Time-dependent quantum transport in correlated systems: applications to electron quantum optics

Bruno Bertin-Johannet

NNT : 2023AIXM0299

THÈSE DE DOCTORAT

Soutenue à Aix-Marseille Université
le 29 septembre 2023 par

Bruno BERTIN-JOHANNET

Transport quantique dépendant du temps dans les systèmes corrélés : applications à l'optique quantique électronique

Discipline
Physique et Sciences de la Matière

Spécialité
Matière Condensée et Nanosciences

École doctorale
ED 352 Physique et science de la matière

Laboratoire/Partenaires de recherche
Centre de Physique Théorique, UMR 7332;
Université de Toulon;
CNRS

Composition du jury

Dominique MAILLY Directeur de recherche au CNRS	Rapporteur
Jérôme CAYSSOL Professeur à l'Université de Bordeaux	Rapporteur
Fabienne MICHELINI Professeure à l'université d'Aix-Marseille	Présidente du jury
Thierry MARTIN Professeur à l'université d'Aix-Marseille	Directeur de thèse
Jérôme RECH Chargé de recherche au CNRS	Membre invité
Benoît GRÉMAUD Directeur de recherche au CNRS	Membre invité

Affidavit

I, undersigned, Bruno Bertin-Johannet, hereby declare that the work presented in this manuscript is my own work, carried out under the scientific supervision of Thierry Martin, Jérôme Rech, Thibaut Jonckheere and Benoît Grémaud, in accordance with the principles of honesty, integrity and responsibility inherent to the research mission. The research work and the writing of this manuscript have been carried out in compliance with both the french national charter for Research Integrity and the Aix-Marseille University charter on the fight against plagiarism.

This work has not been submitted previously either in this country or in another country in the same or in a similar version to any other examination body.

Marseille, July 15, 2023.

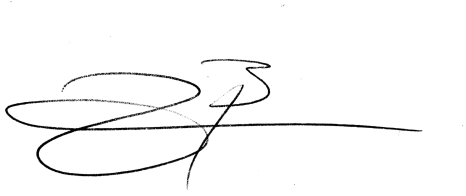

List of publications

List of papers published in the context of the thesis:

1. Bertin-Johannet, B., Rech, J., Jonckheere, T., Grémaud, B., Raymond, L. & Martin, T. Microscopic theory of photoassisted electronic transport in normal-metal/BCS-superconductor junctions. *Physical Review B, 105*(11), 115112 (2022).

2. Bertin-Johannet, B., Raymond, L., Ronetti, F., Rech, J., Jonckheere, T., Grémaud, B. & Martin, T. An on-demand source of energy-entangled electrons using Levitons. *Appl. Phys. Lett.* 122, 202601 (2023)

3. Bertin-Johannet, B., Grémaud, B., Raymond, L., Rech, J., Jonckheere, T. & Martin, T. Current and shot noise in a spin dependent driven normal metal – BCS superconductor junction. arXiv:2311.15684 (2023).

4. Bertin-Johannet, B., Raymond, L., Rech, J., Jonckheere, T., Grémaud, B., Glattli, D. C. & Martin, T. . Photo-assisted current in the fractional quantum Hall effect as a probe of the quasiparticle operator scaling dimension. *Physical Review B, 108*(16), 165425 (2023).

5. Bertin-Johannet, B., Popoff, A., Ronetti, F., Rech, J., Jonckheere, Raymond, L., Grémaud, B., T. & Martin, T. Correlated two-Leviton states in the fractional quantum Hall regime. arXiv:2308.00544 (2023).

6. Ronetti, F., Bertin-Johannet, B., Raymond, L., T. & Martin, T. Periodic source of energy-entangled electrons in helical states coupled to a BCS superconductor. In preparation.

Participation to conferences, meetings and schools during the thesis:

1. Présentation de Poster à
   Meso School 2021: Fundamentals and advances in mesoscopic quantum physics: quantum circuits, topology and correlations, 4/10 - 15/10, Institut d'Etudes Scientifiques de Cargèse, Corsica;

2. Présentation de Poster à
   Topo School Genova 2022: Topological Quantum Matter: theory and applications. 28/03 - 01/04, Santa Margherita Ligure, Italie.

3. Présentation de poster et présentation orale à
   12^{th} Meeting on NanoSciences advances, 13/09-15/09, Porquerolles, France

4. Présentation de poster à
   Session plénière 2021 du GDR 2426 Physique Quantique Mésoscopique, 29/11 - 02/12, Aussois, France.

5. Présentation de poster à
   57^{th} Rencontres de Moriond (2023), session physique mesoscopique, 25/03 - 01/04, La Thuile, Italie.

Résumé

Cette thèse étudie, d'un point du vue théorique, le transport dans des systèmes plus petits que la longueur de cohérence quantique, et plus spécifiquement à travers un contact ponctuel quantique (QPC). Un intérêt particulier est porté aux systèmes corrélés, ici des supraconducteurs de type BCS ainsi que des échantillons dans le régime de l'effet Hall quantique fractionnaire (FQHE). Les jonctions impliquant de tels systèmes sont étudiées en présence d'une tension dépendante du temps. Le cas d'un train de pulses de tension Lorentziens constitue l'un des principaux outils de l'optique quantique électronique pour créer des excitations d'électrons uniques. Un des objectifs de ce travail est d'étudier l'effet des corrélations d'arrière plan sur ces excitations d'électrons uniques.

Il est standard d'étudier le transport grâce au courant électrique moyen à travers le QPC ainsi que ses fluctuations, appelées le bruit. A cette fin, des méthodes de théorie quantique statistique des champs, dans le cadre de la matière condensée, sont appliquées. Le système est décrit par un Hamiltonien, ceci permet d'exprimer le courant et le bruit en termes de fonctions de Green et de self énergies, qui obéissent à la série perturbative de Dyson. Dans des situations hors équilibre, comme à température finie ou en présence d'une tension dépendante du temps, le formalisme de Keldysh est utilisé.

Grâce à ces outils, une description complète du courant et du bruit à l'interface entre un métal normal et un métal supraconducteur de type BCS est atteinte. Celle-ci permet de mettre à jour les différents mécanismes de transport à l'oeuvre dans cette jonction, ainsi que l'effet de leur coexistence. Un résultat principal émerge, à condition que la fréquence de la tension soit faible devant le gap, les Lévitons demi-entiers constituent les états d'excitation minimale de la jonction. Encouragé par ce résultat, un nouveau dispositif est proposé, il s'agit d'une jonction entre un supraconducteur BCS et deux états de bords chiraux dans l'effet Hall quantique de spin. Ce dispositif peut être utilisé afin de générer, à la demande, un état à deux électrons, intriqué en énergie et se propageant dans les deux branches de spin opposé de l'effet Hall quantique de spin.

Le deuxième type de système corrélé étudié est un QPC entre des états de bords Abéliens dans le FQHE. Le couplage tunnel peut soit être modulé en phase en appliquant une source de tension, soit en amplitude en agissant avec une tension de grille. Dans le second cas (et pour un certain régime de paramètres), il est possible de montrer que la dimension d'échelle des quasiparticules (donc l'angle statistique) est égale au décalage de phase de la deuxième harmonique du courant dépendant du temps. Ce résultat peut être considéré comme une proposition de mesure des propriétés des quasiparticules du FQHE. De plus, ce dispositif a l'avantage de n'impliquer qu'une mesure du *courant* à la sortie d'un *seul* QPC plutôt que de recourir à une mesure du bruit dans un système à plusieurs QPCs.

Toujours dans le FQHE, il est possible d'étudier la charge rétrodiffusée lorsque deux Lévitons décalés en temps sont incidents sur le QPC. En général, cette charge n'est pas égale au double de celle induite par un seul Léviton. Ce résultat peut être interprété comme la conséquence d'une interaction effective entre les Lévitons. Le cas, plus accessible expérimentalement, d'une série périodique de paires de Lévitons décalés en temps est examiné en parallèle. Dans les deux cas, il est possible, en jouant sur le décalage en temps, de rendre l'interaction tour à tour attractive ou répulsive. Il s'agit de la seconde proposition, dans cette thèse, de dispositif tirant parti des corrélations d'arrière plan pour donner de nouvelles perspectives à l'optique quantique électronique.

Abstract

This thesis consists in a theoretical study of transport in systems smaller than the quantum coherence length, in particular in quantum point contacts (QPC) connected to leads. Of particular interest are the new phenomena that appear in correlated or interacting mesoscopic systems, such as BCS superconductors or samples in the fractional quantum Hall regime. Junctions involving such systems are studied when a periodic time-dependent voltage drive is applied. The case of Lorentzian voltage pulses constitutes one of the tools used in electron quantum optics to generate single electron excitations. One of the constant concerns throughout the thesis is to study the effects of the embedded correlations on these single electron excitations.

Typically it is possible to characterize transport by computing the average electric current or its fluctuations, the noise, through the QPC. To this end, field theoretical methods for quantum statistical physics in the context of condensed matter are employed. Using a Hamiltonian formalism for the junction, the current and noise can be expressed in terms of Green's functions and self energies, obeying the Dyson's perturbative series. In out-of equilibrium situations, as is the case at finite temperature or under a time-dependent drive, solving Dyson's series will require the use of Keldysh method.

A full description of the current and noise at the junction between a normal metal and a BCS superconductor is derived in such a context. This allows to draw a general picture of transport at the junction, including the interplay between Andreev reflection and quasiparticle transfer. One of the main finding is that, as a consequence of Andreev reflection, half-integer Levitons can be minimal excitation states of the junction (only when the gap is far greater than the frequency). Based on this result, a new type of device is proposed, it consists in a junction between a BCS superconductor and two chiral edge channels of a quantum spin Hall bar. It is shown that it can be operated so as to generate an on-demand energy-entangled two-electron state at the output of the two opposite spin branches of the quantum spin Hall bar.

Next, a quantum point contact between Abelian edge states of the fractional quantum Hall effect is studied with a time-dependent tunnel coupling. It is underlined that the same formalism applies to two types of drives, either a modulation of the coupling phase by a voltage drive or a direct modulation of its amplitude. The main finding is that, in the latter case and with a harmonic modulation (with specific parameters), the scaling dimension of the quasiparticles (thus the statistical angle) coincides with the phase shift of the second harmonics of the current. This result constitutes a proposal to measure properties of the quasiparticles in the fractional quantum Hall effect other than their electric charge. Furthermore, it is achieved via a *current* measurement at a *single* quantum point contact device, rather than a noise measurement with several QPCs.

Still in the fractional quantum Hall effect, the backscattered charge when two time-shifted Levitons are sent to a QPC is studied. It is shown that in general this charge does not correspond to twice that induced by a single Leviton. This is interpreted as the result of an effective interaction between the two Levitons. The more experimentally accessible case of a periodic train of two time-shifted Levitons is also studied in parallel. It is shown that in both cases the interaction between the Levitons can be tuned from attractive to repulsive by changing the time shift between the pulses. This constitutes the second proposition, in this thesis, of device exploiting embedded correlations to provide electron quantum optics with new perspectives.

Résumé étendu

Cette thèse est consacrée à la description du transport quantique dépendant du temps dans des systèmes électroniques mésoscopiques corrélés et en interaction. Une attention particulière est accordée aux applications potentielles de l'optique quantique électronique, la manipulation d'électrons uniques permettant de réaliser des expériences similaires à l'optique quantique [1, 2].

Introduction

La physique mésoscopique [3] est un sous-domaine de la physique de la matière condensée, qui s'intéresse à des systèmes allant de l'échelle nanométrique à quelques micromètres ; sa description théorique repose donc fortement sur la physique statistique quantique. Le transport quantique [4] dans de tels systèmes peut impliquer le spin, la charge, la masse, la température, etc. L'accent est mis ici sur le transport de charge, c'est à dire le déplacement d'électrons dans les métaux. L'aspect quantique de ce domaine a été exploré par Landauer [5] et ses collaborateurs dans les années 50. Ces travaux fondamentaux ont permis de clarifier le processus de base du courant électrique dans les nanostructures, à savoir la diffusion des électrons (et leurs statistiques). La diffusion peut se produire avec n'importe lequel des nombreux éléments présents dans un métal, qui peuvent être des phonons, des impuretés, des ions, d'autres électrons, etc. L'objet canonique de l'étude du courant électrique dans le transport quantique est donc un diffuseur ponctuel unique, c'est-à-dire un contact ponctuel quantique (QPC). Il s'agit d'une jonction tunnel entre deux réservoirs traitée à tous les ordres de la série de perturbations. Les électrons sont transportés d'un côté à l'autre du QPC lorsqu'une différence de tension est appliquée entre les électrodes, ce qui conduit à l'écoulement d'un courant électrique stochastique. Ce courant est donc fluctuant et il s'est avéré, à partir des années 80, que ces fluctuations contiennent des informations sur les processus en jeu dans le transport [6–14]. Par conséquent, la mesure des fluctuations, également appelées bruit, est importante afin d'obtenir une meilleure compréhension du courant électrique. Cette étape a été franchie au milieu des années 90 [15, 16], validant 20 ans de recherche théorique. Enfin, Levitov et ses collaborateurs [13, 17] ont montré que le courant électrique obéit à une statistique binomiale modifiée par des effets de température, ce qui donne une explication cohérente du comportement du bruit et étend cette compréhension à tous les moments du courant électrique.

Parallèlement, à partir des années 60, les expérimentateurs ont commencé à appliquer des tensions périodiques dépendantes du temps à des jonctions tunnel impliquant des supraconducteurs [18, 19], principalement afin d'étudier des régimes particuliers des courbes $I - V$. Le domaine des jonctions tunnel soumises à une tension dépendante du temps n'a pas reçu beaucoup d'attention et a été relativement négligé pendant près de 20 ans. Puis, dans les années 90, la meilleure compréhension du bruit de courant obtenue quelques années auparavant a permis de faire des progrès théoriques importants vers la compréhension et l'utilisation du transport quantique dépendant du temps. En effet, Lesovik, Levitov et Lee ont montré dans une série d'articles [20–22], par le biais de calculs de bruit, que le fait d'alimenter un conducteur avec un train d'impulsions de tension Lorentziennes précisément adapté revient à injecter exactement un électron par période dans le condcucteur. Ils ont montré que, dans cette situation, la mer de Fermi n'est pas perturbée par la tension dépendante du temps. En d'autres termes, la tension ne crée qu'une quasiparticule de charge entière (appelée plus tard Léviton) qui se propage au-dessus de la mer de Fermi à la manière d'un soliton. Des mesures de bruit ont été proposées pour vérifier l'absence de trous dans un tel état. En particulier, le bruit créé par le transport du Léviton devrait être équivalent à celui créé par une tension

continue équivalente. Cette mesure a en effet été réalisée par des expériences pionnières au cours de la dernière décennie [23].

Il existe une similitude frappante entre la manipulation de photons uniques et d'électrons uniques [24]. Dans le cas des photons, cela a motivé la proposition de dispositifs de calcul quantique basés sur des états à un seul *photon* [25–32]. Assez rapidement, il a été réalisé que la manipulation d'excitations *électroniques* uniques dans les systèmes de matière condensée [1, 2, 33–36] a des applications potentielles dans les protocoles d'information quantique [37–40] en codant l'information dans des *électrons* se propageant dans des canaux balistiques. Cependant, le sujet principal de cette thèse n'est pas de fournir des détails sur de telles applications. L'accent est plutôt mis sur la manière de créer de telles excitations électroniques sur des canaux balistiques. Ceci peut être réalisé dans le contexte de l'optique quantique électronique, où les expériences d'optique quantique sont adaptées aux électrons [41–43].

Il s'agit notamment des expériences de type Hanbury-Brown et Twiss [44–47] où l'on observe les corrélations d'intensité des photons cohérents à la sortie. Autrement, dans la configuration Hong-Ou-Mandel [48, 49], les photons entrent en collision à l'emplacement du miroir semi-réfléchissant et les corrélations sont mesurées à la sortie. Un autre exemple célèbre est celui de la preuve expérimentale de la violation de l'égalité de Bell impliquant une paire de photons intriqués en impulsion [50]. Dans le contexte de la matière condensée, les guides d'ondes peuvent être réalisés avec un gaz d'électrons bidimensionnel (2DEG), tandis qu'un QPC joue le rôle du miroir semi-réfléchissant. La différence entre les électrons et les photons réside tout d'abord dans le fait que les électrons possèdent une statistique fermionique, ce qui signifie, qu'ils sont toujours accompagnés d'une mer de Fermi. Deuxièmement, les électrons portent une charge, ils interagissent donc avec leur environnement électromagnétique direct. Dans l'EQO, la première difficulté est contournée par le choix de la forme de l'impulsion de tension, tandis que la seconde est utilisée pour créer les Lévitons.

Cette image de base des Lévitons se propageant sans perturber la mer de Fermi doit être revue lorsque des systèmes plus réalistes ou plus compliqués sont considérés. Il peut s'agir de systèmes en interaction et/ou corrélés, pour lesquels des concepts tels que la mer de Fermi doivent être réexaminés. Typiquement, dans les systèmes où les effets de décohérence [51] ou les corrélations intégrées (comme dans l'effet Hall quantique fractionnaire [52]) opèrent, une description précise du système nécessite un formalisme adapté et de nouveaux effets tels que le fractionnement de la charge [53] ou la cristallisation de Levitons [54] peuvent se produire.

Si, jusqu'à présent, la répulsion de Coulomb a été incluse dans ces scénarios [55–62], d'autres types de corrélations méritent également d'être pris en compte. En effet, par exemple, les guides d'ondes électroniques peuvent être connectés à des supraconducteurs BCS[1], ouvrant la voie à des phénomènes d'optique quantique électronique jusqu'à présent peu explorés [64, 65]. En fait, ces systèmes hébergent des paires de Cooper et des quasiparticules de Bogolubov [66], et pour qu'un courant électrique circule, les électrons doivent être convertis en de telles entités [67]. Un autre exemple de systèmes électroniques en interaction est l'effet Hall quantique fractionnaire (FQHE) [68, 69], qui héberge des quasiparticules portant une charge fractionnaire[2] et qui obéissent à une statistique fractionnaire. L'effet tunnel dans les jonctions composées de tels systèmes pourrait donc impliquer des effets non triviaux, comme le tressage [70], la cristallisation ou la conversion de quasiparticules [71–75].

Être capable de concevoir des jonctions avec de tels matériaux et de les manipuler dans des conditions telles que ces événements remarquables se produisent un par un de manière contrôlée permettrait d'avancer sur plusieurs fronts. Tout d'abord, avec une caractérisation précise des observables de transport, les descriptions théoriques pourraient être comparées aux données expérimentales et les mécanismes ou modèles sous-jacents à ces systèmes pourraient être mieux compris. En fait, dans l'effet Hall quantique fractionnaire, cela pourrait permettre d'étudier plus précisément la validité de l'approche du liquide de Luttinger

[1] Comme ce fut le cas dans les travaux pionniers sur l'effet tunnel quantique dépendant du temps ([18, 63])

[2] Un phénomène habituellement réservé à la physique des hautes énergies, avec les quarks par exemple

chiral et de discriminer entre différentes combinaisons de quasiparticules à différents facteurs de remplissage. Deuxièmement, ces phénomènes peuvent avoir des applications directes, soit dans la conception de nouvelles expériences fondamentales, soit à des fins technologiques. Par exemple, dans les supraconducteurs, l'état fondamental est composé de paires de Cooper, qui sont des paires d'électrons intriqués. L'effet tunnel de ces états de manière cohérente permettrait de propager l'intrication dans différents canaux [14, 76–83]. L'isolation de ces états dans le temps permettrait par exemple de mettre en oeuvre une variété de protocoles quantiques dans des dispositifs à l'état solide. Parmi ce derniers, les principaux exemples sont la téléportation quantique [39], la distribution quantique de clés [37, 38, 40, 84], ou le codage dense quantique [85].

Cette thèse constitue ainsi une tentative de contribuer au processus d'extension des concepts de l'optique quantique électronique à de tels systèmes corrélés et en interaction.

Structure du manuscrit

Cette thèse est divisée en trois parties distinctes. La première présente des résultats déjà connus mais tente d'y apporter un éclairage nouveau afin que les résultats présentés par la suite puissent être facilement interprétés, la deuxième partie expose les nouveaux résultats liés à la supraconductivité BCS et la troisième s'intéresse à l'effet Hall quantique fractionnaire.

Partie I: Transport photo-assisted à travers un contact quantique ponctuel

Chapitre 1: Transport quantique Ce chapitre introduit l'étude du courant électrique dans le contexte du transport quantique. Le contact ponctuel quantique (QPC) qui sera utilisé dans tous les autres chapitres est introduit. Le chapitre continue en présentant rapidement le formalisme Hamiltonien utilisé pour décrire le QPC. Ensuite, la théorie de Floquet est introduite, celle-ci suggère assez simplement une interpretation du transport dans un conducteur soumis à une tension périodique de fréquence Ω. L'état d'un système quantique décrit par un Hamiltonien périodique correspondant à une certaine énergie ω est la somme de Fourier (indice n) des états correspondants à cette énergie plus ou moins la fréquence de l'harmonique de Fourier, i.e., à l'énergie $\omega + n\Omega$.

Chapitre 2: Formalisme pour le contact quantique ponctuel Ce chapitre introduit les principaux détails techniques utilisés dans la suite du manuscrit. Tout d'abord, le lien entre les fonctions de Green et les valeurs moyennes des observables est explicité. Le fait que la jonction soit considérée être hors équilibre implique que le théorème de Wick ne peut pas être utilisé tel quel. La méthode standard pour surmonter ce problème, la théorie de Keldysh, est présentée ensuite. Il paraît judicieux d'écrire les valeurs moyennes dans la représentation énergétique, en termes de fonctions de Green nues et de coefficients de Fourier du couplage tunnel dépendant du temps, qui sont aussi introduits.

Bien qu'il s'agisse d'un chapitre technique, la plupart des complications sont explicitement mentionnées et les équations sont écrites de manière cohérente, pour deux raisons principales. Premièrement, pour montrer à quel point ce formalisme est polyvalent, les effets dits "hors équilibre" (température finie ou autres) étant automatiquement inclus. Deuxièmement, il sera mentionné que ces détails techniques ont une signification physique. Par exemple les états de Floquet agissent comme des états du système d'origine, ce qui est cohérent avec l'image dessinée au premier chapitre. À partir de ce formalisme, des calculs réels d'observables physiques peuvent être effectués dans de nombreuses situations.

Chapitre 3: Variables de transport dans un jonction entre des métaux normaux Ce chapitre applique le formalisme et les idées physiques développés dans les précédents à la jonction la plus simple possible, la jonction $N - N$ soumise à une tension périodique. En particulier, le courant moyenné sur une période et

le bruit sont calculés analytiquement. Ceci permet de dessiner les contours du paradigme de la jonction linéaire, dans laquelle le courant est proportionnel à la tension appliquée et à la transmission, qui peut être exprimée en termes de couplage tunnel. Le bruit présente des propriétés plus intéressantes, il s'agit en effet d'une somme de bruits DC à travers les canaux dits de Floquet. Il sera souligné que cette interprétation est très proche de celle proposée par Tien et Gordon [19] où de tels canaux ont été discutés. Ces derniers correspondent aux harmoniques de Fourier du couplage tunnel, dont les poids peuvent être calculés par simple transformée de Fourier. Ceci permet une description simple des types de tension pouvant mener uniquement à des canaux d'électrons (et pas de trous). Une telle tension est constitué de manière générale d'une combinaison quelconque d'impulsions Lorentziennes respectant un rapport de quantification entre leur amplitude et leur largeur : ce sont les Levitons. Par conséquent, le transport induit par les Lévitons n'implique que des électrons au-dessus de la mer de Fermi et il sera montré que le bruit fournit une mesure de la précision de cette description. En particulier, Il est utile d'introduire le bruit d'excès, c'est à dire la différence de bruit entre une jonction soumise à une tension dépendent du temps et celle soumise à une tension constante équivalente. Il est ensuite possible de démontrer que le bruit d'excès ne contient que des contributions provenant des canaux de trous, et donc qu'il disparaît pour les Lévitons parfaits.

Le bruit en excès peut donc être utilisé comme une mesure pour des expériences impliquant une manipulation précise d'électrons individuels, par exemple pour implémenter des collisions, du transport d'informations, des interférences, etc. En passant, on pourrait remarquer que cela est très similaire à ce qui se fait en optique quantique avec les photons. C'est pourquoi ce domaine est habituellement appelé optique quantique électronique (EQO) et le présent chapitre peut être considéré comme une introduction à l'EQO dans la matière non corrélée (régime du liquide de Fermi).

Les conditions dans lesquelles l'optique quantique électronique peut être réalisée dans des jonctions $N-N$ sont les suivantes : limite de température nulle (bruit linéaire), tension injectant des Levitons (seulement des excitations électroniques), relation de Tien-Gordon pour le bruit, c'est-à-dire canaux de Floquet indépendants (absence de corrélations). Les prochains chapitres décriront comment ces conditions peuvent être assouplies ou adaptées lorsque l'on considère d'autres types de jonctions, impliquant de nouveaux phénomènes physiques, et comment l'EQO peut aider à caractériser ces phénomènes ou même comment ces derniers peuvent aider à concevoir de nouveaux schémas d'EQO.

Partie II: QPC entre des métaux normaux et des supraconducteurs de type BCS

Chapitre 4: Introduction à la supraconductivité BCS Dans ce chapitre, les principaux aspects de la supraconductivité BCS sont résumés. L'image physique derrière une interaction attractive entre les électrons est expliquée en termes d'échange de phonons. C'est l'occasion de calculer l'Hamiltonien de cette interaction au premier ordre dans le couplage des phonons. Il est démontré que cette interaction est effectivement attractive si les deux électrons se trouvent d'un côté opposé de la surface de Fermi. Il sera ensuite montré que cette interaction crée des paires d'électrons avec une énergie nulle. Cette paire étant un singulet de spin, elle conduit à l'instabilité de Cooper et donc à une reconstruction complète de la mer de Fermi.

Ensuite, l'approche standard pour écrire l'état fondamental puis pour décrire les excitations est résumée. Elle consiste à postuler un état fondamental qui "rend l'instabilité de Cooper stable", c'est-à-dire une superposition de paires d'électrons singulets de spin d'énergie nulle. À partir de là, l'Hamiltonien peut être diagonalisé, il est montré qu'il y a un gap en énergie et qu'au-dessus de ce gap, il peut y avoir des excitations uniques, appelées quasiparticules de Bogolubov (ou juste quasiparticules). Ceci permet de trouver une équation pour le gap et pour les facteurs de cohérence, qui sont le poids des trous et des électrons dans les quasiparticules. En particulier, à haute énergie, ces excitations sont simplement des électrons.

Une autre approche de la supraconductivité est présentée, celle de Bogolubov. Elle permet d'inclure des champs externes dans la description et repose sur une représentation dans l'espace réel du gap et des facteurs de cohérence. Cette description permet de trouver les mêmes résultats que BCS en ce qui concerne le spectre

d'excitation dans le cas où le métal est parfaitement homogène et en l'absence de champs externes. Enfin, l'effet de proximité est brièvement décrit, il s'agit de l'apparition de paires de Cooper dans un métal normal à proximité d'un supraconducteur. Cet effet sera utilisé dans les chapitres suivants lorsque le transport dans de telles jonctions sera abordé.

Chapitre 5: La jonction $N-S$ junction under a constant bias Ce chapitre rappelle les résultats standard du transport hors équilibre dans la jonction entre un métal normal et un supraconducteur BCS, la jonction $N-S$. Tout d'abord, l'Hamiltonien de la jonction est dérivé en présence d'une tension (qui peut dépendre du temps) et le courant et le bruit sont exprimés en termes de fonctions de Green. Ceci permet d'utiliser le formalisme développé dans les chapitres précédents pour trouver une formule pour le courant lorsque la jonction est polarisée par une tension constante. Le courant est analysé en utilisant les travaux de Blonder, Tinkham and Klapwijk [67], en particulier, les principaux concepts derrière la réflexion d'Andreev sont rappelés et son implication sur le transport est expliquée. Enfin, le bruit créé par une tension constante est décrit. L'analyse des différents régimes d'énergie est cohérente avec les principaux mécanismes d'effet tunnel introduits pour le courant. Ceci permet d'introduire le facteur de Fano comme un bon outil de diagnostic du régime Poissonnien ainsi que comme une mesure de la charge des particules impliquées dans le transport (ceci est valable seulement dans le régime Poissonnien).

Ce chapitre permet de distinguer trois régimes de fonctionnement différents pour la jonction, dont deux, le régime d'Andreev et le régime normal, sont dits linéaires, car le courant et le bruit sont linéaires en tension. Pour cette raison et comme cela a été montré dans la Sec. 3.4, il paraît raisonnable de supposer que dans ces régimes, le courant et le bruit moyens sous une tension périodique suivent un comportement de Tien-Gordon. Ces deux régimes seront traités ensemble dans le chapitre suivant. Il existe un troisième régime de tension où ni le courant ni le bruit ne sont linéaires en tension, ce régime présente un comportement plus riche et plus complexe et sera traité dans un autre chapitre.

Chapitre 6: La jonction $N-S$ sous un tension alternative dans les régimes linéaires Dans ce chapitre, l'accent est mis sur les régimes linéaires de la jonction $N-S$ soumise à une tension dépendante du temps. Cette situation a été examinée précédemment par Belzig *et al.* [65] grâce à la "full counting statistics" du courant électrique dans le contexte de la théorie des circuits [86]. Dans le régime de faible gap, il a été constaté que le bruit en excès est supprimé pour les Levitons de charge entière, conformément au comportement attendu du continuum à haute énergie, c'est-à-dire celui d'une jonction $N-N$. Dans le régime de grand gap, où le transport est dominé par la réflexion d'Andreev, une suppression du bruit en excès a également été constatée pour des Lévitons de charge demi-entière. L'effet d'une température finie ou le sort de la jonction dans le régime intermédiaire entre ces deux cas limites restent largement inexplorés.

Dans ce chapitre, la jonction $N-S$ dans les régimes linéaires est considérée dans une configuration particulière, lorsque les deux spins du métal normal sont soumis à une tension différente. Le chapitre suivant essaiera de trouver une situation expérimentale où cela est possible, cependant, cette tension séparée est très utile ici pour démêler les propriétés de la jonction. En particulier, les variables de transport comme le courant ou le bruit sont calculées et une interprétation des résultats de Belzig *et. al.* [65] est fournie grâce à la théorie de Floquet et l'image de Tien-Gordon.

Tout d'abord, la jonction dans le régime de tensions bien plus élevées que le gap est rapidement décrite. Comme seul le transfert d'électrons sous forme de quasiparticules dans le continuum du supraconducteur ou la réflexion standard des électrons sont possibles, cette jonction correspond exactement à une jonction $N-N$ dégénérée en spin, qui est étudiée en détail dans le chapitre 3.

Le second cas est celui de tensions très faibles devant le gap, où seules la réflexion d'Andreev ou la réfection standard sont possibles. Les calculs du courant et du bruit sont effectués analytiquement, ce qui permet une analyse détaillée de leur comportement. Il est démontré que le bruit en excès disparaît lorsque la

somme des entraînements sur les spins up et down est un Leviton quantifié. Ceci est expliqué de différentes manières, par l'effet de proximité, ou par l'image dynamique de la réflexion d'Andreev. L'idée principale peut être résumée comme suit : les corrélations supraconductrices lient deux électrons de spins et d'énergie opposés, ce qui fait de ces paires les seuls porteurs de charge responsables de l'effet tunnel. Par conséquent, la tension qui compte est la somme des tensions appliquées sur chacun des spins.

Du point de vue de l'EQO, une fois optimisée, cette jonction peut être utilisée pour manipuler des paires de Cooper uniques dans un supraconducteur, ou inversement, pour diviser les paires de Cooper dans des électrodes. Ce sera le sujet du chapitre suivant, où un nouveau dispositif est proposé pour générer sur demande et de manière contrôlée dans le temps des paires uniques d'électrons intriqués.

Chapitre 7: Source d'électrons intriqués Ce chapitre propose une application des résultats du chapitre précédent : un dispositif utilisant la réflexion d'Andreev pour implémenter une source de paires d'électrons intriqués. L'élément clé réside dans le fait que, comme les paires de Cooper sont intriquées à la fois en énergie et en spin, le fait de les séparer entre deux électrodes polarisées en spin laisse une paire intriquée en énergie. C'est la méthode explorée ici, les électrodes polarisées en spin sont les états de bord de l'effet Hall quantique de spin (QSH), en l'absence de corrélations/interactions entre ces états de bord. Le système étudié consiste en un QPC entre le QSH et un supraconducteur BCS, une tension périodique est appliquée sur les deux états de bord du QSH afin que le dispositif fonctionne dans le régime d'Andreev.

Tout d'abord, l'état créé par la réflexion d'Andreev sur les bords du QSH est calculé de manière perturbative dans le couplage tunnel. Pour une impulsion Lorentzienne de charge totale entière (partagée entre les deux spins), il est montré que, juste après l'impulsion, cet état consiste en une somme de paires d'électrons de spin opposés intriqués en énergie. Le choix du QSH comme plateforme pour héberger ces états est crucial car les deux électrons intriqués formant la paire ont un spin opposé, ils résident donc sur des états bord différents et se propagent dans des directions opposées. À température finie, cette image ne tient plus car l'état final présente également des paires de trous intriqués.

Une généralisation de ce résultat aux trains périodiques d'impulsions Lorentziennes est proposée sur la base des résultats des chapitres précédents. Il est montré que le dispositif correspond formellement à la jonction $N-S$ du Chap. 6, et l'analyse du bruit en excès permettant de sonder la nature strictement électronique de l'état de sortie est répétée. Un ensemble de paramètres expérimentalement réalistes est étudié pour montrer que la jonction peut être utilisée de manière à générer des états électroniques intriqués accompagnés de quelques trous intriqués à cause des effets de température finie, tout en transférant exactement la charge d'une paire de Cooper par période. Il est rappelé que cette description n'est valable que pour des tensions/fréquences faibles par rapport au gap, la solidité de cette condition fera l'objet du chapitre suivant.

Chapitre 8: La jonction $N-S$ soumise à une tension périodique dans le cas général Dans ce chapitre, l'étude de la jonction $N-S$ soumise à une tension périodique a été poussée jusqu'au régime intermédiaire (gap comparable à la fréquence de la tension). D'une part, le courant moyen par période a été calculé analytiquement à tous les ordres du couplage tunnel. D'autre part, le bruit n'a pu être traité analytiquement qu'aux deuxième et quatrième ordres du couplage tunnel. Les régimes généraux de basses et hautes fréquences ainsi que les couplages tunnel ont été étudiés numériquement afin de valider l'analyse développée dans les chapitres précédents.

Lorsque le gap est comparable à la fréquence, le courant moyen par période peut être exprimé analytiquement. Pour les faibles transparences, il présente de fortes discontinuités aux limites du gap correspondant à chaque canal de Floquet. Ces discontinuités marquent le passage d'un courant induit par la réflexion d'Andreev à un courant induit par le transfert de quasiparticules. Dans ce régime, le bruit issu d'une tension périodique peut être plus faible que le bruit dû à une tension constante et contient de nombreuses

discontinuités. Ceci montre que la correspondance habituelle entre le bruit d'excès et le nombre de paires de trous créées par l'entraînement ne tient plus. En outre, le bruit ne peut plus être exprimé sous une forme simple, et il faut recourir à une expansion perturbative de la constante de couplage tunnel, ou à une évaluation numérique à tous les ordres de λ. Cette dernière prouve que les bords du canal de Floquet sont responsables des structures (discontinuités et minimums) du bruit d'excès.

En examinant de plus près les calculs analytiques, il est possible de montrer que le courant moyen par période suit le comportement décrit par Tien-Gordon [19] dans tous les régimes. Il en va de même pour le bruit, qui suit également les relations de type Tien-Gordon, mais uniquement dans les régimes limites, dominés par le transfert de quasiparticules ou la réflexion d'Andreev. Dans le cas général, le bruit suit donc un comportement du type Tien-Gordon seulement au deuxième ordre en tunneling. Il est possible d'interpréter ces résultats en termes de processus physiques principaux, en tenant compte également des effets d'interférence attendus entre les différents canaux de Floquet.

En résumé, ce chapitre démontre que le régime de fréquences intermédiaires (comparables au gap) peut être compris et, en particulier, que le bruit d'excès peut être négatif en raison du fait que la densité d'états dans le supraconducteur n'est pas constante près des bords du gap. En outre, les relations de Tien-Gordon pour le bruit (établies dans la limite où le gap est plus grand que la fréquence d'entraînement) ne tiennent plus dans le régime intermédiaire en raison des interférences entre les différents canaux de Floquet.

Partie III: QPC dans l'effet Hall quantique fractionnaire

Chapitre 9: Fondamentaux de l'effet Hall quantique Ce chapitre introduit les concepts pertinents de l'effet Hall quantique fractionnaire (FQHE) qui seront utiles dans les chapitres suivants. Tout d'abord, un résumé de l'effet Hall quantique lui-même (entier et fractionnaire) est donné et les quantités pertinentes sont introduites avec l'approche quantique la plus simple possible, qui comprend entre autres les niveaux de Landau, le facteur de remplissage ou les orbites cyclotroniques. A des fins de culture générale, un bref résumé de la découverte et des diverses explications théoriques de l'effet Hall entier est aussi proposé. Ceci permet notamment de souligner la nature topologique de l'effet.

Dans la deuxième partie du chapitre, l'FQHE est introduit en résumant brièvement sa contrepartie théorique, c'est-à-dire l'action effective de Chern-Simons. Cette approche a l'avantage d'expliciter les propriétés topologiques du système ainsi que de justifier l'apparition d'états de bord à partir de l'invariance de jauge aux bords de l'échantillon. Il est également expliqué que les états de bord les plus simples de l'effet Hall quantique fractionnaire se comportent comme des liquides de Luttinger chiraux. Par conséquent, les bases de la théorie des liquides de Luttinger chiraux sont rappelées dans le contexte de l'FQHE, y compris la bosonisation et le calcul de la fonction de Green des quasiparticules.

Ensuite, une description du système lorsqu'un QPC relie les deux états de bord a été fournie, le comportement typique en loi de puissance du courant a été expliqué. L'extension de cette description à des états de bord Abéliens plus compliqués a été rapidement résumée. Cela permet d'écrire les trois quantités principales dans ces modèles, la charge des quasiparticules, leur dimension d'échelle et leur angle statistique. Enfin, les principales stratégies expérimentales qui peuvent être utilisées pour mesurer ces quantités sont brièvement rappelées.

Chapitre 10: QPC soumis à une modulation périodique

Ce chapitre décrit une proposition de montage pour mesurer la dimension d'échelle de l'opérateur des quasiparticules. L'investissement théorique considérable pour la recherche de signatures de la statistique des anyons de l'FQHE dans le contexte des configurations de transport quantique électronique a été mis en évidence dans le chapitre précédent. Mais la plupart de ces configurations nécessitent des géométries ou des types de mesures assez compliqués. Étant donné que l'angle statistique des quasiparticules anyoniques

est intimement lié à la dimension d'échelle de l'opérateur des quasiparticules, une question naïve se pose : cette dimension d'échelle peut-elle être détectée par une mesure minutieuse du courant de rétrodiffusion dépendant du temps dans le régime de rétrodiffusion faible ? Bien sûr, la mesure de l'angle statistique est d'un intérêt fondamental, mais il convient de noter que la dimension d'échelle en elle-même est également une quantité importante à mesurer, car elle permettrait de discriminer entre les différents états de bord possibles qui contribuent au courant.

À cette fin, ce chapitre commence par apporter un lumière nouvelle sur la théorie du transport dépendant du temps dans l'FQHE. Il est souligné que le transport peut être induit de deux manières distinctes. Soit en modulant la tension de grille appliquée au QPC (cette situation ne semble pas avoir reçu beaucoup d'attention dans le contexte du transport dépendant du temps), soit en ajoutant une modulation dépendante du temps sur la tension constante appliquées aux électrodes (comme cela a été proposé théoriquement dans Refs. [52, 87]).

Un résultat important du Chap. 2 est rappelé, à savoir que les deux situations peuvent être décrites avec une approche unifiée : la seule différence entre elles réside dans les détails de la décomposition de Fourier de l'amplitude tunnel qui les décrit. Le courant dépendant du temps peut alors être calculé analytiquement en termes de sommes sur ces coefficients de Fourier, impliquant en outre une fonction hypergéométrique de Gauss, un résultat qui est assez abstrait par nature. Pour progresser, il est utile d'effectuer des expansions à l'ordre supérieur dans le paramètre de coupure (au sens du groupe de renormalisation). Il est intéressant de noter que ces expansions dépendent de façon cruciale de la valeur de la dimension d'échelle ν_D et du régime de rétrodiffusion du QPC (faible ou forte).

Dans le régime de rétrodiffusion faible, le courant dépendant du temps peut être décrit comme un terme constant accompagné de ses harmoniques à des multiples de la fréquence de modulation. C'est précisément dans ces harmoniques qu'il pourrait être possible d'isoler la dimension d'échelle de l'opérateur d'effet tunnel des quasiparticules. En effet, en choisissant une simple modulation en cosinus du couplage tunnel, grâce à la tension de grille, il est possible de montrer que le déphasage de la deuxième harmonique du courant dépendant du temps est directement proportionnel à la dimension d'échelle à basse température, ce qui constitue le message central de ce chapitre. Il est aussi souligné que cette connexion est robuste à température finie, ce qui la rend accessible à l'observation expérimentale. Une expérience typique consisterait à multiplier le signal de courant dépendant du temps par une tension harmonique appropriée à deux fois la fréquence de modulation pour détecter ce déphasage.

Par souci d'exhaustivité, un traitement complet de l'expansion des fonctions hypergéométriques qui apparaissent dans l'expression générale du courant dépendant du temps est réalisé. Ceci permet de trouver le courant à la fois pour la limite du liquide de Fermi $\nu = 1$ et pour la limite de la rétrodiffusion forte. Dans le premier cas, une généralisation de la formule de Landauer en fonction du temps est rapidement obtenue dans la limite $\nu = 1$ du modèle de Luttinger chiral. Dans le cas de la rétrodiffusion forte, le courant peut être écrit en termes de dérivée temporelle de la modulation. Une tension dépendante du temps favorise donc un terme capacitif dans le courant moyen de rétrodiffusion forte, ce qui n'avait jamais été observé auparavant.

Le résultat principal concernant le déphasage suggère qu'une mesure minutieuse du courant dépendant du temps pour un dispositif contenant un contact ponctuel quantique pourrait donner un aperçu de la détection (bien qu'indirecte) des statistiques fractionnaires dans l'effet Hall quantique fractionnaire.

Chapitre 11: Lévitons en interaction Dans ce chapitre, l'effet des correlations sur la propagation d'états à deux Lévitons est étudié dans le cas particulier de la séquence de Laughlin de l'FQHE. La largeur des Lévitons ainsi que leur séparation temporelle sont considérés contrôlables. Il est rappelé que les Lévitons, dans le régime tunnel, sont des états d'excitation minimale. En conséquence, ils se déplacent "au-dessus" de la distribution d'équilibre à la manière d'un soliton. En considérant un QPC, la charge rétrodiffusée est

calculée pour la limite de faible transparence. Des résultats analytiques sont dérivés dans le cas d'impulsions isolées et d'une température nulle. Ensuite, la charge rétrodiffusée dans le cas d'un état à deux Lévitons, à savoir Q_2, est calculée et comparée à la charge rétrodiffusée en présence d'une seule impulsion, appelée Q_1. Un calcul explicite montre que $Q_2 > 2Q_1$ dans le régime fractionnaire, contrairement au résultat trivial $Q_2 = 2Q_1$ pour un système sans correlations. Il est intéressant de noter que dans la limite d'impulsions simultanées ($\Delta t \ll \gamma$), la charge rétrodiffusée acquiert une expression simple qui ne dépend que du facteur de remplissage ν. En recourant au formalisme du paquet d'ondes pour les Lévitons, les premiers résultats sont expliqués par l'existence d'une interaction effective entre les deux Lévitons, causée par l'arrière-plan fortement corrélé.

Le cas des impulsions uniques à température finie a ensuite été étudié numériquement. Ces simulations montrent que, pour des températures suffisamment élevées et même pour des impulsions simultanées, $Q_2 < 2Q_1$. En se basant sur l'interprétation de l'interaction effective, cela signifie que la température, ainsi que la séparation temporelle des impulsions, peuvent être utilisées pour contrôler l'intensité et le signe de l'interaction.

Ensuite, afin d'établir un contact avec de potentielles situations expérimentales, le cas d'une température finie et d'une période finie est considéré, il s'appuie sur des calculs numériques dans le formalisme photo-assisté. Dans le cas périodique, on peut régler la charge rétrodiffusée Q_2, en fonction de Δt, pour qu'elle soit inférieure, égale ou supérieure à $2Q_1$. L'effet de l'arrière-plan corrélé est pris en compte dans la dépendance de la charge rétrodiffusée par rapport au facteur de remplissage et à la température. Comme dans le cas d'impulsions uniques, l'interaction effective peut devenir tour à tour positive ou attractive en modifiant la largeur de l'impulsion, la période et la température. Les calculs numériques sont basés sur des estimations réalistes des paramètres qui peuvent être obtenus avec les technologie actuelles.

Remerciements

Je tiens en premier lieu à remercier Thierry Martin en tant que directeur de thèse mais aussi comme professeur et mentor. J'ai appris la plupart des concepts et techniques utilisées dans ce travail en assistant à ses cours de deuxième année de master. Son conseil et son sens de l'organisation m'ont été d'une grande aide. J'ai beaucoup apprécié son habitude de proposer des nouveaux projets accompagnés de célèbres notes manuscrites qui m'ont guidées entre les différents sujets sur lesquels nous avons travaillés. Enfin je le remercie pour sa patience durant les heures de relecture commune des différents articles mais aussi du présent manuscrit.

J'aimerai aussi remercier mon premier co-encadrant de thèse, Jérôme Rech, nos interactions ont toujours été agréables et j'ai beaucoup appris en discutant avec lui. Son aide a notamment été déterminante pour corriger certains de mes codes numériques mais aussi pour les calculs Floquet-Keldysh dans les supraconducteurs. Je voudrai aussi le remercier pour l'intransigence et la rigueur dont il a fait preuve durant la relecture des notes de travail mais aussi de brouillons de publications.

J'étends ma gratitude à Thibaut Jonckheere, mon deuxième co-encadrant de thèse. En effet, son intuition physique durant les discussions que nous avons eues nous ont grandement aidé dans les différents projets. De même, il avait toujours quelque chose à dire sur les notes de travail que je produisait et cela nous menait à chaque fois à une meilleure compréhension du sujet.

Je remercie le reste de l'équipe nanophysique, et particulièrement Benoît Grémaud et Laurent Raymond pour leur aide en informatique et en physique mais aussi pour les longues discussions du vendredi dans le bureau collectif. Je suis aussi très content d'avoir pu travailler avec Flavio Ronetti, depuis qu'il est arrivé dans l'équipe il n'a pas hésité à partager ses connaissances en optique quantique électronique et je l'en remercie. J'ai aussi particulièrement apprécié les moments passés en sa compagnie ainsi que celle du deuxième doctorant de l'équipe, Kishore Iyer, que ce soit lors des conférences, des pauses café au laboratoire ou lorsque nous nous retrouvions dans Marseille.

Merci aussi à Alberto Verga et Laurent Raymond pour m'avoir introduit à la recherche autour de la physique de la matière condensée et plus précisément aux supraconducteurs topologiques lors d'un stage il y a quatre ans de cela.

Je tiens à remercier Catherine Levet, Christelle Chedaille, Stéphanie Suciu et Laura Trano de m'avoir accueilli dans la laboratoire et de leur précieuse aide dans toutes les démarches administratives indispensables au bon déroulé de cette thèse.

Enfin je tiens à remercier ma famille proche, mes parents, Anne et Dominique ainsi que mes trois frères, Pierre, Roland et Louis, mes colocataires, Kostis, Paul, Amelia, Sam et Louis mais aussi toutes les personnes avec lesquelles j'ai partagé des moments de vie agréables durant ces trois années.

Contents

List of Figures

Introduction

This thesis is devoted to describing time-dependent quantum transport in correlated and interacting electronic mesoscopic systems. A particular attention is devoted to potential applications to electron quantum optics, the manipulation of single electrons allowing to perform quantum optics-like experiments [1, 2].

Mesoscopic physics [3] is a subfield of condensed matter physics, concerned with systems ranging from the nanoscale to a few micrometers, its theoretical description therefore relies heavily on quantum statistical physics. Quantum transport [4] in such systems may involve spin, charge, mass, temperature etc. Here the focus is set on charge transport, or displacement of electrons in metals. The quantum aspect of this field was pioneered by Landauer [5] and co-workers starting in the 50's. These foundations have clarified the basic process behind electric current in nanostructure, the scattering of electrons (and their statistics). Scattering can occur with any of the many possible things present in a metal, which can be phonons, impurities, ions, other electrons etc. The canonical object of the study of electric current in quantum transport is therefore a single, point-like, scatterer, i.e., a quantum point contact (QPC). Electrons are transported from one side of the QPC to the other when a voltage difference is applied between the electrodes, leading to the flow of a stochastic electric current. Such a current is therefore fluctuating and it turned out, starting from the 80's, that these fluctuations contain a lot of information about the processes at play in transport [6–14]. As a result, the measurement of the fluctuations, also called the noise, is a crucial step towards a better understanding of electric current. This milestone was achieved in the mid 90's [15, 16], validating 20 years of theoretical research. Finally, Levitov and co-workers [13, 17] showed that the electric current obeys a binomial statistics modified by temperature effects, this gives a consistent explanation for the behavior of the noise and extends this understanding to all the moments of the electric current.

In parallel, starting from the 60's, experimentalists started to apply time-dependent periodic voltage drives on tunnel junctions involving superconductors [18, 19], mainly in order to investigate particular regimes of the $I - V$ curves. The field of time-dependent driven tunnel junctions did not receive much attention and it was relatively neglected for nearly 20 years. Then in the 90's, the better understanding of the current noise achieved just a few years earlier, allowed to make substantial theoretical progress towards understanding and using time-dependent transport. Indeed, Lesovik, Levitov and Lee showed in a series of papers [20–22], through noise calculations, that driving a conductor with a precisely tailored train of Lorentzian pulses of voltage amounts to transferring exactly one electron per period through the junction. They showed that, in this situation, the Fermi sea is unperturbed by the time-dependent drive. Said differently, the drive only creates a quasiparticle of integer charge (later coined Leviton) propagating above the Fermi sea in a soliton manner. Noise measurements were proposed as probes of the absence of holes in such a state, in particular, the noise created by Leviton transport should be equivalent to that created by an equivalent DC voltage drive. This measurement was indeed realized by pioneering experiments in the last decade [23].

There is a striking similarity between the manipulation of single photons and single electrons [24]. In the case of photons, it motivated the proposal of quantum computation schemes based on single-*photon* states [25–32]. Following the same lines, it was quickly realized that the manipulation of single *electronic* excitations in condensed matter systems [1, 2, 33–36] has potential applications in quantum information protocols [37–40] by encoding information in *electrons* propagating in ballistic channels. However, the main subject of this thesis is not to provide details on such applications. Rather, the focus is set on the way to create such electron excitations on ballistic channels. This can be achieved in the context of electron

quantum optics, were quantum optics experiments are adapted to electrons [41–43].

This includes Hanbury-Brown and Twiss like experiments [44–47] where the intensity correlations from coherent photons at the output are observed. Alternatively, in the Hong-Ou-Mandel setup [48, 49], photons collide at the location of the beam splitter and correlations are measured at the output. Another famous example is that of the experimental evidence of the violation of Bell's equality involving momentum-entangled pair of photons [50]. The parallel with electronic excitations is quickly realised as follows, in condensed matter settings, electron wave guides can be achieved with a two dimensional electron gas (2DEG), while a quantum point contact (QPC) mimics the beam splitter. The difference between electrons and photons is first that electrons bear fermionic statistics, this means, in particular, that they are always accompanied by a Fermi sea. Second, electrons carry a charge so they interact with their direct electromagnetic environment. In EQO, the first difficulty is circumvented by the precise tailoring of the voltage pulse while the second one is in fact the very way to excite the Levitons.

This basic picture of Levitons propagating without perturbing the Fermi sea has to be revisited when more realistic or complicated systems are considered. These can include interacting and/or correlated systems where concepts such as the Fermi sea have to be revisited in such cases. Typically, in systems where decoherence effects [51] or embedded correlations (as in the fractional quantum Hall effect [52]) operate, a precise description of the system requires an adapted formalism and new effects such as charge fractionalization [53] or Leviton crystallization [54] can occur.

While so far mostly Coulomb repulsion has been effectively included in such scenarios [55–62], other types of correlations also deserve consideration. Indeed, for example electron waveguides can be connected to BCS superconducting leads[3], opening the way to hitherto scarcely explored EQO phenomena [64, 65]. As a matter of fact, such systems host Cooper pairs and Bogolubov excitations [66], thus for an electric current to flow, electrons must be converted into such entities [67]. Anoter example of interacting electron systems is the fractional quantum Hall effect (FQHE) [68, 69], which hosts quasiparticles carrying a fractional charge[4] and which bear fractional statistics. Tunneling in junctions made up of such systems might therefore involve non-trivial effects, like braiding [70], crystallization or conversion of quasiparticles [71–75].

Being capable to engineer junctions with such materials and to drive them in such a way that these remarkable events occur one at a time in a controlled manner would allow to move forward on several fronts. First with a precise characterization of transport observables, the theoretical descriptions could be compared to experimental data and the underlying mechanisms or models behind these systems could be better understood. In fact in the FQHE, this could permit more precise investigation of the validity of the chiral Luttinger liquid approach and to discriminate between different combinations of quasiparticles for different filling factors. Second, these phenomena can have direct applications, either in designing new fundamental experiments or for technological purposes. For example, in superconductors, the ground state is composed of Cooper pairs, which are pairs of entangled electrons. Tunneling of such states in a coherent way would allow to propagate entanglement to different channels [14, 76–83]. Isolating these states in time would allow for example to implement a variety of quantum protocols in solid-state devices. Among them, major examples are quantum teleportation [39], quantum key distribution [37, 38, 40, 84], or quantum dense coding [85].

This thesis constitutes an attempt to contribute to the process of extending the concepts of electron quantum optics to correlated and interacting systems. An important note is that every equation is written in units where the speed of light $c = 1$, the Planck constant $\hbar = 1$ and the Boltzmann constant $k_B = 1$. A summary of the main results obtained and the references to the original publications follow.

[3] As was the case in the pioneering works on time-dependent quantum tunneling ([18, 63])
[4] A phenomenon usually reserved for high energy physics, with quarks for example

Summary of the new results The junction between a BCS superconductor and a normal metal was studied in [88] with a microscopic model for the junction. Analytical results for the average current and noise to all orders in the tunnel coupling were obtained in the regimes of low and high voltage limits (with respect to the superconducting gap), called the linear regimes. This allowed to draw a physical picture of the tunnel processes in a time-dependent setup, which can be described with the Tien-Gordon approach. This approach was clarified by linking it with Floquet theory, which states that time-dependent transport can be understood as the combination of time-independent processes, taking place in Floquet channels, which were defined by the same occasion. In the regime of large gap, it was shown that half-Levitons actually cancel the excess noise and create exactly one Cooper pair per period, effectively achieving the requirement for EQO to be performed in this junction. This result was already known from [65], but not well understood as it was not derived with a microscopic model and the finite temperature formula was never derived before. In the regime of voltages comparable to the gap, which was so far unexplored, an analytical formula for the average current was found, and it validates the Tien-Gordon picture of transport. Then, the noise was computed to second and fourth order in tunneling, the main result was that the Tien-Gordon picture holds for second order processes in tunneling, but breaks down for higher order terms. This was explained by changing a little this physical picture, the amplitude of the Floquet channels should be considered instead of their probabilities.This result allowed to describe consistently all regimes of tunneling, temperature and voltage of the junction. Finally, to actually implement EQO in the junction, a device operating in accessible regimes of experimental parameters was proposed as an on-demand source of Cooper pairs.

This work was extended in a pair of publications [89, 90], were the BCS superconductor is connected to a quantum spin Hall bar, hosting two opposite spin-polarized chiral edge modes. When operated in the regime of large gap over voltage ratio, it was shown that negative charge half Levitons sent from the edge modes towards the junction are reflected as energy-entangled states shared on the two channels. In this case, the superconductor acts as an "entangler", and experimentally accessible parameters were explored to find an optimized working regime. In particular, through a computation of the noise, similar to that carried out in the first publication [88], it was shown that a finite temperature adds a few entangled hole pairs, and that the entangled electron pair is "fractionalized".

A following paper [91] was needed to explain the underlying mechanism behind the tunneling of a single Cooper pair per period in these junctions and its derivatives. This was done by investigating the junction in the large gap regime when both spins of the normal metal are driven independently, in amplitude and time. Analytical results for the average current as a function of time were found and allowed to understand that the superconducting correlations are responsible for an effective addition of the drives on both spins. As a result, the tolerance of half Levitons to time shift or voltage imbalance between the spins was studied in detail. In particular, it was shown that for integer Levitons, the single electron nature of the state is robust under voltage imbalance or time shift, this is not the case for half Levitons which require perfectly synchronised drives.

Concerning the fractional quantum Hall effect, the capabilities of time-dependent transport to hint for fundamental properties of quasiparticles were investigated in another publication [92]. In particular, it was shown that driving the tunnel contact itself instead of the leads amounts to a much simpler time dependence of the average current. Through Luttinger liquid computations of the average current as a function of time in the weak backscattering regime, it was shown that, in a reasonably large range of parameters, the scaling dimension of anyons is equal to the phase shift of the second harmonics of the average current when the tunnel coupling is a sinusoidal function of time. Therefore, a measurement of the time shift of the harmonics of the average current directly yields the scaling dimension of the quasiparticles, providing a new tool for discriminating between different theories at a given filling factor. Some new results about the strong backscattering regime were also derived, were it was shown that the time-dependent drive gives rise to a new type of tunnel process, which is capacitive, i.e., which involves the time derivative of the voltage

instead of the voltage itself, and dominates the process leading to DC current.

Finally, still in the fractional quantum Hall effect, tunneling of pairs of Levitons at a QPC is investigated in [93]. The charge transmitted through the QPC, as well as its fluctuations, are computed analytically for different time separations of the pulses and in the tunnel limit. It was found that the charge transmitted by two pulses, when they overlap, is not equal to twice that of single pulse. This was directly linked to the effective interaction between the Levitons, induced by the strongly correlated background of the FQHE. It was shown that this interaction can be monitored by the time shift between the pulses, ranging from attractive to repulsive interaction. It was also recalled that interaction between Leviton states in the FQHE is a key ingredient for two qubit gate systems for example.

Structure of the thesis

The thesis is divided in three distinct parts. The first one presents already known results but tries to shine a new light on it so that the subsequently presented findings can be easily interpreted, the second part exposes the results related to BCS superconductivity and the third one is concerned with the fractional quantum Hall effect.

Part I: Photo-assisted transport through a quantum point contact

Chapter 1: Quantum transport Introduces the study of electric current in quantum transport. It describes the quantum point contact (QPC) which will be used in all the other chapters. It continues by presenting the Hamiltonian formalism used to describe the QPC and finishes by presenting Floquet theory and its usefulness in understanding time-dependent transport in the present context.

Chapter 2: Formalism for the quantum point contact Consists in an exposition of the techniques used throughout the thesis to compute transport quantities. The Keldysh Green's function approach is explained, the time dependence of the drive is included through Fourier series and the Dyson equations are summed thanks to the Fourier decomposition.

Chapter 3: Transport quantities in normal metal junctions Applies the last two chapters to the canonical junction, i.e., that between two metals in the normal state. It is shown that this junction has a linear $I-V$ characteristics. The noise is also computed and interpreted thanks to the Tien-Gordon picture helped by Floquet theory, introduced here as well. The specificities of Levitons are introduced through the study of different drive shapes and its link to the noise is clarified.

Part II: QPC between normal leads and BCS superconductors

Chapter 4: Introduction to BCS superconductivity Summarizes the fundamentals of BCS superconductivity. In particular, the phonon origin of the attractive electron-electron interaction is derived. Then the Cooper instability as a hint to the BCS ansatz is explained, this allows to write down the BCS ground state. Finally, the quasiparticle excitations are described, their energy spectrum as well as the coherence factors are derived.

Chapter 5: N-S junction under a constant bias Sums up the main standard results of non-equilibrium transport in the junction between a normal metal and a BCS superconductor, the $N-S$ junction. For example Andreev reflection and quasiparticle transfer above the gap are described and their impact on average current and noise are computed and discussed.

Chapter 6: The AC-driven N-S junction in the linear regimes Describes the $N-S$ junction in the regime where the superconducting gap is large with respect the voltage difference between the leads. In this regime, it is easier to understand the results by separating the processes at play. This is done by considering that the voltage drive applied on the up and down spins of the normal metal are different. It is shown why half Levitons are minimal excitation states of the junction and how they minimize the noise.

Chapter 7: Source of entangled electrons Proposes a device based on the results of the previous chapter, i.e., the use of half Levitons to generate minimal excitation states. More precisely, this device is a junction between a BCS superconductor and the two chiral, spin-polarized, edge modes of a quantum spin Hall bar. It is shown that this junction behaves as an on-demand source of energy entangled two-electron states, devoid of hole excitations. Experimentally accessible parameters are investigated to explain how this proposal could hold in realistic experiments.

Chapter 8: The AC-driven N-S junction in the general case Studies the behavior of the $N-S$ junction in the general case of voltages comparable to the superconducting gap. It is shown how the Tien-Gordon picture is modified, due to both correlations and non linearities of the density of state of the superconductor. In particular, the latter, as a consequence of the former, is responsible for both a reduction of the noise below the DC level when a periodic drive is applied and for interferences between the various channels involved in transport.

Part III: QPC in a fractional quantum Hall bar

Chapter 9: Quantum Hall effect fundamentals Recalls the principal features of both the integer and fractional quantum Hall effects. In the latter case, the chiral Luttinger liquid approach to describe the fractional quantum Hall effect (FQHE) is developed together with the bosonization technique. The main transport properties at a QPC in such systems are then stated.

Chapter 10: Periodically driven QPC Is an application of the so-called gate drive to the computation of the harmonics of the average current in a QPC in the FQHE. More precisely, it is shown that, in the weak backscattering regime (WB) of the QPC, the time shift of the second harmonics is proportional to the scaling dimension of anyons. In the strong backscattering regime, the time-dependent drive favors a capacitive term in the average current, which was never noted before.

Chapter 11: Interacting pulses Analyses the charge transmitted by one or two pulses in a QPC in the FQHE. It is shown that the charge generated by two pulses is not twice that of the single pulse, this is interpreted as due to an effective interaction between two Levitons. In particular it is shown that this interaction can be monitored by the time shift and can be attractive or repulsive. This is generalised to the periodic case, more accessible experimentally, by comparing trains of single pulses to trains of double shifted pulses. As expected in this case, the results hold as long as the width of the pulses and the time shift between them is low with respect to the period of the drive.

Appendices

Appendices containing analytical derivations are provided for the reader interested in understanding the computations. The usage of these computations is scattered in the main text so precise references to the relevant appendices are provided each time.

Part I.

Photo-assisted transport through a quantum point contact

1. Quantum transport

1.1. Introduction

This short chapter consists in a small introduction to the study of electric current in the context of quantum transport. Then the basic quantum conductor studied in this thesis, the quantum point contact (QPC), is described. The formalism chosen to treat such systems is Hamiltonian-based and described in the second part of this chapter. The modification of the Hamiltonian description when a time-dependent voltage drive is applied is also discussed. This is the occasion to introduce Floquet theory as the root of the interpretation of transport developed in the remaining of the thesis.

1.2. General background

The problem of understanding the quantum mechanical processes behind the flow of electric current through a conductor of mesoscopic scale is at the heart of quantum transport, see [4] for an account of the field. Only systems smaller than the coherence length of electrons are studied, so that quantum effects operate. In this framework, pioneered by Rolf Landauer in 1957 [5], the electric current is envisioned as the result of scattering of electrons by all components of the system, usually a metallic device. A central result summarizing these ideas is the Landauer formula for the conductance G of a conductor in the absence of decoherence over the size of the sample:

$$G = G_0 \sum_c \tau_c \,, \tag{1.1}$$

where $G_0 = e^2/2\pi$ is the quantum of conductance (without taking the spins into account) and τ_c is the probability of transmission through the conductor of channel c, simply called the transmission. The current in a mesoscopic conductor is a manifestation of transfer of electrons from one side to the other, which is by essence a probabilistic process for two main reasons. First, transport happens by successive scatterings of electrons, which define a probability for outgoing states, as a function of incoming states, energy levels, angles and other variables depending on the system. Second, mesoscopic physics deals with systems containing thousands of electrons, therefore quantum statistical physics has to be employed, and it describes the occupation of energy levels with a probability distribution, e.g., the Fermi-Dirac distribution. The electric current therefore arises from a combination of random processes. The (quantum) average current $\langle I \rangle$ is the first moment of this distribution, it is often the easiest to compute but not the most interesting. Importantly, in this thesis, the quantum average of the current will be called simply the current[1]. Usually, the fluctuations of the current are not directly characterized by the second moment, rather by current-current correlations, noted $C(t, \tau)$ they read as

$$C(t,\tau) = \langle I(t)I(t+\tau)\rangle - \langle I(t)\rangle \langle I(t+\tau)\rangle \,, \tag{1.2}$$

where $I(t)$ is the current operator at time t an $\langle . \rangle$ is the quantum statistical average value. Historically, current fluctuations were unwanted hindrances to clean experiments, as a result it is customary to call them

[1] This choice is justified by the presence of time averages of the quantum average current later, which will be called period-averaged current.

noise. More precisely, the correlator $C(t,\tau)$ is a function of two times, which is complicated to understand or to measure, it is therefore customary to compute its Fourier transform in both times and to set the frequency associated with the time difference τ to zero. This is what is usually called the current noise power, or just noise,

$$S(\omega) = \frac{1}{T_s}\int_{-T_s/2}^{T_s/2} \mathrm{d}t \int_{-\infty}^{\infty} \mathrm{d}\tau \, \left[\langle I(t)I(t+\tau)\rangle - \langle I(t)\rangle \langle I(t+\tau)\rangle\right] e^{-i\omega t}\,, \tag{1.3}$$

where T_s is any measurement time scale, typically, in this thesis, where the drive is periodic, this will correspond to the period and experimentally, to many periods. Note that the letter S is used as, by Wiener-Kinchine theorem, the noise corresponds to the power spectral density of the current. In actual systems, noise can emerge from various physical phenomena; at low frequencies the atoms of the metal are subject to oscillations between various metastable positions, this gives a noise contribution proportional to the inverse of the typical frequency of such oscillations [94]. In quantum transport, the noise considered is typically a white noise, independent of the frequency, this occurs at higher frequencies, typically around the megahertz where the atoms are considered at rest [95], thus the $1/f$ contribution is suppressed and the noise is independent of the frequency. It is usually around this frequency range that occupation and transmission effects rule the current noise, so that when one speaks of zero-frequency noise, it means between the megahertz and the gigahertz, so that the $1/f$ noise can be ignored. The noise of electric current has been studied for more than a century, Johnson and Nyquist [96] showed that the current white noise in an undriven sample (coined thermal noise) was proportional to the electronic temperature and to the conductance of the electrons, $S_{\mathrm{th}} \propto GT$. On the other hand, when thermal effects are dominated by a voltage drive, Schottky [97] showed that if the current arises from emission of discrete particles, electrons, the noise is proportional to the charge e of the electrons times the current (see [95] for a proof). This voltage-induced noise stems in the quantum nature of the sample and was named shot noise, $S_{\mathrm{sh}} \propto e\,\langle I\rangle$.

Interest in the noise increased again in the late 80's, when, using Landauer's idea of scattering as the main mechanism for the electric current, the proportionality coefficient between the shot noise and the current was expressed in terms of the transmission τ as [6–10, 12].

$$S_{\mathrm{sh}} \propto e(1-\tau)\,\langle I\rangle\ . \tag{1.4}$$

A simple reasoning can help understand this result, the temperature is set to zero and in a single point scatterer, the variables are the direction of propagation and the lead in which the particle is. An incoming electron can either cross the junction at the Fermi surface with probability τ, or be reflected without changing energy, with probability $1-\tau$, thus the current is a Bernoulli process, with probability of success τ. It is well known that Bernoulli processes follow a Binomial distribution, whose first moment is $n\tau$ and second moment reads as $n\tau(1-\tau)$, where n is the number of attempts. This corresponds with the results for the current provided that the number of attempts is proportional to the voltage $V(t)$. It was indeed proven in [13, 17], when the temperature is low enough, i.e., for voltages $eV \gg T$, that the current follows a binomial statistics. This allowed to find an expression for the number of attempts, which is proportional to the voltage. Note that this corresponds to the simple image provided above, the current is proportional to τ and to the voltage, pn in the language of Bernoulli processes. In the other limit, i.e., that of large temperature, transport is dominated by thermal processes which are not the main subject of this thesis. It will be shown that the Landauer formula for the current and the shot noise formula of Schottky can be retrieved in the Hamiltonian approach. This allows to obtain an expression of the transmission τ as a function of the tunnel coupling λ and to check the consistency of the Bernoulli process picture.

1.3. Quantum point contacts

A Quantum point contact (QPC) is a way of connecting two systems of electrons, which can have different dispersion relations, temperatures, band structures, correlations, interactions etc. The two systems are called electrodes or leads depending on the context. The physical distance separating the two leads is typically comparable to, or smaller than the coherence length of electrons, so that coherence-preserving tunneling from one side to the other can occur. For this reason, and in the context of this thesis, a QPC in the regime of weak coupling will also be called a tunnel junction. A QPC can take many forms: a constriction in an electronic wave-guide, a scanning tunneling microscope tip in proximity with the surface of a conductor, a break junction etc. The two electrodes are typically labeled by side, left L or right R, or by type, N for a metal in the normal state or S in the superconducting state, the corresponding junction is called an $N-N$ or an $N-S$ junction. In the language of quantum transport, the conductor is the tunnel region, i.e., a point scatterer with only one incoming direction and one outgoing direction. Thus the method of quantum transport can be used to compute measurable quantities such as the current and the noise at a QPC. Several theoretical descriptions have been used to study such systems, see [98] for a quick review. The so-called Hamiltonian approach was found to be the most relevant for this thesis, so it is explained before anything else, it constitutes the starting point of all calculations presented here.

1.3.1. Hamiltonian approach

This approach was introduced in 1961 for tunneling in an $N-S$ junction [99–101], but it can be extended to other junctions as it relies on simple principles. To summarize briefly the procedure, the aim is to write a second-quantized Hamiltonian describing the junction, for which usual techniques of many-body quantum field theory can be applied. Sketching the discussion from Prange [102], considering the junction as a whole, the system could be described by finding appropriate wave-functions for the left and right leads. However, this would depend on the type of metal involved and such a level of precision would be a hindrance at this point. Writing a Hamiltonian for the whole junction, one can identify three terms, involving only left operators, right ones, or a combination of both, this motivates the following writing

$$H = H_R + H_L + H_T \,, \tag{1.5}$$

where the tunnel Hamiltonian H_T takes the general form

$$H_T = \sum_{k,k'} \left(T_{k,k'} c^\dagger_{k,L} c_{k',R} + \text{H.c.} \right) \,, \tag{1.6}$$

where H.c., stands for Hermitian conjugate and $T_{k,k'}$ is the overlap integral, and can take several forms [99–102], but this is not the point of this discussion. A very important assumption for this approach to be analytically interesting, see [103], is that the applied voltage is very small with respect to the Fermi energy and that the Fermi surface is perfectly metallic, i.e., one can consider one band only enforce that the density of states is constant. This has the direct implication that one can replace $T_{k,k'}$ by its average value on the Fermi surface $\tilde{\lambda}$ which is called the tunnel coupling, this is equivalently called the wide band limit. The tunnel Hamiltonian can therefore be written as

$$H_T = \sum_{k,k'} \left[\tilde{\lambda} c^\dagger_{k,L} c_{k',R} + \text{H.c.} \right] \,. \tag{1.7}$$

Following Cuevas [98], a site representation in real space ($c_{i,L(R)}$ on site i) with a tight binding model can be adopted. Assuming that tunneling involves only one site of each side $c_{L,0}$ and $c_{R,0}$, the Hamiltonian is

written as

$$H_T = \lambda c_L^\dagger c_R + \text{H.c.}\,, \tag{1.8}$$

where the zeros were immediately removed for notational convenience and λ and c were rescaled so that $0 \leq \lambda \leq 1$. When λ is close to zero, the coupling is weak, this is the tunnel limit, on the other hand, when $\lambda = 1$, the coupling is perfect and the junction is in the transparent limit. It is important to raise the problem of $\lambda \approx 1$, where, according to Prange [102], Eq. (1.7) might not be valid anymore. Disregarding this problem, Eq. (1.8) can be taken as a starting point for the description of any QPC as it simply describes a system made of two electron species L and R coupled with strength λ. The above discussion was merely an attempt to link this Hamiltonian with actual physical parameters of a QPC. The total Hamiltonian Eq. (1.5) is therefore used for every calculation performed in this thesis, all the following chapters consider different situations for H_L and H_R, voltage drive, energy distribution, correlations etc.

1.3.2. Voltage drive

As will be explained later, it can be interesting to apply an asymmetric drive to the system, in the case of a voltage drive $V(t)$, the convention is for it to be applied on the left, which has the effect to add a term to the total Hamiltonian, that now reads as

$$H = H_\text{L} + H_\text{R} + H_\text{T} + \sum_i eV(t) c_{i,L}^\dagger c_{i,L}\,. \tag{1.9}$$

Following Rickayzen [103], this can be included in a new set of operators on the left, $\tilde{c}_{i,L}(t)$, which respect the following relation

$$\frac{\mathrm{d}}{\mathrm{d}t}\tilde{c}_{i,L}(t) = i\left[H_L(V=0), \tilde{c}_{i,L}(t)\right] - ieV(t)\tilde{c}_{i,L}(t)\,. \tag{1.10}$$

A convenient choice for the voltage drive is to assume it was adiabatically switched on, more precisely that $V(t<\tau) = 0$ for τ a time long in the past (with respect to the other time scales of the system). The effect of this drive on the left operators is therefore just to add a phase to the c operators as follows:

$$\tilde{c}_{i,L}(t) = e^{-ie\int_{-\infty}^{t}\mathrm{d}t' V(t')} c_{i,L}\,. \tag{1.11}$$

Defining the phase shift for electrons on the left as

$$\phi(t) = e\int_{-\infty}^{t}\mathrm{d}t' V(t')\,, \tag{1.12}$$

the tunnel Hamiltonian reads as

$$H_T = \lambda e^{i\phi(t)} c_L^\dagger c_R + \text{H.c.}\,. \tag{1.13}$$

As a matter of fact, the formalism that will be developed specifically to describe such a system (mainly Fourier analysis, see Sec. 2.2) does not particularly depend on the "shape" or "type" of this time dependence. Therefore, a time-dependent tunnel coupling $\lambda(t)$ can be introduced, that encapsulates every type of time dependence whether it comes from a voltage drive or an experimentally monitored junction width or gate drive. As a result, the tunnel Hamiltonian is written as

$$H_T = \lambda(t) c_R^\dagger c_L + \text{H.c.}\,, \tag{1.14}$$

where $\lambda(t) = \lambda e^{-i\phi(t)}$ for a voltage drive. In this general setting, Fig. 1.1 represents the sites in both sides and the junction itself, with all relevant analytical quantities. Now that the Hamiltonian is clearly written

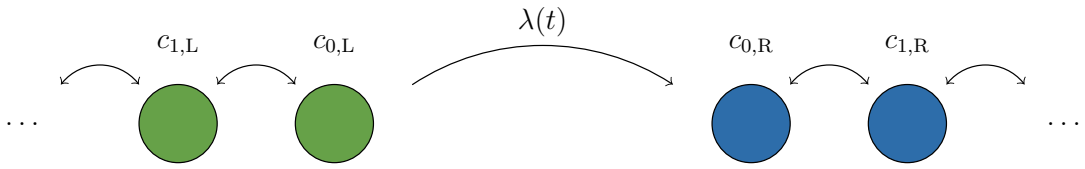

$$H_T = \lambda^*(t) c^\dagger_{0,L} c_{0,R} + \text{H.c.}$$

Figure 1.1.: Simplified drawing of the junction considered. Colored circles correspond to real space electron sites, the double sided arrows represent the kinetic energy coupling between the sites and the single sided arrow materializes the time-dependent tunnel coupling.

a quick physical picture of how a periodic drive affects the system can be provided, this is the purpose of the next section.

1.4. Floquet theory

This section provides a summary of the Floquet theory [104], which is used to characterize quantum systems described by a periodic Hamiltonian. The concepts introduced here are mainly useful as a tool for interpretation, in particular, a link between with Floquet theory and the so-called Tien-Gordon picture of time-dependent quantum transport will be made in Sec. 3.4. As it is independent of the formalism presented in the next chapter and provides a general understanding of time-dependent transport, it was chosen to present Floquet theory to conclude this chapter.

Floquet's theorem states that any periodic linear differential equation can be written (in a different basis) as a constant linear system[2]. This theorem applies to quantum systems with periodic Hamiltonians of frequency Ω, and the so-called Floquet theory was consequently developed in this context, see [104] for details.

This approach stems from the fact that it is much easier to describe a time independent system than a time-dependent one, Floquet theory makes a link between the former and the latter. The main results take place in the Floquet basis, which is spanned by a Fourier expansion of each of the eigenstates of the original Hamiltonian[3]. The Hamiltonian representing the energy of these sates is called the Floquet Hamiltonian and is time-independent. It is therefore possible to write a simple evolution operator between the eigenstates of this time-independent Hamiltonian. As it turns out, the evolution operator of the time-dependent system is a Fourier series with the evolution operators of the Floquet system as Fourier coefficients. The first consequence is that the evolution of the time-dependent eigenstates are the sum of all possible evolutions between the time independent Floquet eigenstates. The second consequence comes from the structure of the Floquet Hamiltonian, which contains a set of eigenvalues for each original eigenstate. This set is built from a fundamental energy E_0 together with all the harmonics $E_0 + n\Omega$ with $n \in \mathbb{N}$. As a result, each evolution operator in the Floquet basis describes the gain or loss of an energy equal to an integer times the frequency. In the context of a voltage drive applied to a system of electrons, these energy shifts in Floquet space can be interpreted as a number of photons exchanged between the drive and the Fermi sea. The energy range used to describe the system can therefore be reduced to $[-\Omega/2 : \Omega/2]$, all other energies arise from the absorption or emission of photons and are said to belong to another Floquet channel.

[2]This is fundamentally very close to Fourier theory but with the inclusion of the differential equation. Hence the ubiquity of Fourier coefficients in this thesis.

[3]It is therefore a tensor product space, Harmonics times states of the time-dependent system

As a small word of anticipation, a parallel with the Tien-Gordon picture of Sec. 3.4 will allow to identify the amplitudes for the absorption of l photons, p_l, corresponding to a probability P_l. The voltage biased lead will then be better described as a Floquet state, a superposition of Fermi seas, which will be referred to as "Floquet channels", with shifted chemical potential $\mu \to \mu + eV_{\mathrm{DC}} + l\Omega$ and an intensity given by the corresponding Floquet weight P_l.

1.5. Conclusion

This chapter was written to set the stage for the next ones. Indeed, the basics of transport in a QPC were recalled, it will be useful to keep this in mind when diving in precise computations of the current and noise. Then, a hand waving derivation of the Hamiltonian used to describe the system was provided. From this simple Hamiltonian, the next chapters will explain in detail the techniques used to write quantum transport operators and extract their expectation values. Finally, a quick reminder of Floquet theory as well as the physical picture it suggests were proposed, it will prove very useful as a tool to interpret the results, first in the simple $N - N$ junction, but also in more complicated systems.

2. Formalism for the quantum point contact

A formalism suitable for the computation of transport properties in time-dependent, out of equilibrium QPC is presented. It is based on techniques developped for quantum field theory such as Wick's theorem, Keldysh Green's functions and Dyson's equations. Time dependence is accounted for by presenting the Fourier counterparts of these techniques.

The Green functions approach is presented from basic quantum mechanics principles in Sec. 2.1. Then, in Sec. 2.2, the time periodicity is included by writing Fourier series of the quantities introduced above. Finally, a way to perform the sum of the Dyson perturbation series in Keldysh space is shown in Sec. 2.3.

2.1. Green's function approach

The Green function formalism is often used in quantum field theory as a way to compute average values of quantum operators. As a simple reminder, some basics of the derivation of these techniques is recalled, and, before performing the full computation of the current, it contours are drawn.

2.1.1. Technical introduction

The physical quantities in quantum mechanics are matrix elements or expectations values, they involve the projection of operators on states, so there can be many choices as to the definition of the states and operators as long as the matrix elements are the same.

First, the traditional one is the Schrodinger picture where the wave function $\psi(t)$ obeys the time-dependent Schrodinger so that

$$\psi_S(t) = e^{-iHt}\psi_S(t_0)\,, \tag{2.1}$$

and the operators are constant in time. The opposite choice is the Heisenberg picture, where the wave function is constant

$$\psi_H = \psi_S(t_0)\,, \tag{2.2}$$

and the operators read as

$$F_H(t) = e^{iHt}F_S e^{-iHt}\,. \tag{2.3}$$

Average values of operators are the sum of the matrix elements over all the possible states, i.e.,

$$\langle O(t)\rangle = \mathrm{Tr}\left[\rho(t)O(t)\right]\,, \tag{2.4}$$

where ρ is the density matrix. It is standard to define operators in the Heisenberg picture (mainly because the density matrix becomes time independent in this picture). Thus, as a first step, the current operator flowing through the left contact and defined as the time derivative of the charge operator, is written in the Heisenberg picture. The latter reads as $Q_L(t) = eN_L(t)$ so that the current can be written as follows,

$$\begin{aligned} I_L(t) = \dot{Q}_L &= ie\left[H_T, c_L^\dagger(t)c_L(t)\right] \\ &= -ie\left[\lambda^*(t)c_L^\dagger(t)c_R(t) - \lambda(t)c_R^\dagger(t)c_L(t)\right]\,, \end{aligned} \tag{2.5}$$

where only one spin species is considered, for simplicity (in the absence of spin flip process, the addition of spin amounts to multiplying the current by two). A simple interpretation of Eq. (2.5) is to say that $c_L^\dagger(t)c_R(t)$ describes the transfer of a particle from right to left, which contributes to the current with a charge $-e$. The second term being the opposite process, it contribute with an opposite charge, hence with an opposite sign[1]. The aim of this chapter is to describe a way to compute the matrix element of such an operator or products of such operators on the ground state, i.e., average values of the type $\left\langle c_L^\dagger(t)c_R(t')\right\rangle$ in the Heisenberg picture.

2.1.2. The Keldysh method

The standard procedure starts by expanding the exponential in Eq. (2.3) so that one is left with the average value of an infinite sum of products of single electron operators. A very important tool to perform such a computation is Wick's theorem [105]. Stated simply, it does two things, first, it provides a recipe to perform all the permutations required to extract normal ordered terms, i.e., terms where the annihilation operators are on the right so that they disappear when applied on the ground state. Second, it allows to write the average value of the initial product in terms of contractions of two operator products. These contractions are the difference between the time ordered product and the normal product in the interaction picture. Hence, when the contraction is not zero, it is proportional to the one-particle average values of the operators in the non-interacting theory[2]. Wick's theorem therefore allows to separate the average value of the full product in a sum of products of two operators average values. This sum is usually hard to compute and one often resorts to various techniques to perform the sum, such as Feynman diagrams, or Dyson's equations in the present case. Wick's theorem is therefore at the heart of such a procedure. It happens however that it is only valid for a single particle initial density matrix *and* for operators in the non-interacting theory[3]. The problem one faces in non-equilibrium many-body theory is therefore twofold, first the Heisenberg operators must be expressed in terms of operators in the non-interacting theory and second the initial density of states has is a many particle one.

One starts by solving the first problem as some concepts which will be introduced are used in solving the second one. To this end, the free Hamiltonian is written H_0 and the interacting term H_T as in Eq. (1.5), this allows to introduce an intermediate representation, the interaction picture (or Dirac picture), where the states contain the interacting part and the operator the non-interacting one. Namely, the states evolve according to

$$\psi_I(t) = e^{iH_0t}\psi_S(t)\,, \tag{2.6}$$

which means that they follow a Schrodinger equation defined by the Hamiltonian

$$H_{T,I}(t) = e^{iH_0t}H_Te^{-iH_0t}\,, \tag{2.7}$$

in the interaction picture. As a result, every operator in the interaction picture evolves in the same way as in the Heisenberg picture for a non-interacting system,

$$\frac{\mathrm{d}}{\mathrm{d}t}F_I(t) = i[H_0, F_I(t)]\,, \tag{2.8}$$

which allows to use Wick's theorem on operators in this representation. Now one is left with the problem of writing Heisenberg operators of the interacting systems in terms of operators in the interaction picture. This is done by writing down the states in the interaction picture first, integrating the Schrodinger equation

[1] The i in front of the current will ensure that the average value of the current be real.
[2] The initial state is chosen so that these average values are known.
[3] This ensures that the contractions can be computed easily

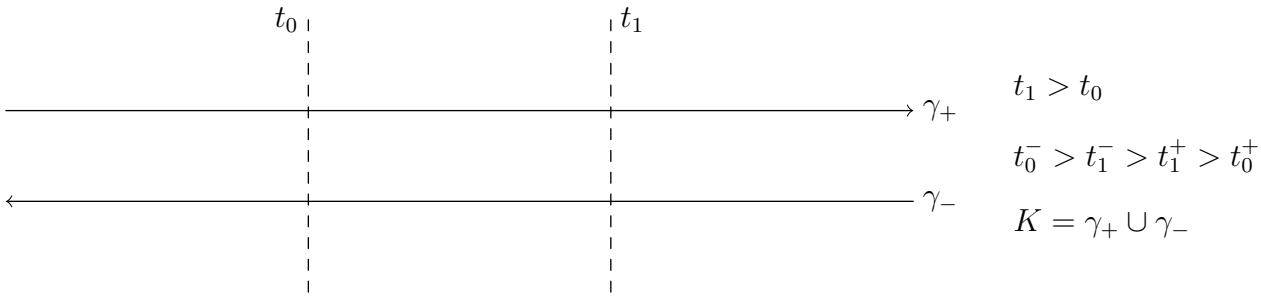

Figure 2.1.: The Keldysh time contour K, defined as the union of two oriented time axes γ_+ and γ_-. The $+$ branch goes forward in time whereas the $-$ branch goes backwards. Time ordering is explained by choosing two times t_0 and t_1.

one is left with

$$\psi_I(t) = \psi_I(t_0) - i \int_{t_0}^{t} \mathrm{d}t_1 H_{T,I}(t_1)\psi_I(t_1)\,, \tag{2.9}$$

which can be written recursively as

$$\psi_I(t) = S(t,t_0)\psi_I(t_0)\,, \tag{2.10}$$

where

$$S(t,t_0) = T\exp\left(-i\int_{t_0}^{t}\mathrm{d}t' H_{T,I}(t')\right)\,, \tag{2.11}$$

is the evolution operator and T the time ordering operator, which places operators at earlier times on the right. As a result, a Heisenberg operator can be written as

$$F_H(t) = S(t_0,t)F_I(t)S(t,t_0)\,. \tag{2.12}$$

The previous equation can conveniently be thought of as an evolution from t_0 to t and then back to t_0. This corresponds to a straight evolution on a time contour c, with two branches, the "plus" branch where time goes forward, and the "minus" branch where it goes backwards. Defining the c time ordering operator T_c which acts on operators at times defined by a branch index, the Heisenberg operators are written as

$$F(t) = T_c S_c(t_0^-, t_0^+)F_I(t)\,, \tag{2.13}$$

where the integral in the new time evolution operator S_c runs on the c time contour. It is underlined that the Heisenberg operators are now written fully in terms of operators in the interacting picture, i.e., which evolve like operators of the non-interacting theory. This solves the first problem in order to use Wick's theorem, it is reminded that the second problem cannot be solved without specifying the properties of the initial density matrix.

In Keldysh theory, it is traditionally argued that the interaction can be switched on adiabatically so that the initial density matrix is ρ_0. As a result, the possible initial correlations are removed by taking the initial time to $-\infty$ and assuming that what happens long in the past will not affect the present state of the system. This amounts to integrating over the Keldysh contour K, from $-\infty$ to $+\infty$ and then back to $-\infty$, which is represented in Fig. 2.1

Now that the essential assumptions allowing one to use Wick's theorem are stated, the actual product to compute can be analyzed.

In the case of products of operators found in the current operator, Eq. (2.5), the average value to compute

can be written as

$$\left\langle c_{i,H}(t)c^{\dagger}_{j,H}(t)\right\rangle = \left\langle T_K c_{i,I}(t^-)c^{\dagger}_{j,I}(t^+)\sum_{n=0}^{\infty}\frac{(-i)^n}{n!}\left[\prod_0^n\int_K \mathrm{d}t_n H_{T,I}(t_n)\right]\right\rangle_0 . \tag{2.14}$$

where the zero index on the average value means it is computed with the ρ_0 density matrix. Wick's theorem can be applied on the products of operators inside the average value on the right hand side of Eq. (2.14), it states that this product can be written as the sum of all possible contractions of two particle operators inside the product, with the right permutation coefficient. One could wonder what is the use of such contractions, in fact it is straightforward to show that the contraction of two single particle operators is equal to the average value of their product. An application of Wick's theorem can therefore be written as

$$\langle T(ABC\dots Z)\rangle = \langle T(AB)\rangle\langle T(CD)\rangle\dots\langle T(YZ)\rangle \pm \langle T(AC)\rangle\langle T(BD)\rangle\dots\langle T(YZ)\rangle \pm \dots . \tag{2.15}$$

A fundamental tool of out of equilibrium quantum field theory is the Keldysh Green's function

$$G^{\eta\eta'}_{ij}(t,t') = -i\left\langle T_K\left[c_{i,H}(t^\eta)c^{\dagger}_{j,H}(t^{\eta'})\right]\right\rangle , \tag{2.16}$$

where η are Keldysh time indices on the contour of Fig.2.1. With this definition, the correlator in Eq. (2.14) is $G^{-+}_{ij}(t,t)$. One notices that the product in Eq. (2.14) involves all the possible combinations of Keldysh and lead indices. A very important result, that was introduced in Keldysh's paper and that is derived in App. A.1, is that all these combinations can be written as a matrix product in Keldysh-lead space. In Keldysh space, the Green's functions read as

$$G_{ij}(t,t') = \begin{pmatrix} G^{++}_{ij}(t,t') & G^{-+}_{ij}(t,t') \\ G^{-+}_{ij}(t,t') & G^{--}_{ij}(t,t') \end{pmatrix} , \tag{2.17}$$

and in lead space, they read as

$$G^{\eta\eta'}(t,t') = \begin{pmatrix} G^{\eta\eta'}_{LL}(t,t') & G^{\eta\eta'}_{LR}(t,t') \\ G^{\eta\eta'}_{RL}(t,t') & G^{\eta\eta'}_{RR}(t,t') \end{pmatrix} . \tag{2.18}$$

Thus the Green's function is a tensor product of two 2×2 matrices, in Keldysh-lead space, which obeys a matrix Dyson equation,

$$G(t,t') = g(t,t') + \int_{\mathbb{R}^2}\mathrm{d}t_1\mathrm{d}t_2\, g(t,t_1)\Sigma(t_1,t_2)G(t_2,t) , \tag{2.19}$$

where $g(t,t')$ is the bare Green's function, computed without interactions, as opposed to $G(t,t')$, the dressed Green's function. $\Sigma(t,t')$ is the self energy, found by computing exactly the first order in λ of the correlator Eq. (2.14), as was done in Sec. A.1:

$$\Sigma^{\eta\eta'}_{LR}(t,t') = \left[\Sigma^{\eta\eta'}_{RL}\right]^*(t,t') = \delta(t-t')\lambda(t)\left[\sigma_z\right]_{\eta\eta'} \quad \text{and} \quad \Sigma^{\eta\eta'}_{LL}(t,t') = \Sigma^{\eta\eta'}_{RR}(t,t') = 0 , \tag{2.20}$$

A quick note about notations, some confusion might appear about the space in which the Green's function is considered. It can in fact be deduced by the indices present, for example $G^{+-}(t,t')$ is a 2×2 matrix in lead space and $G_{LR}(t,t')$ is a 2×2 matrix in Keldysh space. One therefore understands that Eq. (2.20) describes matrices in Keldysh space. Later on, this notation will be extended to spin indices $\uparrow$ or $\downarrow$ and to Fourier harmonics, with latin letters n, m, etc.

2.2. Frequency representation

This section explains how to switch to a description of the system in terms of energy rather than time. This is done for two reasons, first in the case of Fermi liquids or BCS superconductors, the properties of the system are traditionally easier to understand through an energy representation. Second, as periodic systems are considered, Floquet theory will be used as a guide for interpretations, and it takes place in energy space. The Green's functions are functions of two times, periodic in both times, with the same period T, and the following explains how to find their decomposition in Fourier series.

As shown in App. B, if $F(t,t')$ is T-periodic in both t and t', then it can be written as

$$F(t,t') = \sum_{nm} \int_{-\Omega/2}^{\Omega/2} \frac{\mathrm{d}\omega}{2\pi} e^{-i(\omega+n\Omega)t} e^{i(\omega+m\Omega)t'} F_{nm}(\omega)\,, \tag{2.21}$$

where $n, m \in \mathbb{N}$ and

$$F_{mn}(\omega) = \int_{-T/2}^{T/2} \frac{\mathrm{d}\bar{t}}{T} \int_{-\infty}^{\infty} \mathrm{d}\tau\, e^{i(\omega+n\Omega)(\bar{t}+\frac{\tau}{2})} e^{-i(\omega+m\Omega)(\bar{t}-\frac{\tau}{2})} F(\bar{t}+\tau/2, \bar{t}-\tau/2)\,. \tag{2.22}$$

Furthermore, the convolution product between two such functions is a matrix product in harmonics space. This is very convenient in order to solve Dyson's equations, indeed, Eq. (2.19) can immediately be written as

$$G_{nm} = g_{nm} + g_{nk}\Sigma_{kl}G_{lm}\,, \tag{2.23}$$

where summation over repeated indices is assumed and the frequency ω is not written for convenience.

The formulas to find $g(\omega)$ and $\Sigma(\omega)$ are derived in App. A, their Floquet counter parts are derived in App. B. For example, in the case of a normal metal

$$g^{\pm\mp}_{jj,nm}(\omega) = -i\left[\tanh\left(\frac{\omega + n\Omega - e(V_0)_j}{2\theta}\right) \mp 1\right]\delta_{nm}\,, \tag{2.24}$$

where $(V_0)_j$ is the DC voltage in lead j and θ is the temperature, assumed to be the same in both leads. The self energy can be written as

$$\Sigma^{\pm}_{RL,nm} = \lambda p_{n-m}\,, \tag{2.25}$$

where p_l are the Floquet amplitudes, defined by

$$\lambda(t) = \lambda \sum_l p_l e^{-il\Omega t}\,. \tag{2.26}$$

It is interesting to remark that the voltage drive and the gate drive are two different ways to drive the tunnel coupling. In the case of a voltage drive, only the phase of $\lambda(t)$ is time-dependent, i.e., $|\lambda(t)|^2 = \lambda^2$. Driving the coupling with a voltage drive therefore further constrains the Floquet coefficients, namely $\Sigma^{+-}_{LR}(t,t') = \left(\Sigma^{+-}_{RL}\right)^{\dagger}(t,t')$ is unitary, which translates as

$$\Sigma^{+-}_{LR}\Sigma^{+-}_{RL} = \lambda^2 \mathbb{1} \qquad \text{or} \qquad \sum_l p_{m-l}p^*_{n-l} = \delta_{nm}\,. \tag{2.27}$$

Only in this case a simple calculation of the current and the noise to all orders in the tunnel coupling can be performed[4]. From now on, unless specified by indices, the Green functions are written as a function of

[4] Of course, a numerical computation is always possible, even for a gate driven junction.

frequency, hence they are infinite matrices in harmonics space.

2.3. Summing Dyson's equations

One might notice that a relation links the four Green's functions of Eq. (2.16) in Keldysh space,

$$G^{--}(t,t') + G^{++}(t,t') = G^{-+}(t,t') + G^{+-}(t,t')\,. \tag{2.28}$$

This fact is exploited in App. A to provide a simpler Dyson equation. In particular, an alternative basis for Keldysh space, the RAK basis,

$$\begin{aligned} G^r &= G^{++} - G^{+-} \\ G^a &= G^{++} - G^{-+} \\ G^K &= G^{++} + G^{--}\,, \end{aligned} \tag{2.29}$$

is introduced to reduce the number of Green's functions to three (using one of the two relations mentioned above). This basis is useful as Green's function now obey Dyson's equations at the matrix element level, i.e.,

$$\begin{aligned} G^a &= g^a + g^a\Sigma^a G^a \\ G^r &= g^r + g^r\Sigma^r G^r \\ G^K &= g^K + g^r\Sigma^r G^K + g^K\Sigma^a G^a + g^r\Sigma^K G^a\,. \end{aligned} \tag{2.30}$$

This allows to derive a few relations between the Green's functions in the PM basis and the RAK basis, the most important one can take two forms, Dyson I and Dyson II, respectively

$$\begin{aligned} G^{\pm\mp} &= g^{\pm\mp} - g^r\Sigma^{\pm\mp}G^a + g^r\Sigma^r G^{\pm\mp} + g^{\pm\mp}\Sigma^a G^a \\ G^{\pm\mp} &= (\mathbb{1} + g^r\Sigma^r)g^{\pm\mp}(\mathbb{1} + \Sigma^a G^a) - G^r\Sigma^{\pm\mp}G^a\,. \end{aligned} \tag{2.31}$$

This is enough to find a formula for the dressed Green's functions, in lead space for a two lead junction, in terms of the bare ones and the self energies only. This computation is performed in App. A and yields

$$G^{+-}_{RL} = (\mathbb{1} - g^r_{RR}\Sigma^r_{RL}g^r_{LL}\Sigma^r_{LR})^{-1}\left[g^{+-}_{RR} + g^r_{RR}\Sigma^r_{RL}g^{+-}_{LL}(\Sigma^a_{RL}g^a_{LL})^{-1}\right](\mathbb{1} - \Sigma^a_{RL}g^a_{LL}\Sigma^a_{LR}g^a_{RR})^{-1}\Sigma^a_{RL}g^a_{LL}\,. \tag{2.32}$$

A derivation of the bare Green's functions is also provided in App. A. The advantage of frequency representation is that all orders in λ can be obtained by matrix inversion in the case of a voltage drive.

Floquet channels are represented by elements of the Green's functions in Harmonics space and as can be seen in Eq. (2.32), these elements are multiplied with each other between different channels. Therefore, the interactions or correlations between the "pre-Floquet" states, which are encoded in the Green functions, are now present between Floquet states. This means that, in correlated systems, there will be correlations between Floquet states, and, in normal metals, Floquet channels are expected to behave independently of one another.

2.4. Conclusion

This chapter introduced the main technical details used in this work. First the link between Green's functions and average values of observables. Then the complications due to non-equilibrium, which complicates the use of Wick's theorem, and the standard way to overcome them, Keldysh theory. Using the insights from Floquet theory, it is chosen to write the average values in energy representation, in terms of bare Green's functions and Fourier coefficients of the time-dependent tunnel coupling.

Despite the fact that it was a technical chapter, most of the complications were explicitly mentioned and the equations were written consistently, for two main reasons. First to show how versatile this formalism is, temperature and out of equilibrium effects are automatically included. And second, it was considered that these technicalities bear physical meaning. For example, Dyson's equation makes clear the fact that the full behavior of the observables are the sum of all the most simple processes induced by the coupling term of the Hamiltonian. Also, it was possible to see that Floquet states actually act as states of the original system. Therefore on could guess that, in correlated systems, there might be correlations between Floquet states. From this formalism, actual computations of physical observables can be performed in many situations. This will be dealt with in the following chapters.

3. Transport quantities in normal metal junctions

3.1. Introduction

In this chapter, all the formalism and physical ideas developed in the previous chapters are applied to the simplest possible junction, the $N-N$ junction driven by a periodic voltage drive. This allows to draw the contours of the paradigm of the linear junction, in particular, how do the specificities of Leviton physics, which will be introduced, manifest themselves in the noise. Here and there, the possible problems encountered when generalizing these properties to non-linear junctions, typical of correlated systems, are discussed.

A formula for the current is derived in Sec. 3.2, thus making the link with Landauer's picture. Then, in Sec. 3.3, the noise is computed, its structure encourages the next sections. Indeed, Sec. 3.4 explains the link between transport and Floquet theory through the Tien-Gordon picture. Then the difference between the different drive shapes is discussed in Sec. 3.5, in particular, the specificities of Lorentzian pulses are explained, by introducing the so-called minimal excitation state.

3.2. The current

In this section, the tools presented above are used to derive a formula for the current as a function of time, from Eq. (2.5) and Eq. (2.16), it reads as

$$\begin{aligned}\langle I_L\rangle(t) &= -ie\left[\lambda^*(t)\left\langle T_K c^\dagger_{L,H}(t^-)c_{R,H}(t^+)\right\rangle - \lambda(t)\left\langle T_K c^\dagger_{R,H}(t^-)c_{L,H}(t^+)\right\rangle\right]\\ &= e\left[\lambda^*(t)G^{+-}_{RL}(t,t) - \lambda(t)G^{+-}_{LR}(t,t)\right]\,.\end{aligned} \tag{3.1}$$

App. B presents a way to obtain the Fourier series representation:

$$\langle I_L\rangle(t) = e\lambda\sum_{km} e^{-i(k-m)\Omega t}\int_{-\Omega/2}^{\Omega/2}\frac{\mathrm{d}\omega}{2\pi}\left[\mathcal{P}G^{+-}_{RL} - \mathcal{P}^\dagger G^{+-}_{LR}\right]_{km}\,, \tag{3.2}$$

were the trace is over harmonics and

$$\Sigma^r_{LR} = \lambda\mathcal{P}\,. \tag{3.3}$$

The first step is therefore to insert the Green's functions in Eq. (2.32), $g^{r/a}_{L/R} = \mp i\mathbb{1}$, therefore,

$$G^{+-}_{RL} = i\lambda(\mathbb{1}+\lambda^2\mathcal{P}\mathcal{P}^\dagger)^{-1}\left[g^{+-}_{RR} - \mathcal{P}^\dagger g^{+-}_{LL}(\mathcal{P}^\dagger)^{-1}\right](\mathbb{1}+\lambda^2\mathcal{P}\mathcal{P}^\dagger)^{-1}\mathcal{P}^\dagger\,. \tag{3.4}$$

On has to compute the matrix inverse $(\mathbb{1}+\lambda^2\mathcal{P}\mathcal{P}^\dagger)^{-1}$ in order to make progress in an analytical computation. As said earlier, this can be done independently of the drive shape *only in the case of a voltage drive*, in this case

$$(\mathbb{1}+\lambda^2\mathcal{P}\mathcal{P}^\dagger)^{-1} = \frac{1}{1+\lambda^2}\mathbb{1}\,. \tag{3.5}$$

Therefore

$$G_{RL}^{+-} = i\frac{\lambda}{(1+\lambda^2)^2}\left[g_{RR}^{+-}\mathcal{P}^\dagger - \mathcal{P}^\dagger g_{LL}^{+-}\right], \tag{3.6}$$

which can be inserted in Eq. (3.2), yielding

$$\begin{aligned}\langle I_L\rangle(t) = \frac{ie\lambda^2}{(1+\lambda^2)^2}\sum_{klmn} e^{-i(k-m)\Omega t}\int_{-\Omega/2}^{\Omega/2}\frac{\mathrm{d}\omega}{2\pi}\Big[&p_{l-k}^* g_{RR,ln}^{+-} p_{n-m} - p_{l-k}^* p_{l-n} g_{LL,nm}^{+-} \\ &- p_{k-l} g_{LL,ln}^{+-} p_{m-n}^* + p_{k-l} p_{n-l}^* g_{RR,nm}^{+-}\Big].\end{aligned} \tag{3.7}$$

Inserting Eq. (2.24), one finds

$$\begin{aligned}\langle I_L\rangle(t) = \frac{e\lambda^2}{(1+\lambda^2)^2}\sum_{knm} e^{-i(k-m)\Omega t}\int_{-\Omega/2}^{\Omega/2}\frac{\mathrm{d}\omega}{2\pi}\Bigg\{&p_{n-k}^* p_{n-m}^*\left[\tanh\left(\frac{\omega+n\Omega}{2\theta}\right) - \tanh\left(\frac{\omega+m\Omega-eV_0}{2\theta}\right)\right] \\ &- p_{k-n}p_{m-n}^*\left[\tanh\left(\frac{\omega+n\Omega-eV_0}{2\theta}\right) - \tanh\left(\frac{\omega+m\Omega}{2\theta}\right)\right]\Bigg\}.\end{aligned} \tag{3.8}$$

It is useful to remark that the second line is the complex conjugate of the first one[1]. Before performing the integration, one can rename indices $m-n\to m$ and $k-n\to k$ and integration variable $\omega+n\Omega\to\omega$, it allows to isolate n in the integration boundaries, then the sum over n can be performed and one is left with

$$\langle I_L\rangle(t) = \frac{e\lambda^2}{(1+\lambda^2)^2}2\,\mathrm{Re}\sum_{km} e^{-i(k-m)\Omega t}\int_{\mathbb{R}}\frac{\mathrm{d}\omega}{2\pi}\,p_{-k}p_{-m}^*\left[\tanh\left(\frac{\omega}{2\theta}\right) - \tanh\left(\frac{\omega+m\Omega-eV_0}{2\theta}\right)\right], \tag{3.9}$$

This integration can easily be performed and yields

$$\langle I_L\rangle(t) = \frac{e}{\pi}\frac{2\lambda^2}{(1+\lambda^2)^2}\,\mathrm{Re}\sum_{km} e^{-i(k-m)\Omega t}p_{-k}p_{-m}^*(-m\Omega+eV_0). \tag{3.10}$$

Taking the derivative of $e^{-i\phi(t)}$ one can show that

$$\sum_m m p_m e^{-im\Omega t} = \frac{e}{\Omega}V_{AC}(t)e^{-i\phi(t)}. \tag{3.11}$$

As a result, the current can be written as

$$\langle I_L\rangle(t) = \frac{e^2}{\pi}\frac{2\lambda^2}{(1+\lambda^2)^2}V(t). \tag{3.12}$$

This is the reason why such a junction is called a linear junction, the current is directly proportional to the voltage. One remarks that in the case of a DC voltage, Landauer's formula, which holds for a spinful metal, can be retrieved by multiplying by two. This allows to find a formula for the transmission

$$\tau = \frac{4\lambda^2}{(1+\lambda^2)^2}. \tag{3.13}$$

[1]This can be realized by changing indices in the second line to $\tilde{n}=m$ and $\tilde{m}=n$ and $\tilde{k}=n+m+k$.

One can also compute the charge transmitted per period as

$$\langle Q_L \rangle = \int_{-T/2}^{T/2} \mathrm{d}t \, \langle I_L(t) \rangle = eq\tau/2 \,, \tag{3.14}$$

where $q = eV_0/\Omega$ is the charge injected per period, indeed, when the transmission is perfect, no charge is reflected and the charge transmitted is the same as the charge injected.

A comment can be raised about the transmission factor, the perturbative approach developed to find it makes explicit the fact that it comes from the repeated transfer of electrons from one side to the other. Indeed, a non-vanishing current involves an electron leaving the left electrode to end up on the right, this can be achieved with an infinite number of different processes (all the terms of Dyson's equations), from the single transfer to any number of intermediate reflections. The amplitude of the sum of all such processes looks like

$$\lambda - \lambda^3 + \lambda^5 - \cdots = \frac{\lambda}{1+\lambda^2} \,, \tag{3.15}$$

so its probability is just τ.

3.3. The noise

The noise is defined in Eq. (1.3), when the drive is periodic, the integration over t runs over one period only. As a result, the average of the noise over one period of time corresponds to the zero frequency noise,

$$\begin{aligned} S_{LL}(\omega=0) = -e^2 \int_{-T/2}^{T/2} \mathrm{d}t \int_{-\infty}^{\infty} \mathrm{d}\tau \Big[& \lambda^*(t)\lambda^*(t+\tau) \left\langle c_L^\dagger(t) c_R(t) c_L^\dagger(t+\tau) c_R(t+\tau) \right\rangle \\ & -\lambda(t)^*\lambda(t+\tau) \left\langle c_L^\dagger(t) c_R(t) c_R^\dagger(t+\tau) c_L(t+\tau) \right\rangle \\ & +\lambda(t)\lambda(t+\tau) \left\langle c_R^\dagger(t) c_L(t) c_R^\dagger(t+\tau) c_L(t+\tau) \right\rangle \\ & -\lambda(t)\lambda^*(t+\tau) \left\langle c_R^\dagger(t) c_L(t) c_L^\dagger(t+\tau) c_R(t+\tau) \right\rangle \\ & -\lambda^*(t)\lambda^*(t+\tau) \left\langle c_L^\dagger(t) c_R(t) \right\rangle \left\langle c_L^\dagger(t+\tau) c_R(t+\tau) \right\rangle \\ & +\lambda^*(t)\lambda(t+\tau) \left\langle c_L^\dagger(t) c_R(t) \right\rangle \left\langle c_R^\dagger(t+\tau) c_L(t+\tau) \right\rangle \\ & -\lambda(t)\lambda(t+\tau) \left\langle c_R^\dagger(t) c_L(t) \right\rangle \left\langle c_R^\dagger(t+\tau) c_L(t+\tau) \right\rangle \\ & +\lambda(t)\lambda^*(t+\tau) \left\langle c_R^\dagger(t) c_L(t) \right\rangle \left\langle c_L^\dagger(t+\tau) c_R(t+\tau) \right\rangle \Big] \,. \end{aligned} \tag{3.16}$$

Wick's theorem can be used on the first four lines, one sees that only two combinations of operators are available, one corresponds to the last four lines, which therefore cancel out, the remaining pairings yield

$$\begin{aligned} S_{LL} = -e^2 \int_{-\infty}^{\infty} \mathrm{d}\tau \int_{-T/2}^{T/2} \mathrm{d}t \Big\{ & \lambda^*(t) G_{RL}^{-+}(t,t+\tau) \lambda^*(t+\tau) G_{RL}^{+-}(t+\tau,t) \\ & -\lambda^*(t) G_{LL}^{-+}(t,t+\tau) \lambda(t+\tau) G_{RR}^{+-}(t+\tau,t) \\ & +\lambda(t) G_{LR}^{-+}(t,t+\tau) \lambda(t+\tau) G_{LR}^{+-}(t+\tau,t) \\ & -\lambda(t) G_{RR}^{-+}(t,t+\tau) \lambda^*(t+\tau) G_{LL}^{+-}(t+\tau,t) \Big\} \,. \end{aligned} \tag{3.17}$$

Following the steps performed for the current, the noise is written in frequency space, the details as to how to perform the Fourier transform are presented in App. B and yield

$$S_{LL} = -e^2\lambda^2 \int_{-\Omega/2}^{\Omega/2} \frac{\mathrm{d}\omega}{2\pi} \mathrm{Tr_H}\Big\{\mathcal{P}G^{-+}_{RL}\mathcal{P}G^{+-}_{RL} - \mathcal{P}^\dagger G^{-+}_{LL}\mathcal{P}G^{+-}_{RR} + \mathcal{P}^\dagger G^{-+}_{LR}\mathcal{P}^\dagger G^{+-}_{LR} - \mathcal{P}G^{-+}_{RR}\mathcal{P}^\dagger G^{+-}_{LL}\Big\}, \tag{3.18}$$

where $\mathrm{Tr_H}$ is the trace in harmonics (or Fourier) space. From this result, the computation looks similar to that of the current, but are a bit more tedious, hence it is presented in App. C, it yields

$$S_{LL} = \frac{e^2}{2\pi}\left[2\tau^2\theta + \tau(1-\tau)\sum_l (l\Omega + eV_0)|p_l|^2 \coth\left(\frac{l\Omega + eV_0}{2\theta}\right)\right]. \tag{3.19}$$

The noise is made up of two terms, first the Nyquist noise, or thermal noise, proportional to the temperature and to the transmission squared. The second part of the noise is the shot noise, it can be rewritten in a Tien-Gordon fashion, see Sec. 3.4,

$$S_{LL,\mathrm{shot}} = \frac{e^2}{2\pi}\tau(1-\tau)\sum_l P_l S^{\mathrm{shot}}_{LL,DC}(V_0 + l\Omega/e), \tag{3.20}$$

where $P_l = |p_l|^2$, and the shot noise for a DC drive is

$$S_{LL,DC,\mathrm{shot}}(V_0) = \frac{e^2}{2\pi}\tau(1-\tau)eV_0 \coth\left(\frac{eV_0}{2\theta}\right). \tag{3.21}$$

The low temperature limit of the shot noise, $eV_0 \gg \theta$, reads as

$$S_{LL,DC,\mathrm{shot}}(V_0 \gg \theta) = \frac{e^2}{2\pi}\tau(1-\tau)|eV_0|, \tag{3.22}$$

agrees with the claims made in the introduction of this chapter that the current is a binomial process. Indeed the second moment of a binomial distribution is equal to the rate of success, τ time the failure rate $1-\tau$ time the number of trials $\propto V$.

The zero temperature AC noise can be written as

$$S_{LL} = \frac{e^2\Omega}{2\pi}\tau(1-\tau)\sum_l |q+l|P_l, \tag{3.23}$$

where $q = eV_0/\Omega$, is the injected charge. Considering only positive values of q (the noise is symmetric around zero voltage), the sum can be separated in two parts

$$S_{LL} = \frac{e^2\Omega}{2\pi}\tau(1-\tau)\left[\sum_{l\geq -q}(q+l)P_l - \sum_{l<-q}(q+l)P_l\right]. \tag{3.24}$$

Considering only cases where $q > 0$ for simplicity, the first sum can be completed to correspond to the DC noise, by adding the negative channels contributions, i.e.,

$$S_{LL} = S_{LL,DC} - 2\frac{e^2\Omega}{2\pi}\tau(1-\tau)\sum_{l<-q}(q+l)P_l. \tag{3.25}$$

This means that the AC noise differs from the DC one only because of the channels corresponding to energies smaller than eV_0 (i.e. $l < -q$), this is directly probed by the so-called excess noise

$$S_{\text{exc}} = S_{LL,AC+DC} - S_{LL,DC} = \sum_{l<-q} P_l S_{LL,DC}(V_0 + l\Omega/e)\,. \tag{3.26}$$

Hence, the only contributions to the excess noise come from holes-like channels created by the drive. In fact, it can be shown [106], that the noise is proportional to the average number of excitations created by the drive, i.e., the average number of electrons plus the average number of holes. From its definition (3.26), the excess noise is the sum of the noise contribution of the hole channels, one could therefore argue that the excess noise is proportional to the number of holes created by the drive. Following this line of thought, the possibility to minimize this number of excitations so as to create a "minimal excitation state" was also discussed in ref. [106]. The case $V = 0$ is obviously the global minimal excitation states but it is not interesting. From Eq. 3.26, one sees that the excess noise cannot be negative, hence it provides a good signature of minimal excitation states. A minimal excitation state can only occur if $P_l = 0$ for any $l < -q$, i.e., if

$$p_l = \int \mathrm{d}t\, \lambda^*(t) e^{-il\Omega t} = 0 \qquad \text{for any} \qquad l < -q\,. \tag{3.27}$$

This is equivalent to saying that the function $\lambda^*(t)$ is a complex function without poles in the lower half plane. Furthermore, in the case of a voltage drive, the module of $\lambda^*(t)$ has to be unity. Such a function can always be written as a products of such functions

$$\lambda_1^*(t) = \frac{t + iW}{t - iW}\,, \tag{3.28}$$

with different W and possibly shifted t. This function can be written as the result of a phase

$$\frac{t + iW}{t - iW} = e^{-i\phi(t)} \qquad \text{with} \qquad \phi(t) = \arctan\left(\frac{t}{W}\right)\,, \tag{3.29}$$

and this phase corresponds to a particular voltage drive as

$$\phi(t) = \frac{1}{W}\int_{-\infty}^{t} \mathrm{d}t\, \frac{1}{1 + t^2/W^2}\,, \tag{3.30}$$

i.e., to a Lorentzian pulse

$$V(t) = \frac{V_0 T}{W}\frac{1}{1 + (t/W)^2}\,, \tag{3.31}$$

with quantized charge $eV_0T = 1$, where T is any time scale. As a matter of fact, Levitov and Lee [22] first derived the formula for $\phi(t)$ from various considerations, and then they found that this corresponds to a Lorentzian drive. From the structure of Eq. (3.28), any combination of $\lambda_1^*(t)$ leads to a minimal excess noise, i.e., any superposition and shift of quantized Lorentzian pulses creates a minimal excitation state. Hence, in the context of Floquet theory, one can design a periodic drive by promoting the time scale T to the period as

$$V(t) = \sum_k V_0 \frac{\eta}{\eta^2 + (t/T - k)^2}\,, \tag{3.32}$$

where $\eta = W/T$ the width to period ratio. This drive was subsequently called Levitons when $eV_0/\Omega \in \mathbb{N}$ as it only excites electrons above the Fermi sea. This interpretation can get some more footing in the context of the Tien-Gordon picture, described in the next section.

3.4. Tien-Gordon picture

As was already hinted in the previous section, there exists a strong connection between the transport properties of the $N-N$ junction biased simultaneously by DC and AC voltages, and that of the same device in the absence of AC modulation. Such a connection was first unveiled by Tien and Gordon [19] when studying the tunneling current in superconducting diodes biased by a sinusoidal drive of frequency Ω. In this context, they could show that

$$I_{AC+DC}\left(V_0\right) = \sum_l P_l^2 I_0\left(V_0 + l\frac{\Omega}{e}\right), \tag{3.33}$$

so that the current in the presence of a drive $V(t) = V_0 + V_1\sin(\Omega t)$ is a weighted sum of voltage-shifted DC currents (with a shift quantized in the driving frequency), with coefficients which are directly related to the AC power (it is recalled that P_l is a function of the AC power).

This result can actually be readily understood within Floquet theory. Indeed, as argued in Sec. 1.4, the voltage biased normal lead can be described as a set of Floquet channels, i.e., a superposition of Fermi seas shifted in energy with a weight given by the probability of absorbing or emitting a certain number of photons. As a result, from Eq. (3.33), it can be guessed that the fraction of occupied states at a given energy in the metal is no longer given by the standard Fermi distribution but instead by the following weighted sum:

$$\tilde{f}(E) = \sum_{l=-\infty}^{\infty} P_l f(E - eV_{\mathrm{DC}} - l\Omega), \tag{3.34}$$

corresponding to the situation depicted in Fig. 3.1. Invoking scattering theory, one can then argue that the current only involves a linear combination of the leads distribution function, so that in the presence of an AC drive, the current reduces to the sum of the DC contributions arising from all Floquet channels n, with the corresponding probability P_n.

In the case of the $N-N$ junction, the average DC current is linear, i.e., $\langle I\rangle \propto V_0$, therefore, the Tien-Gordon relation reads as

$$\langle I_L\rangle = \sum_l P_l V_0 + \sum_l l P_l, \tag{3.35}$$

and when the junction is driven by a voltage, $|\lambda(t)| = \lambda$, hence

$$\sum_l P_l = 1 \qquad \text{and} \qquad \sum_l l P_l = 0. \tag{3.36}$$

This implies that the Tien-Gordon relation is transparent, i.e., $\langle I_{L,AC+DC}\rangle = \langle I_{L,DC}\rangle$.

For the noise however, see Eq. (3.26), the AC noise is not linear so no compensation between the positive and negative channels is possible. In fact the noise is only impacted by the contribution of the negative channels, which can make it a remarkable tool to investigate the detailed properties of transport at the junction. Before going further in analyzing the excess noise, it is useful to investigate on the structure of the different $|p_l|$.

3.5. Different drive shapes

These Floquet weights are functions of the channel index as well as the injected charge q, but also functional of the voltage shape. A great variety of drives were explored by Vanevic *et al.* [107] while here only three of them are treated: the sinusoidal, square and Lorentzian ones as they display the three most different

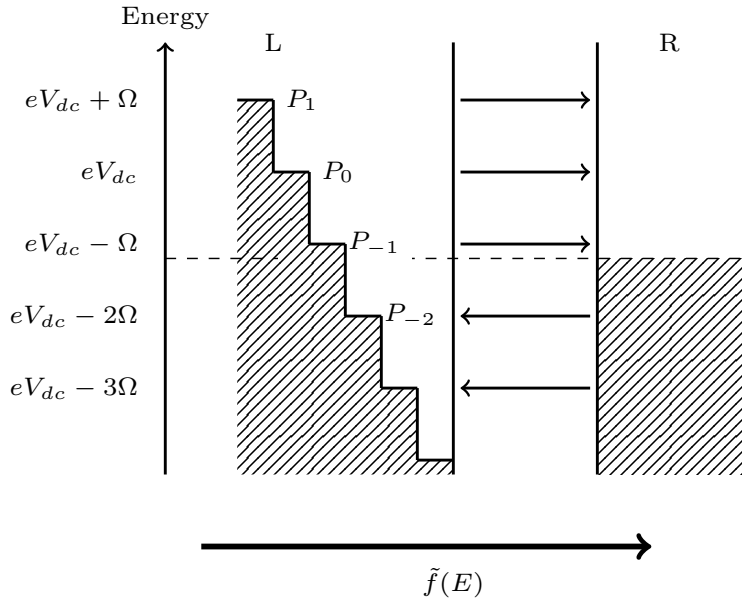

Figure 3.1.: Schematic representation of tunneling events at the $N-N$ junction. Each channel, involving a Fermi sea at level $eV_0+n\Omega$, contributes with a weight P_n in the current, and is represented by a step in the figure. The arrows represent the direction of the electron current. The horizontal axis represents $\tilde{f}(E)$ which is defined in Eq. 3.34.

behaviors. The simplest possible drive shape is a sinusoidal one, in this case the voltage reads as

$$V(t) = V_0(1-\cos\Omega t)\,. \tag{3.37}$$

and yields a Floquet channel amplitude

$$p_l = J_l(-q)\,, \tag{3.38}$$

J_l being the l^{th} Bessel functions of the first kind. This has two main consequences, first the coefficients, p_l are real, which might have an impact on transport when it involves interferences between channels, and second $p_l = p_{-l}$, which means that channels below and above the Fermi sea are symmetric. The sinusoidal time-dependent drive excites electrons and holes in the same manner[2].

The second type of drive considered is that the square drive of half-period width, the voltage is defined as

$$V(t) = V_0\left[1+\operatorname{sgn}\left(\cos\Omega t\right)\right]\,. \tag{3.39}$$

And the associated coefficients are

$$p_l = \frac{2}{\pi}\frac{q}{l^2-q^2}\sin\left[\frac{\pi}{2}(l-q)\right]\,. \tag{3.40}$$

One remarks that they are real and that $p_l = (-1)^l p_{-l}$ so the drive does not affect hole and electrons in the same way, there is a $l\pi$ phase difference in the amplitude of odd channels. This will not affect transport in the $N-N$ junction as only the weights P_l and not the amplitude p_l appears[3].

[2]Remember that there is always a constant voltage V_0 so the Fermi sea is filled up to energy eV_0.

[3]This is equivalent to saying that there is no interferences between different channels. As will be seen, it is not the case anymore when there are interactions or correlations in the leads.

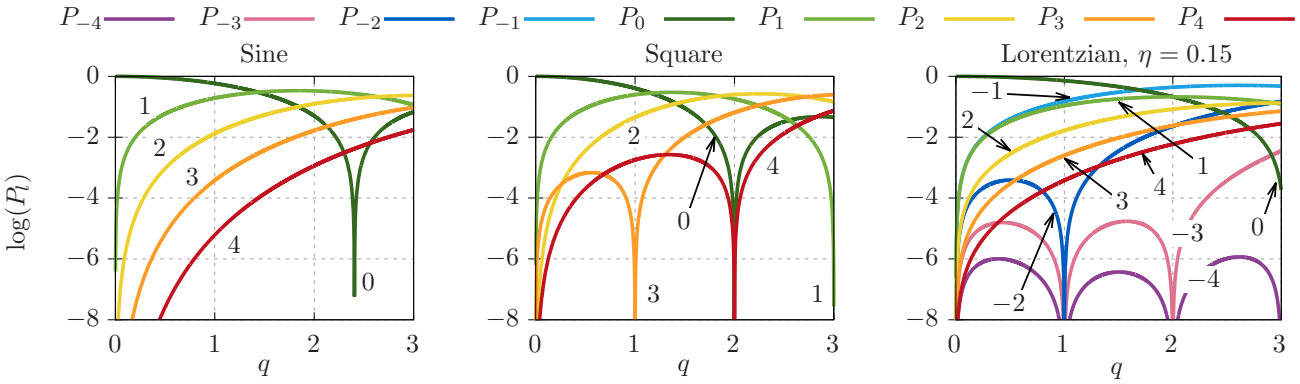

Figure 3.2.: The logarithm of the Floquet weights of the first few channels, as a function of the injected charge per period q, for the three different drives, cosine, square and Lorentzian train of pulses (with $\eta = 0.15$). The index of the coefficient corresponding to each curve is written on the graph. Note that $P_{-l} = P_l$ for the cosine and square drives.

Finally, the most interesting drive, the train of Lorentzian pulses is defined by

$$V(t) = eV_0 \sum_k \frac{1}{1 + \left(\frac{t-kT}{\eta}\right)^2} \,. \tag{3.41}$$

with $\eta = W/T = W\Omega/2\pi$ the ratio between the width of the pulses and the period of the drive. This leads to a Fourier coefficient [52]

$$p_l = \int_{-1/2}^{1/2} \mathrm{d}u \, e^{2i\pi(l+q)u} \left(\frac{\sin[\pi(i\eta + u)]}{\sin[\pi(i\eta - u)]}\right)^q , \tag{3.42}$$

There is no obvious link between p_l and p_{-l} which means that this drive treats electrons and holes differently.

To get more insights on the properties of these drives, the logarithms of the P_l are represented in Fig. 3.2 for the first few values of the index l and the various drives considered. First, for small values of q, only the Floquet weights with the lowest $|l|$ contribute as small q means low eV_0 and a crude image is that the electric field does not have a lot of energy to share as photons, thus one does not expect a high probability to exchange a large number of photons. When q is increased, the higher values of $|l|$ start to have a non-negligible contribution. For all the drives, one remarks that there are some parameters for which P_l vanishes. In the case of a cosine drive (left panel of Fig. 3.2), this corresponds to the zeros of the Bessel functions of the first kind. For the square drive (middle panel of Fig. 3.2), the Floquet weights vanish for $l - q = 2n$ with n integer. Also, as mentioned above, electrons and holes are symmetrically excited only for the square and cosine drives. As a matter of fact, for the Lorentzian pulses (right panel of Fig. 3.2), the Floquet weights vanish for integer values of q such that $q < -l$, i.e., the drive only excites electrons with energies above the Fermi sea.

The different properties of these drives have an impact on the shape of the noise. As was shown above, the excess noise constitutes an interesting tool to measure the effect of the AC drive as it gives a measure of the number of holes excited by the drive.

The excess noise is plotted for different types of drives, a cosine one, a square one and the Lorentzian pulses in Fig. 3.3. The left plot corresponds to low temperature $\theta = 0.01\Omega$. One sees that as q increases, there are successive crossings of the zero energy singularity of the noise for values $q + l = 0$, corresponding

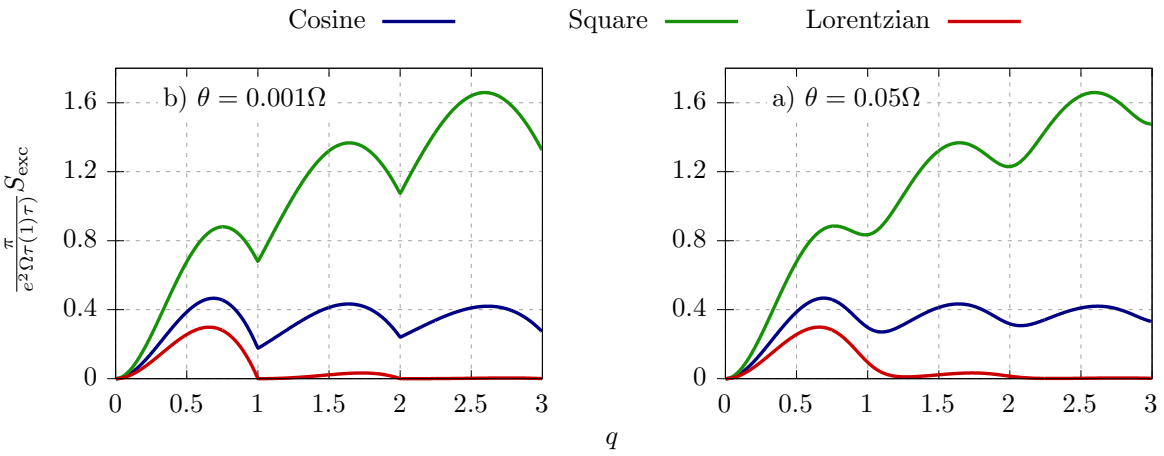

Figure 3.3.: The excess noise as a function of the injected charge for different drives. The green curves correspond to a cosine drive, the green ones to a square drive and the red ones to the train of Lorentzian pulses of width $\eta = 0.15$. Left panel for low temperature, $\theta = 0.001$. Right panel for higher temperatures $\theta = 0.05$.

to the point where the $l^{\rm th}$ channel is at zero energy. This is the reason for the global arch-shapes common to all types of voltages. The main feature of this figure is that the excess noise created by Lorentzian pulses vanishes for integer values of q. As explained above, this is due to the fact that for such a drive, called Leviton, $P_l = 0$ for $l < -q$, hence Eq. (3.26) vanishes, and the drive indeed creates a "minimal excitation state". The right plot of Fig. 3.3 represents the excess noise for higher temperature $\Theta = 0.1\Omega$, the main difference is, as anticipated, a smoothing of the features of the low temperature noise. Another difference is that the minima of excess noise do not correspond to integer values of q (channels crossing zero energy), but to higher, non integer values. The excess noise minimization due to Levitons was observed in [23] at finite temperature. It is to be noted that a Hong-Ou-Mandel experiment, typical of quantum optics, was realized with Levitons in the same paper.

3.6. Conclusion

In this chapter, the current and the noise in the AC-driven $N - N$ junction were computed using the techniques developed in the previous chapters. This allowed to interpret the results and make a link with the general theory of quantum transport of Sec. 1.2 and with Floquet theory as presented in Sec. 1.4.

It was found that the current is proportional to the applied voltage and to the transmission, which was written in terms of the tunnel coupling. On the other hand, the noise displays more interesting properties, indeed it is a sum of equivalent DC noise through the so-called Floquet channels. It was pointed out that this interpretation is very close to that proposed by Tien and Gordon [19] where such channels were discussed. These channels correspond to the Fourier harmonics of the tunnel coupling, this fact allows for a simple derivation of the possible drives leading to electric channels only. Such a drive is made of any combination of quantized Lorentzian pulses called Levitons.[4]. As a result, transport should only involve electrons above the Fermi sea and the excess noise provides a measure of the accuracy of this picture. In particular it was shown that the excess noise only contains contributions from hole channels, it therefore vanishes for perfect Levitons.

[4]This is because they are also seen as states levitating above the Fermi sea and were invented by Levitov.

The excess noise can therefore be used as a probe for experiments involving precise manipulation of single electrons, e.g., collisions, transport of information, interference etc. As a side note, one could remark that this is very similar to what is done in quantum optics with photons, this field could therefore be called quantum electronics. However, usage has preferred electron quantum optics (EQO)[5] and the current chapter can be seen as an introduction to this field in non correlated matter (Fermi liquid regime).

As a quick perspective, the conditions under which electron quantum optics can be performed in $N-N$ junctions are, zero temperature limit (linear noise), Leviton-driven junction (only electronic excitations), Tien-Gordon relation for the noise, i.e., independent Floquet channels (uncorrelated material). The next chapters will describe how these conditions can be relaxed or adapted when considering other types of junctions, involving new physical phenomena, and how can EQO help characterize these phenomena or even how these phenomena can help in designing new EQO schemes.

[5] It would be interesting to propose to rename quantum optics into photon quantum electronics.

Part II.

QPC between normal leads and BCS superconductors

4. Introduction to BCS superconductivity

4.1. Introduction

In this chapter, the basics of BCS superconductivity are recalled in order to make the text self-contained.

Sec. 4.2 starts with a derivation of the interacting Hamiltonian between electrons and phonons, which is at the root of superconductivity. Then it will be shown that this leads to an effective attractive interaction between electrons. In Sec. 4.3, a short description of Cooper's instability as a result of any attractive interaction is provided. This result gives hints towards the BCS ground state ansatz, which is quickly formulated afterwards. Finally, in Sec. 4.4, the quasiparticle excitations are described as well as their spectrum and the BCS coherence factors are derived.

4.2. Electron-electron interaction through phonons

The derivation proposed here is inspired from [108]. Phonons are vibrations of the lattice, i.e., displacements of the basic ions, this amounts to the presence of a charge density that is not due to electrons, $\rho_p(r)$. The electrons interact with this charge density simply with a Hamiltonian

$$H_{e-p} = -e^2 \int \mathrm{d}r\mathrm{d}r' \, \rho_e(r) K(r-r') \rho_p(r') \,, \tag{4.1}$$

where K is an interaction kernel, Coulomb-like, i.e., proportional to the inverse square of the distance. As in metals, the long range interaction between charges is typically screened, the most rough approximation that can be made is that

$$K(r) = \delta(r) a^{-2} \,, \tag{4.2}$$

where a is the lattice constant. As is known from electromagnetism, a local charge density can be understood as the creation of a dipole, i.e., a displacement of two opposite charges. It is therefore characterized by a displacement vector $q(r)$ and a charge Ze. The charge density is equal to the charge times the divergence of the displacement vector. The interaction Hamiltonian can therefore be written as

$$H_{e-p} = -Ze^2 a^2 \int \mathrm{d}r \, \rho_e(r) \mathrm{div}\left[q(r)\right] \,, \tag{4.3}$$

this Hamiltonian can be quantized by choosing the displacement of the lattice points $q_i(r)$ as the generalized coordinates and $\rho_l \dot{q}_i$ as the generalized momentum, with ρ_l the density of the lattice. They obey the following commutation relation

$$\rho_l \left[\dot{q}_i(r,t), q_j(r,t)\right] = -i\delta(r-r')\delta_{ij} \,. \tag{4.4}$$

As argued in [109], the metal can be considered as a box of volume V, thus, as the lattice is a periodic structure, the generalized coordinates can be expanded as Fourier series,

$$q_i(r,t) = \frac{1}{\sqrt{V}} \sum_k \frac{k}{|k|} \left(q_k e^{i(kx-\omega_k t)} + q_k^\dagger e^{-i(kx-\omega_k t)} \right) \,, \tag{4.5}$$

where it was enforced that only longitudinal phonons are of interest in the Hamiltonian. It can be shown that the above commutation relation implies that

$$\rho \sum_k 2i\omega_k \left[q_k^\dagger, q_k\right] = -i\,. \tag{4.6}$$

Thus, new boson fields

$$b_k = \sqrt{2\rho\omega_k} q_k\,, \tag{4.7}$$

that have no dimension and are real valued, can be introduced. The divergence of the displacement operator can be computed, it reads as

$$\begin{aligned} \operatorname{div} q(r) &= \frac{i}{v_s\sqrt{\rho V}} \sum_k \sqrt{\frac{|\omega_k|}{2}} \left(b_k e^{i(kr-\omega_k t)} - b_k^\dagger e^{-i(kr-\omega_k t)}\right) \\ &= \frac{i}{u_0\sqrt{\rho V}}\varphi(r,t)\,, \end{aligned} \tag{4.8}$$

where $v_s = \omega_k/|k|$ is the sound velocity, and $\varphi(r,t)$ is the phonon field. This allows immediately to write the interacting Hamiltonian as

$$H_{e-p} = g\int \mathrm{d}r\, \psi^\dagger(r)\psi(r)\varphi(r)\,, \tag{4.9}$$

where $g = \frac{Ze^2a^2\sqrt{\rho_l}}{u_0}$ is the interaction strength. Now a very nice trick, found in [108] can be used. When computing average values of electron operators, with the Green's function technique, one will have to deal with such expansions

$$\left\langle \psi^\dagger(r,t)\psi(r',t')\right\rangle \approx \left\langle \psi^\dagger(r,t)\psi(r',t')\exp\left(-i\int \mathrm{d}t_1\, g\int \mathrm{d}r_1\, \psi^\dagger(r_1,t_1)\psi(r_1,t_1)\varphi(r_1,t_1)\right)\right\rangle\,. \tag{4.10}$$

When expanding the exponential, only even order terms in the interaction strength will contribute as $\langle\varphi\rangle = 0$. Thus, from the point of view of electrons, the presence of phonons is strictly equivalent to an effective electron-electron interaction (carried by phonons). To lowest order in g in the expansion, this interacting Hamiltonian reads as

$$H_I(t) = \int \mathrm{d}t'\mathrm{d}r'\mathrm{d}t\mathrm{d}r\, \psi^\dagger(r',t')\psi(r',t')U(r-r',t-t')\psi^\dagger(r,t)\psi(r,t)\,. \tag{4.11}$$

where

$$U(r,t) = -ig^2\left\langle T\left[\varphi(r,t)\varphi(0,0)\right]\right\rangle_0\,, \tag{4.12}$$

is the phonons Green's function evaluated on the phonon ground state. Performing the Fourier transform of the interacting Hamiltonian and assuming momentum conservation yields

$$H_I(t) = \sum_{k_1,k_2,p} U_{k_1+p,k_1} c_{k_2-p}^\dagger c_{k_2} c_{k_1+p}^\dagger c_{k_1}\,, \tag{4.13}$$

where the interaction potential of Eq. (4.12), computed in App. A, reads as

$$U_{kk'} = g^2 \frac{v_s^2(k-k')^2}{(\varepsilon_k-\varepsilon_{k'})^2 - v_s^2(k-k')^2}\,. \tag{4.14}$$

This Hamiltonian can simply be interpreted as coming from the following process: two electrons, with momentum k_1 and k_2 exchange a phonon with momentum p and carrying an energy $\varepsilon_{k_1+p} - \varepsilon_{k_1}$. As a first approximation, Debye's result on the number of phonons in a metal can be used to put limits on energy or wave vector sums. It is standard to consider that phonons cannot have an energy above the Debye frequency $\omega_D = \pi v_s n_e$ where n_e is the linear electron density. As a result, in the interaction strength Eq. (4.14), $\varepsilon_k - \varepsilon_{k'} < \omega_D$.

An interesting situation might arise, if the two electrons k_1 and k_2 are on opposite side of the Fermi energy, within an energy shell of a size comparable to the Debye frequency ω_D, then the momentum transferred by the phonon will be comparable to the Debye frequency while its energy will be negligible. According to Eq. (4.14) this would lead to an attractive interaction between the two electrons. The influence of such an interaction on the rest of the Debye shell around the Fermi sea is hinted by the so called Cooper instability.

4.3. Cooper problem and ground state

Cooper [109] had the idea to look at a single two-electron state subject to attractive interaction in the presence of a Fermi sea. The detailed derivation is provided in [66] so only the sketch is given here. Writing the wave function of the pair as

$$\phi(r_1, r_2) = \sum_k \alpha_k e^{ik(r_1 - r_2)}\,, \tag{4.15}$$

the Schrodinger equation can simply be written as

$$(E - 2\varepsilon_k)\alpha_k = \sum_{k>k_F} U_{k,k'}\alpha_{k'}\,. \tag{4.16}$$

Assuming that only the k inside the Debye shell around the Fermi surface contributes in the sum and imposing the wide band limit, $U_{k,k'}$ can be replaced by a constant U. Going from sums over k to integrals over ε and enforcing that the Debye frequency is the maximum of energy, the Schrodinger equation yields

$$\log\left(\frac{2(\varepsilon_F + \omega_D) - E}{2\varepsilon_F - E}\right) = \frac{1}{\nu_0 U}\,, \tag{4.17}$$

where ν_0 is the density of state on the Fermi surface. This is easily solved for E and yields

$$E = 2\varepsilon_F - \frac{2\omega_D}{e^{1/\nu_0 U} - 1}\,, \tag{4.18}$$

And in the low interaction regime

$$E = 2\varepsilon_F - \Delta\,, \tag{4.19}$$

where $\Delta = 2\omega_D e^{-1/\nu_0 U}$ is positive. As a result there is an energy level for a two-electron state inside the Fermi sea, the weaker the interaction and the lower the energy of this state, up to the boundary of the Debye shell. This situation is usually coined Cooper's instability as if it is favorable energetically for a pair to form, then all electrons would pair and the Fermi sea would reorganized entirely.

This computation is nevertheless very useful as it provides hints on what couplings to consider or how to build a trial ground state. For instance, the wave function has to be anti symmetric in spin and positions of the constituent electrons, from Eq. (4.16) the wave function is invariant under $k \to -k$ so the state is a spin singlet and both electrons must have opposite spins[1]. One would therefore be tempted to look at the

[1]This would not the case if the interaction depends on k

following Hamiltonian, called the BCS Hamiltonian,

$$H_{BCS}(t) = \sum_{k,\sigma=\uparrow,\downarrow} \xi_k c^\dagger_{k\sigma} c_{k\sigma} + \sum_{kl} U_{kl} c^\dagger_{l\uparrow} c^\dagger_{-l\downarrow} c_{-k\downarrow} c_{k\uparrow} \,, \tag{4.20}$$

where the Fermi momentum is the zero of wave vectors, $\xi_k = \frac{k^2}{2m} - \varepsilon_F$ and $\overline{\uparrow} = \downarrow$. The ground state might be written as a sum over all possible wave vectors k of the two particle states described above. Therefore, the combination of all the possible pairs of electrons is written as

$$|\Psi_{BCS}\rangle = \prod_k \left(u_k + v_k c^\dagger_{k\uparrow} c^\dagger_{-k\downarrow}\right) |0\rangle \ . \tag{4.21}$$

where u_k and v_k are the coherence factors and are here to ensure the normalization of the state through $u_k^2 + v_k^2 = 1$.

4.4. Quasiparticle excitations

Some constraints on the values of u_k and v_k can be found by minimizing the expectation value of the Hamiltonian on the ground state, i.e., $\langle \Psi_{BCS}| H_{BCS} |\Psi_{BCS}\rangle$. The details are skipped but, assuming that the interaction is constant in the Debye shell around the Fermi sea, i.e.,

$$U_{kl} = \begin{cases} -|U| & \text{for} \quad |\xi_k|, |\xi_l| < \omega_D \\ 0 & \text{otherwise} \,. \end{cases} \tag{4.22}$$

One can show that

$$\begin{aligned} 2u_k v_k &= \frac{\Delta}{\xi_k} \\ u_k^2 - v_k^2 &= \frac{\xi_k}{\varepsilon_k} \,, \end{aligned} \tag{4.23}$$

where

$$\begin{aligned} \Delta &= U \sum_k u_k v_k \theta(|\xi| - \omega_D) \\ E_k &= \xi_k^2 + \Delta^2 \,. \end{aligned} \tag{4.24}$$

which in turns means that

$$\begin{aligned} 2u_k^2 &= 1 + \frac{\varepsilon_k}{E_k} \\ 2v_k^2 &= 1 - \frac{\varepsilon_k}{E_k} \,. \end{aligned} \tag{4.25}$$

And in the weak coupling limit,

$$\Delta \approx 2\omega_D e^{-1/\nu_0 |U|} \,, \tag{4.26}$$

where ν_0 is the density of states in the normal state of the metal at the Fermi level.

4.4.1. Bogolubov-Valatin transformations

It is possible to find the creation and annihilation operators for the BCS ground state, this is done through the Bogolubov-Valatin transformation. They introduce new fermions in the superconductor, see Eq. (2.47a) of [110]:

$$\gamma_{k,\sigma} = u_k c^\dagger_{k,\sigma} + \overline{\sigma} v_k c_{-k,\overline{\sigma}} \,, \tag{4.27}$$

where sign($\downarrow$) $= -$ and sign($\uparrow$) $= +$. As can be shown, the γ fermions act on the BCS ground state as standard fermions act on the void, they are the quasiparticle operators of the BCS Hamiltonian, i.e.,

$$\begin{aligned} \gamma_{k\sigma} |\Psi_{\text{BCS}}\rangle &= 0 \\ \gamma_{k',\sigma'} \gamma^\dagger_{k\sigma} |\Psi_{\text{BCS}}\rangle &= \delta_{k,k'} \delta_{\sigma,\sigma'} |\Psi_{\text{BCS}}\rangle \ . \end{aligned} \tag{4.28}$$

These transformations allow to describe in a few words the excitation spectrum of superconductors. The ground state is made of pairs of electrons with opposite momentum and opposite spin[2] and zero net energy. These pairs form a condensate at the Fermi level and behave like bosons. This ground states constitutes the void of the quasiparticles excitations, which correspond to the addition of an electron of momentum k with energy E_k with weight u_k and of a hole with opposite momentum with weight v_k. These particles therefore have a gapped spectrum, with gap Δ, the part of the spectrum above the gap is called the continuum and the excitations are generically called the quasiparticles. As expected $u_k \to 1$ for high energy excitations, hence, high energy quasiparticles are simply electrons.

4.4.2. Sketch of the Bogolubov method

The method presented above is only valid for the homogeneous gas of electrons with attractive interactions, without impurities or external potential. There exists another method, developed in parallel of the BCS, by Bogolubov [111], explained in detail in [66]. This method is much more versatile to explore the properties of superconductors in real space, or in the presence of magnetic fields for example, like the Meissner effect, or the presence of vertex when there is a magnetic field as well as the distance over which the gap disappears at the boundary of the superconductor. The main feature of this method in the context of this thesis will be to write a simpler Hamiltonian in real space, which will be useful for adapting the tight binding model deployed to described QPCs in the previous sections. The method is based on the Hartree-Fock procedure, i.e., starting from the Hamiltonian in real space

$$\begin{aligned} H_{BCS} = \sum_\sigma \int \mathrm{d}^3 r \, \psi^\dagger_\sigma(r) \left(U_0 - \frac{1}{2m} (\nabla - qA)^2 \right) \psi_\sigma(r) \\ + \sum_{\sigma'} \frac{1}{2} \int \mathrm{d}^3 r \mathrm{d}^3 r' \, V(r - r') \psi^\dagger_\sigma(r) \psi_\sigma(r) \psi^\dagger_{\sigma'}(r') \psi_{\sigma'}(r') \, , \end{aligned} \tag{4.29}$$

where $\psi_\sigma(r)$ is the spin-σ electron annihilation operator in real space and A is the vector potential for an external magnetic field, which will not be considered here[3].

The commutation relation of fermions can be inserted in Eq. (4.29) this Hamiltonian, yielding

$$\begin{aligned} H_{BCS} = \sum_\sigma \int \mathrm{d}^3 r \, \psi^\dagger_\sigma(r) \left(\mathcal{V} - \frac{1}{2m} \nabla^2 \right) \psi_\sigma(r) \\ + \sum_{\sigma'} \frac{1}{2} \int \mathrm{d}^3 r \mathrm{d}^3 r' \, V(r - r') \psi^\dagger_\sigma(r) \psi^\dagger_{\sigma'}(r') \psi_\sigma(r) \psi_{\sigma'}(r') \, , \end{aligned} \tag{4.30}$$

where $\mathcal{U} = U_0 + 2V(0)$. The matrix element of the non-interacting Hamiltonian in real space is now written as $\mathcal{H}_0 = \mathcal{U} - \frac{1}{2m}(\nabla - qA)^2$. The next step is to approximate this quartic Hamiltonian with a quadratic one which is easy to diagonalize, this will require two approximations. First, consistency with the BCS model is found by considering a point-like interaction, i.e., that $V(r - r') = V\delta(r - r')$. Then, following

[2] The pairs are spin singlet, with zero total spin, hence the name s-wave superconductivity.
[3] The vector potential is written explicitly to recall that this method can take it into account.

Bogolubov [111], the four fermion products will be replace by a two fermion product times an average value, by a modified mean field method. A few choices have to be made on which combination is replaced by its average, mainly to respect the antisymmetry of fermions[4]. Terms like $\left\langle \psi_\sigma^\dagger(r)\psi_{\sigma'}(r)\right\rangle$ only contribute for $\sigma = \sigma'$ when no magnetic impurities are present. On the other hand, terms in $\langle\psi_\sigma(r)\psi_{\sigma'}(r)\rangle$ only contribute for $\sigma \neq \sigma'$. Thus, the only reasonable proposal for the quadratic effective Hamiltonian is

$$\begin{aligned} H_{eff} \approx \sum_\sigma \int \mathrm{d}^3 r\, \psi_\sigma^\dagger(r) \left(\mathcal{U} - \frac{1}{2m}\nabla^2\right)\psi_\sigma(r) + \sum_\sigma V \int \mathrm{d}^3 r\, U(r)\psi_\sigma^\dagger(r)\psi_\sigma(r) \\ + \int \mathrm{d}^3 r\, \Delta(r)\psi_\uparrow^\dagger(r)\psi_\downarrow^\dagger(r) + \int \mathrm{d}^3 r\, \Delta^*(r)\psi_\downarrow(r)\psi_\uparrow(r)\,, \end{aligned} \tag{4.31}$$

where the pairing potential $\Delta(r) = -V\langle\psi_\downarrow(r)\psi_\uparrow(r)\rangle$ and the Hartree potential $U(r) = \left\langle\psi_\sigma^\dagger(r)\psi_\sigma(r)\right\rangle$. The fact that this Hamiltonian does not conserve the particle number because of the pairing potential is not disturbing as the BCS ground state itself does not conserve the particle number. This method is called self-consistent because, the values of the pairing potential and the Hartree potential affect the ground state, and they are average values of operators on the same ground state, which can therefore be computed self consistently.

Performing the Bogolubov transformation from space variable r to state indices n, the quasiparticle $\gamma_{n\sigma}$ are introduced as

$$\psi_\sigma(r) = \sum_n \left(u_n(r)\gamma_{\sigma,n} - \mathrm{sign}\,(\sigma)v_n^*(r)\gamma_{n,\bar\sigma}\right)\,. \tag{4.32}$$

Enforcing that these operators diagonalize the effective Hamiltonian, i.e.,

$$H_{eff} = E_g + \sum_{\sigma,n} E_N \gamma_{\sigma,n}^\dagger \gamma_{\sigma,n}\,, \tag{4.33}$$

and computing the commutator $[\psi_\sigma(r), H_{eff}]$ in terms of Bogolubov operators $\gamma_{\sigma,n}$ one gets the matrix eigenvalue equation in spin space

$$\begin{pmatrix} \left(\mathcal{U} - \frac{1}{2m}\nabla^2\right) + U(r) & \Delta \\ \Delta^* & -\left(\mathcal{U} - \frac{1}{2m}\nabla^2\right) - U(r) \end{pmatrix} \begin{pmatrix} u_n(r) \\ v_n(r) \end{pmatrix} = E_n \begin{pmatrix} u_n(r) \\ v_n(r) \end{pmatrix}\,, \tag{4.34}$$

called the Bogolubov-de Gennes equation. This equation can be solved after writing the actual values for the pairing potential $\Delta(r)$ and the Hartree potential $U(r)$ in terms of Bogolubov excitations $\gamma_{\sigma,n}$. From the fermionic nature of $\gamma_{\sigma,n}$ one knows that

$$\left\langle \gamma_{\sigma,n}^\dagger \gamma_{\sigma',n'}\right\rangle = \delta_{\sigma,\sigma'}\delta_{n,n'} f(E_n)\,, \tag{4.35}$$

where f is the Fermi distribution and E_n is the energy of the Bogolubov excitations. One therefore immediately finds that

$$\begin{aligned} \Delta(r) &= V\sum_n u_n(r)v_n^*(r)\left[1 - 2f(E_n)\right] \\ U(r) &= -V\sum_n \left\{|u_n(r)|^2 f(E_n) + |v_n|^2\left[1 - f(E_n)\right]\right\}\,. \end{aligned} \tag{4.36}$$

As $u_n(t)$ and $v_n(r)$ depend on both the Hartree and pairing potentials, these are called the self consistent equations.

[4] It is recalled that this antisymmetry is responsible for the s-wave aspect of BCS superconductivity.

Following De Gennes [66], the pairing potential is assumed to be homogeneous, i.e., $\Delta(r) = \Delta$. Thus,

$$\begin{pmatrix} u_n \\ v_n \end{pmatrix} = w_n(r) \begin{pmatrix} u_0 \\ v_0 \end{pmatrix} , \tag{4.37}$$

where $w_n(r)$ is the wave function of the metal without interaction. As a result, the BdG equation yields

$$E_n = \pm\sqrt{|\Delta|^2 + \xi_n^2} , \tag{4.38}$$

and, imposing normalization $|u_n|^2 + |v_n|^2 = 1$,

$$\begin{aligned} |u_n|^2 &= \frac{1}{2}\left(1 + \frac{\xi_n}{E_n}\right) \\ |u_n|^2 &= \frac{1}{2}\left(1 - \frac{\xi_n}{E_n}\right) . \end{aligned} \tag{4.39}$$

This can be inserted in the self-consistent equation for the pairing potential, Eq. 4.36, yielding

$$\frac{1}{V} = \sum_n |w_n|^2 \frac{\left[1 - 2f(\Delta^2 + \xi_n^2)\right]}{\sqrt{\Delta^2 + \xi_n^2}} . \tag{4.40}$$

Introducing the density of state at the Fermi surface as

$$\nu_0 = \sum_n |w_n|^n \delta(\xi_n) , \tag{4.41}$$

the self consistent equation becomes

$$\frac{1}{\nu_0 V} = \int_{-\omega_D}^{\omega_D} \mathrm{d}\xi \frac{\left[1 - 2f(\Delta^2 + \xi^2)\right]}{\sqrt{\Delta^2 + \xi^2}} . \tag{4.42}$$

This equation allows to derive a value for the gap at zero temperature Δ_0, where $f(x) = H(-x)$ the Heaviside distribution so that the Fermi function does not contribute and the self-consistent equation becomes

$$\frac{1}{\nu_0 V} = \int_{-\omega_D}^{\omega_D} \mathrm{d}\xi \frac{1}{\sqrt{\Delta_0^2 + \xi^2}} = \sinh^{-1}\left(\frac{\omega_D}{\Delta_0}\right) , \tag{4.43}$$

In the weak coupling limit, the gap equation is the same as in the BCS approach, i.e.,

$$\Delta_0 \approx \omega_D e^{-1/\nu_0 V} . \tag{4.44}$$

Equivalently, this equation could be used to derive the transition temperature T_c, at which the gap vanish. This approach allowed to derive the same results as the BCS approach, the difference being that in the BCS approach, the external fields or the inhomogeneities cannot be taken into account.

Proximity effect: This paragraph provides a quick overview of the proximity effect, occurring at the interface between a superconductor and a metal in the normal state or the vacuum. This effect manifests itself by a decreasing superconducting gap close to the boundary of the superconductor, and the appearance of a non vanishing gap at the edge of the normal metal. In the case of interest of the thesis, the traditional approach [66] is not relevant as it consists in expanding the gap in powers of $T_c - T$ which is not small in

the context of the thesis. The result is that indeed, there is a non vanishing superconducting gap in the normal region, it decreases as the inverse distance to the edge, the typical width associated to the gap is $\xi_0 \approx v_F/\Delta$. This means that there are Cooper pairs at the boundary of the normal metal, this fact will be very useful in understanding the properties of the electric current in the next sections. In the current setup the gap function is assumed to be a step function at the boundary of the normal metal with the superconductor.

4.5. Conclusion

In this chapter, the main aspects of standard superconductivity were summarized. The physical picture behind an attractive interaction between electrons was explained in terms of phonon exchange. This was the occasion to derive the Hamiltonian for this interaction to first order in the phonon coupling. It was shown that this interaction is indeed attractive if the two electrons are on the opposite side of the Fermi surface. Then it was shown that this interaction creates pairs of electrons with zero energy, and that this pair is a spin singlet state leading to the Cooper instability and hence a reconstruction of the Fermi sea.

With this in mind the BCS approach was summarized, it consists in postulating a ground state that "makes the Cooper instability stable", i.e., a superposition of zero energy spin singlet pairs of electrons. From there, the Hamiltonian can be diagonalized it was shown that it is gapped and that above the gap there can be single excitations, called Bogolubov excitations. This allowed to derive an equation for the gap and for the coherence factors, which are the weight of holed and electrons in the Bogolubov quasiparticles. In particular, for high energy, these excitations are just electrons.

Another approach to superconductivity was presented, the one from Bogolubov. It allows to include external fields in the description and relies on real space representation of the gap and coherence factors. This description allows to derive the same results as BCS with regards to the excitation spectrum in the case were the metal is perfectly homogeneous and in the absence of external fields. Finally, the proximity effect was quickly described, as the apparition of Cooper pairs in a normal metal when in proximity with a superconductor. This will be used in the following chapters when transport in such junctions will be discussed.

5. N-S junction under a constant bias

5.1. Introduction

This chapter introduces the theoretical framework used to describe transport in the $N-S$ junction, between a normal metal and a BCS superconductor, and then extends it to a multi-lead setup. The detailed computations are not carried out but are illustrated and discussed in detail. In particular, the current and noise in the DC regime of the $N-S$ junction are computed and the main tunneling mechanisms are described. This junction displays different limiting regime depending on the size of the gap with respect to the voltage. This allows to draw a link between certain transport mechanisms and their counterparts in the current and noise. In particular, a new transport observable, the Fano factor, will be defined, it provides a way to identify the charge of the particles responsible for tunneling. All these concepts will be used extensively in the next chapters where time-dependent transport is analyzed.

The Hamiltonian for the junction is introduced in Sec. 5.2, the formulas for the current and the noise in terms of Green's functions are provided. Then, the behavior of these observables is described in detail in Sec. 5.3.

5.2. Multi-lead Hamiltonian and transport observables

This section is devoted to writing the tunnel Hamiltonian for devices with arbitrary number of junctions between superconductors and normal metals. Then the current and noise will be written in terms of Green's functions similarly to what was done in the previous chapters for the $N-N$ junction.

5.2.1. Hamiltonians

The superconducting Hamiltonian is written in the tight binding basis as

$$H_{\mathrm{S}} = \sum_{\sigma=\uparrow,\downarrow} H_{0,\sigma,\mathrm{S}} + \Delta \sum_{i} \left(c^{\dagger}_{i,\mathrm{S},\downarrow} c^{\dagger}_{i,\mathrm{S},\uparrow} + c_{i,\mathrm{S},\downarrow} c_{i,\mathrm{S},\uparrow} \right), \tag{5.1}$$

where the kinetic Hamiltonian is written in the k basis as

$$H_{0,\sigma,S} = \sum_{k,\sigma} \xi_k c^{\dagger}_{k,\mathrm{S},\sigma} c_{k,\mathrm{S},\sigma}\,, \tag{5.2}$$

is the kinetic part of the Hamiltonian in the superconductor (with spin σ), i labels the various sites, Δ is the superconducting gap and the chemical potential is set to zero, $c_{i,S,\sigma}$ is the annihilation operator for electrons in the superconducting lead. The Hamiltonians in the normal metals contain no interacting terms, they are therefore written as

$$H_{\mathrm{N}} = \sum_{\sigma=\uparrow,\downarrow} H_{0,\sigma,\mathrm{N}}\,. \tag{5.3}$$

The tunnel Hamiltonian is the sum of all Hamiltonians at every junction, i.e., considering only a voltage drive,

$$H_T(t) = \sum_{\substack{j=N,S \\ j'=N,S}} \sum_{\sigma} \lambda_{j,j'} e^{i\phi_{j,j'}(t)/2} c^\dagger_{e_{jj'},j,\sigma} c_{e_{j',j},j',\sigma} + \text{H.c.}\,, \tag{5.4}$$

where h.c. stands for hermitian conjugate, $\lambda_{j,j'}$ is the real tunneling amplitude from lead j' to lead j, $c_{j,\sigma}$ is the lead j and spin σ annihilation operator, and $\phi_{j,j'}(t)$ is the time-dependent phase difference between the leads j and j'. As was seen in the previous section, it is convenient to use spinors to write Hamiltonian containing BCS superconductivity. Considering that tunneling is only from a lead to another one ($j \neq j'$), the Hamiltonian is recast into

$$H_T = \sum_{j,j'} \psi^\dagger_j W_{j,j'} \psi_{j'} + \text{h.c.}\,, \tag{5.5}$$

with the Nambu spinor

$$\psi^\dagger = \begin{pmatrix} c^\dagger_{j,\uparrow} & c_{j,\downarrow}\,, \end{pmatrix} \tag{5.6}$$

and the tunneling matrix

$$W_{jj'} = \lambda_{jj'} \sigma_z e^{\sigma_z i\phi(t)/2}\,, \tag{5.7}$$

with σ_z the Pauli matrix. The current operator in lead j can be written as

$$I_j(t) = 2\frac{\delta H_T(t)}{\delta\phi(t)} = \sum_{j'} i\psi^\dagger_j(t)\sigma_z W_{jj'}(t)\psi_{j'}(t) + \text{H.c.}\,. \tag{5.8}$$

As was done in the previous sections, average values are computed with the help of Green's functions. The Keldysh Green's function in Nambu space is introduced, it reads as

$$G^{+-}_{jj'}(t,t) = i \begin{pmatrix} \left\langle c^\dagger_{j',\uparrow}(t) c_{j,\uparrow}(t) \right\rangle & \left\langle c_{j',\downarrow}(t) c_{j,\uparrow}(t) \right\rangle \\ \left\langle c^\dagger_{j',\downarrow}(t) c^\dagger_{j,\uparrow}(t) \right\rangle & \left\langle c_{j',\downarrow}(t) c^\dagger_{j,\downarrow}(t) \right\rangle \end{pmatrix}. \tag{5.9}$$

The current is computed in App. D.1, it is very conveniently written as a trace over Nambu and Lead space,

$$\langle I_j(t) \rangle = 2e\,\mathrm{Re}\,\mathrm{Tr}_{\mathrm{NL}}\left[\sigma_z W_{jj'}(t) G^{+-}_{j'j}(t,t)\right]. \tag{5.10}$$

In the case of a two-terminal device, similarly to what was done for the $N-N$ junction, the period-averaged current is immediately written using Fourier transform as

$$\overline{\langle I_L \rangle} = 2e\lambda \int_{-\Omega/2}^{\Omega/2} \mathrm{d}\omega\,\mathrm{Re}\,\mathrm{Tr}_{\mathrm{NLH}}\left[\sigma_z \mathcal{P} G^{+-}_{RL}(\omega)\right], \tag{5.11}$$

where the following notation was used

$$\Sigma_{LR,nm} = \lambda \mathcal{P}_{nm} = \lambda \begin{pmatrix} p^*_{m-n} & 0 \\ 0 & -p_{n-m} \end{pmatrix}. \tag{5.12}$$

This formula is quite compact, however, the matrices involved in the computation of the current tensor products of their Nambu structure times their Fourier ones.

In the multi-lead setup, the noise (correlations between current at lead j and l) is defined as

$$S_{jl} = \int \mathrm{d}t \int \mathrm{d}t' \left\langle I_j(t')I_l(t) - \left\langle I_j(t')\right\rangle \left\langle I_l(t)\right\rangle \right\rangle . \tag{5.13}$$

It can, similarly to the current, be written in terms of Green's function, see App. D.1. In terms of lead matrix product this is

$$\begin{aligned} S_{jl} = -e^2 \int \mathrm{d}t \int \mathrm{d}t' \mathrm{Tr}_{\mathrm{N}} \Big\{ & \left[\sigma_z W(t) G^{-+}(t,t')\right]_{jl} \left[\sigma_z W(t') G^{+-}(t',t)\right]_{lj} \\ & + \left[G^{-+}(t,t')\sigma_z W^\dagger(t')\right]_{jl} \left[G^{+-}(t',t)\sigma_z W^\dagger(t)\right]_{lj} \\ & - \left[G^{-+}(t,t')\right]_{jl} \left[\sigma_z W(t') G^{+-}(t',t)\sigma_z W^\dagger(t)\right]_{lj} \\ & - \left[\sigma_z W(t) G^{-+}(t,t')\sigma_z W^\dagger(t')\right]_{jl} \left[G^{+-}(t',t)\right]_{lj} \Big\} . \end{aligned} \tag{5.14}$$

In practice, it is very complicated to perform analytical computations of the noise in the multi-lead setup. Therefore, is interesting to write this formula in the case of a 2-terminal device (denoted R and L) where and $W_{LL} = W_{RR} = 0$.

$$S_{LL} = -e^2\lambda^2 \int_{-\Omega/2}^{\Omega/2} \frac{\mathrm{d}\omega}{2\pi} \mathrm{Tr}_{\mathrm{NH}} \left[2\mathrm{Re}\left(\sigma_z \mathcal{P}^\dagger G^{+-}_{LR} \sigma_z \mathcal{P}^\dagger G^{-+}_{LR}\right) - \sigma_z \mathcal{P}^\dagger G^{+-}_{LL} \sigma_z \mathcal{P} G^{-+}_{RR} - \sigma_z \mathcal{P} G^{+-}_{RR} \sigma_z \mathcal{P}^\dagger G^{-+}_{LL}\right] . \tag{5.15}$$

This formula is transportable to the N-N junction by replacing the Green's function by those corresponding to a normal metal, this will automatically make redundant the spin index due to BCS coupling.

5.3. DC behavior

5.3.1. Period-averaged current

In this section, the behavior of the current in the constant bias case is studied, it was studied in details in [98] so the aim here is to describe the link between the current and the main processes responsible for tunneling, described in the famous BTK paper [67]. The current is written in Eq. (5.11), and in the DC case, $\mathcal{P} = \sigma_z$, so that

$$\langle I_L(t)\rangle = 2e\lambda \int_{-\Omega/2}^{\Omega/2} \mathrm{d}\omega \, \mathrm{Re}\, \mathrm{Tr}_{\mathrm{NLH}} \left[G^{+-}_{RL}\right] , \tag{5.16}$$

The computation of the current is carried out in detail in App. D in the AC case, the zero temperature DC behavior can easily be extracted and reads as

$$\langle I_L\rangle = \frac{e}{\pi}\Delta \int_{-eV_0/\Delta}^{eV_0/\Delta} \mathrm{d}x \begin{cases} \dfrac{\tau}{(2-\tau)\sqrt{1-x^{-2}}+\tau} & \text{if} \quad |x|>1 \\ \dfrac{2\tau_A}{2+(\tau_A-2)x^2} & \text{if} \quad |x|<1 \end{cases} , \tag{5.17}$$

where

$$\tau_A = \tau(\lambda^2) = \frac{4\lambda^4}{(1+\lambda^4)^2} , \tag{5.18}$$

is the so-called "Andreev transmission". The effect of finite temperature is, as usual, to smooth the $I-V$ curve, so it is not interesting in a quantitative description. The fact that the current formula involves two distinct expressions reflects the fact that the physics is radically different above and below the gap.

Indeed, for an electron from the normal side incident on the junction, no state is available in the superconductor. However, it might be possible for another electron (with opposite energy with respect to the Fermi sea and opposite spin) to combine in a Cooper pair and tunnel into the superconductor. This means that the charge transferred is twice that of an electron. There are a few complementary ways to understand such a process. The first one assumes that first the Cooper pair forms at the edge of the normal metal because of the proximity effect and then it can tunnel into the zero energy states in the superconductor. The other interpretation describes a single electron tunneling in the continuum of quasiparticles above the gap, effectively gaining an energy $\approx \Delta$, and then another electron, from inside the Fermi sea, forms a Cooper pair with it and annihilates the virtual excited state, leaving a retro-propagating hole behind.

The first interpretation allows to see the physical distance over which such a process is possible, i.e., the superconducting coherence length, $\approx \Delta^{-1}$. This approach is interesting as it would link the magnitude of the tunnel coupling to the size of the gap. It is indeed apparent that in Eq. (5.17), when $x \approx 1$, the probability of Andreev reflection is independent of the tunnel coupling. This is of course caused by a problem in the model, and it seems that the energy dependence of the tunnel coupling should be taken into account to remedy it. In fact, as hinted before, the proximity effect should modify the tunnel coupling as, when the gap is infinite, the superconducting coherence length goes to zero and no proximity effect would be possible.

The second interpretation for Andreev reflection makes clear that this process is only possible over a time shorter than $\approx \Delta^{-1}$, this will be useful when looking at time-dependent Andreev reflection in the next chapters. Both interpretations require that two tunnelings of electrons occur, therefore the formula should only involve λ^4 (instead of λ^2 for single electron tunneling). This is indeed what happens in the second line of Eq. (5.17), where $\tau_A(\lambda) = \tau(\lambda^2)$ is the so-called Andreev reflection. Furthermore, for a voltage very low with respect to the gap and at zero temperature, the current mimics that of the $N - N$ junction, with doubled voltage and squared tunnel coupling. It should also be considered that incident electrons can be reflected, only changing the sign of their wave vectors.

Looking at the other situation, for an electron with an energy above the gap, it is still possible to undergo Andreev reflection as Cooper pair states are available and the Fermi sea is filled. However, it is also possible for such an electron to be transmitted into the continuum of quasiparticles, above the gap, in the superconductor. In the latter case, the charge transmitted is that of a single electron.

Fig. 5.1 shows the current as a function of the applied voltage for different values of the tunnel coupling (color curves) and for low temperature ($\Theta = 0.01\Delta$). In order to understand the curves of the current, it is recalled that the current is the sum of all possible tunneling events at all energies. Because of the Fermi distributions, at low temperatures this sum over energies is usually from $-eV_0$ to eV_0, when the temperature is higher, higher energies start to contribute and lower energies contribute less.

For high transmission (red and orange curves of of Fig. 5.1) and voltages below the gap the effect of Andreev reflection is to double the current with respect to that of the $N - N$ junction as there is a probability one to transfer a Cooper pair. For higher voltages however, the behavior of the $N - N$ junction is retrieved because quasi particle transfer behaves like electron tunneling at high energies. This leads to an excess current due to the fact that Andreev reflection happens for electrons on energy levels $-\Delta < E < \Delta$.

In the tunnel regime (blue and green curves of Fig. 5.1) and low voltages, the current is very low as one Andreev reflection requires two tunnelings, it is therefore proportional to τ_A which is very low in the tunnel regime. However, as the voltage gets closer to the gap, the current suddenly increases as quasiparticle transfer becomes possible and it behaves as τ rather than τ_A like Andreev reflection.

One can therefore distinguish three regimes, two of them are called linear as they reproduce Ohm's law, the Andreev regime (or high gap regime), where $\Delta \gg eV_0$, the normal regimes (or low gap regime), where $\Delta \ll eV_0$, and the non linear regime, where $\Delta \approx eV_0$, is called the intermediate regime.

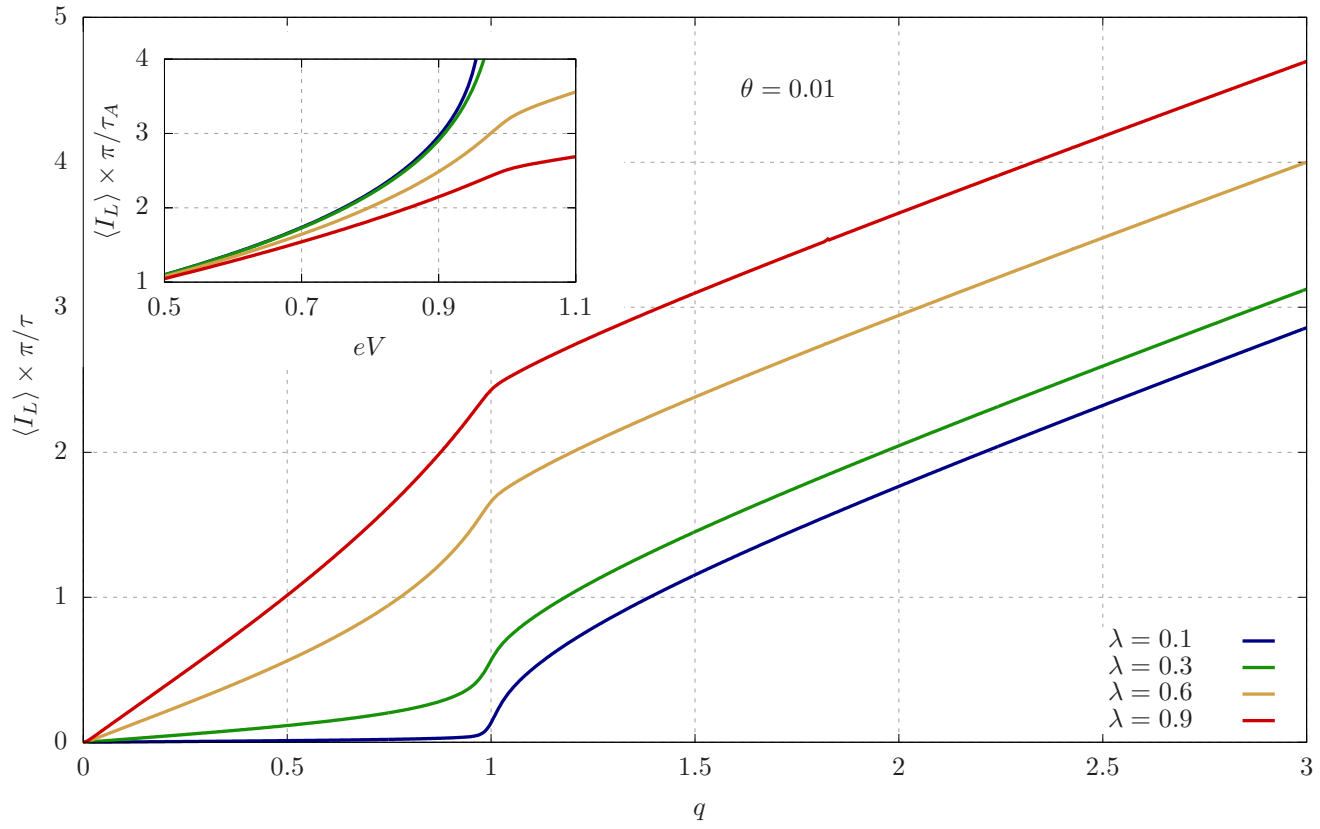

Figure 5.1.: The current in the $N - S$ junction as a function of the applied voltage for different value of the tunnel coupling and at two different temperatures.

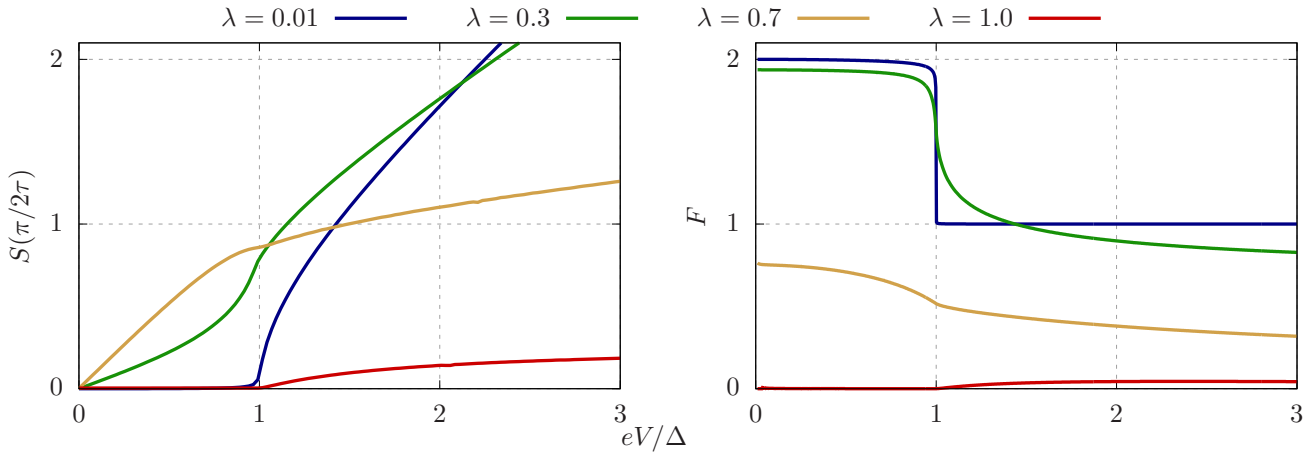

Figure 5.2.: The noise and the Fano factor at the $N-S$ junction biased by a constant voltage drive. Different colors represent different tunnel couplings. The temperature is $\Theta = 10^{-3}\Delta$ for the noise and $\Theta = 10^{-4}\Delta$ for the Fano factor.

5.3.2. DC noise and Fano factor

In the case of the noise, the complete DC behavior was described in [112], where a general formula was obtained at finite temperature. This formula is not reproduced here as it is too long to be of interest, however, the numerical curves of the noise as a function of the applied voltage are displayed in the left panel of Fig. 5.2, for very low temperatures $\Theta = 10^{-3}\Delta$.

At high transparency (red curve) and for voltages under the gap, there is no noise. Indeed, there is a probability one for Andreev reflection, as a result, the charge transfer is a deterministic process and there are no fluctuations and no noise[1]. For voltages just above the gap, an electron can either undergo quasiparticle transfer of Andreev reflection, so the noise increases with voltage. However, when the voltage is increasing, the probability for above gap Andreev reflection is decreasing so the noise is asymptotically reaching a constant value.

In the tunnel regime, i.e., the blue curve, for voltages below the gap, the only possible process is normal reflection as Andreev reflection implies two tunnelings. Therefore, the noise behaves as $\approx \tau_A V$ which is very low in units of τ (which is the scale of the y-axis of Fig. 5.2) for low λ. When the voltage reaches the gap, quasiparticle transfer becomes possible and the current retrieves a probabilistic behavior, hence the noise increases to behave asymptotically like the $N-N$ one.

In the intermediate transparency regimes, displayed as yellow and green curves, the noise displays an intermediate behavior which is an interplay between the two mechanisms described above. It is interesting to remark that the noise undergoes a radical change of behavior around the gap, especially for high or low transparencies.

An interesting quantity that can be computed is the ratio between the noise and the current, it is for example especially useful to remove prefactors common to both and relevant in experimental situations. Another use of this ratio rises in the tunnel limit, when the tunneling processes are known to be Poissonian, in this case, Schottky showed that the shot noise would be twice the current times the charge of the particles carrying the current. It is therefore natural to introduce the Fano factor as

$$F = \frac{S}{2e\,\langle I_L \rangle}\,, \tag{5.19}$$

[1]This is equivalent to a binomial process were the rate of success is one.

so that in the Poissonian regime it will count the charge of the single particles involved in tunneling.

The right panel of Fig. 5.2 shows the Fano factor for different tunnel couplings and for a very low temperature $\Theta = 10^{-4}\Delta$, to obtain sharp features. The most striking feature of the Fano factor appears in the tunnel limit, i.e., the blue curve. In this case, the Fano factor is equal to two for voltages below the gap and to one for voltage above the gap. This is a proof that below the gap, the current is a Poissonian process involving particles with twice the electron charge, i.e., Cooper pairs. This doubling of the shot noise was actually observed experimentally 20 years ago [113]. For voltages above the gap however, the current is only driven by quasiparticle transfer, which, in the Poissonian regime displays a Fano factor of one, hence the current is only carried by electrons.

5.4. Conclusion

In this chapter, the $N - S$ junction was introduced. First, the Hamiltonian for the junction was derived in the presence of a voltage bias (which can be time-dependent) and the current and noise were expressed in terms of Green's functions. This allowed to use the formalism developed in the previous chapters to find a formula for the current when the junction is biased by a constant voltage drive. The current was analyzed with the help of previous literature, in particular, the main concepts behind Andreev reflection were recalled and its implication on transport explained. Finally the noise created by a constant voltage drive was described, the analysis of the different regimes of energy is consistent with the main mechanisms for tunneling. It allows to introduce the Fano factor as a good diagnostic of Poissonian regimes and a measure of the charge of the particles involved in transport in such regimes.

This chapter allowed to separate three different operating regimes for the junction, two of them, the Andreev regimes and the normal regime, are called linear, as the current and the noise are linear in voltage. For this reason and as was shown in Sec. 3.4, one might expected that in these regimes, the AC current and noise will follow a Tien-Gordon behavior. These two regimes will be treated together in the following chapter. There exist a third regime of voltage where neither the current nor the noise are linear in voltage, this regimes displays a richer and more intricate behavior and will be treated in another chapter.

6. The AC-driven N-S junction in the linear regimes

6.1. Introduction

In this chapter, the focus is set on the linear regimes of the $N-S$ junctions, defined in Sec. 5.3, driven by a time-dependent voltage. This situation was discussed earlier by Belzig *et al.* [65] through full counting statistics of the electric current in the context of circuit theory [86]. In the low gap regime, they found that the excess noise (XN) is suppressed for integer charge carrying Levitons, in accordance with the expected behavior of the continuum at high energy, i.e.,that of an $N-N$ junction. In the high gap regime, where transport is dominated by Andreev reflection, they found excess noise suppression also for Levitons carrying half-integer charge. The effect of a finite temperature or the fate of the junction in the intermediate regime between these two limiting cases remained largely unexplored. The latter situation will be explored in a later chapter, in particular, the question as to whether or not the excess noise can be suppressed will be answered.

In this chapter, the work of Belzig *et al.* is extended in two ways. First, the Hamiltonian model, together with Floquet theory and the Tien-Gordon picture, brings physical intuition behind the results. Second, the drive is treated differently on each spin, the can be driven with a separate drive amplitude or be shifted in time.

This chapter is structured as follows. The formalism for spin-dependent drive is described very shortly in Sec. 6.2. In Sec. 6.3, it is shown that in the low gap regime, each spin tunnels independently as there is no correlation between them. The behavior of a normal metal is retrieved, for example, excess noise therefore vanishes for integer injected charge on each spin. In the other limit, that of large gap, described in Sec. 6.4, Andreev reflection dominates and treating both spin separately allows to unveil the basic mechanism responsible for the vanishing of excess noises for half integer Lorentzian pulses. As one might guess, this is due to superconducting correlations, Sec. 6.5 describes a mapping between the junction in the high gap regime and the $N-N$ junction at the level of Dyson's equations. This allows for an interpretation in terms of "minimal excitation states" of Cooper pairs at the junction similar to that of the $N-N$ junction.

6.2. Spin-dependent voltage drive

The Hamiltonian for the junction is recalled,

$$H = H_N + H_S + \psi_N^\dagger W \psi_S + \text{h.c.}\,, \tag{6.1}$$

where the tunnel matrix from the normal lead to the superconducting lead reads as

$$W(t) = \lambda \begin{pmatrix} e^{i\phi_\uparrow(t)} & 0 \\ 0 & -e^{-i\phi_\downarrow(t)} \end{pmatrix}. \tag{6.2}$$

λ_σ are the tunneling amplitudes for each spin species. The functions

$$\phi_\sigma(t) = e\int_{-\infty}^{t} \mathrm{d}t'\, V_\sigma(t')\,, \tag{6.3}$$

are the time-dependent phase differences between the leads accounting for the spin-dependent drives $V_\sigma(t)$ applied on the metallic lead.

This situation could be realized by having a metallic lead actually corresponding to two different leads made of spin-polarized half-metals or a quantum spin Hall effect bar, allowing us, thereby, to drive each spin component independently. This will be discussed in another chapter in the context of an actual proposition of device using superconducting correlations.

6.3. Small-gap regime, $\Delta \ll \Omega$

This regime corresponds to the case of a driving frequency much larger than the gap. One thus expects that transport processes through the junction are largely dominated by QP-transfer. Indeed, the Andreev reflection of an incoming electron of energy ω (with respect to the chemical potential of the superconductor) occurs with a probability [67, 98] Δ^2/ω^2 and is thus strongly suppressed in this limit, as explained in Sec. 5.3.

In order to perform a preliminary analytical computation, the extreme situation of a small superconducting gap with respect to the frequency is considered first. In this limit, the normal-metal and the BCS lead Green functions are identical and read as

$$\hat{g}^{r/a}_{\mathrm{BCS}} \xrightarrow[\Delta\to 0]{} \hat{g}^{r/a}_{N} = \mp i\hat{\mathbb{1}}\,, \tag{6.4}$$

so the junction maps exactly to an $N-N$ junction. Thus, the results of Sec. 3.2 and Sec. 3.3 can be used and the period averaged current reads as

$$\overline{\langle I^N\rangle}_q = \frac{e}{\pi}\tau e V_{\mathrm{DC}} = \frac{e\tau}{\pi} q\Omega\,, \tag{6.5}$$

and the noise as

$$S^N_q = \frac{e^2}{\pi}\left[4\tau^2\theta + 2\tau(1-\tau)\sum_n (eV_{\mathrm{DC}} + n\Omega)P_n(q)\coth\left(\frac{eV_{\mathrm{DC}}+n\Omega}{2\theta}\right)\right]. \tag{6.6}$$

Going beyond this strict zero-gap limit, while still considering $\Delta \ll \Omega$, it is possible to compute the excess noise numerically. The results for the Lorentzian, cosine and square drives at low temperature are summarized in Fig. 6.1. For any drive, there is a local minimum of XN at integer $q = n$. As expected, this is most pronounced for a train of Levitons for which the excess noise is still almost fully suppressed at integer q. Conversely, the sinusoidal bias features a residual finite XN for a quantized drive and the square drive bears local minima with even higher XN. These results are very much in agreement with Sec. 3.5, signaling that the physics at play is well captured by considering only quasiparticle-transfer processes in this small-gap regime.

6.4. Andreev regime, $\Delta \gg \Omega$

In the Andreev regime, which is the opposite of the normal regime, the bare Green's functions in the superconductor simplify to

$$g^{r,a}_{S,nm}(\omega) = -\Delta\sigma_x\delta_{nm} \text{ and } g^{\pm,\mp}_{S,nm}(\omega) \approx 0, \tag{6.7}$$

such that the Keldysh dressed Green's function Eq. (2.32) becomes formally

$$G^{+-}_{SN} = \frac{\lambda^3}{(1+\lambda^4)^2}\left[\sigma_x\mathcal{P}\,(T-\mathbb{1})\,\mathcal{P}^\dagger\sigma_x\mathcal{P} - \sigma_x\sigma_x\mathcal{P}\,(T-\mathbb{1})\right], \tag{6.8}$$

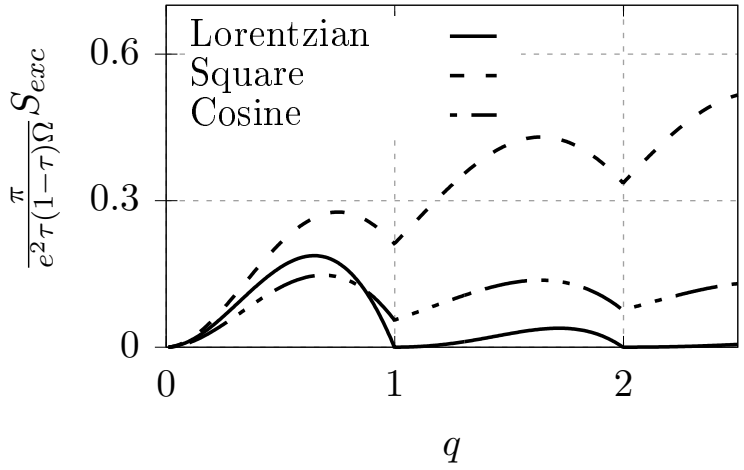

Figure 6.1.: Excess noise for the $N-S$ junction driven by a cosine, a square and a periodic Lorentzian drive (with relative width $\eta = 0.1$) as a function of the injected charge q in the low gap regime, $\Omega = 10^3\Delta$, at low temperature $\theta = 10^{-3}\Omega$. These plots are independent of the tunnel coupling but for the figure, $\lambda = 0.5$ was specified.

with the notations from of App. D, i.e., $\mathcal{P}$ is the tunnel matrix and T describe the thermal distribution of the electrons in the normal lead. Note that, even if $\sigma_x\sigma_x = \mathbb{1}$, it's crucial to keep it in the second term as both terms are divergent taken separately and only their difference is convergent. Thus any rearrangement of the terms has to be made when the sum over harmonics is explicit. In practice, see Eq. (D.34), using the identity $\mathbb{1} = \mathcal{P}^\dagger\mathcal{P}$, the useful form of the Green's function reads, after simplification, as

$$G^{+-}_{SN} = \frac{\lambda^3}{(1+\lambda^4)^2}\left[\sigma_x\mathcal{P}T\mathcal{P}^\dagger\sigma_x\mathcal{P} - \sigma_x\mathcal{P}\mathcal{P}^\dagger\sigma_x\mathcal{P}T\right] . \tag{6.9}$$

One remarks that, as was the case in the $N-N$ junction, in the large gap regime of the $N-S$ junction, there is no dependence in ω other than in the Fermi distribution, this is typical of linear regimes.

6.4.1. Current

It is instructive to start by computing the current as a function of time over a single period. From Eq. (3.2), it reads as

$$\langle I_\sigma(t)\rangle = \frac{e}{2\pi}\sum_{n,m}\int_{-\frac{\Omega}{2}}^{+\frac{\Omega}{2}} d\omega\, e^{-i(n-m)\Omega t}\left(\mathcal{I}^\sigma_{nm}(\omega) + \mathcal{I}^{\sigma*}_{mn}(\omega)\right) , \tag{6.10}$$

with

$$\mathcal{I}^\sigma_{nm}(\omega) = \sigma\sum_k\left[\Sigma_{NS,nk}(\omega)G^{+-}_{SN,km}(\omega)\right]_{\sigma\sigma} , \tag{6.11}$$

such that, in the Andreev regime, one obtains:

$$\langle I_\sigma(t)\rangle = \frac{e}{2\pi}\frac{\lambda^4}{(1+\lambda^4)^2}\sum_{n,m}\int_{-\frac{\Omega}{2}}^{+\frac{\Omega}{2}} d\omega\, e^{-i(n-m)\Omega t}\left(\mathcal{Q}^\sigma_{nm}(\omega) + \mathcal{Q}^{\sigma*}_{mn}(\omega)\right) , \tag{6.12}$$

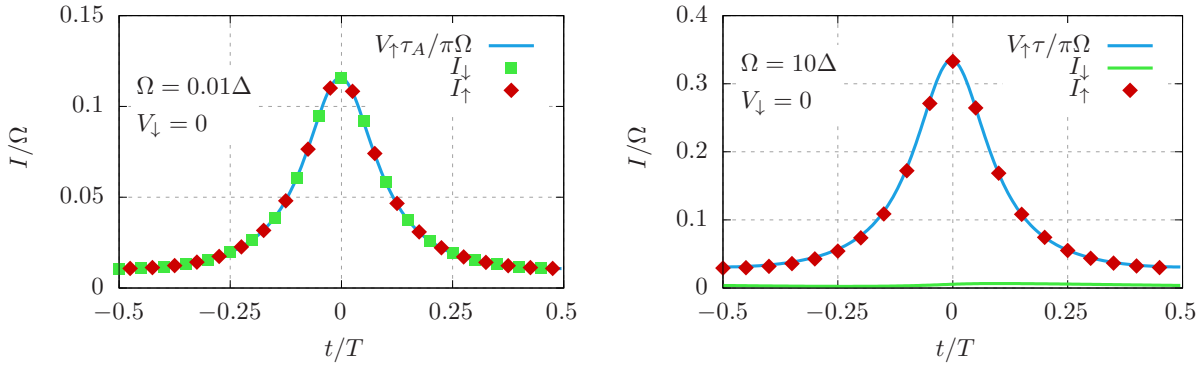

Figure 6.2.: Current of spin up and spin down as a function of time for different drive frequencies Ω where only the spin up are driven, i.e. $V_\downarrow = 0$. The figure was obtained with the following parameters: $\Theta = 10^{-3}$ and $q_\uparrow = 1$.

with

$$\mathcal{Q}^\sigma_{nm}(\omega) = \sigma \left[\mathcal{P}\sigma_x\mathcal{P}^\dagger T\mathcal{P}\sigma_x\mathcal{P}^\dagger - \mathcal{P}\sigma_x\mathcal{P}^\dagger\mathcal{P}\sigma_x\mathcal{P}^\dagger T\right]_{n\sigma,m\sigma} . \tag{6.13}$$

A detailed computation of the current is provided in App. D.4.1 leading to

$$\langle I_\uparrow(t)\rangle = \langle I_\downarrow(t)\rangle = \frac{e^2}{2\pi}\tau_A \left(V_\uparrow(t) + V_\downarrow(t)\right), \tag{6.14}$$

where τ_A is the Andreev transmission. As one can see, both currents are always equal and proportional to the sum of the applied drives, recovering the fact that the $N - S$ junction in the Andreev regime is a linear junction. Furthermore, as the only allowed processes involve pairs of up and down spins the number of transmitted electrons with different spins must always be equal and $\langle I_\uparrow(t)\rangle = \langle I_\downarrow(t)$. This has to be contrasted with the metallic regime, i.e. $\Delta = 0$, in which

$$\langle I_\sigma(t)\rangle = 2\frac{e^2}{\pi}\tau V_\sigma(t), \tag{6.15}$$

where the (normal) transmission $\tau = 4\lambda^2/(1+\lambda^2)^2$. As expected, each spin current is simply proportional to its respective drive.

These properties are visible in Fig. 6.2, where the plots display $I_\sigma(t)$ as a function of time for a vanishing $V_\downarrow = 0$ and $V_\uparrow(t)$ corresponding to a Leviton of charge $q_\uparrow = 1$. In the Andreev regime $\Omega \ll \Delta$ (left plot), one can see that both currents are equal and proportional to $V_\uparrow(t)$, in accordance with Eq. (6.14). In the other limit, as expected, the spin up current $I_\uparrow(t)$ is proportional to $V_\uparrow(t)$ and $I_\downarrow(t)$ is almost vanishing, of the order of $(\Delta/\Omega)^2$ smaller than $I_\uparrow(t)$.

6.4.2. Excess noise

Along similar lines, one can compute the noise averaged over a period, see Sec. D.5 and in particular Eq. (D.70), it reads as

$$\overline{\langle S\rangle} = \frac{e^2}{\pi}\Bigg[2\tau_A(1-\tau_A)\sum_s (s+q_\uparrow+q_\downarrow)\Omega \sum_{nr}\left(p^*_{n,\downarrow}p_{r,\downarrow}p_{s-r,\uparrow}p^*_{s-n,\uparrow}+\text{c.c}\right)\coth\left(\frac{\Omega(s+q_\uparrow+q_\downarrow)}{2\Theta}\right) + 4\tau_A^2\Theta\Bigg], \tag{6.16}$$

This result is to be compared with Eq. (3.19) and it appears that the situation seems to be more complicated than in the $N-N$ case. There is some interaction between the Floquet channels and the amplitudes appear instead of the probabilities. It can be shown that this is directly related to the presence of superconducting correlations at the junction. Using the definition of the coefficients $p_{l\sigma}$, one can show that

$$\sum_r p_{r,\downarrow}p_{s-r,\uparrow} = \frac{1}{T}\int_{T/2}^{T/2} \mathrm{d}t\, e^{-is\Omega t}e^{i\left[\phi_\uparrow(t)+\phi_\downarrow(t)\right]} = p_s(2q)\,, \tag{6.17}$$

which is therefore the Fourier component of $e^{-i\phi_{\rm tot}(t)}$, i.e., of the AC part of the *total* drive $V_{\mathrm{AC}\uparrow}(t)+V_{\mathrm{AC}\downarrow}(t)$. As a result, the formula above for $\overline{\langle S\rangle}$ is the same as the one for zero-frequency noise averaged over a period for a normal-normal junction,

$$\overline{\langle S^N\rangle}_q = \frac{e^2}{\pi}\left[4\tau^2\Theta + 2\tau(1-\tau)\sum_n (eV_{\rm DC}+n\Omega)|p_n|^2\coth\left(\frac{eV_0+n\Omega}{2\Theta}\right)\right], \tag{6.18}$$

driven by $V(t) = V_\uparrow(t) + V_\downarrow(t)$, i.e., the total drive applied to the NS junction. This emphasize that, not only for the current, but also for the noise, the behavior of the junction only depends on the total drive. This has an important consequence for the excess noise: as long as the sum $\phi(t) = \phi_\uparrow(t)+\phi_\downarrow(t)$ corresponds to the phase of a Leviton with an integer charge injected, the excess noise will vanish. This results was first derived by Belzig *et. al.* at zero temperature when both drives are the same and each corresponding to a half-Leviton, i.e., $q_\uparrow = q_\downarrow$. The present computation shows that it extends to any situations where $q_\uparrow + q_\downarrow$ is an integer. This is illustrated in Fig. 6.3, displaying the excess noise in the $(q_\uparrow, q_\downarrow)$ plane, for periodic Lorentzian pulses, q_σ corresponding to the injected charge for each spin component per period. As stated by Eq. (6.16), in the Andreev limit $\Omega \ll \Delta$ (left plot of Fig. 6.3), the excess noise vanishes along lines corresponding to $q_\uparrow + q_\downarrow \in \mathbb{Z}$. For $\Omega \gg \Delta$, i.e., in the $N-N$-equivalent regime of the junction (right plot of Fig. 6.3), the excess noise only vanishes when both q_σ's are integer.

Conversely, even if each drive is a sequence of Lorentzian pulses such that the total injected charge per period $q_\uparrow + q_\downarrow$ is an integer, the excess noise does not necessarily vanishes. For instance, if both drives are the same sequence of half Levitons with a charge $q_s = 1/2$, but being shifted in time one with respect to the other, i.e., $V_\downarrow(t) = V_\uparrow(t+\delta t)$. However, for integer q_σ, each drive V_σ will result in a vanishing excess noise independently of the time shift as the total drive is a sum of Levitons.

Fig. 6.4 makes clear the effects of a time shift on the excess noise. It represents the excess noise as a function of the injected charge, which is the same on both spins, for different time shifts $\delta t/T$ between the drives on each spins. This situation is clearer when looking at the inset, corresponding to the orange curve $\delta t/T = 0.3$, which represents the drives on both spins (blue and purple curves) and the spin-current (which is the same for both spins in the Andreev regime) in orange. For half-integer charge, e.g., $q = 1/2$, the excess noise vanishes only when $\delta t = 0$ (blue curve), and when the dephasing is perfect, $\delta t/T = 0.5$ (red curve), the excess noise behaves as that of the $N-N$ junction. On the other hand, for integer q_s, the excess

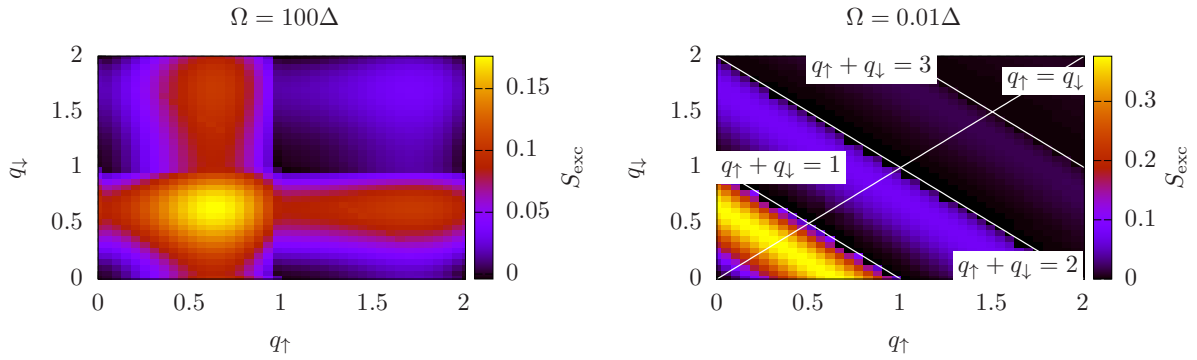

Figure 6.3.: Excess noise at the junction driven by a Lorentzian drive (of width $\eta = 0.1$) as a function of the injected charges $q_\uparrow$ and $q_\downarrow$ and for different frequencies. The temperature is chosen to be $\theta = 10^{-3}\Omega$.

noise vanishes independently of the dephasing between the spins.

The two interpretations of Andreev reflection can be invoked once again to produce two interpretations of time-dependent Andreev reflection. The proximity effect interpretation requires to modify a little the Floquet point of view. The superconducting correlations imply that the normal metal hosts Cooper pairs at its boundary, thus the drive does not exchange photons with electrons but with Cooper pairs. As they are made up of both spins, the tunneling Cooper pairs "see" a drive equal to $V_\uparrow + V_\downarrow$. The Floquet channels therefore do not correspond to shifted Fermi seas but to shifted "Andreev reflection channels".

The time-dependent, or dynamical approach, would say that, for half-integer drives, i.e. $q_\sigma = 1/2$ for instance, the Andreev reflection of each spin component produces a "half-pair" in the superconductor; each of these "half-pairs" must then be produced "at the same time" to allow for a whole pair to be transmitted in the superconductor. This reasoning remains valid as long as $q_\uparrow + q_\downarrow = 1$ and is well visible in Fig. 6.4. On the other hand, for integer drives, the Andreev reflection of each spin component produces a whole pair, independently of the Andreev reflection of the other spin component, allowing for a noiseless current in the junction whatever the time shift.

Both points of views agree with the Tien-Gordon picture provided that the noise is written as

$$\overline{\langle S^A \rangle}_q = \frac{e^2}{\pi}\left[4\tau^2\Theta + 2\tau(1-\tau)\sum_n (eV_{0\uparrow} + eV_{0,\downarrow} + n\Omega)|p_n(q_\uparrow + q_\downarrow)|^2 \coth\left(\frac{eV_{0\uparrow} + eV_{0,\downarrow} + n\Omega}{2\Theta}\right)\right], \quad (6.19)$$

Each Floquet channel is now associated to a Fermi sea at energy $eV_{0\uparrow} + eV_{0,\downarrow}$ and behaves as if the junction were an $N - N$ junction. This picture is represented in Fig. 6.5, with the notation $P_l^A = P_l(q_{\uparrow+\downarrow})$, in order to stress the link to the $N - N$ junction (see Fig. 3.1).

6.5. Mapping to an effective metal-metal junction

The fact that both the current and the noise only depend on the sum of the drives on the up and down spins can be directly inferred from Dyson's equation in the time domain, which is recalled here[1]

$$G(t,t') = g(t-t') + \iint \mathrm{d}t_1 \mathrm{d}t_2 g(t-t_1)\Sigma(t_1,t_2)G(t_2.t')\,, \quad (6.20)$$

[1]It is recalled that, when written without indices, the Green's function represent all the possible spaces, Keldysh, lead and Nambu (not Floquet because it is in the time domain).

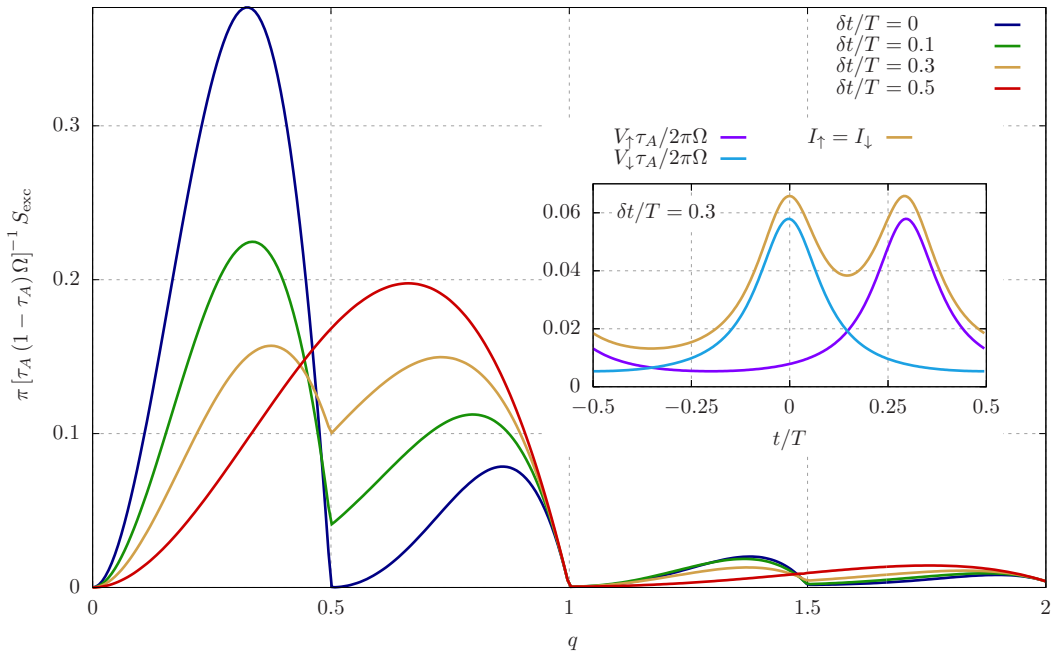

Figure 6.4.: Excess noise at the junction driven by a Lorentzian drive (of width $\eta = 0.1$) as a function of the injected charge $q = q_\uparrow = q_\downarrow$ for various time shifts δt. The frequency of the drive is $\Omega = 0.01$ and the temperature is $\theta = 10^{-3}\Delta$. The inset shows the current $I_\uparrow = I_\downarrow$ and the drives $V_\uparrow$ and $V_\downarrow$ as functions of time.

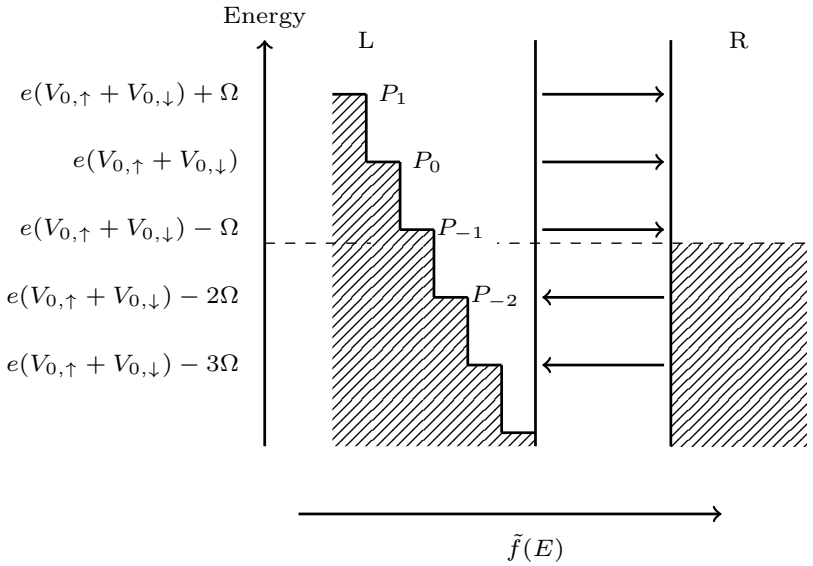

Figure 6.5.: Schematic representation of tunneling events at the $N - S$ junction in the Andreev regime. Each channel, involving a Fermi sea at level $e(V_{0,\uparrow} + V_{0,\downarrow}) + n\Omega$, contributes with a weight P_n in the current and the noise, and is represented by a step in the figure. The arrows represent the direction of the Cooper pair current. The horizontal axis represents $\tilde{f}(E)$ which is defined in Eq. 3.34.

where g is the bare Green function. Every Green function in lead space has the following block structure

$$G = \begin{pmatrix} G_{NN} & G_{NS} \\ G_{SN} & G_{SS} \end{pmatrix}, \tag{6.21}$$

where each G_{ij} is a tensor product of two 2×2 matrices corresponding to Nambu times Keldysh spaces. The self energy Σ reads as

$$\Sigma(t_1, t_2) = \delta(t_1 - t_2) \begin{pmatrix} 0 & \Sigma_{NS} \\ \Sigma_{SN} & 0 \end{pmatrix}, \tag{6.22}$$

where Σ_{NS} is the same as in Eq. (2.20) except that $\lambda(t)$ is replaced by the $W(t)$ of Eq. (6.2), to account for the difference between spins.

Iterating once the Dyson equation, one obtains the following $2 \times 2 \times 2$ matrix product:

$$G(t, t') = g(t - t') + g(t - t_1)V(t_1, t_2)g(t_2 - t') + g(t - t_1)V(t_1, t_2)g(t_2 - t_3)V(t_3, t_4)G(t_4, t'), \tag{6.23}$$

where integration over the intermediate times is implied.

In the Andreev regime, the lead space matrix element of the superconducting bare Green function reads as:

$$g_S(\tau) = \delta(\tau) \begin{pmatrix} -\sigma_x & 0 \\ 0 & \sigma_x \end{pmatrix}, \tag{6.24}$$

such that one obtains the following effective Dyson equation for the normal metal Green function in Keldysh-Nambu space:

$$G_{NN}(t, t') = g_{NN}(t - t') + g_{NN}(t - t_1)\tilde{\Sigma}_{NN}(t_1)G_{NN}(t_1, t'), \tag{6.25}$$

where

$$\begin{aligned} \tilde{\Sigma}_{NN}(t) &= -\begin{pmatrix} W(t) & 0 \\ 0 & -W(t) \end{pmatrix} \begin{pmatrix} \sigma_x & 0 \\ 0 & -\sigma_x \end{pmatrix} \begin{pmatrix} W^\dagger(t) & 0 \\ 0 & -W^\dagger(t) \end{pmatrix} \\ &= -\begin{pmatrix} -\tilde{W}(t) & 0 \\ 0 & \tilde{W}(t) \end{pmatrix}, \end{aligned} \tag{6.26}$$

with

$$\tilde{W}(t) = W(t)\sigma_x W^\dagger(t) = \lambda^2 \begin{pmatrix} 0 & e^{i\left(\phi_\uparrow(t) + \phi_\downarrow(t)\right)} \\ e^{-i\left(\phi_\uparrow(t) + \phi_\downarrow(t)\right)} & 0 \end{pmatrix}. \tag{6.27}$$

It is to be noted that an equivalent of Eq. (6.25) can be written for a $N - N$ junction as well, indeed, it just describes how an electron coming from N can end up in N. It can for example be interpreted as an equation describing a QPC between the normal metal and itself, the only transfer method being the reflection on the other side. In a normal metal, this $\Sigma_{NN}(t)$ would lead to the second term of Eq. (3.15), and hence to an electron being reflected without changing energy or spin.

In the Andreev regime of the $N - S$ junction, this effective Dyson equation describes an $N - N$ junction where one metal is made of spin up and the other of spin down, the effective drive being the sum of the original drives. More precisely, because of the Nambu description of the system, the up spins are electrons, where the down spins correspond to holes, hence the minus sign Eq. (6.26).

From this point of view, the Floquet channels correspond to Fermi seas (of up spins) at energy $eV_\uparrow + l\Omega$ with amplitude p_l tunnel-coupled Fermi seas (of down spins) at energy $eV_\downarrow + m\Omega$ with amplitude p_m. The amplitude for tunneling between such channels being independent of energy (in the Andreev limit only), they can be summed as shown in Eq. (6.17). Thus the Floquet channels can be depicted as Fermi seas at energy $e(V_\uparrow + V_\downarrow) + l\Omega$ with weight $p_l(q_\uparrow + q_\downarrow)$, tunnel-coupled to Fermi seas at the Fermi energy, see Fig. (6.5).

As a result, the minimal excitation state picture valid in the $N-N$ junction can be employed here. In the case of integer Levitons (in the sense of Fig. 6.4), the number of negative channels (reverse Andreev reflection) is minimal, and the excess noise vanishes. As a result it can be inferred that, on average, $q_\uparrow + q_\downarrow \in \mathbb{N}$ Cooper pairs are created per period. For non-quantized drives, the charge transferred is the same but it is shared among Andreev reflection and reverse Andreev reflection, so that much more processes take place, which is the reason for excess noise to appear.

6.6. Conclusion

In this chapter, the $N-S$ junction in the linear regimes was considered in a particular setup, when both spins of the normal metal are supposed to be driven separately. The next chapter will try to find an experimental situation were it is possible, however, this separate driving is very useful here to disentangle the properties of the junction. In particular, transport quantities were computed and an interpretation of the results of Belzig *et. al.* [65] was provided with the use of Floquet theory in the Tien-Gordon picture.

First, the junction driven by voltages far higher than the gap was quickly described. As only electron transfer as QP in the continuum of the superconductor or standard electron reflection are possible, this junction maps exactly to a spin-degenerate $N-N$ one, which was studied in detail in Chapter 3. The second case is that of voltages far below the gap, were only Andreev reflection or standard refection are possible. The computations of the current and noise were carried out analytically allowing for a detailed analysis of their behavior. It was shown that the excess noise vanishes when the sum of the drives on the up and down spins is a quantized Leviton. This was explained in a few different ways, by the proximity effect, or by the dynamical picture of Andreev reflection. The main line can be summarized as follows, the superconducting correlations link two electrons with opposite spins and energy, making these pairs the only charge carrier responsible for tunneling. Therefore, the drive that matters is the sum of the drives experienced by the two constituent particles.

From a quantum electronics point of view (or EQO), when optimized, this junction can be used in order to manipulate single Cooper pairs in a superconductor, or reversely, to split Cooper pairs into metals leads, one by one, in a time resolved way. This will be the subject of the next chapter, where a new device is proposed as a way to generate single pairs of entangled electrons in a time resolved way.

7. Source of entangled electrons

7.1. Introduction

In this chapter, the conclusions of the previous chapters are put in application to design a source of entangled electrons. It might be seen as an extension to the rich history of electronic entanglement in mesoscopic setups and nano-devices [77, 81, 114, 115] started two decades ago. The present idea stems from the fact that BCS superconductors provide a natural source of energy-entangled states, as was already remarked by the people behind the Cooper pair beam splitter [14, 76–83]. It is interesting to recall that energy-entanglement has already been performed for photons by Rarity and Tapster more than 30 years ago [50]. The latter device is built from a hybrid junction between a BCS superconductor and two normal metal leads, and was proposed as a DC source of electronic entangled states where the two constituent electrons propagate in separate leads via a Crossed Andreev Reflection (CAR) process. A manifestation of this entanglement could be found in the prediction of positive noise crossed correlations [14, 76, 77, 80, 116] which were measured experimentally [117]. A definite theoretical proof of this electronic spin entanglement was subsequently proposed through a Bell/Clauser Horne inequality violation test [83, 114]. The subject of this chapter is therefore the time-dependent version of the Cooper pair beam splitter.

In Sec. 7.2, the setup and its modelization are described. In particular, the link with the previous chapters is done through the Hamiltonian. A perturbative computation of the state of the system in the interacting picture when one pulse of voltage is sent is performed in Sec. 7.3. This allows to visualize the entangled state created. Finally, in Sec. 7.4 discusses a way to probe experimentally such a device, as usual through quantum transport experiments.

7.2. Device and model

As the two constituent electrons of a Cooper pair have opposite spins, the superconductor is connected to two leads with opposite spin polarization, see Fig. 7.1. This could be achieved by using two half metals, whose separation needs to be smaller than the superconducting coherence length (see Ref. [118]). Here, however it was chosen to connect the superconductor to a Quantum Spin Hall (QSH) bar. QSH bars are two dimensional topological insulators which (thanks to spin-momentum locking) bear on their edges two spin channels which propagate with opposite chiralities. Andreev reflection splits a Cooper pair in two spin dependent excitations which are thus naturally delocalized

In order to illustrate the dual nature – spin v.s. energy – of entanglement originating from a BCS superconductor, the $\pm\vec{k}$ component of the BCS wave function, see Eq. (4.21), is written as:

$$|\Psi_{BCS}^{(\pm\vec{k})}\rangle \sim u_k v_k \left(c^\dagger_{\vec{k}\uparrow} c^\dagger_{-\vec{k}\downarrow} - c^\dagger_{\vec{k}\downarrow} c^\dagger_{-\vec{k}\uparrow} \right) |0\rangle \ , \tag{7.1}$$

where u_k (v_k) are BCS parameters [119]. Strictly speaking, in the device of Fig. 7.1, energy – rather than momentum – entanglement can be preserved for electrons tunneling to spin polarized leads [77].

As was shown in the previous chapter, an $N-S$ junction in the Andreev regime and driven by a train of fine-tuned Lorentzian pulses can generate one Cooper pair per period. Conversely, applying a negative AC Lorentzian voltage drive to the spin channels of Fig. 7.1, Cooper pairs are expelled from the superconductor

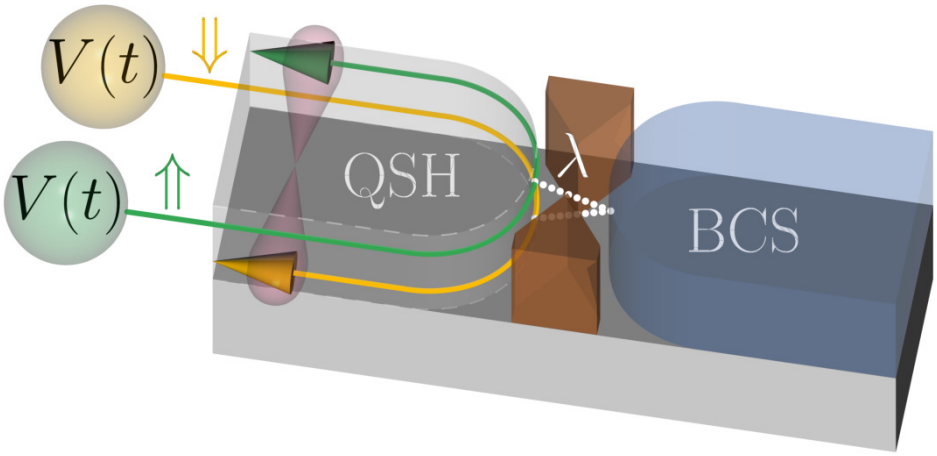

Figure 7.1.: The setup: a superconductor (right) is tunnel coupled to a Quantum spin Hall bar with two opposite edge spin channels via an adjustable QPC. Both channels are driven by the same train of Lorentzian voltage pulses $V(t)$. The shaded area covering the channels (downstream from the injection point of the two electrons ejected from the superconductor) represent the energy-entangled electrons which are generated on the normal side (left).

and their constituent electrons are transferred separately to the two opposite spin channels at the output as energy entangled states (EES) at each period. The link between the $N-S$ junction and the $QSH-S$ junction is easily identified by assuming that there are no correlations in the QSH edge modes. The latter can therefore be formally considered as metals with a unique spin orientation in the normal state, as a result, the Hamiltonians involved read as

$$\begin{aligned} H_{\mathrm{QSH}} &= \sum_{\sigma=\uparrow,\downarrow} H_{0,\sigma,\mathrm{N}} \\ H_{\mathrm{S}} &= \sum_{\sigma=\uparrow,\downarrow} H_{0,\sigma,\mathrm{S}} + \Delta \sum_{i} \left(c^{\dagger}_{i,\mathrm{S},\downarrow} c^{\dagger}_{i,\mathrm{S},\uparrow} + c_{i,\mathrm{S},\uparrow} c_{i,\mathrm{S},\downarrow} \right) , \end{aligned} \tag{7.2}$$

where the notations of Sec. 5.2 are used, i.e., $H_{0,\sigma,j}$ is the kinetic part of the Hamiltonian of lead j (with spin σ), i labels the various sites of these leads, Δ is the superconducting gap and the chemical potential is set to zero.

The tunnel Hamiltonian is defined as

$$H_T(t) = \sum_{\substack{j=N,S \\ j'=N,S}} \sum_{\sigma} \lambda_{j,j'} e^{i\phi_{j,j'}(t)/2} c^{\dagger}_{e_{jj'},j,\sigma} c_{e_{j',j},j',\sigma} + \mathrm{H.c.} , \tag{7.3}$$

where $\lambda_{j,j'}$ is the tunneling amplitude from lead j to lead j', $c_{i,j,\sigma}$ is the annihilation operator for electrons at site i and with spin σ on the lead j, $e_{j,j'}$ denotes the site of lead j from which tunneling to lead j' occurs, and $\phi_{jj'}(t) = e\int_{-\infty}^{t} dt'\, V_{jj'}(t')$ is the time-dependent phase difference between the leads which accounts for the drive-induced voltage difference $V_{jj'}(t)$ between lead j' and lead j.

A tunnel matrix in lead space can be written

$$W_{jj',\sigma\sigma'} = \lambda_{jj',\sigma\sigma'} \sigma_z e^{\sigma_z i \phi_{jj',\sigma\sigma'}(t)} . \tag{7.4}$$

However, for the device considered here, the QSH leads can be labeled by spin index and there is no tunneling between them so $\lambda_{\uparrow\downarrow} = 0$. Furthermore, the tunnel coupling to the BCS superconductor is considered to be the same for each edge mode, as a result $\lambda_{S\uparrow} = \lambda_{S\downarrow} = \lambda$. As a result, the tunnel Hamiltonian describing Fig. 7.1 reads as

$$H_T = \psi_N^\dagger W \psi_S + \text{h.c.}\,, \tag{7.5}$$

where the equivalent tunnel matrix is

$$W(t) = \lambda \begin{pmatrix} e^{i\phi_\uparrow(t)} & 0 \\ 0 & -e^{-i\phi_\downarrow(t)} \end{pmatrix} . \tag{7.6}$$

Thus the formalism is exactly that of the $N-S$ junction discussed in Chapter 6, only the physical meaning of the different variables changes.

7.3. Perturbative approach

This section motivates the design proposed by a perturbative calculation in the Andreev regime of the final quantum state propagating in the QSH channels when a *single* Lorentzian voltage pulse is applied on both of the spin-polarized channels of the QSH lead. From Chapter 6, one knows that the device generates cleaner states when the two pulses are assumed to be synchronized both in time and amplitude between these channels. Furthermore, see Sec. 6.4.2, pulses carrying half integer charge $q = e/2$ per spin lead on average to a $2e$ charge transfer through the tunneling of one Cooper pair per period. Therefore, the following pulse shape is chosen,

$$eV_\uparrow(t) = eV_\downarrow(t) = -\frac{1}{2\pi W}\,\frac{1}{1+t^2/W^2}\,. \tag{7.7}$$

with a width $W \gg \Delta^{-1}$ in order to only excite electrons of energy lower than the gap, i.e., to operate in the Andreev regime.

The final state is written as

$$|\mathcal{F}\rangle = S(+\infty,-\infty)\,|F_\uparrow\rangle \otimes |F_\downarrow\rangle \otimes |\Psi_{\text{BCS}}\rangle\ , \tag{7.8}$$

where $|F_\sigma\rangle$ is the Fermi sea of spin channel σ,

$$S(t,-\infty) = T\exp\left[-i\int_{-\infty}^{t} \mathrm{d}t' H_{TI}(t')\right]\ , \tag{7.9}$$

is the evolution operator and $H_{TI}(t)$ denotes the tunnel Hamiltonian in the interaction picture, i.e.,

$$H_{TI}(t) = e^{iH_0 t} H_T e^{-iH_0 t}\,, \tag{7.10}$$

where H_0 is the Hamiltonian without interaction, $H_0 = H_N + H_{BCS}$, and T is the time ordering operator. As was said earlier, Cooper pair transfer is ruled by the λ^2 terms, they appear in the second order of the perturbation theory of the evolution operator,

$$S(t,-\infty)^{(2)} = -\frac{1}{2}\int_{-\infty}^{t}\mathrm{d}t_1 \int_{-\infty}^{t_1}\mathrm{d}t_2\, T\left[H_{TI}(t_1)H_{TI}(t_2)\right]\,. \tag{7.11}$$

The detailed computations are given in Appendix E,

$$|\mathcal{F}\rangle = i\frac{L^3\lambda^2\sqrt{W}}{2\sqrt{2}\pi^2}\int_{-\infty}^{\infty}\mathrm{d}\varepsilon\,\psi_T(2\varepsilon)\int_{-\varepsilon}^{\varepsilon}\mathrm{d}E c^\dagger_{k(\varepsilon+E),\uparrow}c^\dagger_{k(\varepsilon-E),\downarrow}|F_\uparrow\rangle\otimes|F_\downarrow\rangle\otimes|\Psi_{\mathrm{BCS}}\rangle\ , \tag{7.12}$$

where $|F_\uparrow\rangle$ and $|F_\downarrow\rangle$ are the Fermi seas for the spin-polarized channels at equilibrium with the superconductor. Where

$$\psi_T(\varepsilon) = \sqrt{2W}e^{-W\varepsilon}H(\varepsilon)\,, \tag{7.13}$$

is the wave function of a single Leviton [47, 54, 106, 120], where $H(\epsilon)$ is the Heaviside distribution. It is important to stress that this state is energy-entangled, i.e., one cannot factorize it into a product of two states acting separately on the Fermi seas of the leads. Moreover, this final state is purely electronic, i.e., devoid of additional hole-like excitations. This can be achieved only by pulses with Lorentzian shape carrying a half-integer charge (or an integer multiple of it). In the case of finite temperature, there are allowed states for holes above the Fermi sea, thus, the full Eq. (E.22) should be used

$$\begin{aligned}|\mathcal{F}\rangle = i\frac{L^3\lambda^2}{8\pi^2 v_F^3}\sum_\sigma \mathrm{sign}(\sigma)\int_{-\infty}^{\infty}\mathrm{d}\varepsilon\,\varphi_T(2\zeta)\int_{-\varepsilon}^{\varepsilon}\mathrm{d}\tilde{E}\left[c^\dagger_{k(\tilde{E}+\varepsilon),\sigma}c^\dagger_{k(\varepsilon-\tilde{E}),\overline{\sigma}} - c_{k(\tilde{E}+\varepsilon),\sigma}c_{k(\varepsilon-\tilde{E}),\overline{\sigma}}\right]\\ \times|F_\uparrow\rangle\otimes|F_\downarrow\rangle\otimes|\Psi_{\mathrm{BCS}}\rangle\ ,\end{aligned} \tag{7.14}$$

where $\varphi_T(\varepsilon)$ is the Fourier transform of the exponential of the total phase. The state created by the drive at finite temperature is therefore made of both Cooper pairs splitted on both spin-polarized channels and anti-Cooper pairs, or energy entangled-holes on the same channels.

It seems reasonable to speculate that, in the Andreev regime, these results can be extended to the non-perturbative regime by replacing $\lambda^2 \to \lambda^2/\left(1+\lambda^4\right)$. This conjecture will be justified by the vanishing of excess-noise for quantized Lorentzian pulse in the non-perturbative regime of tunneling.

7.4. Probing the state with excess noise

This section tries to find measurable transport quantities that reflect the absence of hole excitations the state. This is done through excess noise and with realistic parameters.

7.4.1. Analytical reminders

As usual the current operators is written as

$$I_j(t) = \sum_{j'} i\psi^\dagger_j(t)\sigma_z W_{jj'}(t)\psi_{j'}(t) + \mathrm{H.c.}, \tag{7.15}$$

Therefore, the current and the noise are the same as in the $N-S$ junction, see Chap. 6. The total noise is defined as

$$\overline{\langle S_T\rangle} \equiv \sum_{\sigma,\sigma'=\uparrow,\downarrow}\overline{\langle S_{\sigma\sigma'}\rangle}\,, \tag{7.16}$$

It corresponds to the noise in the $N-S$ junction. As, in the high gap regime, only Andreev reflection can transport charge, there is only one transport channel and $\overline{\langle S_{\uparrow\downarrow}\rangle} = \overline{\langle S_{\downarrow\uparrow}\rangle} = \overline{\langle S_{\uparrow\uparrow}\rangle} = \overline{\langle S_{\downarrow\downarrow}\rangle}$, see [77]. Therefore,

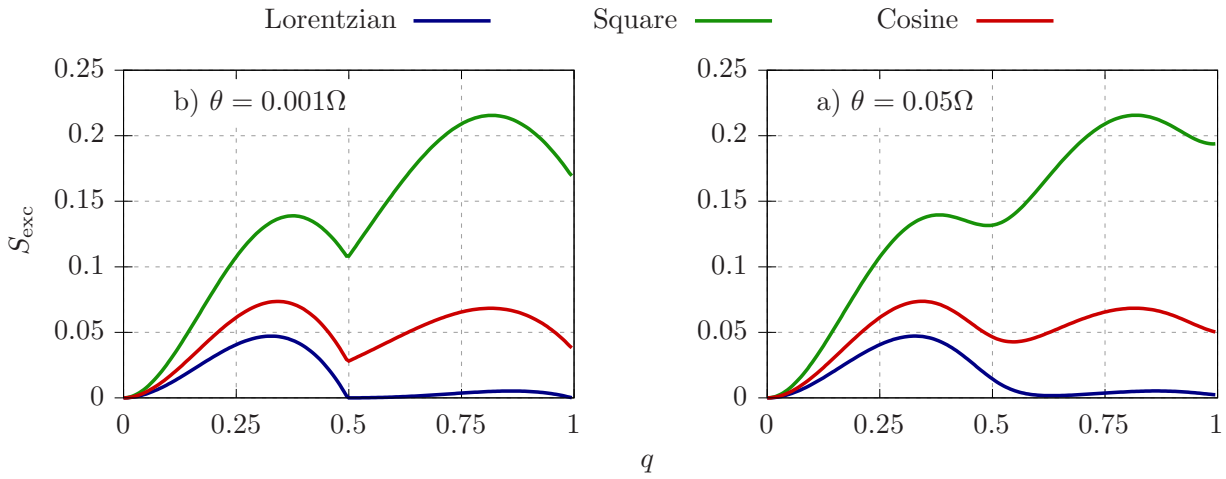

Figure 7.2.: Excess noise for the device driven by a cosine, a periodic square and a periodic Lorentzian drive (with relative width $\eta = 0.15$) as a function of the injected charge q in the Andreev regime $\Omega = 10^{-2}\Delta$. a) experimentally realistic temperature (see below), $\theta = 5 \times 10^{-2}\Omega$ and b) very low reduced temperature $\theta = 10^{-3}\Omega$. These plots are independent of the tunnel coupling (for this figure $\lambda = 0.5$).

in the pure Andreev regime $\Omega \ll \Delta$, the total noise of the source has the analytical expression:

$$\overline{\langle S_T \rangle}_q = \frac{e^2}{\pi}\Bigg(4\tau_A^2\theta + 2\tau_A(1-\tau_A) \times \sum_n (2q+n)\Omega P_n(2q)\coth\left[(2q+n)\frac{\Omega}{2\theta}\right]\Bigg), \tag{7.17}$$

see Chap. 6. The analysis of the noise is repeated here as finite temperature effects are discussed and its relevance for experiments is crucial.

Fig. 7.2 displays the excess noise and was obtained numerically with the full formula. This excess noise is plotted both at finite (left) and zero (right) temperature, minimal noise is achieved for half-integer and integer q at zero temperature, and for slightly higher values of q when the temperature θ is finite. This non-vanishing excess noise is a direct consequence of the fact that for finite temperatures, the drive does not only excite pairs of electrons at the junction but also pairs of holes. The current is therefore not only carried by electrons and the excess noise does not vanish, as explained in Sec. 3.3. However, periodic trains of Levitons still lead to a lower level of noise than cosine, or square voltages.

7.4.2. Realistic parameters

The final step of this study to study experimentally realistic parameters and to find an optimal working regime of the junction for the generation of entangles states. Borrowing from previous experiments on Levitons in metals [23], a realistic electron temperature is $\theta \approx 10$ mK with a drive frequency $f \approx 5$ GHz (this means applying voltages of the order $V_{\rm DC} \approx 10$ µV to reach $q = 0.5$). For example, niobium (with a gap $\Delta_{\rm Nb} \approx 1.55$ meV) corresponds to the Andreev regime, as $\frac{\Delta_{\rm Nb}}{\theta} \approx 2000$ and $\frac{\Delta_{\rm Nb}}{\Omega} \approx 100$. For aluminum ($\Delta_{\rm Al} \approx 0.17$ meV), however, the situation is not as optimal, with $\frac{\Delta_{\rm Al}}{\theta} \approx 200$ and $\frac{\Delta_{\rm Al}}{\Omega} \approx 10$.

To achieve a reliable, controlled source of EES, it is chosen that the average charge $\langle Q \rangle$ transmitted

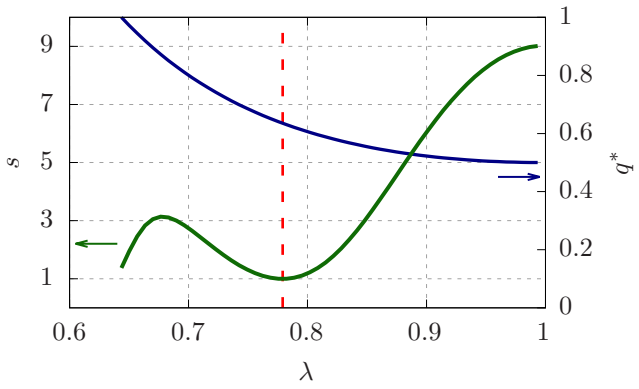

Figure 7.3.: The total excess noise of the source in units of the minimal noise $S_{\min}$ (green line, left axis) and the adjusted value of the injected charge per period (blue line, right axis) as a function of the tunnel parameter λ in the Andreev regime, $\Omega = 10^{-2}\Delta$, at temperature $\theta = 5 \times 10^{-4}\Delta$. λ covers the interval $\tau_A \in [0.5; 1]$. The dashed red line corresponds to a transparency $\tau_A \simeq 0.79$ for which the excess noise is minimal.

through the junction per period should be quantized, corresponding to the Cooper pair charge.

$$\langle Q \rangle = 2\pi \frac{\overline{\langle I \rangle_q}}{\Omega} = 4qe\tau_A \,. \tag{7.18}$$

The device would thus require to operate at near perfect transmission and tune the bias voltage such that the injected charge q is half-integer. As expected, this turns out to be independent of the type of AC drive considered. However, the second property of such an ideal source, the minimization of excess noise, can only be achieved by a Leviton voltage drive. As shown and explained above, at zero temperature, this condition is satisfied for q half-integer. It thus follows that the ideal source of EES corresponds to a $QSH-S$ junction which operates in the Andreev regime driven by a periodic Lorentzian drive with half-integer injected charge q, and operating at zero temperature with perfect transmission.

Unfortunately, none of these conditions can be realistically met in an actual experiment. What happens when such constraints are relaxed? In fact, the average charge transferred per drive period is robust under variations of the electron temperature (of the order of $\approx \Omega\theta/\Delta^2$). This linear behavior in τ_A suggests, however, that while working at finite temperature should hardly affect $\langle Q \rangle$, departing from perfect transmission has severe consequences, as the average transmitted charge is no longer perfectly quantized. One can circumvent this issue by adjusting the injected charge to a new value q^* in order to reach the optimal value $\langle Q \rangle = 2e$ for the source of entangled Levitons.

In the Andreev regime, at $\theta = 0$, the excess noise is proportional to $\tau_A\,(1-\tau_A)$, which is typical of shot noise [95], however, it is sensitive to a nonzero temperature θ. Indeed, as shown in Fig. 7.2a and as explained above, the excess noise gets modified as the temperature is increased, leading to a first arch which, instead of vanishing exactly at $q = 0.5$, now reaches a (nonzero) local minimum for a slightly higher value of q. The value $S_{\min}$ of this local minimum, which, in the Andreev regime, only depends on the drive frequency and temperature, constitutes a good reference point to optimize the quality of the produced entangled states.

In the following, the device is operated with a voltage source maintaining a quantized value of the average transmitted charge $\langle Q \rangle = 2e$, but the tunnel coupling λ is varied. In Fig. 7.3, the ratio $s = \frac{S_{\text{exc}}}{S_{\min}}$ is shown as a function of λ for an injected charge $q^* = \frac{1}{2\tau_A}$ and $\theta = 5 \times 10^{-4}\Delta$ and $\Omega = 10^{-2}\Delta$ (Niobium is chosen). Quite remarkably, there is a range of tunneling amplitudes (which are centered around $\lambda \simeq 0.78$,

i.e., $\tau_A \simeq 0.79$) for which the excess noise is close to the minimum allowed for this choice of temperature and drive frequency. For $q^* \simeq 0.65$, the Lorentzian drive displays the minimal noise, as can be seen in Fig. 7.2. When operated at this optimized transmission, the junction displays the minimal possible noise (taking into account the temperature) while transferring a $2e$ charge per period distributed on both leads on average.

To clarify the situation, and in particular to explain in which way this state is not only made of electrons, a few explanations are required. The injected charge is not integer but the average transmitted charge corresponds to that of a Cooper pair. In fact, the injected charge is distributed in Floquet channels with positive and negative energies (leading to positive and negative charge transfers). Then, at the junction, this distributed charge is "separated" in three processes, electron-like Andreev reflection (charge $2e$), hole-like Andreev reflection (charge$-2e$), or standard reflection (charge 0). The transmission rules the ratio between the latter and the two former while the injected charge rules the ratio between the two former only. The excess noise is minimized for a certain ratio between the two types of Andreev reflection(fixed q^*), while the transmitted charge is maintained quantized by changing λ.

7.5. Conclusion

This chapter proposed an application of the results of the previous one, a device using Andreev reflection as a source of entangled electron pairs. The key element resides in the fact that, as Cooper pairs are entangled both in energy and spin, splitting them between two different spin-polarized leads projects the spin and leaves one with energy entanglement. This was the method explored here, using edge modes of the quantum spin hall (QSH) effect, in the absence of correlations/interactions between the modes. In effect, the system studied consists in a QPC between the QSH and a BCS superconductor and a periodic voltage drive is applied to both QSH edge modes such that the device operates in the Andreev regime.

First the state created by Andreev reflection on the QSH edges was computed perturbatively in the tunnel coupling. For a Lorentzian pulse of integer total charge (shared by both spins), it was shown that the state after the pulse displays energy entanglement of electron pairs shared between the edge modes. The choice of the QSH as a platform to host these states is crucial as the two entangled electrons forming the pair have opposite spin, hence they reside on different edge modes and are counter-propagating. At finite temperature, this picture does not hold anymore as the final state also displays entangled hole pairs.

An generalization of this result to periodic trains of Lorentzian pulses was proposed, based on the findings of the previous chapters. It was shown that the device corresponds formally to the $N-S$ junction of Chap. 6, and the excess noise analysis allowing to probe the strictly electronic nature of the output state was repeated. An experimentally realistic set of parameters was studied to show that the junction can be operated so as to generate entangled electron states accompanied by a few entangled holes because of finite temperature effects, while transferring exactly the charge of a Cooper pair per period. It is reminded that this description only holds for low voltages/frequencies with respect to the gap, relaxing this condition will be the subject of the next chapter.

8. The AC-driven N-S junction in the general case

8.1. Introduction

In this chapter, to conclude the study of the AC-driven $N-S$ junction, the full intermediate regime is studied. In this regime, the voltage is comparable to the superconducting gap so that the energy spectrum of the superconductor is energy dependent and non-linear. It was anticipated in previous chapters that this regime would display interference between Floquet channels, mixing of sub-gap and above-gap transport process, that the Tien-Gordon picture might not apply etc. This will be disentangled with a complete numerical study. It will also be shown through perturbation theory in tunnel coupling that the negative excess noise first noticed by Belzig *et. al.* is a natural feature of non-linear systems. Furthermore, it will be shown that the Floquet channels, obviously visible in the excess noise of linear junctions, also have a dramatic impact on the *period-averaged current* for this non-linear junction, which is computed analytically.

The concept of effective gap that will be used extensively is introduced in Sec. 8.2. The period-averaged current is computed and analyzed in Sec. 8.3. The noise in perturbatively computed analytically up to fourth order in λ in Sec. 8.4. These computations will give some hints on how to interpret the noise in all regimes which is computed exactly numerically for various tunnel couplings, frequencies and drive shapes, in Sec. 8.5.

8.2. Effective gaps

. The analysis carried out in the previous chapters showed that three regimes of voltage can be distinguished. The normal regime, or small-gap regime, in the transport properties are dominated by quasiparticle transfer outside the gap, as Andreev reflection above the gap has a vanishing contribution of high voltages. The second one is the Andreev, or large-gap regime where Andreev reflection inside the gap are the main driving mechanism. In each of these regimes, there is also the possibility for electrons to undergo standard reflection, so that makes a total of four possible processes. In the third regime, the intermediate regime, where $\Omega \sim \Delta$, one expects transport to be impacted the four possible processes, quasiparticle transfers outside the gap, Andreev reflection processes inside and outside the gap, standard reflection and interferences between the four[1].

However, as the junction is periodically driven, transport is described by the sum of the amplitudes of the time-independent Floquet processes. Every Floquet channel is the equivalent of a Fermi sea with chemical potential shifted by an integer times the frequency of the drive. As a result, they are all facing the same gap but shifted in energy by an integer times the frequency. Stated differently, each Floquet channel (with label n) corresponds to a Fermi sea shifted by $eV_{\mathrm{DC}}+n\Omega$, the gap for the channel n is spanned by an energy in the range $[-\Delta-n\Omega,+\Delta-n\Omega]$. Quite importantly, this means that for a given applied DC voltage, some channels are mainly in the Andreev regime, while others are in the quasiparticle-dominated regime. The current and noise then result from the scattering between all these channels.

To better understand the features observed, it is convenient to introduce an effective gap associated with

[1] Actually, for a given energy, never more than three processes are possible

a given Floquet channel n as

$$[\gamma_n^-, \gamma_n^+] \text{ , with } \gamma_n^\pm = -n \pm \frac{\Delta}{\Omega} . \tag{8.1}$$

Since this chapter mostly deals with the evolution of the transport properties as a function of q, which represents the DC bias in units of the driving frequency, the above effective gap is also expressed as a range in energy, given in units of Ω. Within this frame, it corresponds to the range of the injected charge per period q for which the Floquet channel n sees the superconducting gap Δ.

Note that the width of the effective gap is $2\Delta/\Omega$, which naturally implies that the effective gaps of the different channels are large and overlapping when $\Omega < \Delta$, while they are small and well separated for $\Omega > \Delta$. The next sections will try to describe precisely the crossover behavior between the quasiparticle-transfer-dominated regime (small-gap case, $\Delta \ll \Omega$) and the Andreev regime (large-gap case, $\Delta \gg \Omega$). In this situation, analytical calculations are for the most part untractable as it becomes impossible to solve the Dyson equation exactly. One has to resort either to expanding analytic expressions perturbatively in λ or to performing exact numerical calculations, i.e., including contributions to all orders in the tunneling constant.

8.3. Current

.

8.3.1. Period-averaged current

A closed-form analytical expression for the current is not available in the general case. However, one can still work out an intermediate form which turns out to be quite useful, after some lengthy derivation, see App. D), one can find that

$$\overline{\langle I \rangle}_q = 2e\lambda^2 \sum_n P_n(q) \int_{-\infty}^{\infty} \frac{\mathrm{d}\omega}{2\pi} \mathcal{I}(\omega) \left[\tanh\left(\frac{\omega - (n+q)\Omega}{2\theta} \right) - \tanh\left(\frac{\omega + (n+q)\Omega}{2\theta} \right) \right] , \tag{8.2}$$

where

$$\mathcal{I}(\omega) = \begin{cases} \dfrac{2\lambda^2}{(1+\lambda^4)^2 \left(1 - \frac{\omega^2}{\Delta^2}\right) + 4\lambda^4 \frac{\omega^2}{\Delta^2}} & \text{if} \quad |\omega| < \Delta \\ \dfrac{1}{(1+\lambda^4)\sqrt{1 - \frac{\Delta^2}{\omega^2}} + 2\lambda^2} & \text{if} \quad |\omega| > \Delta \, . \end{cases} \tag{8.3}$$

In the presence of an AC drive, the current Eq. (8.2) is therefore the sum of independent contributions coming from all Floquet channels. Interestingly, the behavior of the resulting integral is strongly impacted by the behavior of $|\omega \pm (n+q)\Omega|$ with respect to the superconducting gap Δ, signaling the importance of the effective gap $[\gamma_n^-; \gamma_n^+]$ associated with each Floquet channel n. In particular, as explained in Sec. 5, the integrand of Eq. (8.2) changes sharply for values of the DC voltage near $\gamma_n^\pm$, because in the tunneling regime, there is a huge difference in magnitude between Andreev reflection and QP-transfer. As a result, one would expect the current to undergo a sudden change of behavior close to these values. As a consequence, the transition from a purely Andreev reflection-dominated behavior to a QP-transfer-dominated current should then be visible for each channel in the total current.

This is illustrated in Fig. 8.1 where both the period-averaged current and the differential conductance are plotted as a function of the injected charge q, for $\Omega = 3\Delta$ and different drives. To this transition more

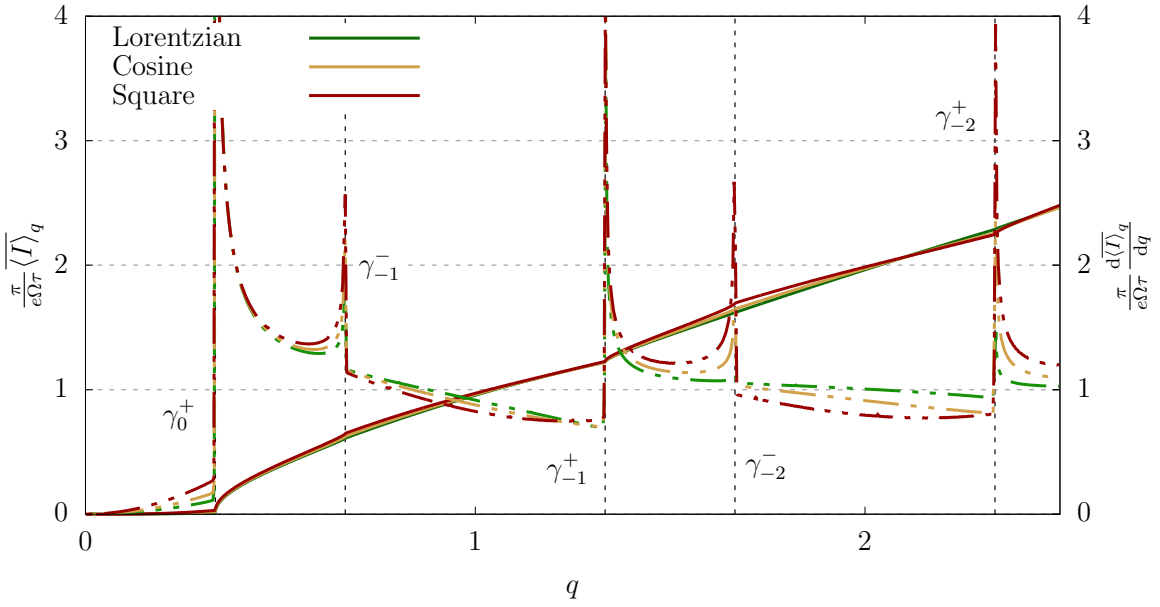

Figure 8.1.: The period-averaged current (full line) and its derivative with respect to q (dashed line) as the junction is driven by different drives (Lorentzian with $\eta = 0.15$, cosine voltage and square voltage), at $\Omega = 3\Delta$, $\beta\Omega = 10^3$ and for a tunnel barrier $\lambda = 10^{-2}$, as a function of q. The edges of the effective gap for conducting channels $n = 0, 1$ and 2 are shown by vertical dashed lines.

dramatic, it was chosen to focus on a low-transparency tunnel barrier, where Andreev processes are strongly suppressed.

The period-averaged current looks smooth exhibiting only small kinks near the effective gaps edges and an overall behavior which looks rather independent of the details of the drive. At low voltage, the current is vanishingly small then suddenly increases near $q \simeq \gamma_0^+$, as one goes from an almost no current regime (Andreev reflection-dominated) to one that is dominated by QP-transfer. These signatures are much more striking in the differential conductance as they manifest as sharp peaks located at the effective gap edges of the different Floquet channels, which are only softened by the finite temperature. Within a given effective gap or in-between gaps, the differential conductance remains continuous and featureless.

8.3.2. Time dependent current

This small section deviates from the main subject of the chapter as it considers that the spins are driven separately, hence the reader should refer to Chap. 6 in order to ensure that it was well understood. Indeed, the current as a function of time over an entire period is computed numerically as no analytical formula was found. It was not treated in Chap. 6 as the intermediate regime was not understood yet.

The results are shown in Fig. 8.2 for a Lorentzian drive of width $\eta = 0.1$ and intermediate frequencies. Close to the Andreev regime $\Omega = 0.1\Delta$ (left plot), both $I_\uparrow$ and $I_\downarrow$ depart from their Andreev value, the main effect is a time shift of the Lorentzian shape. This can be understood with the dynamical picture of Andreev reflection, which takes a time $\delta t \sim \Delta^{-1}$, hence the delay between the drive and the current.

For frequencies close to the gap $\Omega = 0.3\Delta$ (right plot), one can see the impact of the nonlinear behavior of the junction: both $I_\uparrow$ and $I_\downarrow$ display a very different behavior as a function of time, with additional oscillations compared to the drive $V_\uparrow(t)$. One also remarks that the spin up current is increased with respect with the spin down current, indeed, part of the up spins are in Floquet channel below the gap,

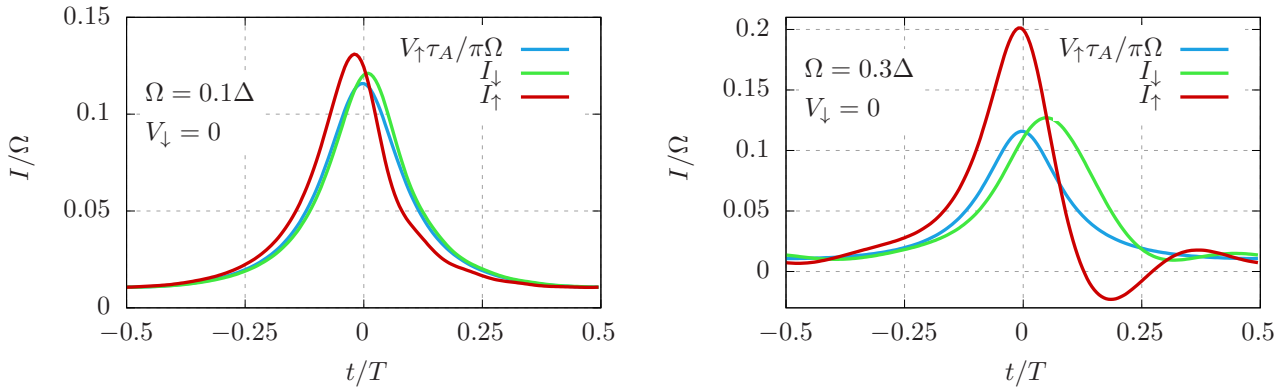

Figure 8.2.: Spin degenerate current as a function of time over one period, for different drive frequencies Ω, where only the spin up is driven, i.e. $V_\downarrow = 0$. The figure was obtained with the following parameters: $\Theta = 10^{-3}$ and $q_\uparrow = 1$.

it therefore creates the spin down current. However, some higher Floquet channels corresponds to energy above their effective gaps, hence they are involved in QP-transfer, leading to a current of the order of τ and therefore higher in magnitude.

8.4. Tunneling noise

The general analytical calculation of the noise turns out to be quite cumbersome and is not shown here. Instead, one can rely on two rather complementary approaches. First, a perturbative expansion in the tunneling constant will give insights on how to interpret the noise when it departs from the linear behavior. Indeed, an expansion in powers of λ (with only even powers contributing) can be performed and the first few terms are accessible analytically. The general expression reads as

$$\overline{S}_q = \sum_{n=1}^{\infty} \overline{\langle S \rangle}_q^{(2n)} , \tag{8.4}$$

where $\overline{S}^{(2n)}$ is the term of order $O\left(\lambda^{2n}\right)$. Here only the $n = 1$ term and the contribution due to in-gap Andreev reflection of the $n = 2$ term are computed exactly . This helps better understand the full picture, as in the low-transparency regime, this allows one to isolate the leading contribution from QP-transfer $\left[\text{of order } O\left(\lambda^2\right)\right]$ and the main modifications arising from Andreev reflection [only present from order $O\left(\lambda^4\right)$ onward. The second approach consists in solving numerically the Dyson equation in order to obtain the evolution of the excess noise as a function of the applied drive. This provides a complete panorama of the different competing physical processes at play in the junction and will be done in Sec. 8.5.

8.4.1. Order λ^2 and negative excess noise

Since the expression for the noise, Eq. (5.15), already contains a prefactor of order λ^2,

$$\overline{S} = -e^2\lambda^2 \int_{-\Omega/2}^{\Omega/2} \frac{\mathrm{d}\omega}{2\pi} \mathrm{Tr}_\mathrm{H}\left\{\mathcal{P}G_{RL}^{-+}\mathcal{P}G_{RL}^{+-} - \mathcal{P}^\dagger G_{LL}^{-+}\mathcal{P}G_{RR}^{+-} + \mathcal{P}^\dagger G_{LR}^{-+}\mathcal{P}^\dagger G_{LR}^{+-} - \mathcal{P}G_{RR}^{-+}\mathcal{P}^\dagger G_{LL}^{+-}\right\}. \tag{8.5}$$

the computation of $\overline{S}^{(2)}$ is carried out by replacing all the dressed Green functions in Eq. 8.5 by their bare equivalent. The second order component of the noise can then be immediately written as

$$\overline{S}_q^{(2)} = 2e^2\lambda^2 \sum_n P_n \int_{|\omega|>\Delta} \frac{d\omega}{2\pi} \frac{|\omega|}{\sqrt{\omega^2-\Delta^2}} \left[1 - \tanh\left(\frac{\omega + eV_{\rm DC} + n\Omega}{2\theta}\right) \tanh\left(\frac{\omega}{2\theta}\right)\right] . \tag{8.6}$$

It naturally arises from the calculation that this contribution only describes QP-transfer above the gap as all the non-diagonal terms in Nambu space from the bare superconducting lead Green function do not contribute in the end. As it turns out, the resulting expression bears some striking resemblance with the corresponding λ^2 contribution from the DC noise $S^{(2)}_{\rm DC}(eV)$, as a result

$$\overline{\langle S\rangle}_q^{(2)} = \sum_n P_n S^{(2)}_{\rm DC}\left(eV_{\rm DC} + n\Omega\right) . \tag{8.7}$$

Therefore, the Tien-Gordon picture applies to the noise to second order in tunneling, it is not surprising as in Chap. 6 it was shown that QP-transfer bears a striking resemblance with electron tunneling *and* Chap. 3 showed that electron tunneling is described by Tien-Gordon noise. However, it was said that a non-linearity like the one observed in Eq. (8.6) would lead to interferences between Floquet channel, thus destroying the Tien-Gordon behavior of the noise. The solution to this gordian knot is readily found by saying that interference between Floquet channels involved in QP-transfer do occur when transport is non linear *but only* to order λ^4 and above.

Eq. (8.6) is however very useful to better understand one of the surprising results obtained at low transparency for intermediate frequency. This is illustrated in Fig. 8.3, where one readily sees that in such a regime the excess noise can become negative, thus signaling that adding an AC component to a DC drive can lead to a reduction of the noise for an appropriately chosen set of parameters. Indeed, while the cusps near $q = \gamma_n^+$ (visible in Fig. 8.3 for all types of drives) are reminiscent of what was observed for the current, and can be understood in terms of a transition between Andreev reflection and QP dominated regimes, the presence of negative excess noise for the Lorentzian and the cosine drives is more intriguing (a regime where this was also true for the square drive was not found).

This can be understood with the help of Eqs. (8.6) and (8.7) where one notices that if the contribution of the different Floquet channels is non-linear in voltage, the noise is not necessarily equal to or larger than its DC counterpart. In practice, this non-linearity occurs primarily near the edges of the gaps $[\gamma_n^-;\gamma_n^+]$, which precisely corresponds to the regions of negative excess noise in Fig. 8.3. Focusing on just a subset of channels, considering only $n = -1$, 0 and 1, and noticing that the DC noise is a monotonically increasing concave function of the voltage (for $eV_{\rm DC} > \Delta$), see Fig. 5.2, it becomes quite easy to find a set of P_n satisfying both $\sum_n P_n = 1$ and

$$P_{-1}S_{\rm DC}\left(eV_{\rm DC} - \Omega\right) + P_1 S_{\rm DC}\left(eV_{\rm DC} + \Omega\right) < \left(1 - P_0\right) S_{\rm DC}\left(eV_{\rm DC}\right) , \tag{8.8}$$

which, in turn, leads to a negative value of the excess noise at this particular voltage. From this, it follows that the negative excess noise arises from the convexity properties of the DC noise, which is itself a consequence of the gap edge singularity in the spectrum of quasiparticles of the superconducting lead. This reduction of the noise below the DC level should be experimentally detectable for cosine or Lorentzian drives and might even be tuned so as to give relatively low total noise.

8.4.2. Excess Andreev noise to order λ^4

For voltages within the gap of a given Floquet channel, the PAN is only due to correlations between Andreev and normal reflections. The lowest order for such correlations is λ^4 and can be obtained analytically

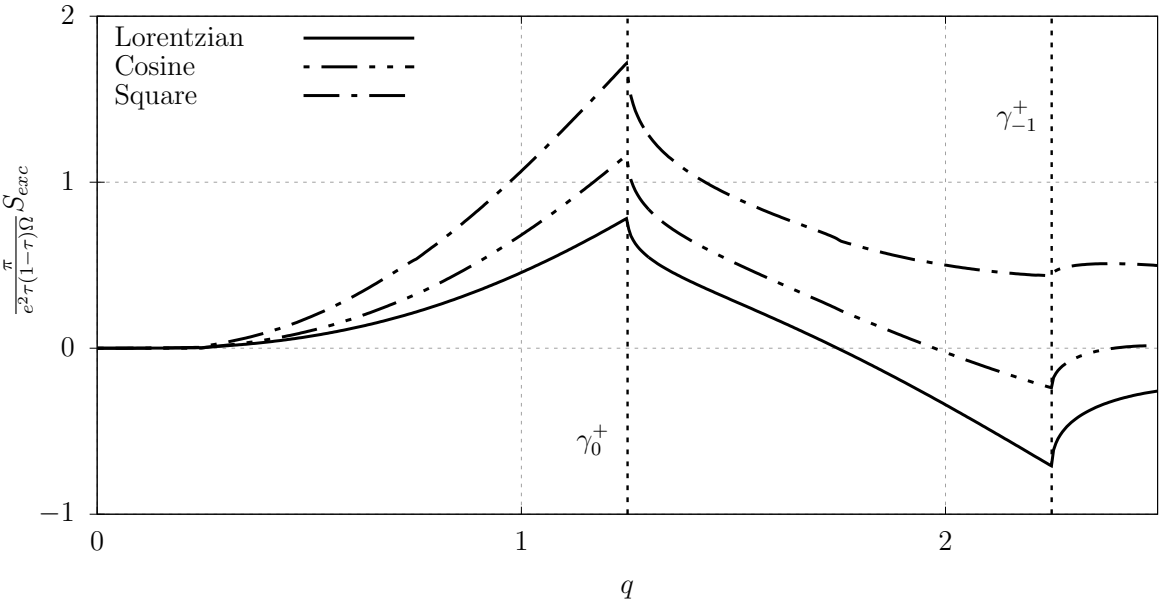

Figure 8.3.: Excess noise as a function of the injected charge q for three different drives (Lorentzian with $\eta = 0.15$, cosine voltage and square voltage), at frequency $\Omega = 0.8\Delta$, $\beta\Omega = 10^3$ and at low transparency ($\lambda = 10^{-2}$).

after some lengthy but straightforward algebra (additional details are presented in App. D.5.2). Indeed, for energies lying inside the effective gap of a particular channel, the retarded and advanced bare Green functions of the superconducting electrode are equal so that the corresponding greater (g^{+-}) and lesser (g^{-+}) Green functions vanish. However, since normal reflection also plays an important role in this regime and transport is non-linear, the calculation no longer simplifies into an expression involving effective Floquet weights, as it did in the Andreev limit of infinite gap, see Chap. 6. Instead, in this situation, the λ^4 noise contribution involving Andreev reflection is a sum over three harmonics indices and reads as

$$\begin{aligned}\overline{\langle S\rangle}^{(4)}_{\text{Andreev}} = 32\int_{-\infty}^{\infty}\frac{\mathrm{d}\omega}{2\pi}\sum_{nsr=-\infty}^{+\infty}\lambda^2\Delta_n\lambda^2\Delta_r p_n^* p_r p_{s-n}^* p_{s-r}\Theta\left(\Delta-|\omega+n\Omega|\right)\Theta\left(\Delta-|\omega+r\Omega|\right)\\ \times\left\{f\left(\frac{\omega-(eV_{\text{DC}}+s\Omega)}{2}\right)\left[1-f\left(\frac{\omega-eV_{\text{DC}}}{2}\right)\right]\right.\\ \left.+f\left(\frac{\omega-eV_{\text{DC}}}{2}\right)\left[1-f\left(\frac{\omega-(eV_{\text{DC}}+s\Omega)}{2}\right)\right]\right\},\end{aligned} \tag{8.9}$$

where $\lambda^2\Delta_n = \lambda^2\frac{\Delta}{\sqrt{\Delta^2-(\omega+n\Omega)^2}}$ is the Andreev reflection amplitude of the Floquet channel n, and $\Theta(x)$ is the Heaviside distribution.

This term cannot be further reduced into a simpler form only involving Floquet weights, as obtained in Eq. (8.7) for the $O\left(\lambda^2\right)$ contribution to the noise. This means that, in this intermediate regime, the noise can no longer be interpreted as a sum of independent contributions coming from all Floquet channels. Instead, the PAN now involves products of two types of terms, for example $\lambda^2\Delta_r p_r p_{s-r}$, which describes the interference between two transport events, Andreev and normal reflections.

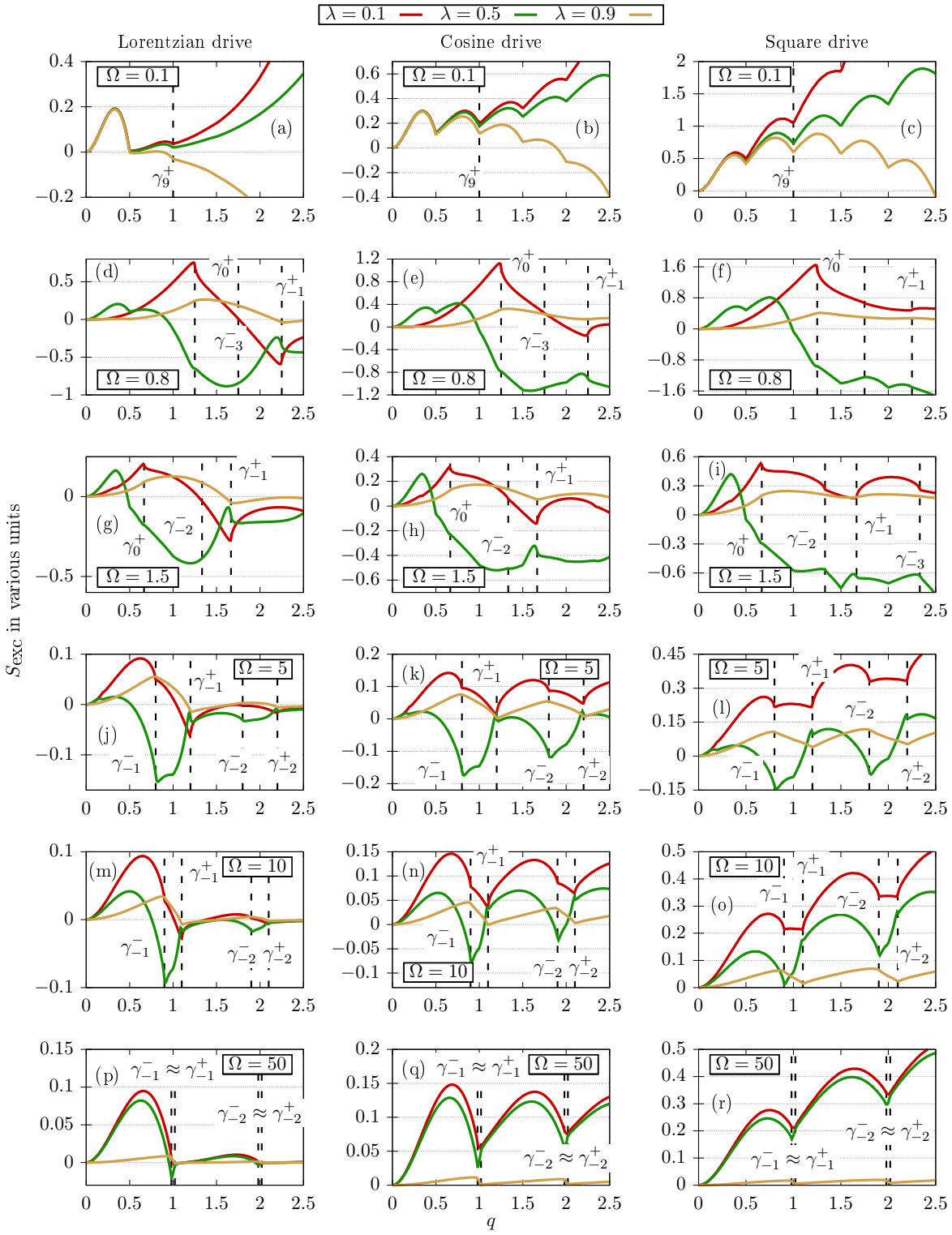

Figure 8.4.: The excess noise at an $N-S$ junction for three different drives and different transparencies as a function of the injected charge q for low temperature: $\beta\Omega = 10^3$. Warning: the curves are not all normalized in the same way. For $\Omega = 0.1\Delta$, i.e., plots (a)-(c), they are all in units of $e^2\Omega\tau_A(1-\tau_A)/\pi$, for $\Omega \neq 0.1\Delta$, the excess noise is in units of $e^2\Omega\tau(1-\tau)/\pi$ *except for the case* $\lambda = 0.9$ *where the excess noise is in units of* $e^2\Omega\tau_A\tau/\pi$.

8.5. Full numerical approach

. The noise can be probed through an excess noise analysis by performing a detailed quantitative investigation. The excess noise is numerically obtained in a wide range of parameters, from low to high transparency, from frequencies smaller to larger than the gap and for three different drives (cosine, square, and Lorentzian). The corresponding plots are displayed in Fig. 8.4.

As explained in the caption of Fig. 8.4, in order to display the curves on the same graph, the normalizations of the excess noise were adjusted as follows. For $\Omega = 0.1\Delta$ [Figs. 8.4(a)–8.4(c)] the normalization is $\tau_A(1-\tau_A)\Omega/\pi$ because this constitutes the Andreev-dominated regime. For $\Omega \neq 0.1\Delta$ [Figs. 8.4(d)–8.4(r)] the excess noise is normalized by $\tau(1-\tau)\Omega/\pi$ for low ($\lambda = 0.1$) and intermediate ($\lambda = 0.5$) transparencies in order to characterise the transition to the normal-metal regime. Finally, for $\Omega \neq 0.1\Delta$ and high transparency ($\lambda = 0.9$), i.e., the red curves in Figs. 8.4(d)–8.4(r), the excess noise is normalized by $\Omega\tau_A\tau/\pi$ as it now involves both Andreev reflection and QP-transfer.

Starting with some general observations, for drive frequencies much smaller than the superconducting gap Δ [Figs. 8.4(a)–8.4(c)], all signals, at all transparencies, exhibit a minimum at $q = 1/2$, depicted by "arches" with a positive excess noise. For the Lorentzian drive, this first arch is characterized by a fully suppressed excess noise at $q = 1/2$, which constitutes the half-Leviton regime. These minima typically persist for larger $q = n/2$ (n integer), although they get less and less visible as the amplitude of the arches quickly decreases. In the opposite limit of frequencies much larger than the gap [Figs. 8.4(p)–8.4(r)], the minima still occur for all signals at all transparencies, only they are now located at integer q, mimicking the excess noise of a normal-metal junction. These integer minima yield a zero excess noise only for the Lorentzian drive.

Tunneling regime. Let us first focus on the tunneling regime, corresponding to all red curves in Fig. 8.4 (associated with $\lambda = 0.1$).

In the low-frequency regime [Figs. 8.4(a)–8.4(c)] , the excess noise is characterized by arches with local minima for half-integer values of q, on top of a monotonously increasing background contribution. For the Lorentzian drive, and unlike the other two, the amplitude of these arches quickly vanishes making them barely visible beyond $q = 1$, while they look much more robust for cosine and square drives. As argued in Chap. 6, in the Andreev regime, these signatures are typically associated with the preeminent role of Andreev reflection processes.

Increasing the driving frequency to values comparable with the superconducting gap [$\Omega = 0.8\Delta$ in Figs. 8.4(d)–8.4(f), $\Omega = 1.5\Delta$ in Figs. 8.4(g)–8.4(i)], these half-integer arches get completely washed out and the only remaining features in the excess noise are cusps located at the edges of the Floquet channel effective gaps. This change of behavior is attributed to the onset of the contribution of QP-transfer. Indeed, for such intermediate frequencies, QP-transfer becomes important, ultimately drowning out the contribution from Andreev reflection processes which involve higher order terms in the tunneling constant. Negative excess noise might be visible for the Lorentzian and cosine drives, as already explained in Sec. 8.4.1.

Increasing further the driving frequency [$\Omega = 5\Delta$ in Figs. 8.4(j)–8.4(l), $\Omega = 0\Delta$ in Figs. 8.4(m)–8.4(o)] leads to the resurgence of arches, only now extending beyond half-integer values of q and all the way to the edge of the effective gaps. For very large frequencies [Figs. 8.4(p)–8.4(r)], these gap edges tend to merge at integer values of the injected charge. The resulting excess noise then fully corresponds to that of a normal junction, recovering the results of Chap. 3 and identically matching the predictions of Ref. [23].

It is important to stress out that these integer arches observed at $\Omega \gg \Delta$ are not a deformed version of the half-integer ones obtained for $\Omega \ll \Delta$, as the two sets rely on very different physical mechanisms, namely QP-transfer and Andreev reflection, respectively. Tuning the driving frequency favors one process over the other, leading to the corresponding set of local minima.

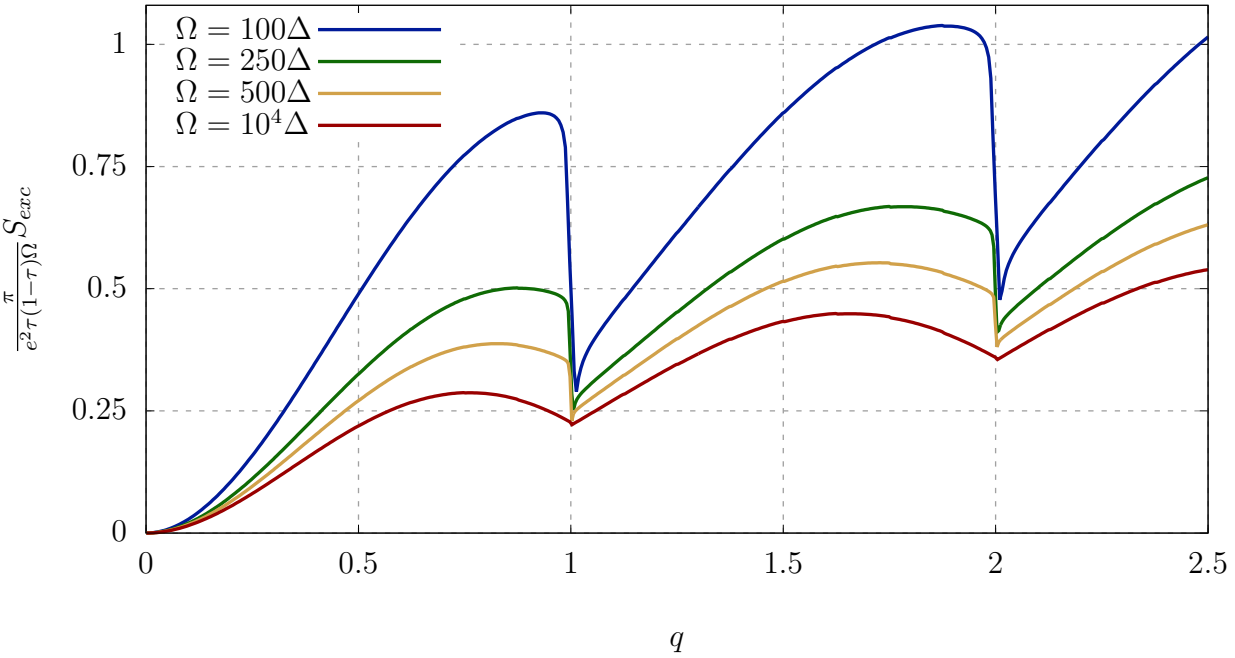

Figure 8.5.: The Excess noise at the highly transparent junction ($\lambda = 0.9$) driven by a square drive of different frequencies (specified on the right of the curves), as a function of the injected charge and at low temperature: $\theta = 10^{-3}\Omega$.

Intermediate transparency regime. This regime corresponds to the green curves in Fig. 8.4 (associated with $\lambda = 0.5$).

As in the low-transparency regime, arches with local minima for half-integer q can be observed at low frequency [$\Omega = 0.1\Delta$, Figs. 8.4(a)–8.4(c)]. They disappear at higher frequency, giving way to marked structures at the edges of the effective gaps of the Floquet channels, which then evolve into another set of arches extending between γ_{n-1}^{+} and γ_n^{-}. At very high driving frequency [Figs. 8.4(p)–8.4(r)], these gap edges satisfy $\gamma_n^{-} \approx \gamma_n^{+}$ and $\gamma_{n+1}^{\pm} - \gamma_n^{\pm} \approx 1$ and, for all drives, the arches with minima at integer q are recoveres as expected from Chap. 3.

However, this regime also differs from the low-transparency case in two important ways. First of all, one needs to go to much higher frequency in order to see the half-integer minima completely disappear, as remnants of these arches can still be observed at frequencies as high as 1.5Δ [Figs. 8.4(g)–8.4(i)]. This can be interpreted as being related to the higher value of the tunneling constant, which thus allows Andreev reflection processes above the gap to remain quite important even at relatively high frequency. Secondly, it appears that negative excess noise can be observed over much larger regions of the bias voltage, and for all considered drives [Figs. 8.4(d)–8.4(n)]. Again, it is believed that this has to do with the larger tunneling constant, as was argued previously, this reduction of the period-averaged noise compared to its DC level counterpart was to be attributed to interference effects between Andreev reflection processes and standard reflection across different Floquet channels, which become much stronger at intermediate transparency.

Quasi-transparent junction. This corresponds to the set of orange curves in Fig. 8.4 (associated with $\lambda = 0.9$).

As in the previous two regimes analyzed, and in accordance with the results from Chap. 6, the excess noise exhibits two different types of arch structures: one present at very low frequency [Figs. 8.4(a)–8.4(c)]

with local minima located at half-integer q, and one at high frequency [Figs. 8.4(p)–8.4(r)] with minima located at integer values of the injected charge.

In-between these limiting regimes, however, the excess noise is rather featureless, only showing slight kinks near the edges of the effective gaps $\gamma_n^{\pm}$. As it turns out, all the physics studied thus far, with the interplay between Andreev reflection and QP-transfer, is strongly dominated by standard reflection up to very high order, which tends to smooth all previously observed signatures.

The only notable feature of this regime lies in the very high frequency regime where, while arches clearly appear with local minima located at integer values of the injected charge q, they typically seem to be much more asymmetric than at lower transparency. This is made clearer in Fig. 8.5 where the excess noise is displayed for increasingly higher frequency, from $\Omega = 10^2\Delta$ to $\Omega = 10^4\Delta$. Here the focused is solely on the square drive for illustrative purposes. It seems that this asymmetry is somewhat related to Andreev reflection processes as the steepest parts of the plots correspond to the effective gaps $[\gamma_n^-;\gamma_n^+]$, which ultimately shrink down to zero as the frequency increases further.

In the end, this may seem like the least interesting regime when looking at the characteristic signatures of the excess noise. However, as argued in Chap. 7, it may also be the most relevant one when it comes to practical applications.

8.6. Conclusion

In this chapter, the study of the $N-S$ junction under a periodic drive was pushed to the intermediate regime. On one hand, the period-averaged current was computed numerically to all orders in the tunnel coupling. The noise on the other hand could only be tracted analytically to second and fourth order in tunneling. The general regimes of low to high frequencies as well as tunnel couplings was studied numerically in order to validate the analysis developped in previous sections.

When the gap is comparable to the frequency, the period-averaged current can be expressed analytically, and for low transparencies it displays strong kinks at the boundaries of the gap of each Floquet channel, surrounding integer values of the integer charge. These sharp discontinuities mark the switch from an Andreev reflection-driven current to a QP-transfer-driven one. In this regime, the AC noise can be lower than the DC one, showing that the usual correspondence between the excess noise and the number of holes pairs created by the drive does not hold anymore. Furthermore, the noise can no longer be expressed in a self-contained form, and one has to resort to a perturbative expansion in the tunneling constant was perform, or to a numerical evaluation to all orders in λ, proving that the Floquet channel gap edges are responsible for the structures (cusps and minima) of the excess noise.

Inspecting more closely the analytic derivations, it was shown that the period-averaged current follows a Tien-Gordon behavior [19], for the whole range of parameters. The same goes for the noise, which also satisfies Tien-Gordon-type relations, but only in the limiting regimes, dominated by QP-transfer or Andreev reflection and to second order in tunneling in all regimes. It was possible to provide an interpretation of these results in terms of the leading physical processes also accounting for the interference effects expected between different Floquet channels. To summarize, it was shown that the full crossover regime of intermediate frequencies (comparable to the gap) can be understood and in particular, the negative excess noise can be attributed to the fact that the density of states in the superconductor is not constant near the gap edges. Furthermore, the Tien-Gordon relations for the noise (established in the limit where the gap is larger than the drive frequency) break down in the intermediate regime because of interferences between different Floquet channels. The present theoretical results could in principle be probed experimentally in normal-metal/superconducting junctions where a microwave photon source irradiates the normal-metal side, in the same spirit as in the pioneering work of Ref. [121] which dealt with diffusive metals and (only) a sinusoidal drive.

Part III.

QPC in a fractional quantum Hall bar

9. Quantum Hall effect fundamentals

9.1. Introduction

This chapter presents the basics of the quantum Hall effect (QHE) and more precisely the fractional quantum Hall effect (FQHE), even though the integer quantum Hall effect (IQHE) is discussed to set the stage. The setup is the following, a two-dimensional electron gas (2DEG) of width W (x axis) and length L (y-axis) is driven by a DC voltage in the y direction V_y. The electric current therefore flows along the y direction and the longitudinal resistance $R_{yy} = I/V_y$ is the typical observable measured. Then the sample is put inside a normal magnetic field B (along the z-axis), a charge imbalance develops along the x direction due to the Lorenz force, leading to the formation of a transverse voltage, called the Hall voltage V_H. Typically in this case, the classical Hall conductivity

$$R_{xy} = V_H/I = B/n_e e\,, \tag{9.1}$$

where n_e is the surface electron density, is also measured. This is the classical Hall effect [122], where typically the Hall resistance is plotted as a function of the magnetic field, with a linear relation allowing to measure the electron density. When the magnetic field is increased quantum effects become important. A quantum theory without interaction between electrons will be enough to understand experimental data for certain values of the magnetic field, this is the integer quantum Hall effect (IQHE). For higher values of the magnetic field, including interactions in higher mobility heterostructures, and in particular Coulomb interaction, is unavoidable in order to construct a proper understanding of the system.

This chapter will start by a short summary of general quantities related to the quantum Hall effect in Sec. 9.2. Then a summary of the history and explanation of the IQHE is provided in Sec. 9.3, very few computations are performed but references to the relevant literature are given. Follows Sec. 9.4 which is longer as it explains the basics of the FQHE, from its action which justifies the presence of edges states in the form of chiral Luttinger liquid, to the techniques of bosonization used to derive transport properties of the simplest edges states. Finally the generalization to all Abelian edge states is presented and the main experimental approaches to probe them are recalled.

9.2. Generalities

The simplest quantum mechanical theory of electrons in a magnetic field yields a Harmonic oscillator behavior, with the cyclotron frequency

$$\omega_c = eB/m \tag{9.2}$$

as the energy scale between the so-called Landau levels

$$E_n = \omega_c \left(n + \frac{1}{2}\right)\,. \tag{9.3}$$

The wave functions for the electrons in this system can be found in any quantum mechanics textbook, they are plane waves along y and are localized in the x direction because of the magnetic field in the Landau gauge. As a result, there can be many different states with the same energy but localized on different places of the sample. In particular they are centered around $x_0(q) = 2\pi q l_B^2/W$ where q is an integer quantum

number and

$$l_B = (eB)^{-1/2}\,, \tag{9.4}$$

is the magnetic length in units where the speed of light $c = 1$ and $\hbar = 1$. Therefore, a sample of size W along x can host a finite number of such states of the same energy, this is the maximal degeneracy of the Landau levels

$$N_{\text{deg, max}} = \frac{WL}{2\pi l_B^2}\,, \tag{9.5}$$

One notices that the maximal degeneracy is also equal to the number of magnetic flux quantum $\phi_0 = 2\pi/e$, hence the electrons arrange themselves spatially such that each one of them can grab exactly one flux quantum. One therefore defines the so-called filling factor as the ratio between the total number of electrons WLn_e and the maximal degeneracy of the Landau level, it reads as

$$\nu = \frac{2\pi eB}{n_e}\,, \tag{9.6}$$

and grows linearly with the magnetic field. This description is lacking for many reasons, the main ones are that the edges are not taken into account, no interactions are considered and collective behavior is absent as this is first quantization. Therefore, it is time to separate the treatment in two sections, with and without coulomb interactions.

9.3. Integer quantum Hall effect

The history of the basic theory behind the IQHE started 40 years ago and was stabilized 30 years ago, there are mainly four stages. First, of course, its experimental discovery in 1980 by von Klitzing, Dorda and Pepper [123] in 1980. The main finding is that the transverse resistivity displays plateaus as a function of the magnetic field and that this behavior is very robust to disorder and perturbations. A hand waving model based on edge modes was introduced by Halperin [124] and Laughlin [125] based on gauge invariance and allowing to derive a conductance matching the experimental results [126, 127]. Extending these two approaches and giving them a solid footing, Buttiker [128] considered a realistic sample and used the scattering approach to compute the conductivity. In particular, he showed that the edge states are chiral because the magnetic fields tends to cancel backscattering, this also explained the robustness of the conductivity when impurities are inserted. This is usually considered as a satisfactory explanation of the IQHE.

However, another theory gave a deep mathematical founding to the robustness of the IQHE, in terms of the topological properties of the band structure of the model. In particular, Thouless *et. al.* [129], in the so-called TKNN paper, studied the band structure of the bulk IQHE, they computed the conductivity with the Kubo formula and showed that it is equal to a certain prefactor times an integer which only depends on the band structure. As shown by Simon [130], the state space defines a fiber bundle over the Brillouin zone, this allows to use all the theorems regarding such mathematical constructions.The main finding of Simon is that the integer found by TKNN is in fact the Chern number[1] associated to this fiber bundle. It is to be noted that this line of thought is now used very often in the context of topology in condensed matter. In the particular case of the IQHE, the quantization of the conductivity is therefore seen as a topological property of the state space for a certain Brillouin zone, this explains the robustness of the conductivity with respect to any perturbations[2] and not only disorder. The problem is that in this approach the current

[1] The Chern number is the integral of the Chern class, and this integral is the number of zeros of any continuous section of the fiber bundle [131], thus it is always integer.

[2] As long as these perturbation do not change the said topological properties that is.

is carried by the bulk and not the edges (as there are no edges in the TKNN model).

This picture is appealing, thus, people looked for a way to put topology in Buttiker's result. For a few years this was done by invoking the mysterious bulk-edge correspondence. It basically keeps the best of both worlds, the current is carried by edge states, but it is robust because of the topological properties of the bulk. Topology was actually brought to the edges by Hatsugai in a series of papers [132, 133] in which a tight binding model with edges and boundary conditions was designed. It allowed, without a particular choice of confining potential, to find that the presence of edges indeed creates gapless states whose wave functions are exponentially suppressed in the bulk, whereas the bulk contains only gapped states. The conductivity was indeed found to be linked to a topological property of the energy space and the Brillouin zone, but not the Chern number this time, a quick overview is tried next. The energy spectrum can be analytically continued to complex space, therefore, to a given state, there will correspond a curve in the complex energy space. This space is found to be a Riemannian surface with genus equal to the number of edge states, hence the topology of the energy space is linked to the number of edge states. The energies of the bulk states were found to correspond to closed loops which do not circle around a hole of the surface whereas the energies of the edge states do correspond to loops around such holes. Therefore, adding 2π to k_y amounts to turning around a hole of the energy surface and the number of turns is defined as the winding number of the edge state. The main result of Hatsugai is that the Hall conductivity is proportional to the sum of the winding numbers of all the edge states present at a given energy. The generality of this result is also important, it only requires two things: that there are gaps in the energy spectrum of bulk states, whatever the size of these gaps and that in each gap there gapless edge states.

This picture holds for the integer quantum Hall effect as it explains the plateaus of the conductance for integer values of the filling factor. However, in 1982 [68], Tsui and Stormer observed plateaus of the Hall conductivity for fractional values of the filling factors. Thus the results of Buttiker and Hatsugai do not hold and one has to consider another Hamiltonian, with Coulomb interaction this time.

9.4. The fractional quantum Hall effect

An absolutely general solution, from first principles, to the problem of electrons in a magnetic field under Coulomb interaction with Hall geometry is still lacking. However, the standard field theoretic approach, that was initiated in the late 80's and that is summarized in Ref. [134], provides a very good description of the effect, as will be showed below. Including interactions gives rise to a plethora of new correlated states of matter which will differ depending on the value of the filling factors. Hence, only the minimal discussion required to understand the transport theory developed later is provided. In particular, the bulk properties will be discussed first and very shortly while the edge states will be discussed in more lengths.

9.4.1. Bulk behavior

This section is strongly inspired by Refs. [135, 136], where the fractional quantum Hall effect is understood as a $U(1)$ Chern-Simons effective theory. The Hamiltonian of the system, for N electrons, in first quantization reads as

$$H = \sum_i^N \frac{1}{2m} \left(p(x_i) - eA(x_i)\right)^2 + eA_0(x_i) + \sum_{i<j} V(|x_i - x_j|)\,, \tag{9.7}$$

where A_0 is the scalar potential and A is the vector potential of the electromagnetic field associated with the electrons. The standard derivation of the action is not performed in detail here as it requires to introduce too much material. The action will typically contain A, the $U(1)$ Maxwell gauge potential of Electrodynamics and possibly other fields describing both the interactions between electrons and the background magnetic

field. In the simplest picture, called the Laughlin series, only one additional gauge field is considered, it is called a. This is an emergent field which describes the collective behavior of the interacting background of electrons. The equations of motion are derived by writing down a conserved current, in the present situation, the sample is made of electrons, thus the conserved current is the electron current, noted $J = (\rho, j)$. It is written in terms of the field a so as to be immediately conserved

$$J_\mu = \frac{e^2}{2\pi}\epsilon^{\mu\nu\lambda}\partial_\nu a_\lambda \,. \tag{9.8}$$

The next step is to write down the action for the coupling between this matter field and the gauge potential. The action contains all the possible terms which respect gauge invariance, however, skipping the details (see [136, 137]) all the irrelevant terms in 2+1 dimensions are removed, those which disappear from rotational invariance are removed, and only the global (non local) gauge invariant term is considered. Considering only the lowest Landau level[3], this action reads as

$$S = \frac{e^2}{2\pi}\int \mathrm{d}^2t\mathrm{d}t\left(\epsilon^{\mu\nu\lambda}A_\mu\partial_\nu a_\lambda + \frac{m}{2}\epsilon^{\mu\nu\lambda}a_\mu\partial_\nu a_\lambda\right) , \tag{9.9}$$

one could say that the first term describes coupling between matter and gauge field and the second one is the purely matter Chern Simons term, where m is its coupling constant.

All the known properties of the FQHE involving one emergent field only can be derived from this action. For example, it is shown in Ref. [137] that in order to respect gauge invariance and to be consistent with Schrodinger's equation, the Chern-Simons coupling constant is quantized $m \in \mathbb{Z}$. Furthermore, after integrating out the matter degree of freedom, a simple computation of the conductivity, as the variation of the action when the matter current varies, yields

$$J_i = \frac{\delta S_{CS}[A]}{\delta A_i} = -\frac{e}{2\pi m}\epsilon_{ij}eV_j \,. \tag{9.10}$$

which immediately means that

$$\sigma_{xy} = \frac{e}{2\pi m} \,. \tag{9.11}$$

Furthermore, the quasiparticle excitations can be characterized by adding a coupling between the emergent field and its current,

$$S_{exc} = \int \mathrm{d}t\mathrm{d}^2x a_\mu j^\mu \,. \tag{9.12}$$

A standard exercise is to considering N excitations strongly localized in space

$$j^0(x,t) = \sum_{n=1}^{N}\delta(x - x_n) \qquad \text{and} \qquad j^i = e\sum_{n=1}^{N}\partial_t x_n \delta(x - x_n) \,, \tag{9.13}$$

Following [136], it can be shown that each of these quasiparticles carry a flux ϕ_0/m and a charge e/m. Further, when one particle is circling around another, after a half circle, it has gained a phase $\theta = 2\pi/m$. This corresponds with Wilczek's result [138], who invented the term anyons in 1982 [139], that charge particles circling around fractional magnetic fluxes behave as a flux-tube-particle composite and have neither fermion nor boson behavior when exchanged but *any* behavior. This is the main result for the FQHE, its excitations have fractional charge and fractional statistics. However, this is not the definite picture for the problem at hand, indeed, as was the case in the IQHE, the bulk behavior is impacted by the presence of

[3] Which amounts to ignoring the Chern Simons action for the Maxwell gauge potential.

edges.

9.4.2. Edge theory and Luttinger liquids

The derivation of the impact of the edge on the action by Wen in 1991 [140] is followed here. Starting from the Chern-Simons action, he remarked that when the boundary is taken into account, the action is not invariant under a $U(1)$ transformation of the gauge potential A. In order to remedy this problem and as usual in field theory with gauge anomalies, it is necessary to introduce another gauge field which, from general grounds, can be shown to be a chiral edge mode. The action of such a mode is originally only here to preserve gauge invariance in the bulk, but ends up ensuring the presence of edge modes. Only from these general considerations, it can be seen that the edge modes are a global properties of the system, hence their topological nature.

Wen proceeds as follows, first, he derives the main properties of the edge action, for example, in order for it to restore gauge invariance and provided that it is local[4], it should include gapless excitations. Then, he focuses on the low energy behavior of these gapless excitations, in particular, when $|kl_b| \ll 1$ and only one branch is present, the new chiral edge modes ρ obey

$$\begin{aligned} [H, \rho_k] &= vk\rho_k \\ [\rho_k, \rho_{k'}] &= v_F k \delta_{k+k'} \,. \end{aligned} \tag{9.14}$$

this is the celebrated Kac-Moody algebra, and the ρ fields can be rewritten in terms of bosons. An important point to raise here is that Eq. (9.14) is the basic operator identity describing the Tomonaga model for *chiral* Luttinger liquids. A very good historical review of how this theory came about (in the non chiral case) is given in Ref. [141].

The following summarizes the essential results of *chiral* Luttinger liquids. Considering only energies close to the Fermi level, there is only one branch in momentum space k and the energy reads as $E_k \approx v_F k$. Hence, the fermionic Hamiltonian reads as

$$H = \sum_k k v_F a^\dagger_{sk} a_k + \frac{1}{2L} \sum_{k,k',q} V(q) a^\dagger_{k-q} a^\dagger_{k'+q} a_{k'} a_k \,. \tag{9.15}$$

There are some constraints on the second term as electrons can only be scattered on the same branch, which is called forward scattering (as opposed to backscattering). Further imposing that the total momentum transfer is conserved the scattering of an electron can only occur by an exchange of momentum $q \ll k_F$, with a weight $g \approx V(0)$. Thus, writing the density operator as

$$\rho_q = \sum_k a^\dagger_{s,k+q} a_{s,k} \,, \tag{9.16}$$

the Hamiltonian reads as

$$H = \sum_k k v_F a^\dagger_k a_k + \frac{1}{2L} \sum_{q \ll k_F} g \rho_q \rho_{-q} \,. \tag{9.17}$$

The second term is just the free Hamiltonian for chiral sound waves of electrons. Furthermore, it can be shown that

$$\begin{aligned} \left[\rho_q, \rho_{q'}\right] &= -\frac{qL}{2\pi} \delta_{q,-q'} \\ [H_0, \rho_q] &= q v_F \rho_q \,, \end{aligned} \tag{9.18}$$

[4] In the sense that the associated current commute at different points in space or that the commutator in momentum space is smooth around $k = 0$.

which is exactly the commutation relations found for the chiral gauge field on the edge of the FQHE sample. This is why they are often described as a chiral Luttinger liquid with interaction density $g = \pi v_F/\nu$. Of course, in the FQHE there are two chiral LL, one on each edge, with opposite chirality, i.e., with opposite velocity. There exist a nice intuitive picture allowing to retrieve the Luttinger liquid behavior of one of the edges and quantify the interaction strength. It is called the hydrodynamical approach to the fractional quantum Hall effect and was invented by Wen in 1995 [134].

9.4.3. Hydrodynamical approach

The starting point is droplet of FQHE with a disc shape, focusing on the edge states, the Hamiltonian reads as

$$H = \frac{1}{2}\int \mathrm{d}x\, e\rho(x)V(x)\,, \tag{9.19}$$

where $V(x)$ is a potential that forces the droplet to keep its shape and x is along the radial direction while y is tangent to the droplet surface. This potential can be expressed as a function of the electric field responsible for the confinement, assuming that the displacement of the droplet around y is $h(x)$, the electric field reads as

$$E(x) = \frac{V(x)}{h(x)}\,. \tag{9.20}$$

Applying a magnetic field in the direction normal to the plane, some excitations will turn around the droplet with a drift velocity v computed from

$$v = \frac{E}{B}\,. \tag{9.21}$$

As a result, the potential will be written as

$$V(x) = vBh(x)\,. \tag{9.22}$$

Then it is recalled that the flux density $n_\phi = N_\phi/S$, where S is the surface, reads as B/ϕ_0. The filling factor links the electron density n_e to the flux density thus one can write

$$n_e = n_\phi \nu = \nu B/\phi_0\,. \tag{9.23}$$

Finally, defining the edge state density as $\rho(x) = n_e h(x)$, the Hamiltonian reads as

$$H = \frac{v\pi}{2\nu}\int \mathrm{d}x\, \rho(x)^2\,. \tag{9.24}$$

Going to Fourier space (with period L), it transforms into

$$H = \frac{v\pi}{2\nu L}\sum_k \rho_k\rho_{-k}\,, \tag{9.25}$$

and the chiral Luttinger liquid with interaction density $\pi v/\nu$ is retrieved. In the next section, the derivation of the correlation function using the bosonization technique is quickly highlighted.

9.4.4. Bosonization

The aim of this section is to derive a formula for the Green's functions of fermions at finite temperature, this was done in the 60's-70's with various techniques, the one used here is that of bosonization. An extensive review of this technique is provided in Ref. [142], so only the results specific to the FQHE are given here.

As a starter, the Hamiltonian is typically written as

$$\mathcal{H} = \frac{v}{4\pi}\int_0^L \mathrm{d}x\ [\partial_x\phi(x)]^2\ , \tag{9.26}$$

where v is the drift/Fermi velocity along the edges and $\phi(x)$ is a bosonic field which is related to the one dimensional electron density $\rho(x) = \sqrt{\nu}\partial_x\phi(x)/2\pi$. Similarly to what was done for phonons in Chap. 4, it is possible to write down the bosonic field $\phi(x)$ in real space as a function of the bosonic fields b_k in momentum space as

$$\phi(x) = \frac{2i\pi}{L}\sum_k \frac{e^{-ka/2}}{\sqrt{k}}\left(e^{ikx}b_k - e^{-ikx}b_k^\dagger\right)\ , \tag{9.27}$$

where a is a small distance that is used to regularize ultraviolet divergences. Due to their fermionic nature, a relation between the electron creation operator $\Psi^\dagger$ and the latter's density $\rho(x)$ can be established:

$$\left[\rho(x),\ \Psi^\dagger(x')\right] = \delta(x-x')\Psi^\dagger(x)\,. \tag{9.28}$$

This means that the electron creation operator can be written as

$$\Psi^\dagger(x) = \frac{1}{\sqrt{2\pi a}}e^{\frac{i}{\sqrt{\nu}}\phi(x)}\,. \tag{9.29}$$

Using the Kac-Moody commutation relation

$$[\phi(x),\phi(x')] = i\pi\mathrm{sgn}(x-x') \tag{9.30}$$

and the Baker-Campbell-Hausdorff identity, it can be shown that:

$$\Psi(x)\Psi(x') = e^{i\frac{\pi}{\nu}\mathrm{sgn}(x-x')}\Psi(x')\Psi(x)\,, \tag{9.31}$$

so electron operators obey anticommutation relations only if $\nu = 1, 1/3, 1/5, 1/7, ...$, i.e., for Laughlin filling factors. Note that other rational values of ν are physically attainable and exhibit the FQHE, but the above derivation needs to be generalized in order to include the presence of several bosonic fields [143]. In what follows, the focus is on the simpler situation of the Laughlin series for clarity's sake. The main results can be readily obtained for the case of a general Abelian FQHE edge involving multiple bosonic modes, but do not fundamentally differ from the Laughlin filling factors. The quasiparticle operator is a local vertex operator[5] and it is required to commute with the electron operator, which justifies the choice:

$$\psi(x) = \frac{1}{\sqrt{2\pi a}}e^{i\sqrt{\nu}\phi(x)}\,. \tag{9.32}$$

From Eq. (9.32), it is also possible to define the statistical angle Θ. Indeed, focusing on a given time $\tau = 0$, one readily obtains a nontrivial phase factor when exchanging two quasiparticles in real space, namely

$$\psi(x)\psi(x') = e^{i\pi\nu\mathrm{sgn}(x-x')}\psi(x')\psi(x)\,, \tag{9.33}$$

which is a clear illustration of anyonic statistics, with a statistical angle specified by $\Theta = \pi\nu$.

Anticipating the question of transport quantities, the Green's function as a function of time for the quasiparticles is computed next. It is usual to compute first the bosonic Green's function and link it with

[5] In the sense of Ref. [144].

the quasiparticle Green's function, this is done in App. F and yields, at the point $x = 0$

$$\left\langle e^{i\sqrt{\nu}\phi(x=0,\tau)} e^{-i\sqrt{\nu}\phi(0,0)} \right\rangle = e^{\nu \mathcal{G}(\tau)} , \tag{9.34}$$

where the bosonic Green's function reads as

$$\mathcal{G}(\tau) = -\log\left[\frac{\sinh\left(\theta\pi(i\tau_0 - \tau)\right)}{\sinh\left(i\theta\pi\tau_0\right)}\right] , \tag{9.35}$$

and $\tau_0 = a/v_F$ is the short time cutoff of the Luttinger liquid theory. At zero temperature, the resulting correlation function, follows a power-law decay in time as

$$\left\langle \psi(0,\tau)\psi^\dagger(0,0) \right\rangle = e^{\nu \mathcal{G}(\tau)} \sim \tau^{-\nu} , \tag{9.36}$$

This allows to define the scaling dimension ν_D of the quasiparticle operator [6], which, in the case of Laughlin filling factors, reduces to $\nu_D = \nu$.

9.4.5. Quantum transport at a QPC

As usual, quantum transport at a QPC, through a measure of current and noise, provides a way to probe the actual excitations of the system. In particular, in the FQHE, as was shown before, the systems carrying the current are the edges. A QPC is defined by a region in which propagating states are scattered, in the case of chiral edge state, in order to have to possible outputs, the two edges have to be close to each other. One can therefore imagine two types of QPC, either two leads are put close to each other or a local constriction is applied to a single bar so that tunneling occurs between the two edge channels. The former case will later be called strong backscattering (SB), and the former weak backscattering (WB), they are illustrated in Fig. 9.1. The current was first computed by Wen [146] in the tunnel limit, he found that the $I - V$ relation is non linear, more precisely that

$$\begin{aligned} \langle I \rangle_{SB,\theta=0} &= V^{2/\nu - 1} \\ \langle I \rangle_{WB,\theta=0} &= V^{2\nu - 1} . \end{aligned} \tag{9.37}$$

The remarkable fact that the strong backscattering regime can be obtained by setting $\nu \to 1/\nu$ was explained by Kane and Fisher [147].They found a renormalization group flow to describe the transition between the strong and weak backscattering regimes. Their findings may be summarized as stating that the action in the weak backscattering case involves ν whereas in the strong backscattering case ν is replaced by ν^{-1}.

A few years later, the current noise at the QPC was also computed in the tunnel limit [147, 148] and was shown to be Poissonian at zero temperature, i.e., it yields the same power law as the current. It is important to keep in mind that the tunnel regime is often called the Poissonian regime even though the current is only Poissonian at zero temperature.

9.4.5.1. Minimal excitation states at the QPC

Importantly, the behavior of Levitons in such a QPC was probed by an excess noise analysis in Ref. [52] in the weak backscattering regime. It was shown that, to second order in λ, the noise follows a Tien-Gordon

[6] There exists an alternate definition in the literature, which only differs by an extra factor 1/2. It is mostly a matter of convention and does not affect the main message and results.

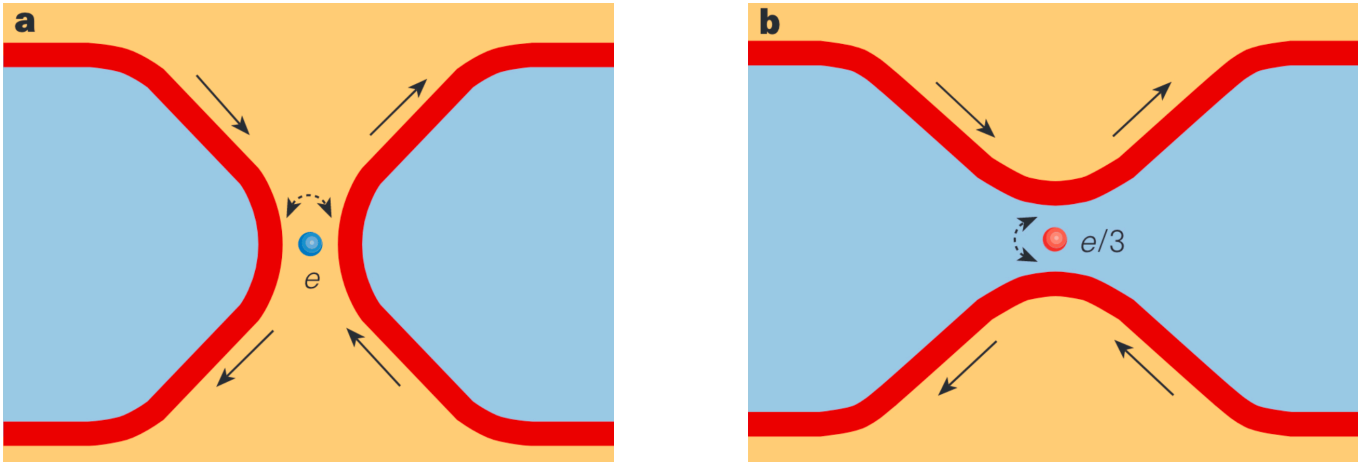

Figure 9.1.: Illustration of a fractional quantum Hall bar, in blue, pinched off by a quantum point contact, the edges are depicted in red (taken from [145]). a) in the strong backscattering regime, the gate drive is important and the bar is broken in two, only electron tunneling occurs at the QPC. b) the gate drive is low enough so that tunneling of quasiparticles can occur between the two edges.

behavior and that it is proportional to the average number of holes created by the drive. As a result, when the injected charge q is integer, no holes are created by the drive but, on average, an integer number of electron charge is involved in tunneling. Thus, a way to excite single quasiparticles or anyons was not found, this is in contrast to other QPC's considered like between normal metals and BCS superconductors.

9.4.6. General model for Abelian fractional quantum Hall edge states

All that was said before is valid for the simplest edge state, that of the Laughlin sequence. This can be extended to more complicated edge structure, these include both Abelian and non-Abelian states [134], though the focus here is on Abelian states. The starting point to extend the previous results is the action of the general Abelian FQHE edge

$$S = \frac{1}{4\pi} \int \mathrm{d}x\, \mathrm{d}t \sum_{l=1}^{N} \left[-\chi_l \partial_x \phi_l \partial_t \phi_l - v_l \left(\partial_x \phi_l\right)^2 \right], \tag{9.38}$$

where ϕ_l are a set of bosonic modes (with $l = 1, ..., N$), with chirality $\chi_l = \pm 1$ and velocity v_l. In the case of a single mode ($N = 1$) this reduces to the standard description of the Laughlin series derived above.

These fields satisfy the commutation relation

$$\left[\phi_l(x,t), \phi_{l'}(x',t')\right] = i\pi\chi_l \delta_{ll'} \mathrm{sgn}\left(x - x' - \chi_l v_l t + \chi_{l'} v_{l'} t'\right), \tag{9.39}$$

and help defining the density operator as

$$\rho = \frac{1}{2\pi} \sum_l q_l \partial_x \phi_l \,, \tag{9.40}$$

where the set of coefficients q_l encode the contribution of the l^{th} mode to charge transport. These coefficients

are related to the filling factor in a nontrivial way as they satisfy the sum rule

$$\sum_l \chi_l q_l^2 = \nu \,. \tag{9.41}$$

In analogy with the Laughlin case, the edge supports quasiparticles, whose creation/annihilation operators involve a linear combination of all bosonic modes, namely

$$\psi_{\mathbf{g}}(x,t) \propto \exp\left[i \sum_{l=1}^{N} g_l \phi_l(x,t) \right] . \tag{9.42}$$

For a given vector $\mathbf{g} = \{g_1, ..., g_N\}$, the corresponding quasiparticle $\psi_{\mathbf{g}}$ is characterized by three important physical quantities:

$$Q_{\mathbf{g}} = e \sum_l \chi_l q_l g_l \qquad \text{its effective charge} \tag{9.43}$$

$$\delta_{\mathbf{g}} = \sum_l g_l^2 \qquad \text{its scaling dimension} \tag{9.44}$$

$$\Theta_{\mathbf{g}} = \pi \sum_l \chi_l g_l^2 \qquad \text{its statistical angle} \,. \tag{9.45}$$

Note that in all generality, the statistical angle is bounded by the scaling dimension, $|\Theta_{\mathbf{g}}| \leq \pi \delta_{\mathbf{g}}$, and even reduces to $|\Theta_{\mathbf{g}}| = \pi \delta_{\mathbf{g}}$ in the special situation where all modes have the same chirality, $\chi_l = \chi$, $\forall l$.

9.4.7. Measurable quantities

The above treatment of FQHE highlight three main quantities describing the quasiparticles arising from different models, the charge, the statistical angle and the scaling dimension.

The simplest of the three to measure is the charge, indeed, as explained in Chap. 5, the Fano factor allows a direct measure of the charge of the particles carrying the current. This was indeed experimentally measured [149, 150], showing that the Fano factor is equal to $\nu = 1/3$ for the first element of the Laughlin sequence. The plot from the original publication is shown in Fig. 9.2 and displays a Fano factor of 1/3. This was the first measure of tunneling of fractionally charged particles and constitutes a success of the Luttinger Liquid theory as well. Other measurements of the charge of the quasiparticle were subsequently performed through identification of the Josephson frequency $\omega_J = e^* V/\hbar$ which is accessed either through a photo assisted transport noise measurement at zero frequency [87, 151], or through a direct finite frequency noise measurement [152]. All the above experiments were performed in the weak backscattering regime of a single quantum point contact (QPC), where the accepted paradigm is that quasiparticle exchange between two opposite edge states constitute the dominant tunneling process.

The detection of fractional statistics has proved to represent an even greater challenge. On the theoretical side, several proposals considered setups with several QPCs in a Hanbury Brown and Twiss geometry [44] where noise crossed correlations were computed [153–156]. Alternatively, more recently, proposals using either Fabry Perot interferometry or Hong-Ou-Mandel collisions of quasiparticles were put forward [157–159]. These proposals generated considerable attention from the experimental community as illustrated by two recent pioneering experiments with a strong claim that the measurement of the statistical angle has been achieved [160, 161]. Nevertheless, the detection of the statistical angle of anyons continues to generate a lot of excitement as illustrated by recent theoretical works, some involving anyon braiding [162–164], or thermal tunneling noise [165].

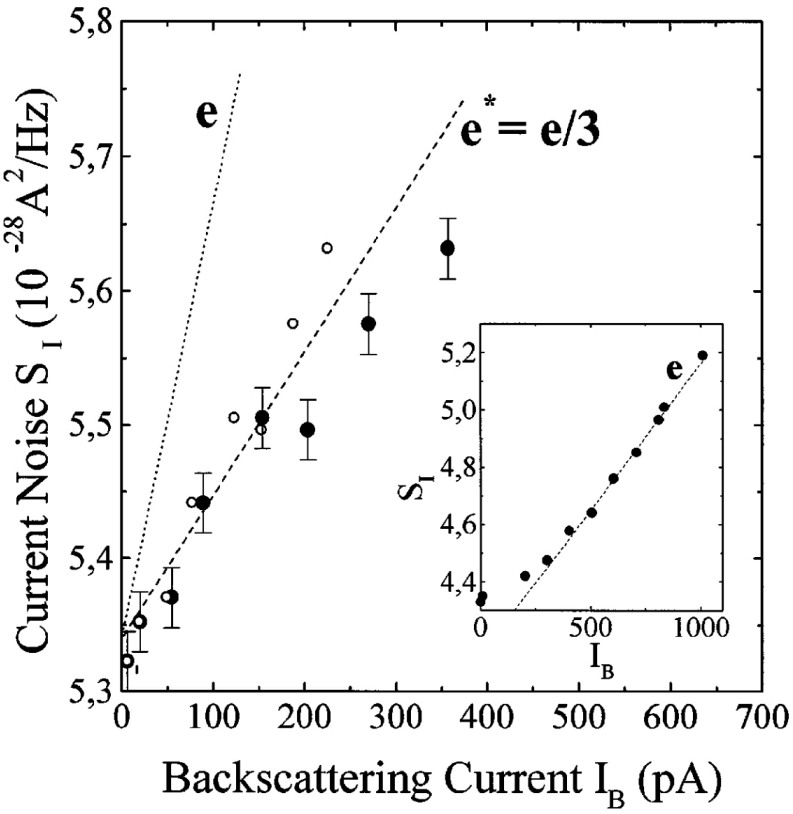

Figure 9.2.: First experimental evidence of the fractional charge of the FQHE quasiparticles, taken from [149]. The plot represents the noise versus the backscattering current with slope proportional to the Fano factor. The two dimensional electron gas is in the $\nu = 1/3$ state of the Laughlin series.

As was shown above, the scaling dimension of the quasiparticle operator is intimately tied to the statistical angle of anyons. For general Abelian states out of the Laughlin sequence, this scaling dimension turns out to provide an upper bound for the statistical angle, the two being equal when all the modes of a given edge have the same chirality (up to a factor π). Naively speaking, one could argue that the scaling dimension of anyons should be accessible via a DC transport measurement in the weak backscattering regime of a single QPC, provided that one measures carefully the backscattering DC current-voltage characteristics. This unfortunately does not seem so realistic due to the complicated analytics which describe the dependence on both the temperature and the DC voltage of the backscattering current [95]. In practice, a quantitative agreement between the backscattering current predicted by theory and experiments seems hard to achieve [166] as it relies on identifying a power-law behavior, which not only requires varying the voltage over several decades but is also easily blurred by non-universal effects.

9.5. Conclusion

This chapter introduced all the relevant concepts of the FQHE that will be useful in the next chapters. First, a summary of the quantum Hall effect itself (integer and fractional) is given and the relevant quantities are introduced with the simplest quantum mechanical picture possible, these include among others the Landau levels, the filling factor or the cyclotron orbits. A short summary of the discovery and various theoretical explanations of the integer effect was provided. This allowed to underline the topological nature of the conductance.

In the second part of the chapter, the fractional quantum Hall effect is introduced by shortly summarizing its field theoretical counterpart, i.e., the effective Chern-Simons action. This approach has the advantage to explicit the topological properties of the system as well as to justify the appearance of edge states from gauge invariance on the boundaries of the sample. It was also explained that the simplest fractional quantum Hall effect edge states behave as a chiral Luttinger liquid. Therefore, the basics of the theory of chiral Luttinger liquids was explained in the context of the FQHE, this included bosonization and a computation of the Green's function of the quasiparticle operator. Next a description of the system when a QPC links the two edge states was provided, the typical power law behavior of the current was explained. The extension of this description to more complicated Abelian edge states was quickly summarized, it allowed to write down the three main quantities of such models, the charge of the quasiparticles, their scaling dimension and their statistical angle. Finally the main experimental strategies that can be used to measure such quantities were quickly recalled.

10. Periodically driven QPC

10.1. Introduction

This chapter serves a different purpose than the previous ones as it is not directly related to electron quantum optics even though it deals with time-dependent transport. Precisely, it focuses on the study of time-dependent transport for the Abelian edge states of a two dimensional electron gas in the fractional quantum Hall regime pinched by a single quantum point contact. The aim is to find a general expression of the current as a function of time, both for an AC voltage drive and for periodically driven tunnel coupling amplitude. Interestingly, in the FQHE, to the knowledge of the author, attention has mainly focused so far on the time-dependent voltage scenario, while the periodic gate drive has been vastly unexplored so far. Unfortunately, for both types of drives, the measurement of the period-averaged current does not provide any striking dependence on the scaling dimension of quasiparticles (other than the power law, which is hard to characterize). However, a complete description of the current requires the knowledge of all of its harmonics at the drive frequency. In practice, this is precisely where the two types of drive lead to significantly different results. It turns out that the gate drive is the most suited of the two to detect the scaling dimension of FQHE quasiparticles. The central result of this chapter is indeed to show that for a simple sinusoidal modulation of the tunneling amplitude the scaling dimension is directly accessible via the measurement of the second harmonic of the current (conversely, for an AC voltage drive, a similar analysis seems difficult to achieve). More precisely, the phase shift of the second harmonic of the current is directly related to the scaling dimension of the quasiparticle operators describing the edge excitations. One can thus find an appreciable range of parameters where the scaling dimension can be easily extracted from a phase shift of the second harmonic of the current.

The formalism used to describe the QPC in the FQHE is exposed in Sec.10.2, this allows to define the tunnel Hamiltonian as well as the current between the edges in the tunnel. In Sec. 10.3, a formula for the current is obtained for any value of the filling factor. It is explained that the general formula has different convergence properties in the weak or in the strong backscattering. The former case is studied in detail in Sec. 10.4 and the harmonics of the current are studied in detail in Sec. 10.5. This allows to derive the main result of the chapter, i.e., that the scaling dimension of the quasiparticles is proportional to the phase shift of the second harmonics. Then the strong backscattering regime is studied in Sec. 10.6, it is shown that in this regime, a voltage drive leads to a capacitive current where a time-dependent tunnel coupling leads to a current proportional to the time derivative of the transmission of the junction.

10.2. Current through the QPC

The simplest quantum transport setup in the FQHE consists of a quantum Hall bar, along which edge excitations propagate, denoted left- and right-movers, further equipped with a QPC (see Fig. 10.1). Voltage sources can be connected to either edges in order to impose a potential bias difference between edge states, and the QPC can be tuned at will, with a special emphasis on two specific regimes. First, in the weak backscattering regime, the QPC is weakly pinched, the quantum Hall fluid spreads over the whole bar, and the dominant charge transfer process between the top and bottom edge is provided by quasiparticle excitations. In this situation, it is typically the backscattering current I_{T} which is computed/measured. This

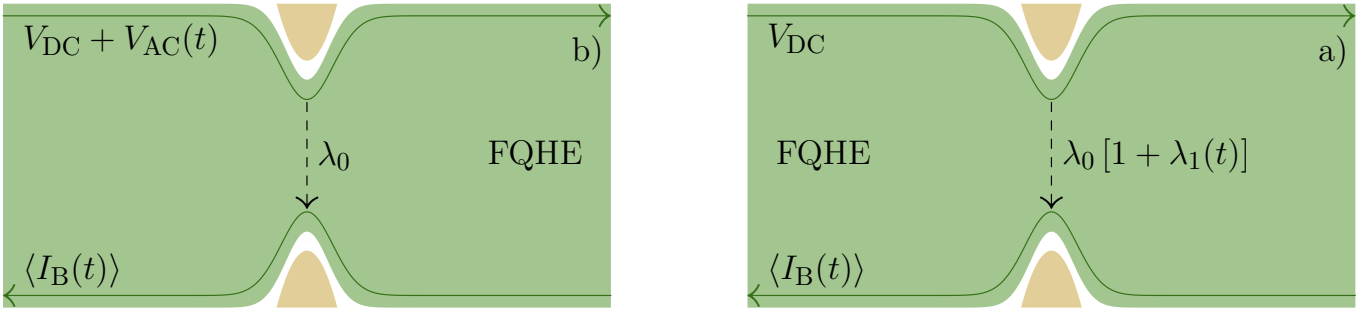

Figure 10.1.: Sketch of the setup, a fractional quantum Hall bar pinched off by a quantum point contact. Left: AC gate drive setup where a DC voltage is applied between edge states and the tunnel coupling is time-dependent. Right: AC voltage drive setup where a periodic voltage is applied on top of the DC voltage and the tunnel coupling is constant.

regime is depicted in both panels of Fig. 10.1. Second, in the opposite limit, called the strong backscattering regime, the QPC is strongly pinched and the quantum Hall fluid is split in two (not shown). Only electrons can then tunnel between the left and right moving edges as they have to cross a vacuum region. The measured current corresponds then to that flowing between the left and right sides of the split Hall fluid.

Assuming that a DC voltage $V_{\rm DC}$ is imposed on the right-moving edge (see Fig. 10.1), the usual tunnel, or backscattering Hamiltonian reads (see Ref. [52]):

$$H_{\rm T} = \sum_{\epsilon=\pm} \left[\lambda^*(t) e^{i\omega_0^* t} \psi_R^\dagger(0)\psi_L(0)\right]^\epsilon , \tag{10.1}$$

where $\epsilon = +$ leaves the expression unchanged, while $\epsilon = -$ specifies the Hermitian conjugate. $\lambda(t)$ is the time-dependent tunnel coupling amplitude and $\omega_0^* = e^* V_{\rm DC}$ in the weak backscattering regime. Two distinct setups for time-dependent transport are considered (left and right panels of Fig. 10.1).

With these conventions, the backscattered current reads:

$$I_{\rm T}(t) = ie^* \sum_{\epsilon=\pm} \epsilon \left[\lambda^*(t) e^{i\omega_0^* t} \psi_R^\dagger(0,t)\psi_L(0,t)\right]^\epsilon . \tag{10.2}$$

In the weak backscattering regime, the fractional charge $e^* = \nu e$ appears both as a prefactor of the current, and through the definition of the DC bias frequency ω_0^*.

The strong backscattering equivalent of the tunnel Hamiltonian and current operator are achieved with the duality transformation $e^* \to e$, $\omega_0^* \to eV_{\rm DC}$, $\psi \to \Psi$.

10.2.1. Reminders for the tunnel coupling

As explained in Chaps. 1 and 2, when the tunnel coupling is driven by a voltage drive, it only modifies its phase. The other situation considered is that of a modulation of the amplitude of the tunnel coupling directly (through a gate drive). This can be summarized by the following

$$\lambda(t) = \begin{cases} \lambda_0(1+\lambda_1(t)) & \text{gate drive,} \\ \lambda_0 \exp\left(ie^* \displaystyle\int_{-\infty}^{t} {\rm d}t'\, V_{ac}(t')\right) & \text{voltage drive}\,, \end{cases} \tag{10.3}$$

Concerning the gate drive, without loss of generality one can choose it to be real valued. It then only makes physical sense to choose $|\lambda_1(t)| < 1$. The Fourier decomposition of the tunnel coupling is written as

$$\lambda(t) = \lambda_0 \sum_l p_l e^{-il\Omega t} \,. \tag{10.4}$$

where the drive frequency is Ω, and $\overline{p_l}$ will be used to denote the complex conjugate[1] of p_l. Then, provided that no assumptions are made on the p_l, the computation can be carried out simultaneously for the voltage drive or the gate drive. However, it is worth mentioning that the Fourier coefficients p_l do not bear the same physical meaning when describing the two different drives. For the gate drive, there is typically a finite number of Fourier coefficients, which satisfy $\overline{p_l} = p_{-l}$ to represent a real valued modulation of the tunnel amplitude. However, for a voltage drive, the p_l's are the Fourier coefficients of a complex number of modulus one. As a consequence, there is an infinite set of coefficients p_l in this case, which obey specific sum rules [23, 88].

10.3. Current for arbitrary ν

The aim of this section is to provide a general derivation of the backscattering current while making minimal assumptions on the Fourier coefficients p_l of either drive. Also, specifically for this section, it should be kept in mind that at any moment, the duality transformation to the strong backscattering regime can be operated. Furthermore, the scaling dimension is explicitly writen as ν_D, although in the Laughlin case, it reduces to $\nu_D = \nu$. It allows to track down the effects which are specific to the scaling dimension. This choice is further reinforced by the general case detailed in App. F.3, where the degeneracy between scaling dimension and filling factor is lifted.

The photo-assisted backscattering current can be computed to second order in the tunnel coupling $\lambda(t)$, using the Keldysh formalism [167]. As shown in Sec. F.2, from Eq. (9.32) and Ref. [95], it reads

$$\langle I_{\mathrm{T}}(t)\rangle = \frac{e^*}{2}\left(\frac{1}{2\pi a}\right)^2 \sum_{\epsilon=\pm} \epsilon \int \mathrm{d}t' e^{i\epsilon\omega_0^*(t-t')} \left[\lambda^*(t)\right]^{\epsilon} \left[\lambda^*(t')\right]^{-\epsilon} \sum_{\eta,\eta'} \eta' e^{2\nu_D \mathcal{G}^{\eta\eta'}(t-t')} \,, \tag{10.5}$$

where η, η' are Keldysh contour indices and $\mathcal{G}^{\eta\eta'}$ is the corresponding bosonic Keldysh Green's function defined in Sec. F.1. At this stage, it is important to stress out that this expression of the tunneling current readily generalizes to any Abelian edge theory comprising multiple bosonic modes, where it then depends on the effective charge and scaling dimension of the quasiparticle $\psi_{\mathbf{g}^*}$ involved in the leading tunneling process at the QPC, as is shown in detail in Sec. F.3,

$$\langle I_T(t)\rangle = \frac{1}{2} Q_{\mathbf{g}^*} \sum_{\epsilon} \epsilon \int \mathrm{d}t' e^{i\epsilon Q_{\mathbf{g}^*} V_{\mathrm{DC}}(t-t')} \left[\Gamma_{\mathbf{g}^*}(t)\right]^{\epsilon} \left[\Gamma_{\mathbf{g}^*}(t')\right]^{-\epsilon} \sum_{\eta\eta'} \eta' e^{2\delta_{\mathbf{g}^*} \mathcal{G}^{\eta\eta'}(t-t')}, \tag{10.6}$$

where $Q_{\mathbf{g}^*}$ and $\delta_{\mathbf{g}^*}$ are respectively the effective charge and scaling dimension of the leading tunneling quasiparticle $\psi_{\mathbf{g}^*}$, while $\Gamma_{\mathbf{g}^*}$ is the corresponding tunneling amplitude. In particular, this expression underlines the importance of the distinction between scaling dimension and filling factor (as the two only turn out to be equal in the Laughlin case), and further emphasizes the major role played by the scaling dimension in the present derivation.

The general calculation of the backscattering current at finite temperature and for arbitrary periodic drives is quite cumbersome, and details of the derivation are provided in App. F.4. First, the summation

[1] The bar notation is adopted in this chapter as the star is already used for the fractional charge.

over the Keldysh indices is performed explicitly using the symmetry properties of the chiral bosonic Green's function components. Next, the time integral is performed and written in terms of Gauss' hypergeometric function ${}_2F_1$. This results in an current

$$\begin{aligned}\langle I_{\mathrm{T}}(t)\rangle = e^*\,(2v\tau_0)^{-2}\,\pi^{-3}\beta\lambda_0^2\sum_{l,m}\overline{p_l}p_m e^{i(l-m)\Omega t}\\ \times\sum_{\eta=\pm}\eta\left[\frac{-i\eta\sin\left(\frac{\pi}{\beta}\tau_0\right)\exp\left(i\eta\frac{\pi}{\beta}\tau_0\right)}{\nu_D-i\frac{m+q}{2\pi\theta}}{}_2F_1\left(1,1-\nu_D-i\frac{m+q}{2\pi\theta};1+\nu_D-i\frac{m+q}{2\pi\theta};\exp\left(2i\eta\frac{\pi}{\beta}\tau_0\right)\right)\right.\\ \left.-(m,q)\to(-l,-q)\right],\end{aligned} \tag{10.7}$$

where $\tau_0 = a/v$ is the short time cutoff, β is the inverse temperature, $\theta = (\beta\Omega)^{-1}$ is the reduced temperature and $q = \omega_0^*/\Omega$. ${}_2F_1$ is the Gauss hypergeometric function and the shorthand notation $f(a,b) - f(c,d) \equiv f(a,b) - (a,b) \to (c,d)$ has been used. An important advantage of this expression is that it remains valid for arbitrary values of the scaling dimension $\nu_D > 0$, allowing us to also obtain the current in various limiting cases, including in the strong backscattering limit using the duality transformation. However, the convergence properties of the resulting hypergeometric function significantly depend on the value of the scaling dimension. For this reason, all physically relevant cases corresponding to, the Laughlin fractions for weak backscattering, the Fermi liquid case, or the Laughlin fractions for strong backscattering, have to be discussed separately. Note that this subtlety does not occur in the standard computation of the current in the presence of a DC voltage, it is specific to time-dependent transport at finite temperature.

10.4. Weak backscattering regime

Here, the focus is set on filling factors $0 < \nu < 1$ in Eq. (10.7), corresponding solely to the weak backscattering regime dominated by quasiparticle transfer through the quantum Hall fluid. One can perform an expansion of the hypergeometric function ${}_2F_1$, which is specific to these filling factors, to leading order in τ_0/β (τ_0 is the short time cutoff of the chiral Luttinger liquid theory). This is achieved in Sec. F.5. Furthermore, without loss of generality (due to the choice of time origin), one can safely assume that the Fourier coefficients p_l are real. This leads to the general expression for the current in terms of cosine and sine harmonics at the drive frequency:

$$\begin{aligned}\langle I_{\mathrm{T}}(t)\rangle = I_0 + \mathcal{I}\sum_{l>0}\left[\cos(l\Omega t)\sum_m\left|\Gamma\left(\nu_D+i\frac{m+q}{2\theta\pi}\right)\right|^2(p_{m-l}p_m+p_m p_{l+m})\sinh\left(\frac{m+q}{2\theta}\right)\right.\\ \left.+\sin(l\Omega t)\tan(\pi\nu_D)\sum_m\left|\Gamma\left(\nu_D+i\frac{m+q}{2\theta\pi}\right)\right|^2(p_m p_{l+m}-p_{m-l}p_m)\cosh\left(\frac{m+q}{2\theta}\right)\right],\end{aligned} \tag{10.8}$$

with the prefactor:

$$\mathcal{I} = \frac{e^*\Omega}{\pi}\left(\frac{\lambda_0}{v}\right)^2\left(\frac{2\pi\theta}{\Lambda}\right)^{2\nu_D-2}\frac{\theta}{\Gamma(2\nu_D)}, \tag{10.9}$$

where $\Lambda = (\Omega\tau_0)^{-1}$ is the reduced high energy cutoff, and the zeroth harmonic is

$$I_0 = \mathcal{I}\sum_m\left|\Gamma\left(\nu_D+i\frac{m+q}{2\theta\pi}\right)\right|^2 p_m^2\sinh\left(\frac{m+q}{2\theta}\right). \tag{10.10}$$

A few comments are in order at this stage. First, this formula for the fully time-dependent current is valid for both a voltage drive and a gate drive. Second, the zeroth harmonic contribution introduced in Eq. (10.10) corresponds naturally to the current averaged over one period of the drive and, in the voltage drive case, satisfies a Tien-Gordon-like formula discussed in Chap. 1 as it corresponds to a weighted sum of DC contributions with a shifted voltage $e^*V_{\rm DC} \to e^*V_{\rm DC} + m\Omega$ and probability p_m^2. Finally, while all harmonics of the current depend on the scaling dimension in a nontrivial way, it turns out that the sine harmonics, in $\sin(l\Omega t)$, all carry a prefactor $\tan(\pi\nu_D)$, which constitutes a striking dependence on the scaling dimension worth exploring further. Note that a similar-looking dephasing in the time-dependent current has been obtained previously in some related cases [87, 168] but has remained unexploited. Indeed, it does not seem obvious to easily isolate this factor from the backscattering current, as the latter involves many contributions of the same order of magnitude.

To this end, the current can be rewritten as

$$\langle I_{\rm T}(t)\rangle = \sum_{n=0}^{\infty} I_n(t)\,, \tag{10.11}$$

where

$$I_{n\neq 0}(t) = \mathcal{I}C_n \cos(n\Omega t + \varphi_n)\,, \tag{10.12}$$

and the formulas for φ_n and C_n are given in Appendix. F.5, see Eq. (F.41).

The analytical continuation of Eq. (10.8) for $\nu_D = 1$ holds, allowing to retrieve the Fermi liquid behavior discussed in Chap. 3.

10.5. Harmonics of the current

This section is devoted to the analysis of the current and its different harmonics in the weak backscattering regime, as defined in Eq. (10.11). The cosine voltage drive is analyzed first, showing that there is no simple way to extract the scaling dimension of the quasiparticles from the current or its harmonics in this setting. On the other hand, for a cosine gate drive, is established, in a second subsection, a proportionality relation between the phase shift of the second harmonic of the current and the scaling dimension of the quasiparticle operator.

10.5.1. Voltage drive

When a voltage drive is applied, the tunnel coupling is modified according to Eq. (10.3). The drive is defined as

$$V(t) = V_{\rm DC} + V_{\rm AC}\cos\Omega t\,, \tag{10.13}$$

where the normalized modulation amplitude is $\alpha = e^*V_{\rm AC}/\Omega$. The Fourier coefficients of the tunnel coupling, are recalled from Chap. 3,

$$p_l = J_l(-\alpha)\,, \tag{10.14}$$

where J_l are Bessel functions of the first kind. One can readily check that these coefficients are real so that the expression for the time-dependent current, Eq. (10.8), can be used as is.

It follows from Eq. (10.14) that the Fourier coefficients p_l are nonzero for any l. The harmonics I_n of the current are therefore written as infinite sums, involving all Fourier coefficients. This significantly complicates the resulting expressions. As a result, in this voltage drive regime, a simple signature of the scaling dimension of the quasiparticle operator has not been extracted from the harmonics of the current

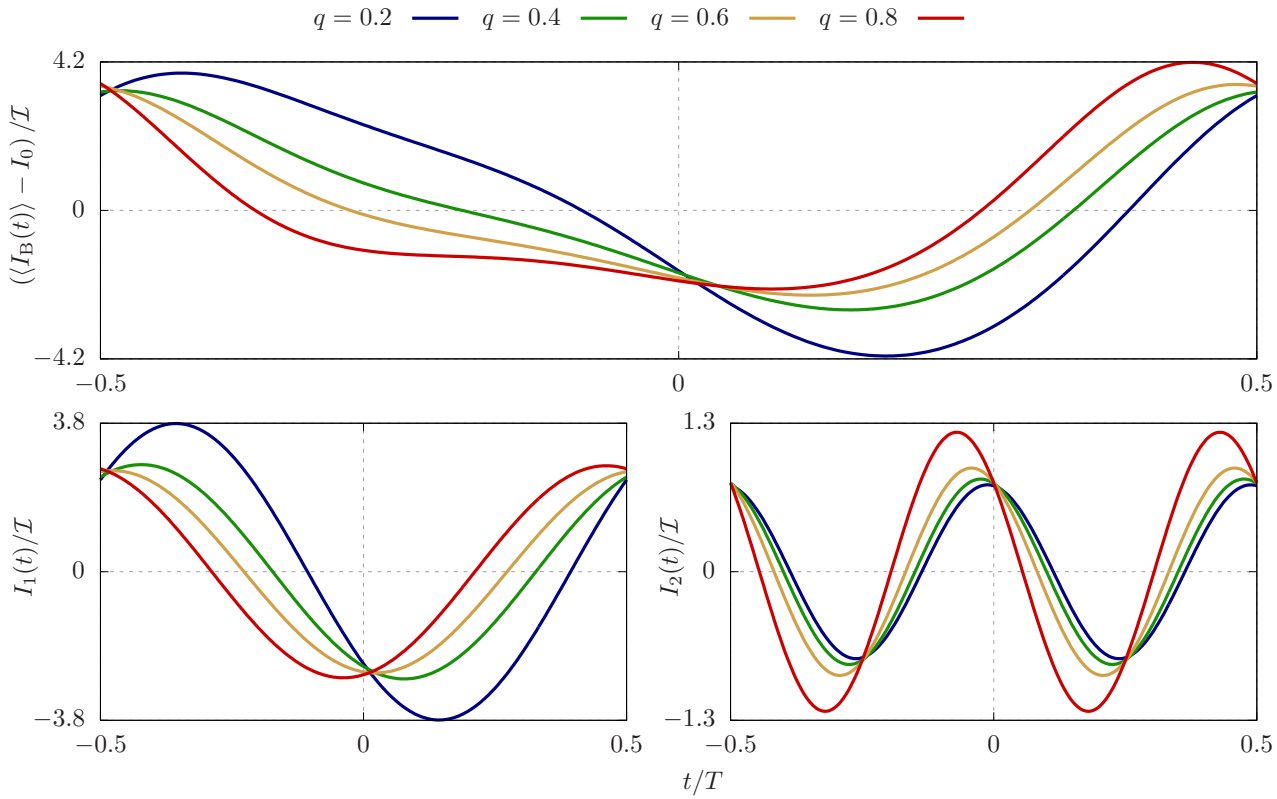

Figure 10.2.: **Voltage drive case:** current through the QPC in the weak backscattering regime under the voltage drive $V(t) = V_{\rm DC} + V_{\rm AC}\cos\Omega t$ and for various values of the average transmitted charge $q = e^* V_{\rm DC}/\Omega$. The filling factor is $\nu = 1/3$, the AC normalized amplitude is $\alpha = 1$, and the temperature is $\theta = 0.1$. The top panel shows the AC part of the current as a function of time, over one period. The lower left panel displays the first harmonic and the lower right the second one.

yet. This situation is not specific of the present choice of a cosine drive, but instead arises from the time dependence of the tunnel coupling, which appears as an exponential of a periodic function.

An illustration of the fully time-dependent current is proposed in Fig. 10.2. It shows the AC part of the current and its first two harmonics as a function of time over a full period for various values of the reduced DC voltage $q < 1$. One remarks that the current displays a rich behavior, in particular, both the amplitude and the phase of the two first harmonics of the current depend on q in a nontrivial way. Indeed, each harmonic involves a large number of Fourier components of the tunnel coupling, making it impractical to extract any valuable information.

10.5.2. Gate drive

The tunnel coupling under a gate drive, as defined in Eq. (10.3), reads, for a cosine drive,

$$\lambda(t) = \lambda_0\left[1 + \lambda_1\cos(\Omega t)\right] . \tag{10.15}$$

Therefore, its Fourier coefficients are given by

$$p_0 = 1\,, \qquad p_{\pm 1} = \frac{\lambda_1}{2}\,, \qquad p_{|n|>1} = 0\,. \tag{10.16}$$

These coefficients are real, allowing the use of the expression for the fully time-dependent current of Eq. (10.8). More importantly, there is only a finite subset of coefficients that are nonzero (two in the present case). This is a major difference between the gate drive and the voltage drive. While in the latter case, the proliferation of nonzero coefficients did not allow to obtain a simple self-contained expression of the current, in the present case of a gate drive, the internal summations over l and m in Eq. (10.8) can be readily performed. The resulting expression for the fully time-dependent current is still quite cumbersome. However, working out explicitly the expression for the amplitudes C_n and phases φ_n [see Eq. (10.12)], one can show that

$$\tan\varphi_2 = \tan\pi\nu_D \frac{\left|\Gamma\left(\nu_D + i\frac{q+1}{2\theta\pi}\right)\right|^2 \cosh\left(\frac{q+1}{2\theta}\right) - \left|\Gamma\left(\nu_D + i\frac{q-1}{2\theta\pi}\right)\right|^2 \cosh\left(\frac{q-1}{2\theta}\right)}{\left|\Gamma\left(\nu_D + i\frac{q+1}{2\theta\pi}\right)\right|^2 \sinh\left(\frac{q+1}{2\theta}\right) + \left|\Gamma\left(\nu_D + i\frac{q-1}{2\theta\pi}\right)\right|^2 \sinh\left(\frac{q-1}{2\theta}\right)} \tag{10.17}$$

which, in the low temperature regime ($\theta \ll 1$), further reduces to

$$\varphi_2 = \pi\nu_D \tag{10.18}$$

provided that the reduced DC voltage satisfies $q < 1$. Quite astonishingly, the phase shift of the second harmonic of the current induced by a cosine gate drive in the low temperature limit is exactly equal to the scaling dimension of the quasiparticle operator.

The same representation of the current as that adopted for the voltage drive (see Fig. 10.2) is proposed in Fig. 10.3, for a finite reduced temperature $\theta = 0.1$. In the lower right panel the phase shift of the second harmonic is indeed equal to $\pi\nu_D$ for a large range of q (the slight discrepancy for the highest $q = 0.8$ disappears at lower temperature). Indeed, from Eq. (10.12), this phase shift can be recast as a shift in time by an amount $t/T = -\varphi_2/(4\pi) = -\nu_D/4$ (taking into account that $C_2 > 0$).

The robustness of this result for finite temperature is explored in Fig. 10.4. It displays the evolution of φ_2 as a function of q for different values of ν_D and at two experimentally realistic reduced temperatures, $\theta = 0.1$ and $\theta = 0.2$. Note that in actual experimental realizations, a reduced temperature $\theta = 0.1$ would correspond to an actual temperature of 50mK for a drive frequency of 10GHz. For this value of the reduced temperature, the results of Fig. 10.4 show a good agreement between the phase shift φ_2 and the scaling dimension, over a large range of DC voltage. Increasing the temperature leads to a small departure between the two, which further grows as one increases the reduced voltage q (as already observed for $q = 0.8$ in Fig. 10.3).

It is relevant to stress that the identification of the phase shift, which gives direct access to the quasiparticle operator scaling dimension requires the experimental measurement of the *time-dependent current*, rather than the measurement of its average value over the period of the drive. Experimentally, it would therefore be necessary to measure the *harmonics* of the current, for instance by multiplying the current signal by a chosen, specific, periodic signal, and subsequently performing the average over the period of the drive.

The present prediction for the phase shift as a signature of the scaling dimension of the quasiparticle operator for a gate voltage modulation constitutes the central result of this chapter. Based on the generalized derivation presented in App. F.3, and the assumptions underlying the above computations, it should hold for a broad range of filling factors, the only requirement being that the scaling dimension of the quasiparticle involved in the leading tunneling process satisfies $0 < \nu_D < 1$ with $\nu_D \neq 1/2$.

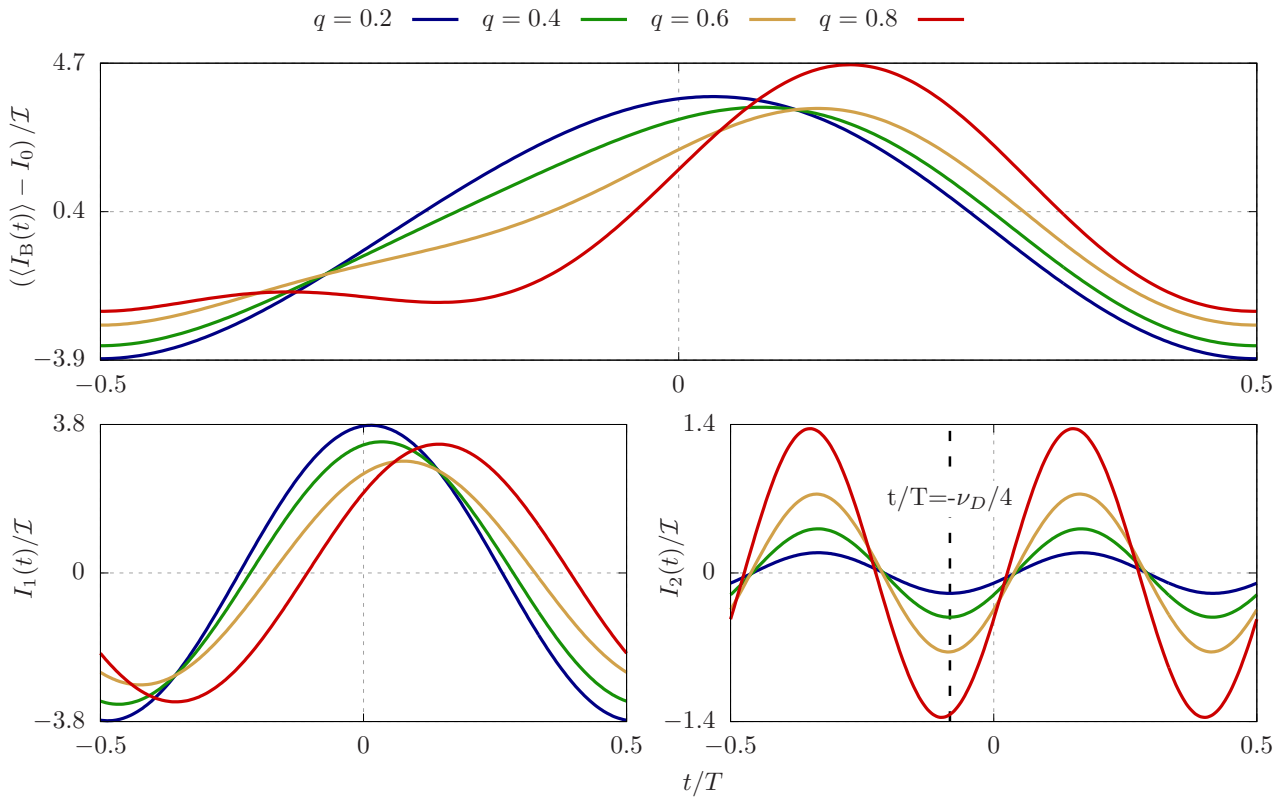

Figure 10.3.: **Gate drive case:** current through the QPC in the weak backscattering regime under the gate drive Eq. (10.15) and for various values of q. The figure was obtained with the following parameters: the filling factor is $\nu = 1/3$, the tunneling amplitude modulation is $\lambda_1 = 1$ and the reduced temperature is $\theta = 0.1$. The top panel shows the AC part of the current as a function of time, over one period. The lower left panel displays the first harmonic of the current and the lower right panel the second harmonic of the current, where all curves depict the same phase shift set by the scaling dimension ν_D.

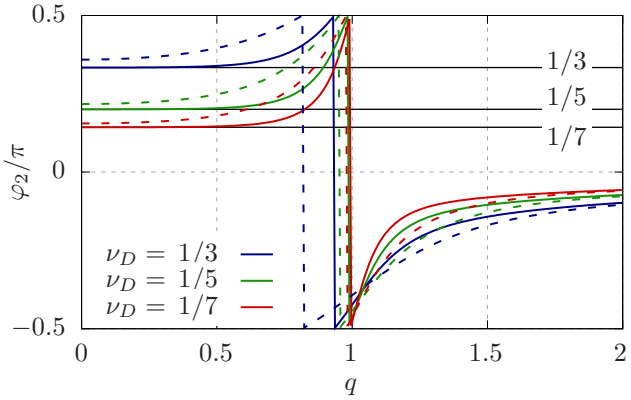

Figure 10.4.: Phase of the second harmonic [as defined in Eqs. (F.41) and (10.17)] of the current through the QPC under the gate drive Eq. (10.15), in the weak backscattering regime, as a function of q, for various filling factors ν. Full lines are for reduced temperature $\theta = 0.1$ and dashed lines for $\theta = 0.2$.

10.5.3. Luttinger liquid approach at $\nu = 1$

In this small subsection, the consistency of the approach developed in this chapter with the Fermi liquid picture of Chap. 3 will be discussed. First, it is recalled that in the QPC in the FQHE at $\nu = 1$, i.e., without correlations, the particles carrying the current are simply electrons, therefore, the current should behave in the same way as a that in a normal metal junction.

As was mentioned in Chap. 3, in the Fermi liquid approach, which was based on the Wick-Keldysh-Dyson method, the current was derived to all orders in λ only when the tunnel coupling was modulated by a voltage drive. In the case of a modulation of the tunnel coupling in amplitude itself, the self energy is not a unitary matrix so the computation is more complicated. A perturbative treatment of the current to second order in λ is performed in App. F.7, in particular it is shown that

$$\langle I_{\mathrm{T}}(t)\rangle = \frac{e^2}{2\pi v_{\mathrm{F}}^2}\begin{cases}\lambda(t)^2 V_{\mathrm{DC}} & \text{for a gate drive}\\ \lambda_0^2 V(t) & \text{for a voltage drive}\end{cases} \tag{10.19}$$

Which is the straightforward time-dependent generalization of the Landauer formula for photo-assisted transport (PAT). The absence of a temperature dependence is a consequence of the wide band approximation. It is interesting to mention the general result, i.e., if one could imagine a way to drive the tunnel coupling periodically both in amplitude and phase, the current would read as

$$\langle I_{\mathrm{T}}(t)\rangle = \frac{e\Omega}{4\pi v_{\mathrm{F}}^2}\left[2q\,|\lambda(t)|^2 + \frac{1}{i\Omega}\partial_t\,|\lambda(t)|^2\right]. \tag{10.20}$$

The second part of the consistency check amounts to finding the current in the Fermi liquid limit of the Luttinger theory. This can be done by setting $\nu_D = \nu = 1$ in the general formula for the current, Eq. (10.7). In this case, the expansion of Eq. (10.7) performed in Sec. F.5 does not hold as it requires $\nu < 1/2$. However, as shown in Sec. F.6, for such values of ν, a logarithmic expansion of the hypergeometric series in powers of τ_0/β can be carried out. This expansion yields two sums, which can be called Fermi/DC [Eq. (F.44)] and correlated-AC [Eq. (F.45)], for reasons that will become clear below. In the particular case of $\nu_D = 1$, the leading term is found in Sec. F.6.1. It corresponds to the first term of the Fermi/DC sum, see Eq. (F.46), and the current is identical to that obtained from the Fermi liquid approach, Eq. (F.53). The chiral Luttinger liquid approach is therefore consistent even in the Fermi liquid regime.

10.6. Strong backscattering regime

In this section the aim is to describe the behavior of the current in the strong backscattering regime, which is obtained from a duality transformation. The latter only holds for filling factors in the Laughlin series, so that, for clarity, a description in terms of the filling factor ν is adopted. This regime is obtained by setting $\nu \to \nu^{-1}$, $e^* \to e$ and $\omega_0^* \to eV_{\mathrm{DC}}/\Omega$ in the expression for the current, Eq. (10.5). As $\nu^{-1} \in \mathbb{N}$ for Laughlin fractions, one has to exploit the expansion of Eq. (10.7) to leading order in the cutoff, which is valid for all integers $\nu^{-1} > 0$, i.e., the logarithmic expansion, Eq. (F.43).

As already pointed out in Sec. 10.5.3, this expansion consists of two sums. In the case $\nu = 1$, the leading term in τ_0/β belongs to the Fermi/DC sum. However, here, the expansion in orders of τ_0/β favors another term, which belongs to the second sum, the correlated-AC sum, see Eq. (F.45). More precisely, the leading

term is of first order in τ_0/β and yields a current:

$$\langle I_{\mathrm{T}}(t)\rangle \approx \frac{-e}{(1-2\nu^{-1})_3}\left(\frac{\lambda_0}{\pi v}\right)^2 \frac{\Omega}{\Lambda}\,\mathrm{Im}\left[\sum_{l,m}\overline{p_l}p_m e^{i(l-m)\Omega t}\,(m+q)^2\right], \tag{10.21}$$

where $(x)_n$ is the Pochhammer symbol, defined in App. F.6. This expression can take a simpler form, since following the steps used to obtain Eq. (10.20), one can write

$$\langle I_{\mathrm{T}}(t)\rangle = \frac{e}{(2\nu^{-1}-1)(2\nu^{-1}-2)(2\nu^{-1}-3)}\frac{1}{\pi^2 v^2\Omega\Lambda}\,\mathrm{Im}\left[\lambda_0^2 e^2 V_{\mathrm{DC}}^2 + 2ieV_{\mathrm{DC}}\lambda(t)\partial_t\overline{\lambda(t)} - \lambda(t)\partial_t^2\overline{\lambda(t)}\right]. \tag{10.22}$$

Finally, computing explicitly the imaginary part, one can express the final result in a unified way for both types of drives defined in Eq. (10.3) as

$$\langle I_{\mathrm{T}}(t)\rangle = \frac{e}{\left(\frac{2}{\nu}-1\right)\left(\frac{2}{\nu}-2\right)\left(\frac{2}{\nu}-3\right)}\frac{1}{\pi^2 v^2\Omega\Lambda}\partial_t\left(\lambda^2 V\right). \tag{10.23}$$

This result is quite intriguing as it involves the time derivative of the AC Landauer formula, Eq. (10.19). As in the Fermi liquid computation, there is no temperature dependence to this order in the cutoff, this reflects the wide band limit of the Luttinger model.

In the case of a voltage drive, the junction in the strong backscattering regime behaves as a standard capacitor, i.e.,

$$\langle I_{\mathrm{T}}(t)\rangle = C\frac{\mathrm{d}V(t)}{\mathrm{d}t}, \tag{10.24}$$

with a capacitance

$$C = \frac{e^2}{\left(\frac{2}{\nu}-1\right)\left(\frac{2}{\nu}-2\right)\left(\frac{2}{\nu}-3\right)}\frac{\lambda_0^2}{\pi^2 v^2\Omega\Lambda}, \tag{10.25}$$

which, after restoring the proper powers of $\hbar$, can be further recast as $C = c\frac{2\pi a}{\left(\frac{2}{\nu}-1\right)\left(\frac{2}{\nu}-2\right)\left(\frac{2}{\nu}-3\right)}\left(\frac{\lambda_0}{\hbar v}\right)^2$, where $c = e^2/(hv)$ is the quantum capacitance by unit length.

In the case of a gate drive the situation is different, defining the transmission of the junction as $\tau(t) = 4\lambda^2(t)$, the current reads

$$\langle I_{\mathrm{T}}(t)\rangle = \frac{e^2 V_{\mathrm{DC}}}{\left(\frac{2}{\nu}-1\right)\left(\frac{2}{\nu}-2\right)\left(\frac{2}{\nu}-3\right)\pi^2 v^2\Omega\Lambda}\frac{\mathrm{d}\tau(t)}{\mathrm{d}t}. \tag{10.26}$$

As very different solutions arise from the same initial formula Eq. (F.38) at integer ν, but in different regimes, a reminder of the differences between these regimes might prove helpful. To summarize, the general expansion of the hypergeometric function in τ_0/β for positive integer ν_D^{-1} yields a current consisting of two sums, see Eq. (F.43). There are three different situations. When the junction is driven by a DC drive only, when the junction is driven by an AC drive and it is in the Fermi regime, $\nu = 1$, or when the junction is driven by an AC drive but correlations are present, i.e., $\nu^{-1} > 1$.

When the junction is in the Fermi liquid regime ($\nu = 1$) or solely driven by a DC drive, the leading terms of the expansion belong to the same sum which can therefore be called the Fermi/DC sum, see Eq. (F.44). In the DC case, this term yields the duality transformation of the already known weak backscattering DC result, see [52]. In the Fermi liquid case it yields a straightforward extension of the Landauer formula which can be called the AC Landauer formula.

When the junction is driven by both a DC and an AC drive (applied to either the edge or the gate) and

correlations are present, i.e. $\nu^{-1} > 1$, the leading contribution to the current comes from another term, which can therefore be called the correlated-AC sum, Eq. (F.45). This term yields a current proportional to the time derivative of the AC Landauer formula, Eq. (10.23).

10.7. Conclusion

This chapter describes a proposition of setup to measure the scaling dimension of the quasiparticle operator. The considerable theoretical investment for the search of signatures of the statistics of anyons of the FQHE in the context of electronic quantum transport setups was highlighted in the previous chapter. But most of these setups require quite complicated geometries or types of measurements. Noting that the statistical angle of anyonic quasiparticles is intimately tied to the scaling dimension of the quasiparticle operator a naive question arises: can this scaling dimension be detected via a careful measurement of the time-dependent backscattering current in the weak backscattering regime? Of course, measuring the statistical angle is of fundamental interest but it is to be noted that the scaling dimension in itself is also an important quantity to measure as it would allow to discriminate between the different possibilities of edge states contributing to the current.

For this purpose, this chapter started with shining a new light on the theory of time-dependent transport in the FQHE. I has been remarked that such transport can be achieved in two distinct ways. Either one modulates the gate voltage applied to the QPC (this type of drive does not appear to have received much attention in the context of time-dependent transport), or one adds an AC modulation on top of the DC voltage drive (as was proposed theoretically in Refs. [52, 87]).

An important result of Chap. 2 was recalled, that both drives can be described with a unified approach: the only difference between them resides in the details of the Fourier decomposition of the tunnel amplitude describing them. The time-dependent current can then be computed analytically in terms of sums over these Fourier coefficients, further involving a Gauss hypergeometric function, a result which is quite abstract in nature. In order to make progress, expansions to leading order in the cutoff need to be subsequently performed. Interestingly, these expansions depend crucially on the value of the scaling dimension ν_D and whether the QPC is in the weak or strong backscattering regime.

For the weak backscattering regime, the time-dependent current can be characterized as a constant term accompanied by its harmonics at multiples of the drive frequency. It is precisely in these harmonics that it might be possible to isolate the scaling dimension of the quasiparticle tunneling operator. Indeed, by choosing a simple cosine modulation for a gate drive, it was possible to show that the phase shift of the second harmonic of the time-dependent current is directly proportional to the scaling dimension at low temperature, which constitutes the central message of this chapter. It was stressed that this connection is robust at finite temperature, rendering it accessible to experimental observation. A typical experiment would require to multiply the time-dependent current signal by a proper harmonic drive at twice the drive frequency to detect this phase shift.

For completeness, a full treatment of the expansion properties of hypergeometric functions which appear in the general expression of the time-dependent current was provided, this allowed to derive results for both the Fermi liquid limit $\nu = 1$ and for the strong backscattering limit. In the former case, a time-dependent generalization of the Landauer formula is quickly obtained in the $\nu = 1$ limit of the chiral Luttinger model. In the case of strong backscattering, the current can be written in terms of time derivative of the drives.

The main result about the phase shift suggests that a careful measurement of the time-dependent current for a device containing a *single* quantum point contact could provide an insight on the detection (albeit indirect) of fractional statistics in the fractional quantum Hall effect.

11. Interacting pulses

11.1. Introduction

This chapter will deal with a new aspect of electron quantum optics in correlated systems, that of interaction between Levitons, due to a correlated background. Following the same lines as Chap. 7, the idea is to propose a setup that would have an experimental or technological application. In this case, the main application of electron quantum optics in quantum computation schemes nowadays is through *single* flying qubit [1, 2, 33–36] propagating in ballistic channels (in a QPC-like setup). Even in the absence of interaction, the qubit operations can be monitored by the length of the tunneling region and the voltage drive applied. In contrast, the realization of *two*-qubit quantum gates requires an interaction between electron flying qubits[36]. The Coulomb interaction in the FQHE introduces a quantum phase between the two states which is at the origin of the entanglement required to implement a two-qubit gate. The aim of this chapter is therefore to describe a system in which two Levitons interact with each other, so far, to the knowledge of the author, no theoretical proposal or experimental evidence of such a system exist.

Due to the intrinsic property of Levitons in non correlated systems, q different Levitons can be injected in a single period and travel without interacting along ballistic channels. The many-body states that are consequently formed are called multi-electron Levitons or, simply, q-Levitons [47, 54, 169]. It is interesting to investigate if this result holds when considering correlations due to the fractional quantum Hall effect. It seems relevant to focus on the Laughlin sequence as the absence of decoherence induced by other propagating channels [55, 170, 171] might be a hindrance. A periodic drive will be applied so as to send two-Leviton states in a single period with a time separation Δt. In the presence of a quantum point contact operating in the weak-backscattering regime the usual tools to characterize the state are that provided by charge transport, hence the aim is to compute the average backscattered charge (by means of the Keldysh technique). Stated simply, the aim of this chapter is therefore to study precisely the transport counterparts of the interaction between Levitons in the FQHE when sent to a QPC.

In the limit of an infinite period and zero temperature, it is shown that the backscattered charge for a two-Leviton state is not equal to twice the backscattered charge for a single Leviton. This result can be interpreted in terms of the wave-packet formalism for Levitons, by an effective interaction between the two Levitons induced by the strongly-correlated background. Finally, numerical calculations, both at finite temperature in the single pulse case *and* in the periodic case, are performed. It is shown that the value of the backscattered charge for two-Leviton states is strongly dependent on the pulse separation, thus opening scenarios where the effective interaction between Levitons can be monitored by a single experimental parameter.

The chapter is organized as follows. Sec. 11.2 introduces the model of the quantum Hall bar with quantum point contact and the source of Levitons. The backscattered charge at the quantum point contact is computed in Sec. 11.3 for isolated pulses of Levitons and for a periodic drive, the interpretation in terms of the wave-packet formalism for Levitons is also given here. The backscattered charge is studied thoroughly in Sec. 11.4. This is done numerically by plotting it as a function of different system parameters.

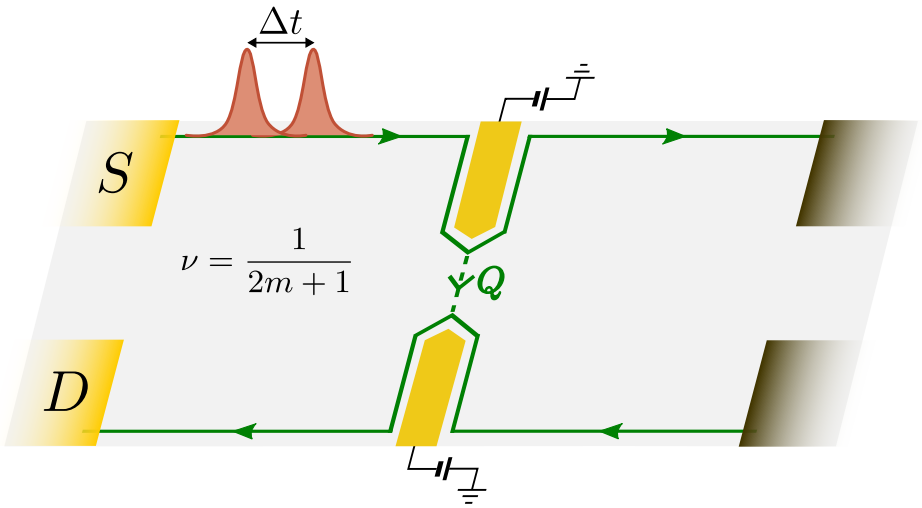

Figure 11.1.: Schematic view of the setup. A two-dimensional electron system is in the Laughlin series of the FQHE, with a single edge state propagating on the boundary. The system is connected to four terminals: a periodic voltage drive $V(t)$ applied to the source terminal S is injecting multiple Levitons in each period separated by a time delay Δt smaller than the period itself. The opposite edges are connected by a QPC placed in $x = 0$. The charge backscattered at the QPC, namely Q, is measured in the drain D. The remaining terminals (in gray) are grounded and they are not involved in any measurement.

11.2. Model

As in the previous chapters, the system considered is a four-terminal FQHE bar at filling factor $\nu = 1/(2n+1)$, with $n \in \mathbb{N}$, hence the bulk is insulating and charge transport occurs at the edges, depicted as chiral Luttinger liquids. Furthermore, at this filling factor only one chiral edge mode emerges at each boundary of the sample. These modes are connected by a QPC, operating in the weak-backscattering regime, where tunneling is dominated by Laughlin quasi-particles with charge $e^* = \nu e$. A time-dependent voltage $V(t)$ is applied to terminal S, the charge backscattered at the QPC is measured in the drain D and the two remaining terminals are assumed to be grounded. An illustration of the situation is provided in Fig. 11.1. The total Hamiltonian that describes this system is given by $H = H_0 + H_B$ and consists of edge states and tunneling terms respectively.

$$H_0 = \sum_{r=R,L} \frac{v}{4\pi} \int \mathrm{d}x \, \left[\partial_x \phi_r(x,t)\right]^2 , \tag{11.1}$$

where $\phi(x,t)$ are the bosonic fields defined in Chap. 9, their time dependence comes from the fact that the voltage transports them along the edge. The voltage drive $V(t)$ is chosen to be a train of Lorentzian pulses and the injected charge is defined as $-qe = \frac{e^2\nu}{2\pi} \int_0^{\mathcal{T}} \mathrm{d}t \, V(t)$. The drive is said to be quantized when q is any integer, thus creating q-Levitons. Furthermore, in order to study the effects of the background correlations on q-Levitons it is important to account for the possibility of injecting multiple Levitons in one period separated by a delay Δt. The corresponding time-dependent potential is

$$V(t) = \sum_{j=0}^{q-1} \sum_{k=-\infty}^{+\infty} \frac{V_0}{\pi} \frac{\gamma^2}{\gamma^2 + (t - k\mathcal{T} - j\Delta t)^2} , \tag{11.2}$$

with period $\mathcal{T} = \frac{2\pi}{\omega}$, amplitude V_0 and width 2γ. Later, the simpler case of an isolated pulse will be considered.

Finally, as before, tunneling between the two edges which occurs at the QPC, i.e., at $x = 0$, hence only the time dependence of the field is considered. Following the tradition of transport in the weak backscattering regime [147, 149, 150], the tunneling of Laughlin quasiparticles between opposite edges is considered to be the only relevant process. Annihilation fields for Laughlin quasiparticles carrying fractional charge $-\nu e$ (with $e > 0$) are defined through the standard procedure of bosonization [134]. Ignoring the Klein factors, they read as

$$\psi_{R/L}(t) = \frac{1}{\sqrt{2\pi a}} e^{i\varphi(t)} e^{-\frac{i}{\sqrt{\nu}}\phi_{R/L}(x)}, \tag{11.3}$$

where a is the short-distance regularization parameter and

$$\Psi_{R/L}(t) = \frac{1}{\sqrt{2\pi a}} e^{i\sqrt{\nu}\phi_{R/L}(t)}, \tag{11.4}$$

are the fermionic fields. The backscattering Hamiltonian therefore reads as

$$H_B = \lambda \sum_{\epsilon=+,-} \left[e^{-i\varphi(t)} \psi_R^\dagger(t) \psi_L(t) \right]^\epsilon . \tag{11.5}$$

where $\epsilon = -$ means Hermitian conjugate and $\varphi(t)$ is the phase difference between the two electrodes, defined as

$$\varphi(t) = e^* \int_{-\infty}^{t} \mathrm{d}t' V(t'). \tag{11.6}$$

11.3. Charge backscattered at the QPC

As shown in Ref. [54], the transport properties before the QPC does not carry any information about the effect of strong correlations of the propagation of q-Levitons. Hence, it is only relevant here to investigate the properties of the charge backscattered at the QPC. It is expected that, due to the non-linear nature of the tunneling at the QPC, effects of interaction will be manifested in the backscattered charge. For a periodic time-dependent voltage, the charge which is backscattered in one period $\mathcal{T}$ is given by

$$Q = \int_{-\mathcal{T}/2}^{\mathcal{T}/2} \mathrm{d}t \, \langle I_B(t) \rangle , \tag{11.7}$$

where the backscattering current reads as

$$I_B(t) = ie^*\lambda \sum_{\epsilon=+,-} \epsilon \left[e^{i\varphi(t)} \psi_R(t)^\dagger \psi_L(t) \right]^\epsilon , \tag{11.8}$$

The restriction to the weak backscattering regime allows to compute the excess charge density perturbatively in the tunneling Hamiltonian H_B. Thermal averages are thus performed over the initial equilibrium density matrix in the absence of tunneling. In order to properly manage the out-of-equilibrium dynamics of the system, calculations are carried out in the Keldysh formalism. To lowest order in the tunneling amplitude λ, the backscattered charge is defined as

$$Q = i \frac{e^*\lambda^2}{2\pi^2 a^2} \int_{-\infty}^{+\infty} \mathrm{d}\tau \, e^{2\nu \mathcal{G}(\tau)} \int_{-\mathcal{T}/2}^{\mathcal{T}/2} \mathrm{d}t \, \sin\left[\varphi(t) - \varphi(t-\tau)\right] , \tag{11.9}$$

where the connected bosonic Green's function $\mathcal{G}$, which was introduced in Chap. 9, is computed in App. F.1.

The expressions for the backscattered charge Q is valid for any arbitrary driving voltage $V(t)$ even though this study will focus on the case of q-Levitons, specifically $q = 1$ and $q = 2$. In the latter case, the time delay separating the two pulses is called Δt. Before performing a numerical evaluation of Q for a finite period $\mathcal{T}$, it is enlightening to consider the case of isolated pulses ($\gamma \ll \mathcal{T}$). In this case, precise analytical expressions are carried out at zero temperature for the backscattered charge in order to set the stage for later discussions. These results are completed with finite temperature plots obtained numerically. For the sake of completeness, the calculations for the charge fluctuations are also performed in the case of isolated pulses at zero temperature.

11.3.1. Isolated pulses

11.3.1.1. Backscattered charge

In the case of isolated pulses the integral over t in Eq. (11.7) can be extended from $-\infty$ to $+\infty$ and can be solved analytically at zero temperature. This limit is well-defined only for voltage pulses that go to zero at $t = \pm\infty$, which is the case for Lorentzian-shaped pulses. The expression for the charge becomes

$$Q = i\frac{e^*\lambda^2}{2\pi^2 a^2}\int_{-\infty}^{+\infty}\frac{\mathrm{d}\tau}{\left(1+i\frac{\tau}{\tau_0}\right)^{-2\nu}}\int_{-\infty}^{+\infty}\mathrm{d}t\,\sin\left[\varphi(t)-\varphi(t-\tau)\right], \tag{11.10}$$

where the zero-temperature limit of the bosonic Green's function (defined in Eq. (9.35)),

$$\mathcal{G}(\tau) = -\log\left(1+i\frac{\tau}{\tau_0}\right), \tag{11.11}$$

was used. The integral over t can be performed analytically for integer values of q. For $q = 1$, the computation is carried out thanks to the residue theorem, one finds

$$Q_1 = e^*\left(\frac{\lambda}{v_F}\right)^2\left(\frac{2\gamma}{\tau_0}\right)^{2-2\nu} + \mathcal{O}\left[\left(\frac{\tau_0}{\gamma}\right)^{2\nu-1}\right], \tag{11.12}$$

where only the leading order in τ_0/γ is kept. In the case $q = 2$, where the isolated pulses are separated by a constant delay Δt, the integral over t gives a backscattered charge

$$Q_2 = 16\pi\gamma^2 i\frac{e^*}{2\pi^2 a^2}\lambda^2\int_{-\infty}^{+\infty}\mathrm{d}\tau\,\left(1+i\frac{\tau}{\tau_0}\right)^{-2\nu}\frac{\tau\left[\left(4\gamma^4+\Delta t^2\right)^2-\tau^2\left(3\Delta t^2+4\gamma^2\right)+2\tau^4\right]}{(\tau^2+4\gamma^2)((\Delta t+\tau)^2+4\gamma^2)((\Delta t-\tau)^2+4\gamma^2)}. \tag{11.13}$$

This integral can also be computed using the residue theorem and, to leading order in τ_0/γ, it yields

$$Q_2 = Q_1\left\{2\,\mathrm{Re}\left[\left(1+\frac{2i\gamma}{\Delta t}\right)^2\left(1-\frac{i\Delta t}{2\gamma}\right)^{-2\nu}\right]+2\left(1+\frac{4\gamma^2}{\Delta t^2}\right)\right\}+\mathcal{O}\left[\left(\frac{\tau_0}{\gamma}\right)^{2\nu-1}\right]. \tag{11.14}$$

The backscattered charge for two pulses is therefore proportional to that generated by a single pulse. For the integer filling factor $\nu = 1$, it yields the trivial result that $Q_2 = 2Q_1$. Nevertheless, for fractional filling factor, the constant of proportionality depends on Δt and γ and $Q_2 \neq 2Q_1$. As a result the charge backscattered when two Levitons are impinging at the QPC does not amount in general to twice the charge backscattered when a single Leviton is injected. This is an immediate consequence of the strong

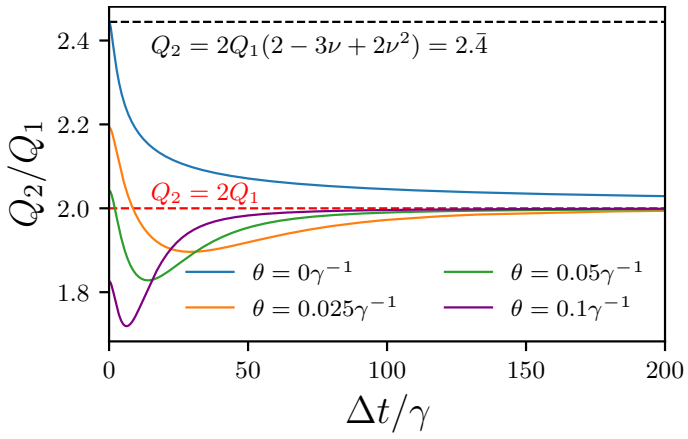

Figure 11.2.: Backscattered charge for a two-Leviton state Q_2, in units of that induced by a single Leviton and as a function of $\Delta t/\gamma$ at zero temperature. The black and red dotted lines represent respectively the limits of simultaneous ($\Delta t/\gamma \to 0$) and well-separated pulses ($\Delta t/\gamma \to \infty$). The figure was obtained filling factor $\nu = 1/3$.

correlations that characterize Laughlin states (and which are also responsible for the non-linear current-to-voltage characteristic in the presence of the tunneling of quasi-particles at the QPC).

Before concluding this part, it is instructive to analyze two extreme limits of the ratio $\Delta t/\gamma$. The limit of simultaneous pulses, which is obtained when $\Delta t/\gamma \ll 1$ in Eq. (11.14), yields

$$\lim_{\Delta t/\gamma \to 0} Q_2 = 2Q_1 \left(2 - 3\nu + 2\nu^2\right) . \tag{11.15}$$

In this limit the constant of proportionality acquires a simple expression, becoming independent of γ and being determined solely by the filling factor ν. It is to be noted that, both when $\nu = 1$ *and* $\nu = 1/2$ this yields the non-interacting result $Q_2 = 2Q_1$. In the opposite case of well-separated pulses, i.e., when $\Delta t/\gamma \to \infty$ in the expression for Q_2,

$$\lim_{\Delta t/\gamma \to \infty} Q_2 = 2Q_1 . \tag{11.16}$$

Indeed, in this case, for any filling factor the charge backscattered for two Levitons is twice the one obtained with a single Leviton. For well-separated injection time, the system has relaxed to equilibrium when the second pulse comes in. As a result, the two Levitons behave as two independent single pulses. These results, together with their finite temperature counterparts, are summarized in Fig. 11.2, where the black and red dotted lines represents the two limits of simultaneous and well-separated pulses. It seems relevant to remark that, at zero temperature (blue curve), the limit of well-separated pulses not reached exponentially but as $\approx \Delta t^{-2}$ due to the long-tail feature of Lorentzian pulses.

At finite temperature, numerical computations of the backscattered charge can be preformed. The results are also represented in Fig. 11.2, the backscattered charge when two pulses are sent simultaneously is decreasing with temperature. For low enough temperatures, see the purple curve of Fig. 11.2, this charge can be lower than twice that induced by a single pulse. Furthermore, the backscattered charge as a function of the time shift shows a minimum which gets closer and closer to 0 as the temperature increases. The time shift at which this minima is reached appears to be roughly proportional to the inverse temperature $\Delta t_{\min} \approx \theta^{-1}$. Finally, for time shift higher than $\Delta t_{\min}$, the limit of well separated pulses seems to reach the exponentially the limit of well-separated pulses.

11.3.1.2. Charge fluctuations

In order to further characterize the transport properties of this system it is useful to consider the analytical calculations of charge fluctuations. These fluctuations are defined as

$$\mathcal{S}_Q = \int_{-\infty}^{+\infty} \mathrm{d}t \int_{-\infty}^{+\infty} \mathrm{d}t' \left\langle I_B(t) I_B(t') \right\rangle - Q^2 \,. \tag{11.17}$$

Similarly to the backscattered charge fluctuations, the above integral can be computed at zero temperature and for isolated quantized Lorentzian pulses, in order to provide the analytical expressions of charge fluctuations for $q = 1$ and $q = 2$. An important new feature with respect to the charge is that their fluctuations diverges at zero temperature: as discussed in Ref. [172], the integral should be regularized by subtracting its value at equilibrium, i.e in the absence of voltage pulses. The regularized quantity reads as

$$\tilde{\mathcal{S}}_Q = \left(\frac{e^*\lambda}{\pi a}\right)^2 \int_{-\infty}^{+\infty} \mathrm{d}\tau \, e^{2\nu\mathcal{G}(\tau)} \int_{-\infty}^{\infty} \mathrm{d}t \, \left\{\cos\left[\varphi(t) - \varphi(t-\tau)\right] - 1\right\} \,, \tag{11.18}$$

where the notation $\tilde{\mathcal{S}}_Q$ for the regularized charge fluctuations was adopted. The calculation of the integrals over t can be performed analytically for integer values of q using the residue theorem, one finds

$$\tilde{\mathcal{S}}_{Q,1} = -e^* \frac{4e^*\lambda^2\gamma}{\pi v_{\mathrm{F}}^2 \tau_0^2} \int_{-\infty}^{+\infty} \mathrm{d}\tau \, \frac{\tau^2}{\tau^2 + 4\gamma^2} e^{2\nu\mathcal{G}(\tau)} \tag{11.19}$$

for $q = 1$ and

$$\tilde{\mathcal{S}}_{Q,2} = -2\pi\gamma \left(\frac{2e^*\lambda}{\pi a}\right)^2 \int_{-\infty}^{\infty} \mathrm{d}\tau\tau^2 \frac{32\gamma^4 + \left(\Delta t^2 - \tau^2\right)^2 + 4\gamma^2\left(3\Delta t^2 - \tau^2\right)}{\Delta t\left(\tau^2 + 4\gamma^2\right)\left[(\Delta t + \tau)^2 + 4\gamma^2\right]\left[(\Delta t - \tau)^2 + 4\gamma^2\right]} \left(1 + i\frac{\tau}{\tau_0}\right)^{-2\nu} \tag{11.20}$$

for $q = 2$. The residue theorem can be used once again to perform both integrals over τ and the final expressions for the charge fluctuations for $q = 1$ and $q = 2$ are

$$\tilde{\mathcal{S}}_{Q,1} = 2\left(\frac{2e^*\lambda\gamma}{v_F\tau_0}\right)^2 \left(1 + \frac{2\gamma}{\tau_0}\right)^{-2\nu} \,. \tag{11.21}$$

and

$$\tilde{\mathcal{S}}_{Q,2} = 2\left(\frac{e^*\lambda}{v_{\mathrm{F}}}\right)^2 \left(\frac{2\gamma}{\tau_0}\right)^{2-2\nu} \left[2\left(1 + \frac{4\gamma^2}{\Delta t^2}\right) + 2\,\mathrm{Re}\left(1 + \frac{2i\gamma}{\Delta t}\right)^2 \left(1 - \frac{i\Delta t}{2\gamma}\right)^{-2\nu}\right] , \tag{11.22}$$

to leading order in $\tau_0/\gamma \to 0$. It is instructive to introduce a Fano factor for the charge as

$$F_Q = \frac{\tilde{\mathcal{S}}_{Q,1,2}}{Q_{1,2}} \,. \tag{11.23}$$

Therefore as usual, $F_Q = 2e^*$ for $q = 1$ and also for $q = 2$ independently of the separation between the Levitons. However, the above Fano factor has been defined by employing the regularized charge fluctuations in order to yield Fano relations similar to those existing between current and noise in other setups, see e.g. Refs. [52] and [173]. Due to the proportionality between regularized charge fluctuations and backscattered charge, the plot of $\mathcal{S}_{Q,2}/\mathcal{S}_{Q,1}$ as a function of $\Delta t/\gamma$ has the exact same behavior as the one depicted in Fig. 11.2 and is not displayed here.

The natural prolongation of these results reside in the extension to periodic trains of such pairs of Levitons.

However, it makes more sense to first present a physical interpretation of the above results in terms of the wave-packet formalism of Levitons.

11.3.2. Correlated two-Levitons state

In this part, the aim is to recast the expression for the backscattered charges Q_1 and Q_2 at zero temperature in terms of the wave-function of an isolated Leviton. The latter was derived in Ref. [174] is given by

$$\chi(t) = \sqrt{\frac{\gamma}{\pi}} \frac{1}{t - i\gamma} \,. \tag{11.24}$$

For the following discussion, it is useful to introduce the excess charge ΔQ as

$$\Delta Q \equiv Q_2 - 2Q_1, \tag{11.25}$$

which represents the backscattered charge in excess compared to the trivial case at $\nu = 1$. By using Eq. (11.24), the charge Q_1 can be recast into

$$Q_1 = -\frac{e^*\lambda^2}{2\pi^2 a^2} \int_{-\infty}^{\infty} \mathrm{d}t \int_{-\infty}^{\infty} \mathrm{d}\tau \ \mathrm{Re}\left[\chi(t)\chi^*(t-\tau)\right] \tau \left(1 + i\frac{\tau}{\tau_0}\right)^{-2\nu} . \tag{11.26}$$

The charge Q_1 contains a product of Leviton wave-function χ, as a result, it is determined directly by the charge density of the state injected on the system ground state. Following the same lines, the excess charge ΔQ can be written in terms of Leviton wave-functions as

$$\Delta Q = \frac{e^*\lambda^2}{4\pi^2 a^2 (i)^{2\nu-2}} \int_{-\infty}^{\infty} \mathrm{d}t \big[\chi(t) g_\nu(t, \Delta t) \chi(t + \Delta t) - \mathrm{h.c.}\big] \tag{11.27}$$

where

$$g_\nu(t, \Delta t) = \int_{-\infty}^{\infty} \mathrm{d}\tau \, \chi^*(t-\tau)\chi^*(t-\tau+\Delta t)\tau^{2-2\nu} \,. \tag{11.28}$$

In contrast with Q_1, the excess charge is related to the product of four Leviton wave-functions, hence it is related to a density-density interaction between Levitons. A possible interpretation of this result is that the strongly-correlated background mediates an effective interaction between the two Levitons. In the above expression τ_0 was set to zero since the integrated function is well-behaved around $\tau = 0$. Remarkably, for $\nu = 1$ (no interactions), this function vanishes

$$g_{\nu=1}(t, \Delta t) = \int_{-\infty}^{\infty} \mathrm{d}\tau \, \chi^*(t-\tau)\chi^*(t-\tau+\Delta t) = 0 \,, \tag{11.29}$$

which is the standard solitonic behavior of Levitons in non-correlated media. Tracing back this result, the function g_ν is different from zero for fractional filling factors because of the propagator $e^{2\nu\mathcal{G}(\tau)}$. The power law decay for fractional filling factors is slower than τ^2, thus inducing long-time correlations between the two Levitons. These correlations do not affect the charge only when the pulses are well separated (limit of Δt very big). Otherwise, correlations induce an effective interaction between Levitons that effectively enhance the value of the charge Q_2 compared to the limit of two well-isolated pulses.

It is important to mention that the effect described above cannot be ascribed to braiding effects related to the anyonic statistics of the excitations in the fractional regime. Indeed, as was shown in Ref. [74], one should not expect any kind of braiding effects for pulses carrying an integer multiple of the electronic charge. This is one of the reasons for considering only integer values of q rather than generic fractional values, where

braiding effects may also affect the charge backscattered at the QPC.

11.3.3. Periodic train of Levitons

In order to discuss possible experimental realization of such interacting pairs of Levitons, it is essential consider the periodic drive. Furthermore, not only do the previous results hold but also new phenomena arise. In the case of a periodic signal, no close analytical expression can be derived for the backscattered charges Q_1 and Q_2 and one has to resort to a numerical calculation. The latter is conveniently carried on in the photo-assisted formalism, where the transport properties are expressed in terms of the Fourier coefficients of the phase associated with the periodic signal [175]. In the following, only Lorentzian-shaped pulses with $q = 1$ and $q = 2$ are considered. From the results of the previous chapter[1], the photo-assisted expressions for the backscattered charges Q_1 and Q_2 are

$$Q_1 = \mathcal{Q}\sum_m p_m^2 \left|\Gamma\left(\nu + i\frac{m+1}{2\theta\pi}\right)\right|^2 \sinh\left(\frac{m+1}{2\theta}\right), \tag{11.30}$$

$$Q_2 = \mathcal{Q}\sum_m \tilde{p}_m^2 \left|\Gamma\left(\nu + i\frac{m+2}{2\theta\pi}\right)\right|^2 \sinh\left(\frac{m+2}{2\theta}\right), \tag{11.31}$$

where

$$\mathcal{Q} = \frac{2e^*}{\mathcal{T}}\left(\frac{\lambda}{v}\right)^2 (2\pi\theta\tau_0)^{2\nu-2}\frac{\theta}{\Gamma(2\nu)}. \tag{11.32}$$

and the reduced temperature $\theta = \theta/\hbar\omega$. The photo-assisted coefficients are computed $q = 2$ in App. G.2 in terms of the rescaled pulse width $\eta = \gamma/\mathcal{T}$ and the pulse separation $\alpha = \Delta t/(2\mathcal{T})$. For $q = 1$ they read as

$$p_m = \begin{cases} e^{-2\pi\eta m}\left(1 - e^{-4\pi\eta}\right) & m \geq 0 \\ -e^{-2\pi\eta} & m = -1 \\ 0 & m < -1. \end{cases} \tag{11.33}$$

and for $q = 2$,

$$\tilde{p}_m = \begin{cases} \frac{\left[1-e^{i\pi\alpha(m+1)}\right]-e^{-4\pi\eta-i\pi\alpha}\left[1-e^{i\pi\alpha(m+3)}\right]}{(1-e^{i\pi\alpha})e^{i\pi\alpha m}} p_m & m \geq 0 \\ e^{i\pi\alpha}\left(e^{-i\pi\alpha}+1\right)\left(1-e^{-4\pi\eta}\right)p_{-1} & m = -1 \\ e^{i\pi\alpha}p_{-1}^2. & m = -2 \\ 0 & m < -2 \end{cases}. \tag{11.34}$$

The sums appearing in Eqs. (11.30) and (11.31) can be evaluated numerically: their convergence is assured by the negative exponential of coefficients p_m in Eq. (11.33). As for the case of isolated pulses, the excess charge is defined as $\Delta Q = Q_2 - 2Q_1$ for the periodic drive. A meticulous numerical exploration of the parameters can be found in the next sections.

It has been shown in Ref. [173] that a Fano relation exist between noise and backscattered current for one-Leviton and multi-Leviton states regardless of the value of the time separation Δt. As a result, apart from the fact that transport is Poissonian, the fluctuations do not give more information on the interaction between the pulses than the current . The following study therefore focuses on the current and no discussion about noise is provided. Moreover, it is instructive to point out that the regularized charge fluctuations introduced for isolated pulse in Eq. (11.18) do correspond to the equivalent expression from the periodic case in the limit $\eta \to 0$.

[1] Indeed, the backscattered charge is the average value of the current over a full period times the period.

Before concluding this section, an interesting situation is discussed, that of the injection of two excitations with opposite charge, i.e., one Leviton and one anti-Leviton, separated by a time delay Δt in the same period. The applied voltage is

$$V(t) = \sum_{s=\pm} s \sum_{k=-\infty}^{+\infty} \frac{V_0}{\pi} \frac{\gamma^2}{\gamma^2 + (t - k\mathcal{T} + s\Delta t/2)^2}\,, \tag{11.35}$$

It is therefore an even function of time, i.e $V(t) = V(-t)$. The first consequence, as shown in App.G.1 is that the backscattered charge induced by this voltage vanishes for any value of Δt. As a result, the current is not Poissonian and the interaction between the Leviton and the anti-Leviton cannot be probed by a measure of the backscattered charge. A computation of the charge fluctuations might therefore prove to be useful. To this end, the equivalent of the calculation leading to Eq. (11.22) can be performed. The charge fluctuations induced by a single couple of Leviton anti-Leviton, read as

$$\tilde{S}_{Q,l\bar{l}} = 2\left[\left(\frac{2\gamma}{\Delta t}\right)^2 + 1\right]^{-1} \tilde{S}_{Q,l}\,, \tag{11.36}$$

Where l stands for Leviton and $\bar{l}$ stands for anti-Leviton. This result bears a simple physical meaning, when $\Delta t/\gamma \to 0$, the Leviton is superposed with the anti-Leviton in the drive, resulting in no drive at all, and when $\Delta t/\gamma \to \infty$ they are well separated and give twice the fluctuations of a single Leviton.

Finally, it is worth to point out that the case of Leviton and anti-Leviton is equivalent to an HOM interferometer, where two Levitons with the same charge are injected from two opposite terminals, e.g., terminal S and the gray terminal of left moving particles in the setup of Fig. 11.1, separated by a controllable time delay. Indeed, the charge fluctuations for the case of two excitations with opposite charge separated by a time delay correspond to the well-known analytical expression for the charge noise computed in an Hong-Ou-Mandel configuration, see for instance Ref. [52].

11.4. Results

In the previous section, a connection was established between the excess charge ΔQ and the effect of the strongly-correlated background on the two-Leviton state. Follows an analysis and a few plots of this quantity as a function of different parameters.

11.4.1. Comparison with the isolated pulse case and effects of time separation

Before investigating the excess charge, a plot of the backscattered charge Q_2 as a function of $\Delta t/\gamma$ in the periodic case is presented in Fig. 11.3. The filling factor is $\nu = 1/3$, Q_2 is normalized with respect to Q_1, and different values of the parameter $\eta = \gamma/\mathcal{T}$ correspond to different colors. In order to provide an estimation for the experimentally realistic value of γ, the width of the pulse is chosen to be that tailored for future applications in the quantum information domain. The pulses should be as short as possible in order to maximize the time over which the single-electron excitations stay the micrometric tunneling region. It has been estimated that the required pulse width to perform a single-qubit rotation is roughly $\gamma \sim 10$ ps, which is at the limit of state-of-the-art technology [36]. Shorter pulses can be envisioned by resorting to schemes based on optoelectronics generation [176]. Generally, the frequency is set to $\Omega/2\pi = 5$ GHz in experiments involving Levitons, the resulting value for the dimensionless width is $\eta = 5 \times 10^{-2}$. For theoretical purposes, i.e., a comparison with purely isolated pulses, values of η far lower than this estimation are also considered, see Fig. 11.3. Indeed, for $\eta = 10^{-4}, 10^{-5}$ the colored lines corresponding to the periodic case approach the black dashed line, which correspond to the case of isolated pulses. The limit of isolated pulses therefore

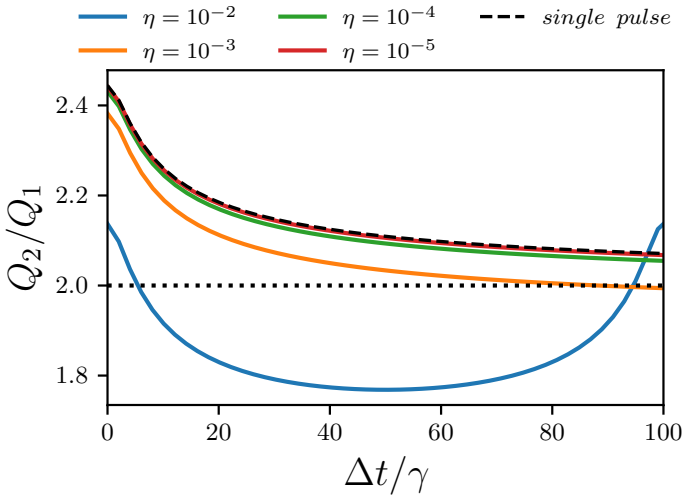

Figure 11.3.: Backscattered charge for a two-Leviton state Q_2 in units of that induced by a single Leviton, as a function of $\Delta t/\gamma$ and at zero temperature. The black dashed line represents the limit of a single pulse. Solid lines are computed for the periodic case with $\eta = 10^{-2}, 10^{-3}, 10^{-4}, 10^{-5}$. The black dotted line is a visual guide for $Q_2 = 2Q_1$. The figure was obtained at filling factor $\nu = 1/3$.

corresponds to infinitely large periods $\gamma \ll \mathcal{T}$, as anticipated in the model section. For $\eta = 10^{-4}, 10^{-5}$ the ratio Q_2/Q_1 is always greater than or equal to 2: the effect of the correlated background is always to enhance the backscattered charge compared to the case $\nu = 1$ as for the case of an isolated pulse. On the other hand, for $\eta = 10^{-2}, 10^{-3}$, the ratio Q_2/Q_1 can also be smaller than or equal to 2, which means that the effect of the correlated background is strongly affected by the width of Lorentzian pulses in the periodic case. In passing, this additional feature occurs for values of η which are closer to realistic estimation. For this reason, it is interesting to explore further the dependence of the backscattered charge on the other parameters: $\alpha = \Delta t/(2\mathcal{T})$ and $\eta = \gamma/\mathcal{T}$. The excess charge, Eq. (11.25), gives a diagnosis on the type of interaction, for $\Delta Q > 0$ ($\Delta Q < 0$), the backscattered charge is increased (reduced) by strong correlations with respect to the trivial case at $\nu = 1$. In Fig. 11.4, the excess charge as a function of α is presented for different values of η. Generally, for a large range of η, the sign of ΔQ can be monitored by tuning the parameter α. Interestingly, there exist some values of α where the excess charge ΔQ vanishes. The effect of strong correlations on two-Leviton states can therefore be tuned on and off by acting on the separation time Δt. Above a certain value of η, the sign of ΔQ is negative for any value of α at zero temperature and $\nu = 1/3$. While the specific values of η depend on temperature and filling factor, the important result is that there always exists a width of Lorentzian pulse above which the sign of ΔQ is strictly negative.

11.4.2. Effects of the pulse width

Similarly, in Fig. 11.5 the behavior of the excess charge is depicted as a function of η. In particular, for increasing values of η all the lines reach the asymptotic excess charge $\Delta Q = Q_1\left(2^{2\nu-1} - 2\right)$, which corresponds to the limit of a constant voltage $V_{DC} = \hbar\Omega q/e$. In the inset of this figure, these curves are zoomed-in around the range $\eta = 10^{-3} - 10^{-2}$. The black dotted is a visual guide for the limit $\eta \to \infty$: in this case the periodic drive corresponds to a constant voltage with $q = 2$ and one finds the analytical value of $\Delta Q = Q_1\left(2^{2\nu-1} - 2\right)$. Again, for some values of α and η the excess charge ΔQ vanishes and by tuning these parameters its sign can be reversed. More precisely, one can see that ΔQ changes sign only for $\alpha = 0.01$ and $\alpha = 0.1$.

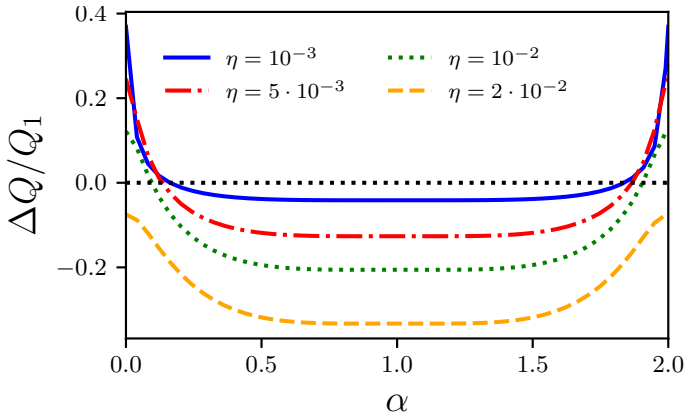

Figure 11.4.: Excess backscattered charge ΔQ in units of the backscattered charge Q_1 due to a single Leviton, as a function of $\alpha = \Delta t/2\mathcal{T}$ at zero temperature. The black dotted line is a visual guide for $\Delta Q = 0$. Solid lines are computed for the periodic case with $\eta = 10^{-3}, 5 \cdot 10^{-3}, 10^{-2}, 2 \cdot 10^{-2}$. The figure was obtained at filling factor $\nu = 1/3$.

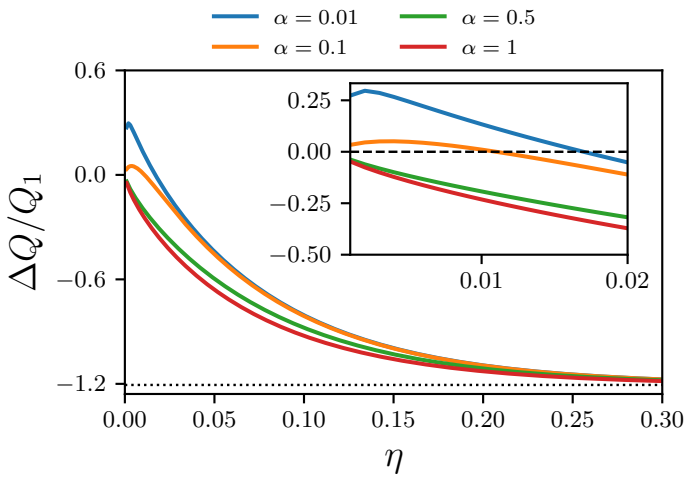

Figure 11.5.: Excess backscattered charge ΔQ in units of the backscattered charge Q_1 due to a single Leviton, as a function of $\eta = \gamma/\mathcal{T}$ and at zero temperature. Various values of α are represented with different colors, $\alpha = 0.01, 0.1, 0.5, 1$. The figure was obtained at filling factor $\nu = 1/3$. (Inset) Zoom of the same plot between $\eta = 0$ and $\eta = 2 \cdot 10^{-2}$

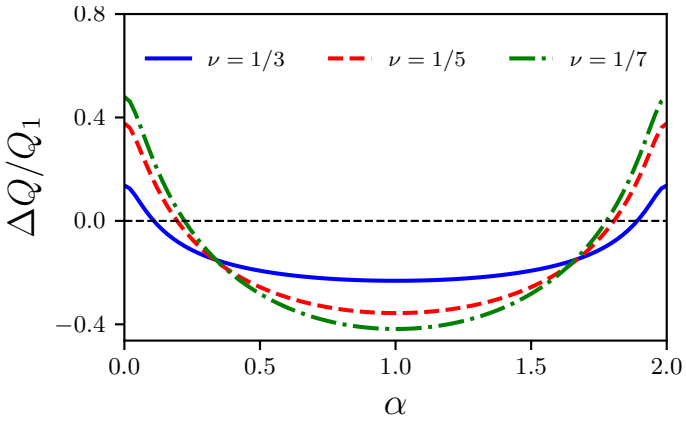

Figure 11.6.: Excess backscattered charge ΔQ in units of the backscattered charge Q_1 for a single Leviton, as a function of $\alpha = \Delta t/2\mathcal{T}$ and at zero temperature. The black dotted line is a visual guide for $\Delta Q = 0$ and corresponds to the case $\nu = 1$. Different filling factors are represented by different colors for the following values $\nu = 1/3, 1/5, 1/7$. The figure was obtained at $\eta = 10^{-2}$.

11.4.3. Effects of the filling factor and the temperature

Finally, the dependence of ΔQ on the properties of the strongly-correlated background is explored. The latter are encoded in the Green's function which in turns depends on the filling factor ν and the temperature θ. The dependence of ΔQ on the filling factor and, therefore, on the strength of the interaction is presented in Fig. 11.6 for $\nu = 1/3, 1/5, 1/7$. In general, two behaviors emerge as the filling factor is reduced. First of all, the values of α for which the excess charge vanishes increase, thus a stronger interaction requires larger separation time Δt to compensate its effect on the two-Leviton state. Moreover, for stronger correlations, the absolute value of the maximum (in $\alpha = 0$) and the minimum (in $\alpha = 1$) of ΔQ are also increasing. The effect of temperature in Fig. 11.7 can be summarized as follows. A qualitatively different behavior of the current as a function of α arise for different regimes of temperature. For low temperature, the excess charge behaves as in the zero-temperature case (blue line), i.e., a single minimum appears at $\alpha = 1$. As the temperature is increased, a plateau develops for intermediate values of α. In the high temperature limit, two minima appear for values of α different from $\alpha = 1$ and which depend on the specific temperature. Furthermore, in this regime, ΔQ reaches a local maximum in $\alpha = 1$. Finally, the excess charge ΔQ is changing sign as a function of α, except for the highest value of $\theta = \Omega$: in this case ΔQ is always negative. In order to make contact with experiments it can be said that for $\Omega = 2\pi \times 5$ GHz, the temperature $\theta = \Omega$ corresponds to roughly 1.5 K.

11.5. Conclusion

In this chapter, the effect of a strongly-correlated system on the propagation of two-Leviton states were studied in the particular case of a two-dimensional electron gas in the Laughlin sequence of the fractional quantum Hall effect. These Levitons are injected by periodic trains of quantized Lorentzian-shaped pulses with controllable width and time separation. It was recalled that Levitons, in the tunnel regime, are minimal excitations states. Considering a quantum point contact, the backscattered charge was computed for the low-transparency limit. Analytical results are derived in the case of isolated pulses (i.e., infinite period) and zero temperature. Then, the charge backscattered for the two-Leviton state, namely Q_2, is computed and compared with the backscattered charge in the presence of a single pulse, termed Q_1. By an explicit calculation, it is shown that $Q_2 > 2Q_1$ in the fractional regime, in contrast to the trivial result $Q_2 = 2Q_1$

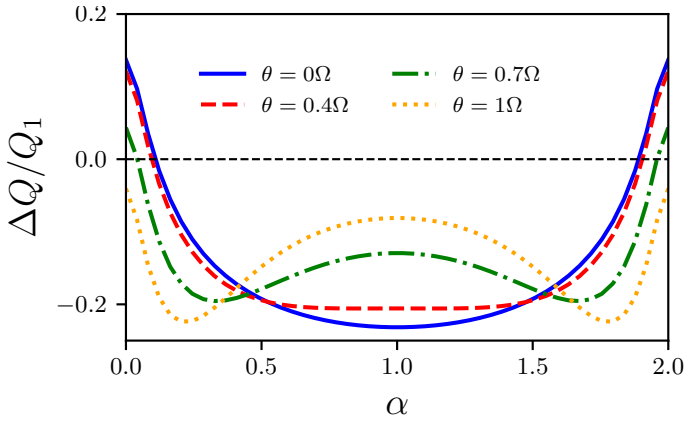

Figure 11.7.: Excess backscattered charge ΔQ, in units of the backscattered charge Q_1 for a single Leviton, as a function of $\alpha = \Delta t/2\mathcal{T}$ and for different values of temperature. The black dotted line is a visual guide for $\Delta Q = 0$. The different curves were obtained at different temperatures $\theta = 0, 0.4\Omega, 0.7\Omega, \Omega$. For higher temperatures, two local minima appear at the left and at the right of $\alpha = 1$. The figure was obtained at $\nu = 1/3$ and $\eta = 10^{-2}$.

at $\nu = 1$. Interestingly, in the limit of simultaneous pulses ($\Delta t \ll \gamma$), the backscattered charge acquires a simple expression depending only on the filling factor ν. By resorting to the wave-packet formalism for Levitons, the former results are explained by conjecturing the existence of an effective interaction between the two Levitons, caused by the strongly-correlated background.

The case of single pulses at finite temperature was then studied numerically. These simulations show that, for high enough temperatures and even for simultaneous pulses, $Q_2 < 2Q_1$. Relying on the effective interaction interpretation, this means that the temperature, together with the time separation of the pulses, can be used to monitor the intensity and the sign of the interaction.

Then, in order to make contact with experimental situations, the case of both finite temperature and finite period is considered, it relies on numerical calculations in the photo-assisted formalism. In the periodic case, one can tune the backscattered charge Q_2, as a function of Δt, to be smaller than, equal to or greater than $2Q_1$. The effect of the correlated background are considered in the dependence of the backscattered charge on the filling factor and on temperature. As in the case of single pulses, the effective interaction can be tuned from positive to attractive by monitoring the width of the pulse, the period and the temperature. The numerical calculations are based on realistic estimations of the parameters that can be achieved with state-of-the-art technology.

Interesting extension of the present work can be the calculation of the backscattered charge in the presence of extended or multiple quantum point contacts, thus taking into account the effect of quantum interference [177–179]. Indeed, the realization of quantum computing architecture with Levitons requires the presence of multiple tunneling regions.

Conclusion

Summary In this thesis, time-dependent quantum transport through a quantum point contact in correlated systems was studied and proposals of applications to electron quantum optics were put forward. It started by recalling the basics of quantum transport in quantum point contacts, as well as the formalism suitable for computing observables, like the average electric current or the current noise, in out-of-equilibrium situations (finite temperature and voltage-driven junction). The focus was directly set on periodic voltage drives, the principal features of Floquet theory, describing quantum systems with periodic Hamiltonians, were explained as a tool providing a physical interpretation for transport observables in such systems. An application of this interpretation was proposed for the simplest non-correlated system, the $N-N$ junction. This allowed, using the Tien-Gordon picture, to show that the current noise created by the periodic drive is equal to the DC equivalent when no holes are excited by the drive. From this, as was done by Levitov *et. al.*, it is possible to design a drive which only excites electrons above the Fermi sea without perturbing it. Furthermore, measuring the noise in excess allows to actually ascertain that the Fermi sea is not perturbed. This constitutes the paradigm of electron quantum optics with Levitons in non-correlated systems.

The second part of the thesis provided an extension to the concept of Levitons to systems with superconducting correlations. To this end, the basics of BCS superconductivity were recalled as well as transport in the DC-driven $N-S$ junction. Studying this junction under a periodic drive, the first thing to show was that in the regime where the drive frequency is far greater than the superconducting gap, the behavior of the $N-N$ junction is retrieved, i.e., integer Levitons are minimal excitation states of the junction. On the other hand, it was found that, in the Andreev regime of the junction (frequency of the drive far lower than the gap), when two equivalent half Levitons of opposite spin are sent at the $N-S$ junction, they create a minimal excitation state of the junction. Using the fact the BCS ground state is entangled both in spin and energy, these so-called Andreev Levitons were used to design an on-demand, time-resolved source of energy-entangled states in a junction involving a BCS superconductor and two spin-polarized edge states of a quantum spin Hall bar. This might constitute the first proposition of an electron quantum optics device generating on-demand energy-entangled state with Lorentzian pulses. For completeness the $N-S$ junction was studied in detail in every regime of the drive frequency, this allowed for example to explain, from the simple Tien-Gordon picture, how a non-linear density of states (due to interactions) can lead to negative excess noise. Further, thanks to the Floquet interpretation, it was possible to understand how does the Tien-Gordon picture break down when taking into account both non-linear density of states *and* higher order tunneling events.

Finally the third part of this thesis focused on time-dependent transport in the fractional quantum Hall effect (FQHE). After recalling the basics of the FQHE and of the chiral Luttinger liquid theory used to describe its the edge states, the standard results for tunneling at quantum point contact in the FQHE were recalled. A robust way to measure the scaling dimension from the time-dependent current instead of the noise was proposed. It relies on the fact that the QPC can be driven either by a superposition of DC plus AC voltage drive or by an AC modulation of the amplitude. In the latter case and for a harmonic modulation, it was shown that the second harmonic of the current is directly proportional to the scaling dimension of the quasiparticles. Finally, when two Levitons per period are sent at a QPC, it was shown that the backscattered charge is not twice that of a single Leviton, this is interpreted as the result of an effective interaction between the two Levitons carried by the strongly correlated background. Performing a precise study of this interaction, it was shown that it can be tuned from attractive to repulsive by the time shift

between the two Levitons. This appears to be the first theoretical proposal for a platform implementing two Levitons in interaction and where this interaction can be fully monitored by a time-shift in the drive.

Perspectives The theoretical work presented here has formal aspects, yet it was shown that it can have applications in an experimental context. In particular, the results presented here were illustrated with realistic experimental parameters.

In the first original part of this study, the focus was set on electron quantum optics in junctions between a normal metal and conventional superconductors, described by BCS theory. Yet in the last decade or more, a lot of excitement (on the theoretical and the experimental side) has been generated on unconventional superconductors. Among these are topological superconductors, which are expected to host Majorana fermions. The toy model in this case is the Kitaev model, which relies on p-wave pairing in a one-dimensional system of spinless electron on a lattice. For specific parameters of this model (chemical potential, nearest neighbor hopping, p-wave pairing amplitude) this system bears Majorana fermions at its extremities (whose creation and annihilation operators coincide). This toy model has potential applications to quantum computing, as a delocalized fermion - built from these two Majorana fermions - can be built and its occupancy/parity (zero or one) can be used as a qubit which is thus topologically protected. It is important to note that physical realizations of the Kitaev model have been proposed by theorists and experimentalists. A possible extension of the present work would therefore be to generalize the results to a spin polarized fermion system composed of a normal metal branch and a topological superconductor (TS). In principle all the ingredients to repeat the analysis in this case are already present, allowing to make predictions on the photo-assisted current and noise. This extension goes well beyond the scope of this thesis, but constitutes a very solid prolongation of the present formalism.

The contribution of this thesis on the on-demand source of energy-entangled states paves the way to the study of quantum Hall systems coupled to a BCS superconductor. The case of a quantum spin Hall model was studied specifically because of the opposite chirality of the two spin branches, which allow physical separation of the outgoing states. First, a generalization to the (conventional) integer quantum Hall effect at filling factor two (with two spin species) seems straightforward and could be addressed in future work. In the long run, it would be also interesting to study the coupling between the fractional quantum Hall bar and a BCS superconductor. The difficulty here would be to include spin flip processes at the junction so that the constituent electrons of a Cooper pair can be converted in a superposition of Laughlin quasiparticles in the Hall system.

A. Keldysh's method

This Appendix provides various results related to Keldysh's formalism used in the main text.

A.1. From Keldysh through Wick to Dyson

In this section, it is shown that the following formula for the Green's function

$$G_{ij}^{\eta_1\eta_2}(t,t') = -i\left\langle T_K c_{i,I}(t^{\eta_1}) c_{j,I}^\dagger(t^{\eta_2}) \sum_{n=0}^{\infty} \frac{(-i)^n}{n!} \left[\prod_0^n \int_K \mathrm{d}t_n H_{T,I}(t_n)\right]\right\rangle_0 . \tag{A.1}$$

obeys a Dyson equation in Keldysh-lead space. First the Hamiltonian in the interaction picture reads as

$$H_{T,I} = \lambda(t) c_{R,I}^\dagger(t) c_{L,I}(t) + \text{H.c.}\,, \tag{A.2}$$

and the integral over the Keldysh can be written as

$$\int_K \mathrm{d}t = \int_{-\infty}^{\infty} \mathrm{d}t^+ + \int_{\infty}^{-\infty} \mathrm{d}t^- . \tag{A.3}$$

As a result, to first order in λ, the Green's function reads as

$$\begin{aligned} G_{ij}^{\eta_1\eta_2}(t,t') = &-i\left\langle T_K c_{i,I}(t^{\eta_1}) c_{j,I}^\dagger(t'^{\eta_2})\right\rangle_0 \\ &+(-i)^2\Bigg\langle T_K c_{i,I}(t^{\eta_1}) c_{j,I}^\dagger(t'^{\eta_2})\Bigg[\int_{-\infty}^{\infty} \mathrm{d}t_1^+ \left\{\lambda(t_1^+) c_{R,I}^\dagger(t_1^+) c_{L,I}(t_1^+) + \lambda^*(t_1^+) c_{L,I}^\dagger(t_1^+) c_{L,I}(t_1^+)\right\} \\ &\qquad + \int_{\infty}^{-\infty} \mathrm{d}t_1^- \left\{\lambda(t_1^-) c_{R,I}^\dagger(t_1^-) c_{L,I}(t_1^-) + \lambda^*(t_1^-) c_{L,I}^\dagger(t_1^-) c_{R,I}(t_1^-)\right\}\Bigg]\Bigg\rangle_0 \\ &\qquad + O(\lambda^2) . \end{aligned} \tag{A.4}$$

The first term immediately corresponds to the bare Green's function $g_{ij}^{\eta_1\eta_2}(t,t')$. It is important to remark that $g_{RL} = 0$ as, without interaction, the leads are not linked in any way. Wick's theorem can be used on the second and third lines to separate the average values of four fermion operators into two fermion average values. Developing all the terms, and writing them explicitly, one finds that

$$\begin{aligned} G_{ij}^{\eta_1\eta_2}(t,t') = g_{ij}^{\eta_1\eta_2}(t,t') &+ g_{iR}^{\eta_1,+}(t,t_1)\lambda(t_1) g_{Lj}^{+,\eta_2}(t_1,t') + g_{iL}^{\eta_1,+}(t,t_1)\lambda^*(t_1) g_{Rj}^{+,\eta_2}(t_1,t') \\ &- g_{iR}^{\eta_1,-}(t,t_1)\lambda(t_1) g_{Lj}^{-,\eta_2}(t_1,t') - g_{iL}^{\eta_1,-}(t,t_1)\lambda^*(t_1) g_{Rj}^{-,\eta_2}(t_1,t') + O(\lambda^2) . \end{aligned} \tag{A.5}$$

One immediately recognizes a convolution and a matrix product in the Keldysh-lead tensor product space[1], where the Green's function is trivially defined, and the self energy

$$\Sigma^{\eta\eta'}_{LR}(t,t') = \left[\Sigma^{\eta\eta'}_{RL}\right]^*(t,t') = \delta(t-t')\lambda(t)\left[\sigma_z\right]_{\eta\eta'} \quad \text{and} \quad \Sigma^{\eta\eta'}_{LL}(t,t') = \Sigma^{\eta\eta'}_{RR}(t,t') = 0\,, \tag{A.6}$$

is introduced, note that σ_z is the third Pauli matrix in Keldysh space where the first line and row represent the + contour. As a result, the Green's function can be written in a compact way,

$$G(t,t') = g(t,t') + \iint_{\mathbb{R}^2} \mathrm{d}t_1\mathrm{d}t_2 g(t,t_1)\Sigma(t_1,t_2)g(t_2,t') + O(\lambda^2)\,. \tag{A.7}$$

This result can be extended to all order by writing the full Green's function recursively, one can indeed check that

$$G(t,t') = g(t,t') + \int_{\mathbb{R}^2} \mathrm{d}t_1\mathrm{d}t_2\, g(t,t_1)\Sigma(t_1,t_2)G(t_2,t)\,, \tag{A.8}$$

A.2. Keldysh rotation

This section aims at deriving the equations commonly called Dyson I and Dyson II for the Green's functions in Keldysh space. They allows to design an algorithm to compute the dressed Green's functions in terms of the bare ones and the self energy. As these are Keldysh space equations the lead indices are not specified (summation over these indices is assumed). Furthermore the Green's functions are evaluated in frequency representation, this has two advantages, first the convolution products become simple products. And second, when there is a time-dependent drive, the harmonics can be encapsulated in a matrix representation so the convolution products becomes a matrix product. First, the definition of the Green's functions in the standard Keldysh basis are given

$$G^{\eta\eta'}(t,t') = -i\left\langle T_{\mathrm{K}} c_{\mathrm{H}}(t^\eta) c^\dagger_{\mathrm{H}}(t'^{\eta'})\right\rangle\,. \tag{A.9}$$

One notices that this system is twice degenerate as there exists only two different correlators, $\left\langle c_{\mathrm{H}}(t)c^\dagger_{\mathrm{H}}(t'^{\eta'})\right\rangle$ and $\left\langle c_{\mathrm{H}}(t'^{\eta'})c^\dagger_{\mathrm{H}}(t)\right\rangle$. This suggests that some relations can be found between the four Keldysh Green's functions, indeed, one can show that

$$G^{++}(r,t,r',t') + G^{--}(r,t,r',t') = -i\left\langle \psi(t)\psi^\dagger(t') - \psi^\dagger(t')\psi(t)\right\rangle = G^{-+}(r,t,r',t') + G^{+-}(r,t,r',t')\,. \tag{A.10}$$

This motivates a change of basis from the matrix

$$G = \begin{pmatrix} G^{++} & G^{+-} \\ G^{-+} & G^{--} \end{pmatrix}\,, \tag{A.11}$$

to a more useful one, where Eq. (A.10) is directly used to have a zero in the matrix representation.

An appropriate basis is found by using the rotation matrix $L = \frac{1}{\sqrt{2}}(\mathbb{1} - i\sigma_y)$, where σ_y is the second Pauli matrix. Using Eq. (A.10), it is straightforward to show that

$$LGL^\dagger = \begin{pmatrix} 0 & G^a \\ G^r & G^K \end{pmatrix}\,, \tag{A.12}$$

[1]The matrix element are defined by two sets of indices, Keldysh indices *and* lead indices.

where the retarded, advanced, and Keldysh Green's functions where introduced, namely,

$$\begin{aligned} G^r &= G^{++} - G^{+-} \\ G^a &= G^{++} - G^{-+} \\ G^K &= G^{++} + G^{--} \,. \end{aligned} \tag{A.13}$$

This is the so-called RAK basis.

Some constraints on the self energy in the RAK basis can also be found from the rotated Dyson equation:

$$LGL^\dagger = LGL^\dagger + LgL^{-1} \otimes L\Sigma L^{-1} \otimes LGL^\dagger \,. \tag{A.14}$$

writing the self energy in the new basis as

$$L\Sigma L^\dagger = \frac{1}{2}\begin{pmatrix} \Sigma^{++} - \Sigma^{+-} - \Sigma^{-+} + \Sigma^{--} & \Sigma^{++} + \Sigma^{+-} - \Sigma^{-+} - \Sigma^{--} \\ \Sigma^{-+} - \Sigma^{--} + \Sigma^{-+} + \Sigma^{--} & \Sigma^{-+} + \Sigma^{--} + \Sigma^{++} + \Sigma^{+-} \end{pmatrix} = \begin{pmatrix} \alpha & \beta \\ \gamma & \delta \end{pmatrix} , \tag{A.15}$$

Eq. (A.14) reads as

$$\begin{pmatrix} 0 & G^a \\ G^r & G^K \end{pmatrix} = \begin{pmatrix} g^a \delta G^r & g^a(\gamma G^a + \delta G^K) \\ g^r \beta G^r + g^K \delta G^r & g^r(\alpha G^a + \beta G^K) + g^K(\gamma G^a + \delta G^K) \end{pmatrix} , \tag{A.16}$$

This immediately means that $\delta = 0$ which in turns [from Eq. (A.15)] implies that

$$\Sigma^{-+} + \Sigma^{--} + \Sigma^{++} + \Sigma^{+-} = 0 \,, \tag{A.17}$$

and finally,

$$L\Sigma L^\dagger = \begin{pmatrix} \Sigma^{++} + \Sigma^{--} & \Sigma^{++} + \Sigma^{+-} \\ \Sigma^{-+} + \Sigma^{++} & 0 \end{pmatrix} , \tag{A.18}$$

which is used to define the advanced, retarded and Keldysh self energies. Writing the rotated version of Dyson's equations allow to understand the usefulness of the RAK basis as

$$\begin{aligned} G^a &= g^a + g^a \Sigma^a G^a \\ G^r &= g^r + g^r \Sigma^r G^r \\ G^K &= g^K + g^r \Sigma^r G^K + g^K \Sigma^a G^a + g^r \Sigma^K G^a \,. \end{aligned} \tag{A.19}$$

The important result is that the retarded and advanced Green's function directly obey the standard Dyson equation.

This can be used to find some useful formulas for $G^{\pm\mp}$ which are the functions involved in the current and the noise. The function G^K is usually complicated so one usually writes it in terms the retarded and advanced ones, this is the first step of this paragraph. As a first step, it is recalled that

$$G^r = g^r + g^r \Sigma^r G^r = g^r + G^r \Sigma^r g^r \,. \tag{A.20}$$

The first consequence is that

$$(\mathbb{1} - g^r \Sigma^r) G^r = g^r \,. \tag{A.21}$$

which can be written as

$$\begin{aligned} (\mathbb{1} - g^r \Sigma^r)^{-1} &= G^r (g^r)^{-1} \\ &= \mathbb{1} + G^r \Sigma^r \,, \end{aligned} \tag{A.22}$$

where Eq. (A.20) was used to get the second line. This is useful when writing the third line of Eq. (A.19) as

$$(\mathbb{1} - g^r\Sigma^r)G^K = g^K(\mathbb{1} + \Sigma^K G^a) + g^r\Sigma^K G^a\,. \tag{A.23}$$

Indeed, applying Eq. (A.22) gives

$$G^K = (\mathbb{1} + G^r\Sigma^r)g^K(1 + \Sigma^K G^a) + (\mathbb{1} + G^r\Sigma^r)g^r\Sigma^K G^a\,, \tag{A.24}$$

which is in itself an important result as some authors directly use this function to compute $G^{\pm\mp}$ through

$$G^{\pm\mp} = \frac{1}{2}(\pm G^a \mp G^r + G^K)\,. \tag{A.25}$$

An independent way to compute $G^{\pm\mp}$ is through a direct replacement of Eq. (A.19) in Eq. (A.25), this gives

$$\begin{aligned} G^{\pm\mp} &= \frac{1}{2}\left(\pm g^a \mp g^r + g^K + g^r[\Sigma^K G^a + \Sigma^r(G^K \mp G^r)] + (\pm g^a + g^K)\Sigma^a G^a\right) \\ &= \frac{1}{2}\left(2g^{\pm\mp} + g^r[(-2\Sigma^{\pm\mp} \pm \Sigma^r \mp \Sigma^a)G^a + \Sigma^r(2G^{\pm\mp} \mp G^a)] + (\pm g^r + 2g^{\pm\mp})\Sigma^a G^a\right)\,, \end{aligned} \tag{A.26}$$

Summing it up, one finds Dyson I

$$G^{\pm\mp} = g^{\pm\mp} - g^r\Sigma^{\pm\mp}G^a + g^r\Sigma^r G^{\pm\mp} + g^{\pm\mp}\Sigma^a G^a\,. \tag{A.27}$$

An alternative form can be found, factorizing $G^{\pm\mp}$ one finds

$$(\mathbb{1} - g^r\Sigma^r)G^{\pm\mp} = g^{\pm\mp}(\mathbb{1} + \Sigma^a G^a) - g^r\Sigma^{\pm\mp}G^a\,, \tag{A.28}$$

applying Eq. (A.22) on the left yields Dyson II

$$G^{\pm\mp} = (\mathbb{1} + G^r\Sigma^r)g^{\pm\mp}(\mathbb{1} + \Sigma^a G^a) - G^r\Sigma^{\pm\mp}G^a\,. \tag{A.29}$$

In the case of a QPC system, the last term does not contribute.

A.3. Dressed Green's function for a QPC based system

In this section, an expression of the dressed Green's functions $G^{\pm\mp}$ are derived in terms of the bare ones and the self energy matrices. It is assumed that the Green's functions do not commute with each other or with the self energy as they can be non-diagonal matrices. The only assumption is that the system is a QPC, described by the Hamiltonian Eq. (1.8), which means for the bare Green's function that $g_{LR} = g_{RL} = 0$.

To summarize the route of the calculation, the starting point is G^{+-}_{LR} which is recast in terms of G^{+-}_{RR} and bare Green's functions using Dyson I. Then Dyson II is used to get a formula involving only $G^{r,a}_{RL,LR}$ and $G^{r,a}_{RR}$'s. The latter obey a Dyson equation involving the two former, allowing to write the current and the noise in terms of $G^{r,a}_{RL,LR}$ only, whose Dyson's equation can be solved recursively.

As mentioned, one starts with Dyson I:

$$G^{+-}_{RL} = G^{+-}_{RR}\Sigma^a_{RL}g^a_{LL} + G^r_{RR}\Sigma^r_{RL}g^{+-}_{LL}\,, \tag{A.30}$$

in which Dyson II for G^{+-}_{RR}, i.e.,

$$G^{+-}_{RR} = (\mathbb{1} + G^r_{RL}\Sigma^r_{LR})g^{+-}_{RR}(\mathbb{1} + \Sigma^a_{RL}G^a_{LR}) + G^r_{RR}\Sigma^r_{RL}g^{+-}_{LL}\Sigma^a_{LR}G^a_{RR}\,, \tag{A.31}$$

is plugged. After a few steps of simple algebra, this yields

$$G^{+-}_{RL} = (\mathbb{1} + G^r_{RL}\Sigma^r_{LR})\Big[g^r_{RR}\Sigma^r_{RL}g^{+-}_{LL} + (g^{+-}_{RR} + g^r_{RR}\Sigma^r_{RL}g^{+-}_{LL}\Sigma^a_{LR}g^a_{RR})(\mathbb{1} + \Sigma^a_{RL}G^a_{LR})\Sigma^a_{RL}g^a_{LL}\Big]\,. \tag{A.32}$$

Next it is possible to show that

$$\mathbb{1} + G^r_{RL}\Sigma^r_{LR} = (\mathbb{1} - g^r_{RR}\Sigma^r_{RL}g^r_{LL}\Sigma^r_{LR})^{-1}\,. \tag{A.33}$$

and

$$\mathbb{1} + \Sigma^a_{RL}G^a_{LR} = (\mathbb{1} - \Sigma^a_{RL}g^a_{LL}\Sigma^a_{LR}g^a_{RR})^{-1}\,. \tag{A.34}$$

Using Eq. (A.34) and Eq. (A.33) in Eq. (A.32), one finds

$$\begin{aligned} G^{+-}_{RL} = (\mathbb{1} - g^r_{RR}\Sigma^r_{RL}g^r_{LL}\Sigma^r_{LR})^{-1}\Big[g^{+-}_{RR} + g^r_{RR}\Sigma^r_{RL}g^{+-}_{LL}(\Sigma^a_{RL}g^a_{LL})^{-1}\Big] \\ \times (\mathbb{1} - \Sigma^a_{RL}g^a_{LL}\Sigma^a_{LR}g^a_{RR})^{-1}\Sigma^a_{RL}g^a_{LL}\,. \end{aligned} \tag{A.35}$$

This expression can directly be used in various case, for different types of drives or different bare green's functions.

A.4. Bare Green's functions

In this section, the bare Green's functions in different systems are derived, namely, a normal metal, a BCS superconductor.

A.4.1. Normal metal

In the case of a normal metal, no interactions are present and the Green's function can be computed by going to the site basis. Enforcing the wide band limit and writing the Green's in units of the density of state at the Fermi surface, one gets

$$g^{r/a}_{\alpha\alpha}(\omega) = \mp i\,. \tag{A.36}$$

A.4.2. BCS superconductor

It was shown in [180], by solving Keldysh Dyson's equation for the electrons when electron-phonon interaction is included, that the bare Green function of electrons in the superconductor can be written as

$$g^{r/a}_{BCS}(\omega) = -\lim_{\delta\to 0}\frac{\omega\mathbb{1} + \Delta\sigma_x}{\sqrt{\Delta^2 - (\omega \pm i\delta)^2}}\,, \tag{A.37}$$

A.4.3. Phonon Green's function

Here a quick computation of the phonon Green's function on its ground state is proposed, it is used in the derivation of the effective attraction between electrons at the root of BCS theory of superconductivity. Using Eq. (4.8), the phonon correlator in real space can be computed and reads as

$$\begin{aligned} D(r,t) &= -i\,\langle T(\varphi_{\mathrm{I}}(r,t)\varphi_{\mathrm{I}}(0,0))\rangle \\ &= i\sum_k \frac{\omega_k}{2}\left(\Theta(t)e^{i(kr-\omega_k t)} + \Theta(-t)e^{-i(kr-\omega_k t)}\right)\,. \end{aligned} \tag{A.38}$$

Now switching to Fourier space, allows to write

$$\begin{aligned} D(l,\varepsilon) &= Vi \int \frac{\mathrm{d}^3k}{(2\pi)^3} \int \frac{\mathrm{d}^3r}{V} \frac{\omega_k}{2} \left[e^{i(k-l)r} \int_0^{+\infty} \mathrm{d}t\, e^{-i(\omega_k-\varepsilon)t} + e^{-i(k+l)r} \int_{-\infty}^{0} \mathrm{d}t\, e^{i(\omega_k+\varepsilon)t} \right] \\ &\approx \frac{\omega_l^2}{\varepsilon^2-\omega_l^2}\,. \end{aligned} \tag{A.39}$$

using the linear dispersion relation of phonons, $lv_s = \omega_l$, this is finally written as

$$D(l,\varepsilon) = \frac{v_s^2 l^2}{\varepsilon^2 - v_s^2 l^2}\,. \tag{A.40}$$

B. Double Fourier transform

In this Appendix, the Fourier series of a general double periodic function is defined. Then its application to the Green's functions, bare and dressed, and the self energy is discussed.

B.1. Double Fourier transform

If $F(t,t')$ is T-periodic in the first and second argument, one defines its harmonics as

$$F_{nm}(\omega) = \int_{-T/2}^{T/2} \frac{\mathrm{d}\bar{t}}{T} \int_{-\infty}^{\infty} \mathrm{d}\tau \, e^{i(\omega+n\Omega)\left(\bar{t}+\frac{\tau}{2}\right)} e^{-i(\omega+m\Omega)\left(\bar{t}-\frac{\tau}{2}\right)} F\left(\bar{t}+\frac{\tau}{2}, \bar{t}-\frac{\tau}{2}\right) , \tag{B.1}$$

with $\Omega T = 2\pi$, the total time $2\bar{t} = t + t'$ and the relative time $\tau = t - t'$. This definition allows for an alternative expression of F in the time domain. Indeed,

$$\begin{aligned}
&\sum_{nm} \int_{-\Omega/2}^{\Omega/2} \frac{\mathrm{d}\omega}{2\pi} \, e^{-i(\omega+n\Omega)t} e^{i(\omega+m\Omega)t'} F_{nm}(\omega) \\
&\qquad = \sum_{nm} \int_{-\Omega/2}^{\Omega/2} \frac{\mathrm{d}\omega}{2\pi} \, e^{-i\omega(t-t'-\tau)} \int_{-T/2}^{T/2} \frac{\mathrm{d}\bar{t}}{T} \int_{-\infty}^{\infty} \mathrm{d}\tau \\
&\qquad\qquad \times e^{-in\Omega\left(t-\bar{t}-\frac{\tau}{2}\right)} e^{im\Omega\left(t'-\bar{t}+\frac{\tau}{2}\right)} F\left(\bar{t}+\frac{\tau}{2}, \bar{t}-\frac{\tau}{2}\right) \\
&\qquad = \int_{-T/2}^{T/2} \frac{\mathrm{d}\bar{t}}{T} \, \delta\left(\frac{t+t'}{2} - \bar{t}\right) F\left(\bar{t}+\frac{t-t'}{2}, \bar{t}-\frac{t-t'}{2}\right) \\
&\qquad = F(t,t') \, .
\end{aligned} \tag{B.2}$$

To summarize, the following development in harmonics was proven to hold

$$F(t,t') = \sum_{nm} \int_{-\Omega/2}^{\Omega/2} \frac{\mathrm{d}\omega}{2\pi} \, e^{-i(\omega+n\Omega)t} e^{i(\omega+m\Omega)t'} F_{nm}(\omega) \, . \tag{B.3}$$

B.2. Convolution product

One is interested in the convolution product of such functions, as this is what appears in the current, the noise, or even Dyson's equations. The calculation is explicitly performed here:

$$\begin{aligned}(F\circ G)(t,t') &= \int_{-\infty}^{+\infty} \mathrm{d}t_1\, F(t,t_1)G(t_1,t') \\ &= \sum_{n_1m_1n_2m_2} \int_{-\infty}^{+\infty} \mathrm{d}t_1 \int_{-\Omega/2}^{\Omega/2} \frac{\mathrm{d}\omega_1}{2\pi} \int_{-\Omega/2}^{\Omega/2} \frac{\mathrm{d}\omega_2}{2\pi} \\ &\qquad \times e^{-i(\omega_1+n_1\Omega)t} e^{i(\omega_1+m_1\Omega)t_1} F_{n_1m_1}(\omega_1) \\ &\qquad \times e^{-i(\omega_2+n_2\Omega)t_1} e^{i(\omega_2+m_2\Omega)t'} F_{n_2m_2}(\omega_2) \\ &= \sum_{n_1m_1n_2m_2} \int_{-\Omega/2}^{\Omega/2} \frac{\mathrm{d}\omega_1}{2\pi} \int_{-\Omega/2}^{\Omega/2} \frac{\mathrm{d}\omega_2}{2\pi}\, \delta\left[\frac{\omega_1-\omega_2}{\Omega} - (n_2-m_1)\right] \\ &\qquad \times e^{-i(\omega_1+n_1\Omega)t} e^{i(\omega_2+m_2\Omega)t'} F_{n_1m_1}(\omega_1) F_{n_2m_2}(\omega_2)\,.\end{aligned} \tag{B.4}$$

As the Fourier decomposition of the frequencies is unique, the Dirac distribution can be separated in two as $\delta((\omega_1-\omega_2)/\Omega - (n_2-m_1)) = \delta(\omega_1-\omega_2)\delta(n_2-m_1)$. This can be seen by looking at the frequency interval $\omega \in]-\frac{\Omega}{2};\frac{\Omega}{2}]$

$$(F\circ G)(t,t') = \sum_{mn} \int_{-\Omega/2}^{\Omega/2} \frac{\mathrm{d}\omega}{2\pi}\, e^{-i(\omega+n\Omega)t} e^{i(\omega+m\Omega)t'} (F\circ G)_{nm}(\omega)\,, \tag{B.5}$$

where the harmonic component of the convolution product is $(F\circ G)_{nm}(\omega) = \sum_q F_{nq}(\omega)G_{qm}(\omega)$. The main advantage of this formulation is therefore that a convolution product in real time is the matrix product of the Fourier components.

B.3. Fourier Dyson's equations

Dyson's equations involve convolution products between periodic functions, as was shown earlier, these can be written as matrix products in harmonics space. One therefore needs to derive the expressions for the Green's functions and the self energies in harmonics space. At equilibrium, the bare Green's function only depends on the time difference $g(t,t') = g(\tau)$ with $\tau = t-t'$. The harmonics read

$$\begin{aligned}g_{nm}(\omega) &= \int_{-T/2}^{T/2} \frac{\mathrm{d}\bar{t}}{T} \int_{-\infty}^{\infty} \mathrm{d}\tau\, e^{i(\omega+n\Omega)\left(\bar{t}+\frac{\tau}{2}\right)} e^{-i(\omega+m\Omega)\left(\bar{t}-\frac{\tau}{2}\right)} g(\tau) \\ &= \int_{-\Omega/2}^{\Omega/2} \frac{\mathrm{d}\omega'}{2\pi} \int_{-T/2}^{T/2} \frac{\mathrm{d}\bar{t}}{T} \int_{-\infty}^{\infty} \mathrm{d}\tau\, e^{i\bar{t}\Omega(n-m)} e^{-i\tau\left(\omega'-\omega-\frac{n+m}{2}\Omega\right)} g(\omega') \\ &= \int_{-\Omega/2}^{\Omega/2} \frac{\mathrm{d}\omega'}{2\pi} \int_{-\infty}^{\infty} \mathrm{d}\tau\, e^{-i\tau(\omega'-\omega-n\Omega)} g(\omega')\delta_{nm} \\ &= g(\omega+n\Omega)\delta_{nm}\,.\end{aligned} \tag{B.6}$$

The self energy reads as $\Sigma_{RL}(t,t') = W_{RL}(t)\delta(t-t')$, where $W_{RL}(t) = \lambda(t)$ in the case of a normal metal.

Its harmonics components can be computed,

$$\begin{aligned}\Sigma_{RL,nm}(\omega) &= \int_{-T/2}^{T/2}\frac{\mathrm{d}\bar{t}}{T}\int_{-\infty}^{\infty}\mathrm{d}\tau\, e^{i(\omega+n\Omega)\left(\bar{t}+\frac{\tau}{2}\right)}e^{-i(\omega+m\Omega)\left(\bar{t}-\frac{\tau}{2}\right)} \\ &\qquad\qquad \times W_{RL}\left(\bar{t}+\frac{\tau}{2}\right)\delta\left(\bar{t}+\frac{\tau}{2}-\bar{t}+\frac{\tau}{2}\right) \\ &= \int_{-T/2}^{T/2}\frac{\mathrm{d}\bar{t}}{T}e^{i(\omega+n\Omega)\bar{t}}e^{-i(\omega+m\Omega)\bar{t}}W_{RL}(\bar{t})\,.\end{aligned} \tag{B.7}$$

Using the Fourier transform of the tunnel coupling

$$\lambda(t) = \lambda\sum_l p_l e^{-i\Omega l t}\,, \tag{B.8}$$

it is rewritten as

$$\begin{aligned}\Sigma_{RL,nm}(\omega) &= \int_{-T/2}^{T/2}\frac{\mathrm{d}\bar{t}}{T}\sum_l \lambda e^{i(n-m)\Omega\bar{t}}e^{-i\Omega l\bar{t}}p_l \\ &= \lambda p_{n-m}\,,\end{aligned} \tag{B.9}$$

in the case of a normal metal. For the NS junction, the Nambu structure is non-trivial, it is however easily found that

$$\Sigma_{RL,nm}(\omega) = \lambda\begin{pmatrix} p_{n-m} & 0 \\ 0 & -p^*_{m-n}\end{pmatrix}\,, \tag{B.10}$$

The coefficients p_l will be computed for different drive shapes.

B.4. Going to Fourier representation

B.4.1. The current

The current can generally be written as a sum of such terms

$$\langle I(t)\rangle \approx W(t)G(t,t)\,, \tag{B.11}$$

which, using the previous definition of the free energy, can be written in terms of a convolution:

$$\begin{aligned}\langle I(t)\rangle &= \int_{-\infty}^{\infty}\mathrm{d}t'\delta(t'-t)W(t')G(t',t) \\ &= (\Sigma\circ G)(t,t) \\ &= \sum_{nm}e^{-i(k-m)\Omega t}\int_{-\Omega/2}^{\Omega/2}\frac{\mathrm{d}\omega}{2\pi}\,\Sigma_{kl}(\omega)G_{lm}(\omega)\,.\end{aligned} \tag{B.12}$$

B.4.2. The noise

Once again, loosely speaking, the noise is the sum of typical terms:

$$S \propto \int_{-\infty}^{\infty}\mathrm{d}t'\int_{-T/2}^{T/2}\frac{\mathrm{d}t}{T}\,W_1(t)G_1(t,t')W_2(t')G_2(t',t)\,. \tag{B.13}$$

Defining $A(t,t') = W_1(t)G_1(t,t')$ and $B(t,t') = W_2(t')G_2(t',t)$, one sees that this integral can be recast as

$$\begin{aligned} S &= \int_{-T/2}^{T/2} \frac{\mathrm{d}t}{T} (A \circ B)(t,t) \\ &= \sum_{nm} \int_{-\Omega/2}^{\Omega/2} \frac{\mathrm{d}\omega}{2\pi} A_{nm}(\omega) B_{mn}(\omega) \,. \end{aligned} \tag{B.14}$$

The next step is to specify the Fourier coefficients $A_{nm}(\omega)$ in terms of those of the Green functions and the self energies,

$$(WG)_{mn}(\omega) = \int_{-T/2}^{T/2} \frac{\mathrm{d}\bar{t}}{T} \int_{-\infty}^{\infty} \mathrm{d}\tau \, e^{-i(\omega+m\Omega)\left(\bar{t}+\frac{\tau}{2}\right)} e^{i(\omega+n\Omega)\left(\bar{t}-\frac{\tau}{2}\right)} W\left(\bar{t}+\frac{\tau}{2}\right) G\left(\bar{t}+\frac{\tau}{2}, \bar{t}-\frac{\tau}{2}\right) . \tag{B.15}$$

The similarity between this equation and the convolution product encourages to write down the latter and to compare them.

$$\begin{aligned} \sum_q \Sigma_{ml}(\omega) G_{ln}(\omega) = \sum_l \int_{-T/2}^{T/2} \frac{\mathrm{d}\bar{t}_1}{T} \int_{-T/2}^{T/2} \frac{\mathrm{d}\bar{t}_2}{T} \int_{-\infty}^{\infty} \mathrm{d}\tau_1 \int_{-\infty}^{\infty} \mathrm{d}\tau_2 \\ \times e^{-i(\omega+m\Omega)\left(\bar{t}_1+\frac{\tau_1}{2}\right)} e^{i(\omega+l\Omega)\left(\bar{t}_1-\frac{\tau_1}{2}\right)} \\ \times e^{-i(\omega+l\Omega)\left(\bar{t}_2-\frac{\tau_2}{2}\right)} e^{i(\omega+n\Omega)\left(\bar{t}_2+\frac{\tau_2}{2}\right)} \\ \times \Sigma\left(\bar{t}_1-\frac{\tau_1}{2}, \bar{t}_1+\frac{\tau_1}{2}\right) G\left(\bar{t}_2+\frac{\tau_2}{2}, \bar{t}_2-\frac{\tau_2}{2}\right) . \end{aligned} \tag{B.16}$$

The first task is to perform the sum over l which yields a Dirac distribution that, when computing the integral over $\bar{t}_1$, gives

$$\begin{aligned} \sum_l \Sigma_{ml}(\omega) G_{ln}(\omega) = \int_{-T/2}^{T/2} \frac{\mathrm{d}\bar{t}_2}{T} \int_{-\infty}^{\infty} \mathrm{d}\tau_1 \int_{-\infty}^{\infty} \mathrm{d}\tau_2 \, e^{-i(\omega+m\Omega)\left(\bar{t}_2+\tau_1-\frac{\tau_2}{2}\right)} e^{i(\omega+n\Omega)\left(\bar{t}_2-\frac{\tau_2}{2}\right)} \\ \times \Sigma\left(\bar{t}_2-\frac{\tau_2}{2}, \bar{t}_2+\tau_1-\frac{\tau_2}{2}\right) G\left(\bar{t}_2+\frac{\tau_2}{2}, \bar{t}_2-\frac{\tau_2}{2}\right) . \end{aligned} \tag{B.17}$$

Using the definition of the self energy once again, one gets

$$\begin{aligned} \sum_l \Sigma_{ml}(\omega) G_{ln}(\omega) = \int_{-T/2}^{T/2} \frac{\mathrm{d}\bar{t}_2}{T} \int_{-\infty}^{\infty} \mathrm{d}\tau_2 \, e^{-i(\omega+m\Omega)\left(\bar{t}_2+\frac{\tau_2}{2}\right)} e^{i(\omega+n\Omega)\left(\bar{t}_2-\frac{\tau_2}{2}\right)} \times \\ \times W\left(\bar{t}_2+\frac{\tau_2}{2}\right) G\left(\bar{t}_2+\frac{\tau_2}{2}, \bar{t}_2-\frac{\tau_2}{2}\right) . \end{aligned} \tag{B.18}$$

One recognizes (B.15), allowing to write the final result for the noise as

$$\begin{aligned} S &= \sum_{klmn} \int_{-\Omega/2}^{\Omega/2} \frac{\mathrm{d}\omega}{2\pi} \Sigma_{1,kl}(\omega) G_{1,lm}(\omega) \Sigma_{2,mn}(\omega) G_{2,nk}(\omega) \\ &= \int_{-\Omega/2}^{\Omega/2} \frac{\mathrm{d}\omega}{2\pi} \mathrm{Tr}_{\mathrm{H}}\left[\Sigma_1(\omega) G_1(\omega) \Sigma_2(\omega) G_2(\omega)\right] , \end{aligned} \tag{B.19}$$

which is again a trace on harmonic space.

C. Computation of the noise in the $N-N$ junction

In this Appendix, the steps to obtain the noise in the $N-N$ junction, Eq. (3.19) are presented. As shown in the main text

$$S_{LL} = -e^2\lambda^2 \int_{-\Omega/2}^{\Omega/2} \frac{\mathrm{d}\omega}{2\pi} \mathrm{Tr}_{\mathrm{H}}\Big\{\mathcal{P}G_{RL}^{-+}\mathcal{P}G_{RL}^{+-} - \mathcal{P}^\dagger G_{LL}^{-+}\mathcal{P}G_{RR}^{+-} + \mathcal{P}^\dagger G_{LR}^{-+}\mathcal{P}^\dagger G_{LR}^{+-} - \mathcal{P}G_{RR}^{-+}\mathcal{P}^\dagger G_{LL}^{+-}\Big\}. \tag{C.1}$$

Eq. (3.6) can be used here but is not sufficient, its equivalents for different lead indices can be computed and read as

$$\begin{aligned}
G_{RL}^{\pm\mp} &= i\frac{\lambda}{(1+\lambda^2)^2}\Big[g_{RR}^{\pm\mp}\mathcal{P}^\dagger - \mathcal{P}^\dagger g_{LL}^{\pm\mp}\Big] \\
G_{LR}^{\pm\mp} &= i\frac{\lambda}{(1+\lambda^2)^2}\Big[g_{LL}^{\pm\mp}\mathcal{P} - \mathcal{P}g_{RR}^{\pm\mp}\Big] \\
G_{RR}^{\pm\mp} &= \frac{1}{(1+\lambda^2)^2}\Big[g_{RR}^{\pm\mp} + \lambda^2\mathcal{P}^\dagger g_{LL}^{\pm\mp}\mathcal{P}\Big] \\
G_{LL}^{\pm\mp} &= \frac{1}{(1+\lambda^2)^2}\Big[g_{LL}^{\pm\mp} + \lambda^2\mathcal{P}g_{RR}^{\pm\mp}\mathcal{P}^\dagger\Big].
\end{aligned} \tag{C.2}$$

The noise can therefore be written as

$$\begin{aligned}
S_{LL} = \frac{e^2\tau}{8\pi\,(1+\lambda^2)^2}\int_{-\Omega/2}^{\Omega/2}\mathrm{d}\omega\,\mathrm{Tr}_{\mathrm{H}}\Big\{&\lambda^2\mathcal{P}\Big[g_{RR}^{-+}\mathcal{P}^\dagger - \mathcal{P}^\dagger g_{LL}^{-+}\Big]\mathcal{P}\Big[g_{RR}^{+-}\mathcal{P}^\dagger - \mathcal{P}^\dagger g_{LL}^{+-}\Big] \\
&+\mathcal{P}^\dagger\Big[g_{LL}^{-+} + \lambda^2\mathcal{P}g_{RR}^{-+}\mathcal{P}^\dagger\Big]\mathcal{P}\Big[g_{RR}^{+-} + \lambda^2\mathcal{P}^\dagger g_{LL}^{+-}\mathcal{P}\Big] \\
&+\lambda^2\mathcal{P}^\dagger\Big[g_{LL}^{-+}\mathcal{P} - \mathcal{P}g_{RR}^{-+}\Big]\mathcal{P}^\dagger\Big[g_{LL}^{+-}\mathcal{P} - \mathcal{P}g_{RR}^{+-}\Big] \\
&+\mathcal{P}\Big[g_{RR}^{-+} + \lambda^2\mathcal{P}^\dagger g_{LL}^{-+}\mathcal{P}\Big]\mathcal{P}^\dagger\Big[g_{LL}^{+-} + \lambda^2\mathcal{P}g_{RR}^{+-}\mathcal{P}^\dagger\Big]\Big\}.
\end{aligned} \tag{C.3}$$

Grouping all the terms, on finds the following factorization

$$\begin{aligned}
S_{LL} = \frac{e^2\tau}{8\pi\,(1+\lambda^2)^2}\int_{-\Omega/2}^{\Omega/2}\mathrm{d}\omega\,\mathrm{Tr}_{\mathrm{H}}\Big[&4\lambda^2(g_{RR}^{-+}g_{RR}^{+-} + g_{LL}^{-+}g_{LL}^{+-}) \\
&+[1-2\lambda^2+\lambda^4]\left(g_{RR}^{-+}\mathcal{P}^\dagger g_{LL}^{+-}\mathcal{P} + g_{RR}^{+-}\mathcal{P}^\dagger g_{LL}^{-+}\mathcal{P}\right)\Big].
\end{aligned} \tag{C.4}$$

After a little bit of algebra, one is left with the following

$$\begin{aligned}
S_{LL} = -\frac{e^2\tau}{8\pi}\sum_n\int_{-\Omega/2}^{\Omega/2}\mathrm{d}\omega\Bigg\{&\tau\left(\left[\tanh^2\left(\frac{\omega+n\Omega}{2\theta}\right)-1\right] + \left[\tanh^2\left(\frac{\omega+n\Omega-eV_0}{2\theta}\right)-1\right]\right) \\
&+(1-\tau)\sum_m|p_{n-m}|^2\left[\tanh\left(\frac{\omega+n\Omega}{2\theta}\right)\tanh\left(\frac{\omega+m\Omega-eV_0}{2\theta}\right)-1\right]\Bigg\}.
\end{aligned} \tag{C.5}$$

C. Computation of the noise in the $N-N$ junction –

As was done for the current, a change of variable $\omega + n\Omega = x$ can be performed and, renaming $l = n - m$ in the second line, the sum over n can be performed to change the integration boundaries. Then, the noise reads as

$$S_{LL} = -\frac{e^2\tau}{8\pi}\int_{-\infty}^{\infty} \mathrm{d}x \left\{ \tau \left(\left[\tanh^2\left(\frac{x}{2\theta}\right) - 1 \right] + \left[\tanh^2\left(\frac{x - eV_0}{2\theta}\right) - 1 \right] \right) \right. \\ \left. + (1-\tau)\sum_l |p_l|^2 \left[\tanh\left(\frac{x}{2\theta}\right) \tanh\left(\frac{x - l\Omega - eV_0}{2\theta}\right) - 1 \right] \right\}. \tag{C.6}$$

Now the integrals are easily performed[1] and the noise reduces to

$$S_{LL} = \frac{e^2}{\pi}\left[2\tau^2\theta + \tau(1-\tau)\sum_l (l\Omega + eV_0)|p_l|^2 \coth\left(\frac{l\Omega + eV_0}{2\theta}\right) \right]. \tag{C.7}$$

[1] Indeed $\int \mathrm{d}x\, \tanh(x/a + b/a)\tanh(x/a) - 1 = a\coth(b/a)\left\{\log[\cosh(x/a)] - \log[\cosh(b/a + x/a)]\right\}$.

D. Computations related to the $N-S$ junction

This Appendix gathers all the computations, Green's functions, current and noise, related to the NS junction. First, a fomula for the current and the noise in terms of Green's functions is derived. Then, a few functions are introduced as they will be useful for later computations. Next, the dressed Green's function is expressed in terms of the bare ones and the tunnel matrices. Finally, the current and the noise are computed in different situations.

D.1. Current and Wick's theorem for the noise

The Keldysh Green's function in Nambu space is introduced, it reads as

$$G^{+-}_{jj'}(t,t) = i\begin{pmatrix} \left\langle c^\dagger_{j',\uparrow}(t)c_{j,\uparrow}(t)\right\rangle & \left\langle c_{j',\downarrow}(t)c_{j,\uparrow}(t)\right\rangle \\ \left\langle c^\dagger_{j',\downarrow}(t)c^\dagger_{j,\uparrow}(t)\right\rangle & \left\langle c_{j',\downarrow}(t)c^\dagger_{j,\downarrow}(t)\right\rangle \end{pmatrix}. \tag{D.1}$$

This allows to identify the pairings present in the current (see Eq. (5.8)) and to write it as

$$\begin{aligned} \langle I_j(t)\rangle &= i\sum_{j'}\big\langle W_{jj',\uparrow\uparrow}(t)c^\dagger_{j,\uparrow}(t)c_{j',\uparrow}(t) - W_{jj',\downarrow\downarrow}(t)c_{j,\downarrow}(t)c^\dagger_{j',\downarrow}(t) \\ &\qquad -W^*_{jj',\uparrow\uparrow}(t)c^\dagger_{j',\uparrow}(t)c_{j,\uparrow}(t) + W^*_{jj',\downarrow\downarrow}(t)c_{j',\downarrow}(t)c^\dagger_{j,\downarrow}(t)\big\rangle \\ &= \sum_{j'}\Big[W_{jj',\uparrow\uparrow}(t)G^{+-}_{j'j,\uparrow\uparrow}(t,t) - W_{jj',\downarrow\downarrow}(t)G^{+-}_{j'j,\downarrow\downarrow}(t,t) \\ &\qquad\qquad - W^*_{jj',\uparrow\uparrow}(t)G^{+-}_{jj',\uparrow\uparrow}(t,t) + W^*_{jj',\downarrow\downarrow}(t)G^{+-}_{j'j,\downarrow\downarrow}(t,t)\Big] \\ &= \sum_{j',\sigma}\sigma\Big[W_{jj',\sigma\sigma}(t)G^{+-}_{j'j,\sigma\sigma}(t,t) - W^*_{jj',\sigma\sigma}(t)G^{+-}_{jj',\sigma\sigma}(t,t)\Big]. \end{aligned} \tag{D.2}$$

noticing that $\sum_{\sigma'}\sigma'\delta_{\sigma\sigma'} = (\sigma_z)_{\sigma\sigma}$, one recognizes the components of a Pauli matrix and a trace in Nambu space (denoted with a N index) in the previous expression of the current. This allows to write the current as a Nambu trace:

$$\langle I_j(t)\rangle = e\sum_{j'}\mathrm{Tr}_N\left[\sigma_z\big(W_{jj'}(t)G^{+-}_{j'j}(t,t) - W^*_{jj'}(t)G^{+-}_{jj'}(t,t)\big)\right]. \tag{D.3}$$

Furthermore,

$$(G^{+-}_{LR})^\dagger(t,t) = i\left\langle\psi^\dagger_R(t)\psi_L(t)\right\rangle^\dagger = -i\left\langle\psi^\dagger_L(t)\psi_R(t)\right\rangle = -G^{+-}_{LR}(t,t), \tag{D.4}$$

and $W^\dagger_{j,j'} = W_{j',j}$, thus

$$\sigma_z W_{jj'}(t)G^{+-}_{j'j}(t,t) = -\left(G^{+-}_{jj'}(t,t)W_{j'j}(t)\sigma_z\right)^\dagger. \tag{D.5}$$

The tunnel matrix is diagonal in Nambu space and can therefore be written as a combination of σ_z's and σ_0, which commutes with σ_z. Using the cyclic properties of the trace, the current can be written as

$$\langle I_j(t)\rangle = 2e\,\mathrm{Re}\,\mathrm{Tr}_{\mathrm{NL}}\left[\sigma_z W(t) G^{+-}(t,t)\right]_{jj}, \tag{D.6}$$

where the L index of trace means lead space. In the case of a two-terminal device, similarly to what was done for the $N-N$ junction, the period-averaged current is immediately written using Fourier transform as

$$\overline{\langle I_L\rangle} = 2e\lambda \int_{-\Omega/2}^{\Omega/2} \mathrm{d}\omega\,\mathrm{Re}\,\mathrm{Tr}_{\mathrm{NLH}}\left[\sigma_z \mathcal{P} G^{+-}_{RL}(\omega)\right], \tag{D.7}$$

where the following notation was used

$$\Sigma_{LR,nm} = \lambda \mathcal{P}_{nm} = \lambda \begin{pmatrix} p^*_{m-n} & 0 \\ 0 & -p_{n-m} \end{pmatrix}. \tag{D.8}$$

Now the noise will be expressed in terms of Green's functions and tunnel matrices, its definition is recalled here:

$$S_{jl} = \int \mathrm{d}t \int \mathrm{d}t' \left\langle I_j(t') I_l(t) - \langle I_j(t')\rangle \langle I_l(t)\rangle \right\rangle. \tag{D.9}$$

The first term to compute is the irreducible correlator,

$$\begin{aligned} \langle I_j(t') I_l(t)\rangle = -\sum_{j'l'} \Big\langle \Big[& W_{jj',\uparrow\uparrow}(t) c^\dagger_{j,\uparrow}(t) c_{j',\uparrow}(t) - W_{jj',\downarrow\downarrow}(t) c_{j,\downarrow}(t) c^\dagger_{j',\downarrow}(t) \\ & - W^*_{jj',\uparrow\uparrow}(t) c^\dagger_{j',\uparrow}(t) c_{j,\uparrow}(t) + W^*_{jj',\downarrow\downarrow}(t) c_{j',\downarrow}(t) c^\dagger_{j,\downarrow}(t) \Big] \\ & \times \Big[W_{ll',\uparrow\uparrow}(t') c^\dagger_{l,\uparrow}(t') c_{l',\uparrow}(t') - W_{ll',\downarrow\downarrow}(t') c_{l,\downarrow}(t') c^\dagger_{l',\downarrow}(t') \\ & - W^*_{ll',\uparrow\uparrow}(t') c^\dagger_{l',\uparrow}(t') c_{l,\uparrow}(t') + W^*_{ll',\downarrow\downarrow}(t') c_{l',\downarrow}(t') c^\dagger_{l,\downarrow}(t') \Big] \Big\rangle. \end{aligned} \tag{D.10}$$

There are four types of terms, which will be treated separately. Computing the mean value of a product of four operators involves Wick's theorem and results in three types of pairings. The first one is typically of the form $\left\langle c_{j',\downarrow}(t) c^\dagger_{j,\downarrow}(t)\right\rangle \left\langle c^\dagger_{l',\uparrow}(t') c_{l,\uparrow}(t')\right\rangle$ and is obviously contained in the second term of (D.9). The second one describes spin switching of electrons or holes at the junction. These are typically of the form $\langle c_{j,\downarrow}(t) c_{l,\downarrow}(t)\rangle = \left\langle c^\dagger_{j,\downarrow}(t) c_{l,\uparrow}(t)\right\rangle = 0$. The absence of magnetic impurities allows to remove them and to simplify the product (D.9). Finally, the third type, involving transfer of electrons or Cooper pairs, typically of the form $\langle c_{j,\downarrow}(t) c_{l,\uparrow}(t)\rangle$ or $\left\langle c^\dagger_{j,\downarrow}(t) c_{l,\downarrow}(t)\right\rangle$, is the only one of interest.

It is relevant to provide a list of all the Green's functions definitions needed:

$$\begin{aligned} \left\langle c^\dagger_{j,\uparrow}(t) c_{l,\uparrow}(t')\right\rangle &= iG^{+-}_{lj,\uparrow\uparrow}(t',t) & \left\langle c^\dagger_{j,\uparrow}(t) c^\dagger_{l,\downarrow}(t')\right\rangle &= -iG^{-+}_{lj,\downarrow\uparrow}(t,t') \\ \left\langle c_{j,\downarrow}(t) c^\dagger_{l,\downarrow}(t')\right\rangle &= iG^{+-}_{lj,\downarrow\downarrow}(t,t') & \langle c_{j,\downarrow}(t) c_{l,\uparrow}(t')\rangle &= -iG^{-+}_{jl,\uparrow\downarrow}(t,t') \\ \left\langle c_{j,\uparrow}(t) c^\dagger_{l,\uparrow}(t')\right\rangle &= -iG^{-+}_{jl,\uparrow\uparrow}(t,t') & \left\langle c^\dagger_{j,\uparrow}(t) c_{l,\downarrow}(t')\right\rangle &= iG^{+-}_{lj,\downarrow\uparrow}(t',t) \\ \left\langle c^\dagger_{j,\downarrow}(t) c_{l,\downarrow}(t')\right\rangle &= -iG^{-+}_{jl,\downarrow\downarrow}(t,t') & \left\langle c^\dagger_{j,\downarrow}(t) c^\dagger_{l,\uparrow}(t')\right\rangle &= iG^{+-}_{lj,\uparrow\downarrow}(t',t). \end{aligned} \tag{D.11}$$

The computation starts by writing all the terms of Eq. (D.10) involving $W_{jj'}W_{ll'}$ (keeping the minus sign

out of the sum in (D.9)). Once the first product and Wick's theorem has been applied, these terms read as

$$\begin{aligned}
&W_{jj',\uparrow\uparrow}(t)\left[W_{ll',\uparrow\uparrow}(t')\left\langle c^\dagger_{j,\uparrow}(t)c_{l',\uparrow}(t')\right\rangle\left\langle c_{j',\uparrow}(t)c^\dagger_{l,\uparrow}(t')\right\rangle - W_{ll',\downarrow\downarrow}(t')\left\langle c^\dagger_{j,\uparrow}(t)c^\dagger_{l',\downarrow}(t')\right\rangle\left\langle c_{j',\uparrow}(t)c_{l,\downarrow}(t')\right\rangle\right]\\
&\quad - W_{jj',\downarrow\downarrow}(t)\left[W_{ll',\uparrow\uparrow}(t')\left\langle c_{j,\downarrow}(t)c_{l',\uparrow}(t')\right\rangle\left\langle c^\dagger_{j',\downarrow}(t)c^\dagger_{l,\uparrow}(t')\right\rangle - W_{ll',\downarrow\downarrow}(t')\left\langle c_{j,\downarrow}(t)c^\dagger_{l',\downarrow}(t')\right\rangle\left\langle c^\dagger_{j',\downarrow}(t)c_{l,\downarrow}(t')\right\rangle\right]\\
&= W_{jj',\uparrow\uparrow}(t)\left[W_{ll',\uparrow\uparrow}(t')G^{+-}_{l'j,\uparrow\uparrow}(t',t)G^{-+}_{j'l,\uparrow\uparrow}(t,t') - W_{ll',\downarrow\downarrow}(t')G^{+-}_{l'j,\uparrow\downarrow}(t',t)G^{-+}_{j'l,\downarrow\uparrow}(t,t')\right]\\
&\quad - W_{jj',\uparrow\uparrow}(t)\left[W_{ll',\uparrow\uparrow}(t')G^{+-}_{l'j,\downarrow\uparrow}(t',t)G^{-+}_{j'l,\uparrow\downarrow}(t,t') - W_{ll',\downarrow\downarrow}(t')G^{+-}_{l'j,\downarrow\downarrow}(t',t)G^{-+}_{j'l,\downarrow\downarrow}(t,t')\right]\\
&= \sum_{\sigma,\sigma'}\sigma W_{jj',\sigma\sigma}(t)G^{-+}_{j'l,\sigma\sigma'}(t,t')\sigma' W_{ll',\sigma'\sigma'}(t')G^{+-}_{l'j,\sigma'\sigma}(t',t)\\
&= \mathrm{Tr}_{\mathrm{N}}\left[\sigma_z W_{jj'}(t)G^{-+}_{j'l}(t,t')\sigma_z W_{ll'}(t')G^{+-}_{l'j}(t',t)\right].
\end{aligned} \tag{D.12}$$

There is no need to perform a similar calculation for the term $W^*_{jj'}W^*_{ll'}$ of Eq. (D.10) since it is exactly the same as in Eq. (D.12) with j,l changed to j',l'. Therefore, it reads as

$$\text{Second term} = \mathrm{Tr}_{\mathrm{N}}\left[\sigma_z W^*_{jj'}(t)G^{-+}_{jl'}(t,t')\sigma_z W^*_{ll'}(t')G^{+-}_{lj'}(t',t)\right]. \tag{D.13}$$

An analogous computation can be carried out on the mixed terms, a sign changes and only one of the index is changed; j,l,j',l' becomes j',l,j,l' for the term $W^*_{jj'}W_{ll'}$ and j,l,j',l' becomes j',l,j,l for the term $W_{jj'}W^*_{ll'}$. Furthermore, $W^*_{jj'} = (W^\dagger)_{jj'}$, which allows to write all the terms of the noise as a matrix products as

$$\begin{aligned}
S_{jl} = -e^2\int \mathrm{d}t\int \mathrm{d}t' \mathrm{Tr}_{\mathrm{N}}\Big\{&\left[\sigma_z W(t)G^{-+}(t,t')\right]_{jl}\left[\sigma_z W(t')G^{+-}(t',t)\right]_{lj}\\
&+\left[G^{-+}(t,t')\sigma_z W^\dagger(t')\right]_{jl}\left[G^{+-}(t',t)\sigma_z W^\dagger(t)\right]_{lj}\\
&-\left[G^{-+}(t,t')\right]_{jl}\left[\sigma_z W(t')G^{+-}(t',t)\sigma_z W^\dagger(t)\right]_{lj}\\
&-\left[\sigma_z W(t)G^{-+}(t,t')\sigma_z W^\dagger(t')\right]_{jl}\left[G^{+-}(t',t)\right]_{lj}\Big\}.
\end{aligned} \tag{D.14}$$

In the case of a 2-terminal device (denoted R and L) where and $W_{LL} = W_{RR} = 0$, the noise becomes

$$\begin{aligned}
S_{LL} = -e^2\int \mathrm{d}t\int \mathrm{d}t'\,\mathrm{Tr}_{\mathrm{N}}\big[&\sigma_z W_{LR}(t)G^{-+}_{RL}(t,t')\sigma_z W_{LR}(t')G^{+-}_{RL}(t',t)\\
&+G^{-+}_{LR}(t,t')\sigma_z W_{RL}(t')G^{+-}_{LR}(t',t)\sigma_z W_{RL}(t)\\
&-\sigma_z W_{LR}(t)G^{-+}_{RR}(t,t')\sigma_z W_{RL}(t')G^{+-}_{LL}(t',t)\\
&-G^{-+}_{LL}(t,t')\sigma_z W_{LR}(t')G^{+-}_{RR}(t,t')\sigma_z W_{RL}(t)\big].
\end{aligned} \tag{D.15}$$

This result is in accordance with that of [98]. Using the same arguments as those allowing to obtain Eq. (D.7), the first two terms of the noise can be recast into

$$S_{LL} = -e^2\lambda^2\int_{-\Omega/2}^{\Omega/2}\frac{\mathrm{d}\omega}{2\pi}\,\mathrm{Tr}_{\mathrm{NH}}\left[2\mathrm{Re}\left(\sigma_z\mathcal{P}^\dagger G^{+-}_{LR}\sigma_z\mathcal{P}^\dagger G^{-+}_{LR}\right) - \sigma_z\mathcal{P}^\dagger G^{+-}_{LL}\sigma_z\mathcal{P}G^{-+}_{RR} - \sigma_z\mathcal{P}G^{+-}_{RR}\sigma_z\mathcal{P}^\dagger G^{-+}_{LL}\right]. \tag{D.16}$$

D.2. Definitions

The following definition are introduced, they will be relevant for all superconductor-related calculations

$$\begin{aligned}
\omega_n^{\pm} &= \lim_{\delta\to 0}\frac{\omega+n\Omega}{\sqrt{\Delta^2-(\omega+n\Omega\pm i\delta)^2}} & \Delta_n^{\pm} &= \lim_{\delta\to 0}\frac{\Delta}{\sqrt{\Delta^2-(\omega+n\Omega\pm i\delta)^2}}\\
\xi_n^{\pm} &= \frac{1}{1+\lambda^4\mp 2i\lambda^2\omega_n^{\pm}} & \zeta_n^{\pm} &= \left[\tanh\left(\frac{\omega+n\Omega}{2\Theta}\right)\mp 1\right]\\
\overline{\Delta}_n &= \frac{\Delta_n^- - \Delta_n^+}{2} & \overline{\omega}_n &= \frac{\omega_n^- - \omega_n^+}{2}\\
\tau_N &= \frac{4\lambda^2}{(1+\lambda^2)^2} & \tau_A &= \frac{4\lambda^4}{(1+\lambda^4)^2}\\
g^{r,a}_{RR,nm} &= -\left(\Delta_n^{\pm}\sigma_x+\omega_n^{\pm}\mathbb{1}\right)\delta_{nm} & g^{r,a}_{LL,nm} &= \mp i\mathbb{1}\delta_{nm}\\
g^{\pm\mp}_{RR,nm} &= \left(\overline{\omega}_n\mathbb{1}+\overline{\Delta}_n\sigma_x\right)\zeta_n^{\pm}\delta_{nm} & g^{\pm\mp}_{LL,nm} &= -i\left(T\mp\mathbb{1}\right)\delta_{nm}\\
\Sigma^{r,a}_{LR,nm} &= \lambda\begin{pmatrix} p^*_{m-n,\uparrow} & 0\\ 0 & -p_{m-n,\downarrow}\end{pmatrix} = \lambda\mathcal{P}_{nm} & T_{nm} &= \begin{pmatrix}\tanh\left(\frac{\omega+n\Omega-eV_{0,\uparrow}}{2\Theta}\right) & 0\\ 0 & \tanh\left(\frac{\omega+n\Omega+eV_{0,\downarrow}}{2\Theta}\right)\end{pmatrix}\delta_{nm}\,.
\end{aligned} \tag{D.17}$$

it is recalled that the period-averaged current and the noise are defined as

$$\overline{\langle I\rangle} = 2e\lambda\int_{-\Omega/2}^{\Omega/2}\frac{\mathrm{d}\omega}{2\pi}\,\mathrm{Re}\Big(\mathrm{Tr}_{\mathrm{NH}}\left[\sigma_z\mathcal{P}G^{+-}_{RL}\right]\Big)\,, \tag{D.18}$$

and

$$S_{LL} = -e^2\lambda^2\int_{-\Omega/2}^{\Omega/2}\frac{\mathrm{d}\omega}{2\pi}\,\mathrm{Tr}_{\mathrm{NH}}\big[2\mathrm{Re}\left(\sigma_z\mathcal{P}^\dagger G^{+-}_{LR}\sigma_z\mathcal{P}^\dagger G^{-+}_{LR}\right)-\sigma_z\mathcal{P}^\dagger G^{+-}_{LL}\sigma_z\mathcal{P}G^{-+}_{RR}-\sigma_z\mathcal{P}G^{+-}_{RR}\sigma_z\mathcal{P}^\dagger G^{-+}_{LL}\big]\,. \tag{D.19}$$

D.3. Computation of $G^{\pm\mp}_{LR}$ for an NS junction.

For the current there is only one Green function to compute, $G^{\pm}_{LR}$, see Eq. (A.35) and for the noise two more are required. The calcuation can start by examining the following term,

$$\begin{aligned}
\left(\mathbb{1}-g^{r,a}_{RR}\Sigma_{RL}g^{r,a}_{LL}\Sigma_{LR}\right)_{nm} &= \left[(1\mp i\lambda^2\omega_n^{\pm})\mathbb{1}\mp i\lambda^2\Delta_n^{\pm}\sigma_x\right]\delta_{nm}\\
&= \left(\mathbb{1}-\Sigma_{RL}g^{r,a}_{LL}\Sigma_{LR}g^{r,a}_{RR}\right)_{nm}\,,
\end{aligned} \tag{D.20}$$

where the last lines comes from the fact that $\Sigma_{RL}g^{r,a}_{LL}\Sigma_{LR}$ is proportional to the identity. The inverse of Eq. (D.20) is that of a two by two matrix:

$$\left(\mathbb{1}-g^{r,a}_{RR}\Sigma_{RL}g^{r,a}_{LL}\Sigma_{LR}\right)^{-1}_{nm} = \xi_n^{\pm}\left[(1\mp i\lambda^2\omega_n^{\pm})\mathbb{1}\pm i\lambda^2\Delta_n^{\pm}\sigma_x\right]. \tag{D.21}$$

Now the second term of the product in Eq. A.35 is found to be which allows to write

$$\begin{aligned}
\left[g^{\pm\mp}_{RR}+g^{r}_{RR}\Sigma_{RL}g^{\pm\mp}_{LL}\left(\Sigma_{RL}g^{a}_{LL}\right)^{-1}\right]_{nm} =&\Delta_n^+\sigma_x\mathcal{P}^\dagger_{nk}T_k\mathcal{P}_{km}+(\zeta_n^{\pm}\overline{\Delta}_n\mp\Delta_n^+)\sigma_x\delta_{nm}\\
&+\omega_n^+\mathcal{P}^\dagger_{nk}T_k\mathcal{P}_{km}+(\zeta_n^{\pm}\overline{\omega}_n\mp\omega_n^+)\mathbb{1}\delta_{nm}\,.
\end{aligned} \tag{D.22}$$

Thus, one can write

$$\begin{aligned}
&(\mathbb{1}-g^r_{RR}\Sigma_{RL}g^r_{LL}\Sigma_{LR})^{-1}_{nk}\left[g^{\pm\mp}_{RR}+g^r_{RR}\Sigma_{RL}g^{\pm\mp}_{LL}\left(\Sigma_{RL}g^a_{LL}\right)^{-1}\right]_{km}\\
&\qquad=\xi^+_n\Big[\mathcal{P}^\dagger_{nk}T_k\mathcal{P}_{km}\left\{\omega^+_n+i\lambda^2\left[\left(\Delta^+_n\right)^2-\left(\omega^+_n\right)^2\right]\right\}\\
&\qquad\quad+\sigma_x\mathcal{P}^\dagger_{nk}T_k\mathcal{P}_{km}\left[\Delta^+_n\right]+\sigma_x\left\{\zeta^\pm_n\left[\overline{\Delta}_n-i\lambda^2\left(\omega^+_n\overline{\Delta}-\Delta^+_n\overline{\omega}_n\right)\right]\mp\Delta^+_n\right\}\\
&\qquad\quad+\mathbb{1}\left\{\zeta^\pm_n\left[\overline{\omega}_n+i\lambda^2\left(\overline{\Delta}_n\Delta^+_n-\omega^+_n\overline{\omega}_n\right)\right]\mp\omega^+_n\pm i\lambda^2\left[\left(\omega^+_n\right)^2-\left(\Delta^+_n\right)^2\right]\right\}\Big],
\end{aligned}\tag{D.23}$$

A simplification can be performed by considering that,

$$\begin{aligned}
\Delta^\pm_n\Delta^\pm_n-\omega^\pm_n\omega^\pm_n&=1\\
\Delta^\pm_n\Delta^\mp_n-\omega^\pm_n\omega^\mp_n&=\mathrm{sgn}\left[\Delta-(\omega+n\Omega)\right]\\
\Delta^\pm_n\omega^\mp_n-\omega^\pm_n\Delta^\mp_n&=0\\
\omega^\pm_n\overline{\Delta}_n-\Delta^\pm_n\overline{\omega}_n&=0\,,
\end{aligned}\tag{D.24}$$

for all ω. Hence

$$\begin{aligned}
&(\mathbb{1}-g^r_{RR}\Sigma_{RL}g^r_{LL}\Sigma_{LR})^{-1}_{nk}\left[g^{\pm\mp}_{RR}+g^r_{RR}\Sigma_{RL}g^{\pm\mp}_{LL}\left(\Sigma_{RL}g^a_{LL}\right)^{-1}\right]_{km}\\
&\qquad=\xi^+_n\Big\{\sigma_x\mathcal{P}^\dagger_{nk}T_k\mathcal{P}_{km}\Delta^+_n+\mathcal{P}^\dagger_{nk}T_k\mathcal{P}_{km}(\omega^+_n+i\lambda^2)+\sigma_x\left[\zeta^\pm_n\overline{\Delta}_n\mp\Delta^+_n\right]\delta_{nm}\\
&\qquad\quad+\mathbb{1}\left[\zeta^\pm_n\left[\overline{\omega}_n+i\lambda^2\left(\overline{\Delta}_n\Delta^+_n-\omega^+_n\overline{\omega}_n\right)\right]\mp(\omega^+_n+i\lambda^2)\right]\delta_{nm}\Big\}.
\end{aligned}\tag{D.25}$$

One is left with only one term to compute in order to get the full Green's function. It is easily obtained from Eq. (D.21)

$$\left[\left(\mathbb{1}-\Sigma_{RL}g^a_{LL}\Sigma_{LR}g^a_{RR}\right)^{-1}\Sigma_{RL}g^a_{LL}\right]_{nm}=i\lambda\xi^-_n\left[\mathcal{P}^\dagger_{nm}(1+i\lambda^2\omega^-_n)-i\lambda^2\Delta^-_n\sigma_x\mathcal{P}^\dagger_{nm}\right].\tag{D.26}$$

Finally the Green's function is the product of the latter two terms:

$$\begin{aligned}
G^{\pm\mp}_{RL,nm}=i\lambda\xi^+_n\xi^-_r\Big[&\sigma_x\mathcal{P}^\dagger_{nk}T_k\mathcal{P}_{kr}\mathcal{P}^\dagger_{rm}\left[\Delta^+_n+i\lambda^2\Delta^+_n\omega^-_r\right]+\sigma_x\mathcal{P}^\dagger_{nk}T_k\mathcal{P}_{kr}\sigma_x\mathcal{P}^\dagger_{rm}\left[-i\lambda^2\Delta^+_n\Delta^-_r\right]\\
&+\mathcal{P}^\dagger_{nk}T_k\mathcal{P}_{kr}\mathcal{P}^\dagger_{rm}\left[\omega^+_n+i\lambda^2+i\lambda^2\omega^+_n\omega^-_r-\lambda^4\omega^-_r\right]\\
&+\mathcal{P}^\dagger_{nk}T_k\mathcal{P}_{kr}\sigma_x\mathcal{P}^\dagger_{rm}\left[-i\lambda^2\Delta^-_r\omega^+_n+\lambda^4\Delta^-_r\right]\\
&+\mathcal{P}^\dagger_{nm}\Big\{\zeta^\pm_n\left[\overline{\omega}_n+i\lambda^2(1+i\lambda^2\omega^-_n)\left(\overline{\Delta}_n\Delta^+_n-\omega^+_n\overline{\omega}_n\right)+i\lambda^2\left(\omega^-_n\overline{\omega}_n-\overline{\Delta}_n\Delta^-_n\right)\right]\\
&\qquad\pm\left[-i\lambda^2+i\lambda^2(\Delta^+_n\Delta^-_n-\omega^+_n\omega^-_n)-\omega^+_n+\lambda^4\omega^-_n\right]\Big\}\\
&+\sigma_x\mathcal{P}^\dagger_{nm}\left\{\zeta^\pm_n\left[\overline{\Delta}_n+\lambda^4\Delta^-_n\left(\overline{\Delta}_n\Delta^+_n-\omega^+_n\overline{\omega}_n\right)\right]\mp\left(\Delta^+_n+\lambda^4\Delta^-_n\right)\right\}\Big].
\end{aligned}\tag{D.27}$$

D.4. The current

D.4.1. High gap regime, as a function of time

The spin-resolved currents in the junction are defined as:

$$\begin{aligned}\langle I_\sigma(t)\rangle &= e\int_{-\infty}^{\infty}\mathrm{d}t'\,\left[\sigma_z W_{\mathrm{NS}}(t)\delta(t-t')G_{\mathrm{SN}}(t',t)-\sigma_z G_{\mathrm{SN}}(t,t')W_{\mathrm{NS}}(t)\delta(t-t')\right]_{\sigma\sigma}\\ &= \frac{e}{2\pi}\sum_{n,k,m}\int_{-\frac{\Omega}{2}}^{\frac{\Omega}{2}}\mathrm{d}\omega\, e^{-i(n-m)\Omega t}\left[\sigma_z\Sigma_{\mathrm{NS},nk}(\omega)G^{+-}_{\mathrm{SN},km}(\omega)-\sigma_z G^{+-}_{\mathrm{NS},nk}(\omega)\Sigma_{\mathrm{SN},km}(\omega)\right]_{\sigma\sigma}.\end{aligned} \tag{D.28}$$

Using the following relations,

$$G^{\pm\mp}_{\mathrm{NS}} = -\left(G^{\pm\mp}_{\mathrm{SN}}\right)^\dagger \qquad \text{and} \qquad \Sigma^\dagger_{\mathrm{NS}} = \Sigma_{\mathrm{SN}}\,, \tag{D.29}$$

the currents can be written as

$$\langle I_\sigma(t)\rangle = \frac{e}{2\pi}\sum_{n,k,m}\int_{-\frac{\Omega}{2}}^{\frac{\Omega}{2}}\mathrm{d}\omega\, e^{-i(n-m)\Omega t}\left\{\left[\sigma_z\Sigma_{\mathrm{NS},nk}(\omega)G^{+-}_{\mathrm{SN},km}(\omega)\right]_{\sigma\sigma}+[(n,m)\to(m,n)]^*\right\}, \tag{D.30}$$

where the second term is the complex conjugate of the first one after taking $m\to n$ and $n\to m$. Since the terms in G^{+-}, see Eq. (D.27), that contains an odd number of σ_x do not contribute to the diagonal matrix elements of $\sigma_z\Sigma G^{+-}$, one is left with

$$\begin{aligned}\langle I_\sigma(t)\rangle = \frac{e}{2\pi}\lambda^2\sum_{n,m,r,k,s}\int_{-\frac{\Omega}{2}}^{\frac{\Omega}{2}}\mathrm{d}\omega\, e^{-i(n-m)\Omega t}\\ \Bigg\{i\xi^+_k\xi^-_r\sigma_z\mathcal{P}^\dagger_{nk}\Big[\sigma_x\mathcal{P}_{ks}T_s\mathcal{P}^\dagger_{sr}\sigma_x\mathcal{P}_{rm}\left[-i\lambda^2\Delta^+_k\Delta^-_r\right]\\ +\mathcal{P}_{ks}T_s\mathcal{P}^\dagger_{sr}\mathcal{P}_{rm}\left[\omega^+_k+i\lambda^2+i\lambda^2\omega^+_k\omega^-_r-\lambda^4\omega^-_r\right]\\ +\delta_{sr}\delta_{rm}\mathcal{P}_{km}\Big(\zeta^+_k\Big[\overline{\omega}_k+i\lambda^2\left(\omega^-_k\overline{\omega}_k-\overline{\Delta}_k\Delta^-_k\right)+i\lambda^2(1+i\lambda^2\omega^-_k)\left(\overline{\Delta}_k\Delta^+_k-\omega^+_k\overline{\omega}_k\right)\Big]\\ +\Big[-i\lambda^2+i\lambda^2(\Delta^+_k\Delta^-_k-\omega^+_k\omega^-_k)-\omega^+_k+\lambda^4\omega^-_k\Big]\Big)\Big]+[(n,m)\to(m,n)]^*\Bigg\}_{\sigma\sigma}.\end{aligned} \tag{D.31}$$

Working in the high gap regime amounts to setting

$$\omega^\pm_n=\overline{\omega}_n=\overline{\Delta}_n=0 \quad\text{and}\quad \Delta^\pm_n=1 \quad\text{thus}\quad \xi^\pm_n=1/(1+\lambda^4)\,, \tag{D.32}$$

so the current, Eq. (D.31), becomes

$$\begin{aligned}\langle I_\sigma(t)\rangle = \frac{e}{2\pi}\frac{\lambda^4}{(1+\lambda^4)^2}\sum_{n,m,r,k,s}\int_{-\frac{\Omega}{2}}^{\frac{\Omega}{2}}\mathrm{d}\omega\Big\{e^{-i(n-m)\Omega t}\Big[\sigma_z\mathcal{P}^\dagger_{nk}\sigma_x\mathcal{P}_{ks}T_s\mathcal{P}^\dagger_{sr}\sigma_x\mathcal{P}_{rm}\\ -\sigma_z\mathcal{P}^\dagger_{nk}\mathcal{P}_{ks}T_s\mathcal{P}^\dagger_{sr}\mathcal{P}_{rm}\Big]_{\sigma\sigma}\\ +[(n,m)\to(m,n)]^*\Big\}.\end{aligned} \tag{D.33}$$

Formally, the second term , one could use that $\sum_{n,r,s}\mathcal{P}^{\dagger}_{kn}\mathcal{P}_{ns}T_s\mathcal{P}^{\dagger}_{sr}\mathcal{P}_{rm}=\delta_{ns}T_s\delta_{sm}$, but that would make the whole expression divergent for all $k\neq m$, i.e., for all terms but the currents averaged over a period. Therefore, when expanding the sums, one must always pay attention to keep convergent series. Performing a careful expansion, in the Andreev regime, of Eq. (D.27), one can show that the Keldysh dressed Green's function reads

$$G^{+-}_{SN}=\frac{\lambda^3}{(1+\lambda^4)^2}\left[\sigma_x\mathcal{P}\left(T-\mathbb{1}\right)\mathcal{P}^{\dagger}\sigma_x\mathcal{P}-\sigma_x\sigma_x\mathcal{P}\left(T-\mathbb{1}\right)\right], \tag{D.34}$$

such that a properly converging expression of the current is

$$\begin{aligned}\langle I_\sigma(t)\rangle=\frac{e}{2\pi}\frac{\lambda^4}{(1+\lambda^4)^2}\sum_{n,m,r,k,s}\int_{-\frac{\Omega}{2}}^{\frac{\Omega}{2}}\mathrm{d}\omega\Big\{e^{-i(n-m)\Omega t}\Big[&\sigma_z\mathcal{P}^{\dagger}_{nk}\sigma_x\mathcal{P}_{ks}T_s\mathcal{P}^{\dagger}_{sr}\sigma_x\mathcal{P}_{rm}\\&-\sigma_z\mathcal{P}^{\dagger}_{nk}\sigma_x\mathcal{P}_{ks}\mathcal{P}^{\dagger}_{sr}\sigma_x\mathcal{P}_{rm}T_m\Big]_{\sigma\sigma}\\&+[(n,m)\to(m,n)]^*\Big\}.\end{aligned} \tag{D.35}$$

More precisely, the 2×2 matrices $\sigma_z\mathcal{P}^{\dagger}_{nk}\sigma_x\mathcal{P}_{ks}T_s\mathcal{P}^{\dagger}_{sr}\sigma_x\mathcal{P}_{rm}-\sigma_z\mathcal{P}^{\dagger}_{nk}\sigma_x\mathcal{P}_{ks}\mathcal{P}^{\dagger}_{sr}\sigma_x\mathcal{P}_{rm}T_m$ are diagonal with the following entries

$$\begin{aligned}&p^*_{k-n,\uparrow}p^*_{s-k,\downarrow}p_{r-s,\downarrow}p_{r-m,\uparrow}\left[\tanh\left(\frac{\omega+s\Omega+eV_{\mathrm{DC},\downarrow}}{2\Theta}\right)-\tanh\left(\frac{\omega+m\Omega-eV_{\mathrm{DC},\uparrow}}{2\Theta}\right)\right]\\&-p_{n-k,\downarrow}p_{k-s,\uparrow}p^*_{r-s,\uparrow}p^*_{m-r,\downarrow}\left[\tanh\left(\frac{\omega+s\Omega-eV_{\mathrm{DC},\uparrow}}{2\Theta}\right)-\tanh\left(\frac{\omega+m\Omega+eV_{\mathrm{DC},\downarrow}}{2\Theta}\right)\right].\end{aligned} \tag{D.36}$$

Thereby, one gets

$$\begin{aligned}\langle I_\uparrow(t)\rangle=\frac{e}{2\pi}\frac{\lambda^4}{(1+\lambda^4)^2}\sum_{n,m,r,k,s}\int_{-\frac{\Omega}{2}}^{\frac{\Omega}{2}}\mathrm{d}\omega\,e^{-i(n-m)\Omega t}&\\\times\Big\{p^*_{k-n,\uparrow}p^*_{s-k,\downarrow}p_{r-s,\downarrow}p_{r-m,\uparrow}\left[\tanh\left(\frac{\omega+s\Omega+eV_{\mathrm{DC},\downarrow}}{2\Theta}\right)-\tanh\left(\frac{\omega+m\Omega-eV_{\mathrm{DC},\uparrow}}{2\Theta}\right)\right]&\\+[(n,m)\to(m,n)]^*\Big\}.&\end{aligned} \tag{D.37}$$

Perform the following change of variables, $x=\omega+(s+q_\downarrow)\Omega$and shift all the indices by s (except s itself), one can perform the sum over s, which yields

$$\begin{aligned}\langle I_\uparrow(t)\rangle=\frac{e}{\pi}\frac{\lambda^4}{(1+\lambda^4)^2}\sum_{n,r,k,m}\int_{-\infty}^{\infty}\mathrm{d}x\,e^{i(m-n)\Omega t}p^*_{k-n,\uparrow}p^*_{s-k,\downarrow}p_{r-s,\downarrow}p_{r-m,\uparrow}&\\\times\left[\tanh\left(\frac{x}{2\Theta}\right)-\tanh\left(\frac{x+m\Omega-(q_\uparrow+q_\downarrow)}{2\Theta}\right)\right].&\end{aligned} \tag{D.38}$$

The integral can be performed and the preceding expression current becomes

$$\langle I_\uparrow(t)\rangle=\frac{2e}{\pi}\frac{\lambda^4}{(1+\lambda^4)^2}\sum_{n,r,k,m}e^{i(m-n)\Omega t}p^*_{k-n,\uparrow}p^*_{-k,\downarrow}p_{-r,\downarrow}p_{r-m,\uparrow}\Big(q_\uparrow+q_\downarrow-m\Big), \tag{D.39}$$

which using the definition of the $p_{l\sigma}$ leads to

$$\langle I_\uparrow(t)\rangle = \frac{e^2}{\pi}\frac{\tau_A}{2}(V_\uparrow(t)+V_\downarrow(t))\,, \tag{D.40}$$

and, similarly, $\langle I_\downarrow(t)\rangle = \frac{e^2}{\pi}\frac{\tau_A}{2}(V_\uparrow(t)+V_\downarrow(t))$.

D.4.2. General case, period-averaged current

This section focuses on the computation of the period-averaged current defined in Eq. (D.18), the Harmonics trace is hereby developed as

$$\begin{aligned}\overline{\langle I_L\rangle} = 2ie\lambda^2 \int_{-\Omega/2}^{\Omega/2}\frac{\mathrm{d}\omega}{2\pi}\sum_{lm}\delta_{lm}\mathrm{ReTr_N}\Big\{&\sigma_z\mathcal{P}_{ln}\xi_n^+\xi_r^- \\ &\times\Big[\sigma_x\mathcal{P}^\dagger_{nk}T_k\mathcal{P}_{kr}\mathcal{P}^\dagger_{rm}\left[\Delta_n^+ + i\lambda^2\Delta_n^+\omega_r^-\right] + \sigma_x\mathcal{P}^\dagger_{nk}T_k\mathcal{P}_{kr}\sigma_x\mathcal{P}^\dagger_{rm}\left[-i\lambda^2\Delta_n^+\Delta_r^-\right] \\ &+ \mathcal{P}^\dagger_{nk}T_k\mathcal{P}_{kr}\mathcal{P}^\dagger_{rm}\left[\omega_n^+ + i\lambda^2 + i\lambda^2\omega_n^+\omega_r^- - \lambda^4\omega_r^-\right] \\ &+ \mathcal{P}^\dagger_{nk}T_k\mathcal{P}_{kr}\sigma_x\mathcal{P}^\dagger_{rm}\left[-i\lambda^2\Delta_r^-\omega_n^+ + \lambda^4\Delta_r^-\right] \\ &+ \mathcal{P}^\dagger_{nm}\big\{\zeta_n^\pm\left[\overline{\omega}_n + i\lambda^2(1+i\lambda^2\omega_n^-)\left(\overline{\Delta}_n\Delta_n^+ - \omega_n^+\overline{\omega}_n\right) + i\lambda^2\left(\omega_n^-\overline{\omega}_n - \overline{\Delta}_n\Delta_n^-\right)\right] \\ &\qquad \pm\left[-i\lambda^2 + i\lambda^2(\Delta_n^+\Delta_n^- - \omega_n^+\omega_n^-) - \omega_n^+ + \lambda^4\omega_n^-\right]\big\}\delta_{nr} \\ &+ \sigma_x\mathcal{P}^\dagger_{nm}\left\{\zeta_n^\pm\left[\overline{\Delta}_n + \lambda^4\Delta_n^-\left(\overline{\Delta}_n\Delta_n^+ - \omega_n^+\overline{\omega}_n\right)\right] \mp \left(\Delta_n^+ + \lambda^4\Delta_n^-\right)\right\}\delta_{nr}\Big]\Big\}\,.\end{aligned} \tag{D.41}$$

It is important to remark that the Nambu trace will remove some terms. First, the ones containing only one σ_x, the first, fourth and last ones. Second, the one containing σ_z, i.e., the last but one. Thus

$$\langle I\rangle = 2e\lambda^2\sum_{kn}\int_{-\Omega/2}^{\Omega/2}\frac{\mathrm{d}\omega}{2\pi}\,\mathrm{Re}\,\xi_n^+\xi_n^-\mathrm{Tr_N}\left(\sigma_z P^\dagger_{nk}T_kP_{kn}\right)\left[-\lambda^2(\Delta_n^-\Delta_n^+ + \omega_n^+\omega_n^-) + i\omega_n^+ - \lambda^2 - i\lambda^4\omega_n^-\right]\,. \tag{D.42}$$

The Nambu trace involved can be computed simply as

$$\left(\sigma_z P^\dagger T P\right)_{nn} = \begin{pmatrix} p^*_{n-k,\uparrow}p_{n-k,\uparrow}\tanh\left(\frac{\omega+k\Omega-eV_{0,\uparrow}}{2\Theta}\right) & 0 \\ 0 & -p^*_{k-n,\downarrow}p_{k-n,\downarrow}\tanh\left(\frac{\omega+k\Omega+eV_{0,\downarrow}}{2\Theta}\right)\end{pmatrix}\,, \tag{D.43}$$

plugging it in the current yields

$$\begin{aligned}\langle I\rangle = 2e\lambda^2\sum_{nk}\int_{-\Omega/2}^{\Omega/2}\frac{\mathrm{d}\omega}{2\pi}\,\mathrm{Re}\,\xi_n^+\xi_n^-&\left[-\lambda^2(\Delta_n^-\Delta_n^+ + \omega_n^+\omega_n^-) + i\omega_n^+ - \lambda^2 - i\lambda^4\omega_n^-\right] \\ &\times\left\{|p_{n-k,\uparrow}|^2\tanh\left(\frac{\omega+k\Omega-eV_{0,\uparrow}}{2\Theta}\right) - |p_{k-n,\downarrow}|^2\tanh\left(\frac{\omega+k\Omega+eV_{0,\downarrow}}{2\Theta}\right)\right\}\,.\end{aligned} \tag{D.44}$$

As was done in the $N-N$ computation, a simple shift of indices can be performed, $\tilde{k}=k-n$, as well as a new definition of $\omega+n\Omega=\tilde{\omega}$. This allows to sum over the n index and yields

$$\begin{aligned}\langle I\rangle = 2e\lambda^2\sum_{\tilde{k}}\int_{-\infty}^{\infty}\frac{\mathrm{d}\tilde{\omega}}{2\pi}\,\mathrm{Re}\,\xi^+\xi^-\left[-\lambda^2(\Delta^-\Delta^+ + \omega^+\omega^-) + i\omega^+ - \lambda^2 - i\lambda^4\omega^-\right] \\ \times\left\{\left|p_{-\tilde{k},\uparrow}\right|^2\tanh\left(\frac{\tilde{\omega}+\tilde{k}\Omega - eV_{0,\uparrow}}{2\Theta}\right) - \left|p_{\tilde{k},\downarrow}\right|^2\tanh\left(\frac{\tilde{\omega}+\tilde{k}\Omega + eV_{0,\downarrow}}{2\Theta}\right)\right\}.\end{aligned} \tag{D.45}$$

The next step is to use the expressions of $\omega_n^\pm$ and $\Delta_n^\pm$. Because of the square root in their denominator, one has to separate the sub-gap and above-gap regimes. Also the tildes are dropped for convenience.

Above the gap, $\omega>\Delta$: The denominator present in the Green function of the superconductor is $\sqrt{\Delta^2-(\omega\pm i\delta)^2}$, and its real and imaginary parts will be studied separately. One uses the fact that $\omega\pm i\delta=\omega e^{\pm i\delta/\omega}$, for $\delta\ll\omega$. As a result,

$$\sqrt{\Delta^2-(\omega\pm i\delta)^2} = \sqrt{\Delta^2-\omega^2e^{\pm 2i\delta/\omega}} = \sqrt{e^{i\pi}e^{\pm 2i\delta/\omega}\left(\omega^2-\Delta^2\right)} \tag{D.46}$$

In order to compute the square root, one has to consider the branch cut in the definition of the logarithm, indeed $x^{1/2}=e^{\frac{1}{2}\ln(x)}$ and $\ln(z)=\ln(|z|)+i\arg(z)$; therefore, one needs to glue the logarithms at some angle. The choice made here is to define the logarithm for angles $\phi\in[-\pi;\pi]$ so if $\phi+2\pi n\in[-\pi;\pi]$, the logarithm is defined as $\ln(z)=\ln(|z|)+i(\phi-2\pi n)$. As result, the square root $\sqrt{e^{i\pi}e^{\pm 2i\delta/\omega}}$ can take two values depending on the sign of ω:

$$\sqrt{1-\omega^2e^{\pm 2i\delta/\omega}} = \begin{cases} e^{\pm i\pi/2}\sqrt{\omega^2-\Delta^2} & \text{if} \quad \omega<0 \\ e^{\mp i\pi/2}\sqrt{\omega^2-\Delta^2} & \text{if} \quad 0<\omega\,. \end{cases} \tag{D.47}$$

As a result, the following holds

$$\begin{aligned}\omega^\pm &= \pm i\mathrm{sgn}(\omega)\frac{\omega}{\sqrt{\omega^2-\Delta^2}} \\ \Delta^\pm &= \pm i\mathrm{sgn}(\omega)\frac{\Delta}{\sqrt{\omega^2-\Delta^2}} \\ \xi_\pm &= \frac{\sqrt{\omega^2-\Delta^2}}{(1+\lambda^4)\sqrt{\omega^2-\Delta^2}+2\lambda^2|\omega|}\,.\end{aligned} \tag{D.48}$$

Thus the frequency dependent term in the current reads as

$$-\lambda^2(\Delta^-\Delta^+ + \omega^+\omega^-) + i\omega^+ - \lambda^2 - i\lambda^4\omega^- = \frac{-|\omega|}{\omega^2-\Delta^2}\left[2\lambda^2|\omega| + (1+\lambda^4)\sqrt{\omega^2-\Delta^2}\right]. \tag{D.49}$$

This immediately simplifies with the denominator of $\xi^\pm$, leaving

$$\begin{aligned}\lambda^2\xi^+\xi^-\left[-\lambda^2(\Delta^-\Delta^+ + \omega^+\omega^-) + i\omega^+ - \lambda^2 - i\lambda^4\omega^-\right] &= \lambda^2\frac{|\omega|}{(1+\lambda^4)\sqrt{\omega^2-\Delta^2}+2\lambda^2|\omega|} \\ &= \frac{\tau}{(2-\tau)\sqrt{1-(\Delta/\omega)^2}+\tau}\,.\end{aligned} \tag{D.50}$$

As a result, the above gap (AG) contribution to the current can be greatly simplified

$$\langle I_{L,\mathrm{AG}}\rangle = 2e\sum_k \left(\int_{-\infty}^{-\Delta} + \int_{\Delta}^{\infty}\right)\frac{\mathrm{d}\omega}{2\pi}\,\frac{\tau}{(2-\tau)\sqrt{1-(\Delta/\omega)^2}+\tau} \times \sum_\sigma \mathrm{sign}\,(\sigma)|p_{k,\sigma}|^2 \tanh\left(\frac{\omega+\sigma[eV_{0\sigma}k\Omega]}{2\Theta}\right), \tag{D.51}$$

where k was transformed into $-k$ in one of the terms, and $\mathrm{sign}\,(\uparrow)=1$ and $\mathrm{sign}\,(\downarrow)=-1$.

Below the gap, $\omega<\Delta$: In this case, the different functions to use are

$$\begin{aligned}\Delta^{\pm} &= \frac{1}{\sqrt{\Delta^2-\omega^2}}\\ \omega^{\pm} &= \frac{\omega}{\sqrt{\Delta^2-\omega^2}}\\ \xi^{\pm} &= \frac{\sqrt{\Delta^2-\omega^2}}{(1+\lambda^4)\sqrt{\Delta^2-\omega^2}\mp 2i\lambda^2\omega}\,.\end{aligned} \tag{D.52}$$

The frequency dependent term in the current can therefore be written

$$\mathrm{Re}\left(-\lambda^2(\Delta_n^-\Delta_n^+ + \omega_n^+\omega_n^-) + i\omega_n^+ - \lambda^2 - i\lambda^4\omega_n^-\right) = -\frac{2\lambda^2\Delta^2}{\Delta^2-\omega^2}\,. \tag{D.53}$$

As a result, the sub-gap contribution to the current is

$$\langle I_{L,\mathrm{SG}}\rangle = \frac{e}{2\pi}\sum_k \int_{-\Delta}^{\Delta}\mathrm{d}\omega\,\frac{2\tau_A}{2+(\tau_A-2)(\omega/\Delta)^2}\sum_\sigma \mathrm{sign}\,(\sigma)|p_{k,\sigma}|^2\tanh\left(\frac{\omega+\sigma[eV_{0\sigma}+k\Omega]}{2\Theta}\right), \tag{D.54}$$

where k was transformed to $-k$ in one of the terms.

To summarize, the general formula is written here

$$\langle I_L\rangle = \frac{e}{2\pi}\sum_k\int_{-\infty}^{\infty}\mathrm{d}\omega\sum_\sigma \mathrm{sign}\,(\sigma)|p_{k,\sigma}|^2\tanh\left(\frac{\omega+\sigma[eV_{0\sigma}+k\Omega]}{2\Theta}\right) \times \begin{cases}\dfrac{\tau}{(2-\tau)\sqrt{1-(\Delta/\omega)^2}+\tau} & \text{if} \quad |\omega|>\Delta\\ \dfrac{2\tau_A}{2+(\tau_A-2)(\omega/\Delta)^2} & \text{if} \quad |\omega|<\Delta\end{cases}. \tag{D.55}$$

D.5. The noise

In this section, the noise is computed first in the high gap regime and then in the tunnel limit.

D.5.1. Infinite gap regime

D.5.1.1. Preliminaries

It is recalled that the high gap regime is implemented by setting

$$\begin{aligned} g^{r,a}_{RR,nm} &= -\sigma_x \delta_{nm} & g^{r,a}_{LL,nm} &= \mp i\mathbb{1}\delta_{nm} \\ g^{\pm\mp}_{RR,nm} &= 0 & g^{\pm\mp}_{LL,nm} &= -i\left(T \mp \mathbb{1}\right)\delta_{nm}\,. \end{aligned} \tag{D.56}$$

In order to compute the noise, one has to find formulas for $G^{\pm\mp}_{SS}$ and $G^{\pm\mp}_{NN}$. One starts by $G^{r,a}_{RR,nm}$,

$$\begin{aligned} G^{r,a}_{RR,nm} &= \left(\mathbb{1} - g^{r,a}_{RR}\Sigma_{RL}g^{r,a}_{LL}\Sigma_{LR}\right)^{-1}_{nr} g^{r,a}_{RR,rm} \\ &= -\frac{1}{1+\lambda^4}\left(\sigma_x \pm i\lambda^2\mathbb{1}\right)\delta_{nm}\,. \end{aligned} \tag{D.57}$$

The next one is obtained only by matrix multiplication

$$\begin{aligned} G^{r,a}_{RL} &= G^{r,a}_{RR}\Sigma_{RL}g^{r,a}_{LL} \\ &= \pm i\frac{\lambda}{1+\lambda^4}\left(\sigma_x P_{nm} \pm i\lambda^2 P_{nm}\right)\,. \end{aligned} \tag{D.58}$$

This can be used to compute the next function

$$\begin{aligned} G^{r,a}_{LR} &= g^{r,a}_{LL}\Sigma_{LR}G^{r,a}_{RR} \\ &= \pm i\frac{\lambda}{1+\lambda^4}\left[\left(P^\dagger\right)_{nm}\sigma_x \pm i\lambda^2\left(P^\dagger\right)_{nm}\right]\,. \end{aligned} \tag{D.59}$$

This can be used to compute the dressed Green's function in the $\pm$ basis:

$$\begin{aligned} G^{\pm\mp}_{LL,nm} &= g^{\pm\mp}_{LL,nm} + G^r_{LR,nq}\Sigma_{RL,qr}g^{\pm\mp}_{LL,rs}\Sigma_{LR,st}G^a_{RL,tm} + G^r_{LR,nq}\Sigma_{RL,qr}g^{\pm\mp}_{LL,rm} \\ &\quad + G^r_{LL,nq}\Sigma_{LR,qr}g^{\pm\mp}_{RR,rs}\Sigma_{RL,st}G^a_{LL,tm} + g^{\pm\mp}_{LL,nq}\Sigma_{LR,qr}G^a_{RL,rm} \\ &= \frac{1}{(1+\lambda^4)^2}\Big[\left[P^\dagger\sigma_x P,\, T\right]_{nm}\lambda^2(1+\lambda^4) - iT_{nm} \pm i(1+\lambda^4)\mathbb{1}\delta_{nm} - i\left(P^\dagger\sigma_x PTP^\dagger\sigma_x P\right)_{nm}\Big]\,. \end{aligned} \tag{D.60}$$

The next Green's function reads

$$\begin{aligned} G^{\pm\mp}_{RR,nm} &= g^{\pm\mp}_{RR,nm} + G^r_{RR,nq}\Sigma_{RL,qr}g^{\pm\mp}_{LL,rs}\Sigma_{LR,st}G^a_{RR,tm} + G^r_{RL,nq}\Sigma_{LR,qr}g^{\pm\mp}_{RR,rm} \\ &\quad + G^r_{RL,nq}\Sigma_{LR,qr}g^{\pm\mp}_{RR,rs}\Sigma_{RL,st}G^a_{LR,tm} + g^{\pm\mp}_{RR,nq}\Sigma_{RL,qr}G^a_{LR,rm} \\ &= -i\lambda^{-2}\frac{1}{\left(1+\lambda^4\right)^2}\Big\{\sigma_x\left(PTP^\dagger\right)_{nm}\sigma_x - i\lambda^2\left[\sigma_x,\,\left(PTP^\dagger\right)_{nm}\right] \\ &\quad + \lambda^4\left(PTP^\dagger\right)_{nm} \mp \left(1+\lambda^4\right)\mathbb{1}\delta_{nm}\Big\}\,. \end{aligned} \tag{D.61}$$

D.5.1.2. The actual computation

The noise is defined as

$$\begin{aligned}\overline{S_{LL}} = -e^2 \int_{-\Omega/2}^{\Omega/2} \frac{\mathrm{d}\omega}{2\pi} \mathrm{Tr}_{\mathrm{NH}} \big[2\mathrm{Re}\left(\sigma_z \Sigma_{RL} G^{+-}_{LR} \sigma_z \Sigma_{RL} G^{-+}_{LR}\right) \\ -\sigma_z \Sigma_{RL} G^{+-}_{LL} \sigma_z \Sigma_{LR} G^{-+}_{RR} - \sigma_z \Sigma_{LR} G^{+-}_{RR} \sigma_z \Sigma_{RL} G^{-+}_{LL} \big] ,\end{aligned} \tag{D.62}$$

The three terms can be computed separately and read as

$$\mathrm{Tr}_{\mathrm{NH}} \left[2\mathrm{Re}\left(\sigma_z \Sigma_{RL} G^{+-}_{LR} \sigma_z \Sigma_{RL} G^{-+}_{LR}\right)\right] = \frac{\tau_A}{2} \mathrm{Tr}_{\mathrm{NH}} \left[(1-\tau_A) PTP^\dagger \sigma_x PTP^\dagger \sigma_x - \mathbb{1} + \tau_A T^2 \right] \tag{D.63}$$

and

$$\begin{aligned}-\mathrm{Tr}_{\mathrm{NH}} \left[\sigma_z \Sigma_{RL} G^{+-}_{LL} \sigma_z \Sigma_{LR} G^{-+}_{RR} + \sigma_z \Sigma_{LR} G^{+-}_{RR} \sigma_z \Sigma_{RL} G^{-+}_{LL} \right] \\ = \frac{\tau_A}{2} \mathrm{Tr}_{\mathrm{NH}} \left[(1-\tau_A) PTP^\dagger \sigma_x PTP^\dagger \sigma_x - \mathbb{1} + \tau_A T^2 \right] .\end{aligned} \tag{D.64}$$

Thus the noise reads as

$$\overline{S_{LL}} = -e^2 \tau_A \int_{-\Omega/2}^{\Omega/2} \frac{\mathrm{d}\omega}{2\pi} \mathrm{Tr}_{\mathrm{NH}} \left[(1-\tau_A) PTP^\dagger \sigma_x PTP^\dagger \sigma_x - \mathbb{1} + \tau_A T^2 \right] . \tag{D.65}$$

Writing

$$\begin{aligned}&P_{nk} T_k P^\dagger_{kr} \sigma_x P_{rs} T_s P^\dagger_{sn} \sigma_x \\ &\qquad = \mathrm{diag} \left[p^*_{k-n,\downarrow} p_{k-r,\downarrow} p_{r-s,\uparrow} p^*_{n-s,\uparrow} \tan\left(\frac{\omega_k + eV_{\mathrm{DC}}}{2\theta\Omega}\right) \tan\left(\frac{\omega_s - eV_{\mathrm{DC}}}{2\theta\Omega}\right) , \right. \\ &\qquad\qquad \left. p_{n-k,\uparrow} p^*_{r-k,\uparrow} p^*_{s-r,\downarrow} p_{s-n,\downarrow} \tan\left(\frac{\omega_k - eV_{\mathrm{DC}}}{2\theta\Omega}\right) \tan\left(\frac{\omega_s + eV_{\mathrm{DC}}}{2\theta\Omega}\right) \right]\end{aligned} \tag{D.66}$$

and remarking that $\mathbb{1} = \sum_{nkrs} P_{nk} P^\dagger_{kr} \sigma_x P_{rs} P^\dagger_{sn} \sigma_x$ so that $T_n^2 = \sum_{nkrs} P_{nk} P^\dagger_{kr} \sigma_x P_{rs} P^\dagger_{sn} \sigma_x T_n^2$ and the total noise reads as

$$\begin{aligned}\overline{S_{LL}} = -\Omega e^2 \tau_A \sum_{nkrs} \int_{-1/2}^{1/2} \frac{\mathrm{d}x}{2\pi} \Bigg\{ &\left[\tan\left(\frac{x+k+q}{2\theta}\right) \tan\left(\frac{x+s-q}{2\theta}\right) - 1 \right] p^*_{k-n,\downarrow} p_{k-r,\downarrow} p_{r-s,\uparrow} p^*_{n-s,\uparrow} \\ &+ \left[\tan\left(\frac{x+k-q}{2\theta}\right) \tan\left(\frac{x+s+q}{2\theta}\right) - 1 \right] p_{n-k,\uparrow} p^*_{r-k,\uparrow} p^*_{s-r,\downarrow} p_{s-n,\downarrow} \\ -\tau_A &\left[\tan\left(\frac{x+k+q}{2\theta}\right) \tan\left(\frac{x+s-q}{2\theta}\right) - \tan^2\left(\frac{x+n-q}{2\theta}\right) \right] p^*_{k-n,\downarrow} p_{k-r,\downarrow} p_{r-s,\uparrow} p^*_{n-s,\uparrow} \\ -\tau_A &\left[\tan\left(\frac{x+k-q}{2\theta}\right) \tan\left(\frac{x+s+q}{2\theta}\right) - \tan^2\left(\frac{x+n+q}{2\theta}\right) \right] p_{n-k,\uparrow} p^*_{r-k,\uparrow} p^*_{s-r,\downarrow} p_{s-n,\downarrow} \Bigg\} .\end{aligned} \tag{D.67}$$

which is rewritten as

$$\begin{aligned}\overline{S_{LL}} = -\Omega e^2\tau_A \sum_{nkrs}\Big(p^*_{k-n,\downarrow}p_{k-r,\downarrow}p_{r-s,\uparrow}p^*_{n-s,\uparrow}+p_{n-s,\uparrow}p^*_{r-s,\uparrow}p^*_{k-r,\downarrow}p_{k-n,\downarrow}\Big)\\ \times\int_{-1/2}^{1/2}\frac{\mathrm{d}x}{2\pi}\Bigg\{(1-\tau_A)\left[\tan\left(\frac{x+k+q}{2\theta}\right)\tan\left(\frac{x+s-q}{2\theta}\right)-1\right]\\ +\tau_A\left[\tan^2\left(\frac{x+n-q}{2\theta}\right)-1\right]\Bigg\}.\end{aligned} \tag{D.68}$$

This way, both terms are bounded and variables can safely be shifted. Changing indices as $\tilde{n}=n-k$, $\tilde{r}=r-k$, $\tilde{s}=s-k$ and $x+k=\tilde{x}$ and removing the tildes for comfort, one gets

$$\begin{aligned}\overline{S}_{LL} = -\Omega e^2\tau_A \sum_{nkrs}\Big(p^*_{-n,\downarrow}p_{-r,\downarrow}p_{r-s,\uparrow}p^*_{n-s,\uparrow}+p_{n-s,\uparrow}p^*_{r-s,\uparrow}p^*_{-r,\downarrow}p_{-n,\downarrow}\Big)\\ \times\int_{k-1/2}^{k+1/2}\frac{\mathrm{d}x}{2\pi}\Bigg\{(1-\tau_A)\left[\tan\left(\frac{x+q}{2\theta}\right)\tan\left(\frac{x+s-q}{2\theta}\right)-1\right]\\ +\tau_A\left[\tan^2\left(\frac{x+n-q}{2\theta}\right)-1\right]\Bigg\},\end{aligned} \tag{D.69}$$

where x was shifted to $x+k$. The sum over k can be performed and changes the integration boundaries. Then, performing the integration and changing the sign of all the summation indices, one find

$$\overline{S_{LL}} = \frac{\Omega e^2\tau_A}{\pi}\left[(1-\tau_A)\sum_{nrs}(p^*_{n,\downarrow}p_{r,\downarrow}p_{s-r,\uparrow}p^*_{s-r,\uparrow}+\text{c.c})(2q+s)\coth\left(\frac{2q+s}{2\theta}\right)+4\tau_A\theta\right]. \tag{D.70}$$

D.5.2. λ^4 noise

Here the λ^4 contribution associated with photo-assisted noise, solely due to AR, is computed.

The first term of the noise. One starts by the first term of Eq. (D.62). It can be written, after performing the trace over harmonics degrees of freedom, as

$$\begin{aligned}&\sigma_z\Sigma_{LR,nq}G^{+-}_{RL,qr}\sigma_z\Sigma_{LR,rm}G^{-+}_{RL,mn}\\ &=-\lambda^4\sigma_z\mathcal{P}^\dagger_{nq}\Big\{\sigma_x\mathcal{P}_{qr}T_r\Delta^+_q+\mathcal{P}_{qr}T_q\omega^+_q+\mathcal{P}_{qr}\Big[\omega^+_q-i\zeta^+_q\bar{\omega}_q\Big]+\sigma_x\mathcal{P}_{qr}\Big[-i\zeta^+_q\bar{\Delta}_q+\Delta^+_q\Big]\Big\}\\ &\times\sigma_z\mathcal{P}_{rm}\Big\{\sigma_x\mathcal{P}_{mn}T_n\Delta^+_m+\mathcal{P}_{mn}T_n\omega^+_m+\mathcal{P}_{mn}\Big[-\omega^+_m-i\zeta^-_m\bar{\omega}_m\Big]+\sigma_x\mathcal{P}_{mn}\Big[-i\zeta^-_m\bar{\Delta}_m-\Delta^+_m\Big]\Big\}.\end{aligned} \tag{D.71}$$

When looking at Andreev process in the gap only, both $\omega^\pm$ and $\Delta^\pm$ are real so $\bar{\omega}=\bar{\Delta}=0$, $\omega^+=\omega^-$ and $\Delta^-=\Delta^+$. The trace of this term therefore reduces to

$$\begin{aligned}&\mathrm{Tr}_\mathrm{N}\Big[\sigma_z\Sigma_{LR,nq}G^{+-}_{RL,qr}\sigma_z\Sigma_{LR,rm}G^{-+}_{RL,mn}\Big]\\ &\qquad=\mathrm{Tr}_\mathrm{N}\Big[-\lambda^4\Big(-\sigma_x\mathcal{P}_{qr}T_r\mathcal{P}^\dagger_{rm}\Delta_q+\mathcal{P}_{qr}T_r\mathcal{P}^\dagger_{rm}\omega_q+\delta_{qm}\omega_q-\delta_{qm}\sigma_x\Delta_q\Big)\\ &\qquad\times\Big(\sigma_x\mathcal{P}_{mn}T_n\mathcal{P}^\dagger_{nq}\Delta_m+\mathcal{P}_{mn}T_n\mathcal{P}^\dagger_{nq}\omega_m-\delta_{mq}\omega_m-\delta_{mq}\sigma_x\Delta_m\Big)\Big].\end{aligned} \tag{D.72}$$

The noise is obtained by performing a Nambu trace so only the diagonal terms are kept, yielding

$$\begin{aligned}&\mathrm{Tr_N}\Big[\sigma_z\Sigma_{LR,nq}G^{+-}_{RL,qr}\sigma_z\Sigma_{LR,rm}G^{-+}_{RL,mn}\Big]\\&=\mathrm{Tr_N}\Big[-2\lambda^4\left(-\sigma_x\mathcal{P}_{qr}T_r\mathcal{P}^\dagger_{rm}\sigma_x\mathcal{P}_{mn}T_n\mathcal{P}^\dagger_{nq}\Delta_m\Delta_q+\mathcal{P}_{qr}T_r\mathcal{P}^\dagger_{rm}\mathcal{P}_{mn}T_n\mathcal{P}^\dagger_{nq}\omega_m\omega_q+\mathbb{1}(\Delta_m^2-\omega_m^2)\right)\Big]\,.\end{aligned}\tag{D.73}$$

The second and third terms. The rest of the terms of Eq. (D.62) are computed here. One starts by computing (note that some permutations have been performed as one is only interested in the trace)

$$\begin{aligned}&\lambda^2\sigma_z\mathcal{P}G^{\pm\mp}_{LL}\sigma_z\mathcal{P}^\dagger G^{\mp\pm}_{RR}\\&=\lambda^2\sigma_z(\mathbb{1}-\lambda^2g^r_R\mathcal{P}g^r_L\mathcal{P}^\dagger)^{-1}\mathcal{P}\big(g^{\pm\mp}_L+\lambda^2g^r_L\mathcal{P}^\dagger g^{\pm\mp}_R\mathcal{P}g^a_L\big)\mathcal{P}^\dagger(\mathbb{1}-\lambda^2\mathcal{P}g^a_L\mathcal{P}^\dagger g^a_R)^{-1}\mathcal{P}\sigma_z\mathcal{P}^\dagger\\&\quad\times(\mathbb{1}-\lambda^2g^r_R\mathcal{P}g^r_L\mathcal{P}^\dagger)^{-1}\big(g^{\mp\pm}_R+\lambda^2g^r_R\mathcal{P}g^{\mp\pm}_L\mathcal{P}^\dagger g^a_R\big)(\mathbb{1}-\lambda^2\mathcal{P}g^a_L\mathcal{P}^\dagger g^a_R)^{-1}\,.\end{aligned}\tag{D.74}$$

Some simplifications can be performed, first g_L commutes in Nambu and harmonics space with $\mathcal{P}^\dagger$ so the second parentheses can be simplified. Furthermore, the inverse of $(\mathbb{1}-\lambda^2\mathcal{P}g^a_L\mathcal{P}^\dagger g^a_R)^{-1}$ is diagonal in harmonic space, the same goes for g_L. As a result, the frequencies at which this term is evaluated will be that of $g^{\pm\mp}_R$ and therefore it vanishes when looking at in-gap AR. The next step is to keep only λ^4 terms. As

$$(\mathbb{1}-\lambda\mathcal{P}g^a_L\lambda\mathcal{P}^\dagger g^a_R)^{-1}_{nm}\sigma_z(\mathbb{1}-g^r_R\lambda\mathcal{P}g^r_L\lambda\mathcal{P}^\dagger)^{-1}_{mq}=\sigma_z(\xi^+_n\xi^-_n)^2\delta_{nq}=\sigma_z\delta_{nq}+o(\lambda^4)\,,\tag{D.75}$$

the total term to evaluate becomes

$$\begin{aligned}&\Big[\lambda\mathcal{P}g^{\pm\mp}_L\lambda\mathcal{P}^\dagger\sigma_zg^r_R\lambda\mathcal{P}^rg^{\mp\pm}_L\lambda\mathcal{P}^\dagger g^a_R\sigma_z\Big]_{nn}\\&\qquad=-\lambda^4\mathcal{P}_{nq}(T_q\mp\mathbb{1})\mathcal{P}^\dagger_{qr}\sigma_z(\omega_r\mathbb{1}+\Delta_r\sigma_x)\mathcal{P}_{rs}(T_s\pm\mathbb{1})\mathcal{P}^\dagger_{sn}(\omega_n\mathbb{1}+\Delta_n\sigma_x)\sigma_z\,.\end{aligned}\tag{D.76}$$

As the $\mp$ and the $\pm$ results are summed in the noise so only half of the terms will count and the sum yields

$$\begin{aligned}&\Big[-\sigma_z\lambda\mathcal{P}G^{+-}_{LL}\sigma_z\lambda\mathcal{P}^\dagger G^{-+}_{RR}-\sigma_z\lambda\mathcal{P}^\dagger G^{-+}_{RR}\sigma_z\lambda\mathcal{P}G^{+-}_{LL}\Big]_{nn}\\&\qquad=2\lambda^4\mathcal{P}_{nq}\Big[T_q\mathcal{P}^\dagger_{qr}\sigma_z(\omega_r\mathbb{1}+\Delta_r\sigma_x)\mathcal{P}_{rs}T_s\mathcal{P}^\dagger_{sn}(\omega_n\mathbb{1}+\Delta_n\sigma_x)\\&\qquad\quad-\mathcal{P}^\dagger_{qr}\sigma_z(\omega_r\mathbb{1}+\Delta_r\sigma_x)\mathcal{P}_{rs}\mathcal{P}^\dagger_{sn}(\omega_n\mathbb{1}+\Delta_n\sigma_x)\Big]\sigma_z\,.\end{aligned}\tag{D.77}$$

The term contributing to the trace therefore reduces to

$$\begin{aligned}\mathrm{Tr_{NH}}\Big[\lambda^2\sigma_z\mathcal{P}G^{\pm\mp}_{LL}\sigma_z\mathcal{P}^\dagger G^{\mp\pm}_{RR}\Big]=2\lambda^4\sum_n\mathrm{Tr_N}\Big[&\mathcal{P}_{nq}T_q\mathcal{P}^\dagger_{qr}\mathcal{P}_{rs}T_s\mathcal{P}^\dagger_{sn}\omega_n\omega_r\\&+\sigma_x\mathcal{P}_{nq}T_q\mathcal{P}^\dagger_{qr}\sigma_x\mathcal{P}_{rs}T_s\mathcal{P}^\dagger_{sn}\Delta_n\Delta_r-\mathbb{1}(\omega_n^2+\Delta_n^2)\Big]\,.\end{aligned}\tag{D.78}$$

Sum of the terms. Summing both terms yields

$$\overline{\langle S\rangle}_q=-4e^2\lambda^4\int_{-\Omega/2}^{\Omega/2}\frac{\mathrm{d}\omega}{2\pi}\sum_{nsr=-\infty}^{+\infty}\mathrm{Tr_N}\left[\sigma_x\mathcal{P}_{nq}T_q\mathcal{P}^\dagger_{qr}\sigma_x\mathcal{P}_{rs}T_s\mathcal{P}^\dagger_{sn}\Delta_n\Delta_r-\Delta_n^2\mathbb{1}\right]\,.\tag{D.79}$$

After performing the Nambu trace, redefining the indices and performing one harmonics sum one is left with Eq. (8.9).

E. Perturbation in the $QSH - S$ junction

In this Appendix, the state of a $QSH - S$ junction after a single, quantized, Lorentzian pulse is sent is computed perturbatively. The final state will be written

$$|\mathcal{F}\rangle = S(+\infty, -\infty)\,|F_\uparrow\rangle \otimes |F_\downarrow\rangle \otimes |\Psi_{\mathrm{BCS}}\rangle\ , \tag{E.1}$$

where $|F_\sigma\rangle$ is the Fermi sea of spin channel σ, and

$$S(t, -\infty) = T \exp\left[-i \int_{-\infty}^{t} \mathrm{d}t' H_{TI}(t')\right]\ , \tag{E.2}$$

is the evolution operator and $H_{TI}(t)$ denotes the tunnel Hamiltonian in the interaction picture, i.e.,

$$H_{TI}(t) = e^{iH_0 t} H_T e^{-iH_0 t}\,, \tag{E.3}$$

where H_0 is the Hamiltonian without interaction, $H_0 = H_N + H_{BCS}$, and T is the time ordering operator. Cooper pair transfer is ruled by the λ^2 terms, they appear in the second order of the perturbation theory of the evolution operator,

$$S(+\infty, -\infty)^{(2)} = -\frac{1}{2} \int_{-\infty}^{\infty} \mathrm{d}t_1 \int_{-\infty}^{t_1} \mathrm{d}t_2\, T\left[H_{TI}(t_1) H_{TI}(t_2)\right]\ . \tag{E.4}$$

The two edge modes of the QSH are considered to be normal metals.

E.1. Writing the state in terms of electron operators

The action of electron operators on the BCS ground state is complicated, therefore, they will be expressed in terms of the free quasiparticles of the BCS Hamiltonian. The inverse Bogolubov-Valatin relations are recalled,

$$c^\dagger_{S,k,\sigma} = u_k \gamma^\dagger_{k,\sigma} + v_k \mathrm{sign}(\sigma) \gamma_{-k,\overline{\sigma}}\,. \tag{E.5}$$

where $\gamma_{k,\sigma}$ are quasiparticle annihilation operators. The second order term in λ in the evolution operator expansion therefore reads as

$$\begin{aligned} S(+\infty, -\infty)^{(2)} = -\frac{1}{4} \sum_{\substack{k_N, k'_N \\ k_S, k'_S \\ \sigma_1, \sigma_2 \\ \epsilon_1 \epsilon_2 = \pm}} \int_{-\infty}^{+\infty} \mathrm{d}t_1 \int_{-\infty}^{t_1} \mathrm{d}t_2 \\ \left[e^{-i\phi(t_1)} c^\dagger_{k_N,\sigma_1}(t_1) \left(u_{k_S} \gamma_{k_S,\sigma_1}(t_1) + v_{k_S} \mathrm{sign}(\sigma_1) \gamma^\dagger_{-k_S,\overline{\sigma_1}}(t_1)\right)\right]^{\epsilon_1} \\ \times \left[e^{-i\phi(t_2)} c^\dagger_{k'_N,\sigma_2}(t_2) \left(u_{k_S} \gamma_{k'_S,\sigma_2}(t_2) + v_{k_S} \mathrm{sign}(\sigma_2) \gamma^\dagger_{-k'_S,\overline{\sigma_2}}(t_2)\right)\right]^{\epsilon_2}\ , \end{aligned} \tag{E.6}$$

where $\epsilon = -$ means hermitian conjugate and $\epsilon = +$ does not change anything. Note that only the phase factor ϕ is the same in the two terms.

As only the Andreev regime will be considered, it can be assumed that the BCS ground state is not modified by the drive, this has the direct implication that only terms involving $\gamma_{k_1,\sigma_1}\gamma^\dagger_{k_2,\sigma_2}\delta_{k_1,k_2}\delta_{\sigma_1,\sigma_2}$ in Eq. (E.6) are taken into account. This reduces the number of term, for each ϵ combination, from four to one.

There are no restriction on the Fermi sea other than fermionic rules, i.e., $c_{k,\sigma}c_{k,\sigma} = 0$ so one can start writing down these terms:

- $\epsilon_1 = +$
  - $\epsilon_2 = +$, so that the only term is the one containing $c^\dagger_{k_N,\sigma_1}c^\dagger_{k'_N,\sigma_2}\gamma_{k_S,\sigma_1}\gamma^\dagger_{-k'_S,\overline{\sigma_2}}$
  - $\epsilon_2 = -$, so that the only term is the one containing $c^\dagger_{k_N,\sigma_1}c_{k'_N,\sigma_2}\gamma_{k_S,\sigma_1}\gamma^\dagger_{k'_S,\sigma_2}$
- $\epsilon_1 = -$
  - $\epsilon_2 = +$, so that the only term is the one containing $c_{k_N,\sigma_1}c^\dagger_{k'_N,\sigma_2}\gamma_{-k_S,\overline{\sigma_1}}\gamma^\dagger_{-k'_S,\overline{\sigma_2}}$
  - $\epsilon_2 = -$, so that the only term is the one containing $c_{k_N,\sigma_1}c_{k'_N,\sigma_2}\gamma_{-k_S,\overline{\sigma_1}}\gamma_{k'_S,\sigma_2}\dagger$

These terms are now written in the interaction picture, i.e.,

$$\begin{aligned} c_{k,\sigma}(t) &= c_{k,\sigma}e^{-iE_N(k)t} \\ \gamma_{k,\sigma}(t) &= \gamma_{k,\sigma}e^{-iE_S(k)t}\,. \end{aligned} \tag{E.7}$$

Using Eq. (4.28) in Eq. (E.1) after writing explicitly the sum over ϵ, k'_s and σ_2, changing variable $t_2 \to t_1$ in the second time-ordered term yields

$$\begin{aligned} |\mathcal{F}\rangle = -\frac{\lambda^2}{4}\sum_{\substack{k_N,k'_N\\k_S\sigma}}\int_{-\infty}^{\infty}\mathrm{d}t_1\int_{-\infty}^{t_1}\mathrm{d}t_2 \\ \Big[& e^{-i\phi(t_1)}e^{i[E_N(k_N)-E_S(k_S)]t_1}e^{-i\phi(t_2)}e^{i\left[E_N(k'_N)+E_S(k_S)\right]t_2}\mathrm{sign}(\sigma)u_{k_S}v_{k_S}c^\dagger_{k_N,\sigma}c^\dagger_{k'_N,\overline{\sigma}} \\ & + e^{-i\phi(t_1)}e^{i\phi(t_2)}e^{i[E_N(k_N)-E_S(k_S)]t_1}e^{i\left[-E_N(k'_N)+E_S(k_S)\right]t_2}u^2_{k_S}c^\dagger_{k_N,\sigma}c_{k'_N,\sigma} \\ & + e^{i\phi(t_1)}e^{-i\phi(t_2)}e^{i[-E_N(k_N)-E_S(-k_S)]t_1}e^{i\left[E_N(k'_N)+E_S(-k_S)\right]t_2}v^2_{k_S}c_{k_N,\sigma}c^\dagger_{k'_N,\sigma} \\ & + e^{i\phi(t_1)}e^{i[-E_N(k_N)-E_S(-k_S)]t_1}e^{i\phi(t_2)}e^{i\left[-E_N(k'_N)+E_S(-k_S)\right]t_2}\mathrm{sign}(\sigma)u_{k_S}v_{k_S}c_{k_N,\sigma}c_{k'_N,\overline{\sigma}}\Big] \\ & \times |F_\uparrow\rangle\otimes|F_\downarrow\rangle\otimes|\Psi_{\mathrm{BCS}}\rangle\,, \end{aligned} \tag{E.8}$$

It will be useful write the phase in terms of its Fourier transform as

$$e^{-i\phi(t)} = \int_{-\infty}^{\infty}\mathrm{d}\varepsilon\varphi(\varepsilon)e^{-i\varepsilon t}\,. \tag{E.9}$$

Another intermediate result is necessary here, let I be the following integral

$$\begin{aligned} I &= \lim_{\alpha\to 0}\int_{-\infty}^{t_1} \mathrm{d}t_2 \exp\left[i(E-i\alpha)t_2\right] \\ &= \lim_{\alpha\to 0}\frac{-ie^{iEt_1}}{E-i\alpha}\,, \end{aligned} \tag{E.10}$$

These two results will be plugged separately in the four terms of Eq. (E.8).

E.2. Andreev reflection terms

This term is the main contribution at low frequency which involves Andreev processes, therefore it is denoted with an index A. Using the fact that $u_k v_k = \pm\Delta/2E_S(k)$

$$\begin{aligned} |\mathcal{F}_A\rangle = -\frac{\lambda^2\Delta}{2}\sum_{\substack{k,k'\\ k_S\sigma}}\int_{-\infty}^{\infty}\mathrm{d}\varepsilon_1\int_{-\infty}^{\infty}\mathrm{d}\varepsilon_2\int_{-\infty}^{\infty}\mathrm{d}t_1\int_{-\infty}^{t_1}\mathrm{d}t_2\,\mathrm{sign}(\sigma)e^{\alpha t_2}E_S(k_S)^{-1} \\ \Big[\varphi(\epsilon_1)e^{i[E_N(k)-E_S(k_S)-\varepsilon_1]t_1}\varphi(\epsilon_2)e^{i[E_N(k')+E_S(k_S)-\varepsilon_2]t_2}c^\dagger_{k,\sigma}c^\dagger_{k',\bar\sigma} \\ -\varphi(\epsilon_1)e^{i[-E(k)-E_S(-k_S)+\varepsilon_1]t_1}\varphi(\epsilon_2)e^{i[-E(k')+E_S(-k_S)+\varepsilon_2]t_2}c_{k,\sigma}c_{k',\bar\sigma}\Big] \\ \times|F_\uparrow\rangle\otimes|F_\downarrow\rangle\otimes|\Psi_{\mathrm{BCS}}\rangle\,. \end{aligned} \tag{E.11}$$

Where α is a positive regularization parameter that will be taken to zero, ensuring that the contribution at $-\infty$ vanishes. The integral over t_2 is performed with the help of Eq.(E.10),

$$\begin{aligned} |\mathcal{F}_A\rangle = i\frac{\Delta\lambda^2}{2}\sum_{\substack{k,k'\\ k_S\sigma}}\int_{-\infty}^{\infty}\mathrm{d}\varepsilon_1\int_{-\infty}^{\infty}\mathrm{d}\varepsilon_2\int_{-\infty}^{\infty}\mathrm{d}t_1\,\mathrm{sign}(\sigma)E_S(k_S)^{-1} \\ \Big[\varphi(\epsilon_1)\varphi(\epsilon_2)e^{i[E_N(k)+E_N(k')-(\varepsilon_1+\varepsilon_2)]t_1}\frac{1}{E_N(k')+E_S(k_S)-\varepsilon_2-i\alpha}c^\dagger_{k,\sigma}c^\dagger_{k',\bar\sigma} \\ -\varphi(\epsilon_1)\varphi(\epsilon_2)e^{i[-E(k)-E_N(k')+\varepsilon_1+\varepsilon_2]t_1}\frac{1}{-E_N(k')+E_S(k_S)+\varepsilon_2-i\alpha}c_{k,\sigma}c_{k',\bar\sigma}\Big] \\ \times|F_\uparrow\rangle\otimes|F_\downarrow\rangle\otimes|\Psi_{\mathrm{BCS}}\rangle\,. \end{aligned} \tag{E.12}$$

Now, provided that the $\exp(-i\phi(t))$ is a continuous function, one can show that its Fourier transform respects

$$\varphi(\varepsilon) \le \frac{1}{2}\int_{\mathbb{R}}\mathrm{d}t\,\left|\exp\left[-i\phi(t)\right]-\exp\left[-i\phi\left(t+\frac{\pi}{\varepsilon}\right)\right]\right|\,. \tag{E.13}$$

It is useful to introduce a typical time scale in $\exp(i\phi(t))$, W, which describes the time over which the function changes substantially. For a periodic function, this would be the period, for a unique pulse, it would be the width of the pulse etc. The Fourier transform in Eq. (E.13) will give a vanishing contribution as soon as $\varepsilon \gg W^{-1}\pi$. The Andreev regime is valid for $\Delta \gg 1/W$, which in turns imply that, $\varepsilon_2 \ll \Delta$ and $\varepsilon_1 \ll \Delta$ in Eq. (E.12). This is basically saying that the exponential of the phase does not vary over times

shorter than the inverse gap.

Considering that creation operators vanish for negative energy states and annihilation operator for positive energy states, and that $E_N(k) \propto k$, the following constraint are enforced. For the first term, $E_N(k)$, $E_N(k') > 0$ for the first term and $E_N(k)$, $E_N(k') < 0$ for the second one. Furthermore, as $E_S(k) > \Delta$, the ε_2 and the $i\alpha$ can safely be removed of the fraction and the Fourier transform of the phase can be reverted to get[1]

$$\begin{aligned}|\mathcal{F}_A\rangle = i\frac{\Delta\lambda^2}{2}\sum_{\substack{k,k'\\k_S\sigma}}\int_{-\infty}^{\infty}\mathrm{d}t_1\,\mathrm{sign}(\sigma)E_S(k_S)^{-1}\Bigg[&e^{-2i\phi(t_1)}e^{i[E_N(k)+E_N(k')]t_1}\frac{1}{E_N(k')+E_S(k_S)}c^\dagger_{k,\sigma}c^\dagger_{k',\overline{\sigma}}\\&-e^{2i\phi(t_1)}e^{i[-E(k)-E_N(k')]t_1}\frac{1}{-E_N(k')+E_S(k_S)}c_{k,\sigma}c_{k',\overline{\sigma}}\Bigg]\\&\times|F_\uparrow\rangle\otimes|F_\downarrow\rangle\otimes|\Psi_{\mathrm{BCS}}\rangle\ ,\end{aligned}\tag{E.14}$$

Going back to energies, and writing the Fourier transform of the total phase as $\varphi_T(\varepsilon)$.

$$\begin{aligned}|\mathcal{F}_A\rangle = i\frac{\Delta\lambda^2}{2}\sum_{\substack{k,k'\\k_S\sigma}}\int_{-\infty}^{\infty}\mathrm{d}t_1\int_{-\infty}^{\infty}\mathrm{d}\varepsilon\,\mathrm{sign}(\sigma)E_S(k_S)^{-1}&\\\Bigg[\varphi_T(\varepsilon)e^{i[E_N(k)+E_N(k')-\varepsilon]t_1}\frac{1}{E_N(k')+E_S(k_S)}c^\dagger_{k,\sigma}c^\dagger_{k',\overline{\sigma}}&\\-\varphi^*_T(\varepsilon)e^{i[-E(k)-E_N(k')+\varepsilon]t_1}\frac{1}{-E_N(k')+E_S(k_S)}c_{k,\sigma}c_{k',\overline{\sigma}}\Bigg]&\\\times|F_\uparrow\rangle\otimes|F_\downarrow\rangle\otimes|\Psi_{\mathrm{BCS}}\rangle\ ,&\end{aligned}\tag{E.15}$$

the integral over t_1 is easily performed now and yields

$$\begin{aligned}|\mathcal{F}_A\rangle = i\frac{\Delta\lambda^2}{2}\sum_{\substack{k,k'\\k_S\sigma}}\int_{-\infty}^{\infty}\mathrm{d}\varepsilon\,\mathrm{sign}(\sigma)E_S(k_S)^{-1}\Bigg[&\varphi_T(\varepsilon)\frac{\delta\left[E_N(k)+E_N(k')-\varepsilon\right]}{E_N(k')+E_S(k_S)}c^\dagger_{k,\sigma}c^\dagger_{k',\overline{\sigma}}\\&-\varphi^*_T(\varepsilon)\frac{\delta\left[-E(k)-E_N(k')+\varepsilon\right]}{-E_N(k')+E_S(k_S)}c_{k,\sigma}c_{k',\overline{\sigma}}\Bigg]\\&\times|F_\uparrow\rangle\otimes|F_\downarrow\rangle\otimes|\Psi_{\mathrm{BCS}}\rangle\ .\end{aligned}\tag{E.16}$$

In order for the delta function to be reduced, one has to translate k sums to energy integrals in the normal metals. It can be assumed that the range of valid k are the same in the normal metal as in the superconductor, so that the following analysis apply both to k_N and k_S. In the context of the BCS theory, $-k_{\omega_D} < k - k_F < k_{\omega_D}$, where $\omega_D \ll \varepsilon_F$ is the Debye frequency. Therefore it is relevant to define $\delta k = k - k_F$ and go from sum over k to integral over δk as

$$\sum_k = \frac{L}{2\pi}\int_{-k(\omega_D)}^{k(\omega_D)}\mathrm{d}\delta k\,,\tag{E.17}$$

[1] going backwards, one can see that 2ϕ is in fact $\phi_\uparrow + \phi_\downarrow$

where L is the typical size of the system. Then, for the normal metal only, writing the k dependence of the energy as $E(k) = \frac{1}{2m}(k - k_F)(k + k_F)$ and enforcing that $\omega_D \ll \varepsilon_F$, the spectrum is linear. Therefore, defining the Fermi velocity as $v_F = k_F/m$, one gets the following relation

$$\sum_k = \frac{L}{2\pi v_F} \int_{-\omega_D}^{\omega_D} \mathrm{d}\xi \,, \tag{E.18}$$

where $\xi = \frac{k^2}{2m} - \varepsilon_F$, in the normal metal this corresponds to energy, so it is called E. This is not the case in the superconductor where $E_S(k) = \sqrt{\xi(k)^2 + \Delta^2}$, so the notation ξ is kept in this case. Therefore

$$\begin{aligned} |\mathcal{F}_A\rangle = i\frac{L^3\lambda^2}{16\pi^3 v_F^3} \sum_\sigma \mathrm{sign}(\sigma) \int_{-\omega_D}^{\omega_D} \mathrm{d}E \int_{-\omega_D}^{\omega_D} \mathrm{d}E' \int_{-\omega_D}^{\omega_D} \mathrm{d}\xi \int_{-\infty}^{\infty} \mathrm{d}\varepsilon \, \frac{\Delta}{\sqrt{\xi^2+\Delta^2}} \\ \times \left[\varphi_T(\varepsilon) \frac{\delta\left[E + E' - \varepsilon\right]}{E' + \sqrt{\xi^2+\Delta^2}} c^\dagger_{k(E),\sigma} c^\dagger_{k(E'),\bar\sigma} - \varphi_T^*(\varepsilon) \frac{\delta\left[-E - E' + \varepsilon\right]}{-E' + \sqrt{\xi^2+\Delta^2}} c_{k(E),\sigma} c_{k(E'),\bar\sigma} \right] \\ \times |F_\uparrow\rangle \otimes |F_\downarrow\rangle \otimes |\Psi_{\mathrm{BCS}}\rangle \,. \end{aligned} \tag{E.19}$$

As said earlier, the E are positive in the first term, and negative in the second one, furthermore, ε is far lower that Δ, and finally, the delta function enforces that $\varepsilon = E + E'$. Thus, for all terms, one has $|E|, |E'| \ll \Delta$. This means that, in the denominator, the E' do not contribute and the integral over E' can be performed. It yields

$$\begin{aligned} |\mathcal{F}_A\rangle = i\frac{L^3\lambda^2}{16\pi^3 v_F^3} \sum_\sigma \mathrm{sign}(\sigma) \int_{-\omega_D}^{\omega_D} \mathrm{d}E \int_{-\omega_D}^{\omega_D} \mathrm{d}\xi \int_{-\infty}^{\infty} \mathrm{d}\varepsilon \, \frac{\Delta}{\xi^2+\Delta^2} \\ \times \left[\varphi_T(\varepsilon) c^\dagger_{k(E),\sigma} c^\dagger_{k(\varepsilon-E),\bar\sigma} - \varphi_T^*(\varepsilon) c_{k(E),\sigma} c_{k(E'),\bar\sigma} \right] |F_\uparrow\rangle \otimes |F_\downarrow\rangle \otimes |\Psi_{\mathrm{BCS}}\rangle \,. \end{aligned} \tag{E.20}$$

The integral over ξ yields a factor π (as $\omega_D \gg \Delta$) and the final state reads as

$$\begin{aligned} |\mathcal{F}_A\rangle = i\frac{L^3\lambda^2}{16\pi^2 v_F^3} \sum_\sigma \mathrm{sign}(\sigma) \int_{-\omega_D}^{\omega_D} \mathrm{d}E \int_{-\infty}^{\infty} \mathrm{d}\varepsilon \, \left[\varphi_T(\varepsilon) c^\dagger_{k(E),\sigma} c^\dagger_{k(\varepsilon-E),\bar\sigma} - \varphi_T^*(\varepsilon) c_{k(E),\sigma} c_{k(\varepsilon-E),\bar\sigma} \right] \\ |F_\uparrow\rangle \otimes |F_\downarrow\rangle \otimes |\Psi_{\mathrm{BCS}}\rangle \,. \end{aligned} \tag{E.21}$$

This result can be symmetrized by defining $\tilde E = E - \frac{\varepsilon}{2}$. The boundaries of the E integration are not modified as the only non vanishing contributions of ε are at $\varepsilon \ll \Delta \ll \omega_D$. Then, for comfort, one defines $2\zeta = \varepsilon$, the general result is

$$\begin{aligned} |\mathcal{F}_A\rangle = i\frac{L^3\lambda^2}{8\pi^2 v_F^3} \sum_\sigma \mathrm{sign}(\sigma) \int_{-\infty}^{\infty} \mathrm{d}\zeta \, \varphi_T(2\zeta) \int_{-\zeta}^{\zeta} \mathrm{d}\tilde E \left[c^\dagger_{k(\tilde E+\zeta),\sigma} c^\dagger_{k(\zeta-\tilde E),\bar\sigma} - c_{k(\tilde E+\zeta),\sigma} c_{k(\zeta-\tilde E),\bar\sigma} \right] \\ \times |F_\uparrow\rangle \otimes |F_\downarrow\rangle \otimes |\Psi_{\mathrm{BCS}}\rangle \,. \end{aligned} \tag{E.22}$$

E.2.1. Quantized Levitons

In the case of a drive such that $q_\uparrow + q_\downarrow$ is integer,

$$\varphi_T(\varepsilon) = \delta(\varepsilon) + 2We^{-W\varepsilon}\theta(\varepsilon) \,. \tag{E.23}$$

This imposes that $\zeta \geq 0$, so that at zero temperature the second term disappears identically.

$$|\mathcal{F}_A\rangle = i\frac{L^3\Delta\lambda^2}{8\pi^2 v_F^3}\int_{-\infty}^{\infty}\mathrm{d}\zeta\,\varphi_T(2\zeta)\int_{-\zeta}^{\zeta}\mathrm{d}\tilde{E}\left[c^\dagger_{k(\tilde{E}+\zeta),\uparrow}c^\dagger_{k(\zeta-\tilde{E}),\downarrow} - c^\dagger_{k(\tilde{E}+\zeta),\downarrow}c^\dagger_{k(\zeta-\tilde{E}),\uparrow}\right]|F_\uparrow\rangle\otimes|F_\downarrow\rangle\otimes|\Psi_{\mathrm{BCS}}\rangle\ . \quad \text{(E.24)}$$

E.3. Quasiparticle transfer terms

Here the second and third terms of Eq. (E.8) are computed. The state is denoted by an index Q as it involves only quasiparticle transfer above the gap:

$$\begin{aligned}|\mathcal{F}_Q\rangle = -\frac{\lambda^2}{4}\sum_{\substack{k_N,k'_N\\ k_S\sigma_1}}\int_{-\infty}^{\infty}\mathrm{d}t_1\int_{-\infty}^{t_1}\mathrm{d}t_2 \\ \times\Big[e^{-i\phi(t_1)}e^{i\phi(t_2)}e^{i[E_N(k_N)-E_S(k_S)]t_1}e^{i\left[-E_N(k'_N)+E_S(k_S)\right]t_2}u^2_{k_S}c^\dagger_{k_N,\sigma}c_{k'_N,\sigma} \\ +e^{i\phi(t_1)}e^{-i\phi(t_2)}e^{i[-E_N(k_N)-E_S(-k_S)]t_1}e^{i\left[E_N(k'_N)+E_S(-k_S)\right]t_2}v^2_{k_S}c_{k_N,\sigma}c^\dagger_{k'_N,\sigma}\Big] \\ \times|F_\uparrow\rangle\otimes|F_\downarrow\rangle\otimes|\Psi_{\mathrm{BCS}}\rangle\ .\end{aligned} \quad \text{(E.25)}$$

The phases are replaced by their expression in Fourier space

$$\begin{aligned}|\mathcal{F}_Q\rangle = -\frac{\lambda^2}{4}\sum_{\substack{k_N,k'_N\\ \sigma}}A_S\int_{-\infty}^{\infty}dk_S\int_{-\infty}^{\infty}\mathrm{d}t_1\int_{-\infty}^{t_1}\mathrm{d}t_2\int_{-\infty}^{\infty}\mathrm{d}\epsilon_1\int_{-\infty}^{\infty}\mathrm{d}\epsilon_2\ \varphi(\epsilon_1)\varphi(\epsilon_2) \\ \times\Big[e^{-i\epsilon_1 t_1}e^{i\epsilon_2 t_2}e^{i[E_N(k_N)-E_S(k_S)]t_1}e^{i\left[-E_N(k'_N)+E_S(k_S)\right]t_2}u^2_{k_S}c^\dagger_{k_N,\sigma}c_{k'_N,\sigma} \\ +e^{i\epsilon_1 t_1}e^{-i\epsilon_2 t_2}e^{i[-E_N(k_N)-E_S(-k_S)]t_1}e^{i\left[E_N(k'_N)+E_S(-k_S)\right]t_2}v^2_{k_S}c_{k_N,\sigma}c^\dagger_{k'_N,\sigma}\Big] \\ \times|F_\uparrow\rangle\otimes|F_\downarrow\rangle\otimes|\Psi_{\mathrm{BCS}}\rangle\ ,\end{aligned} \quad \text{(E.26)}$$

Integration over t_2 in both terms can be performed by introducing a convergence factor $e^{\alpha t_2}$ to take care of the limit $t_2 \to -\infty$, thus

$$\begin{aligned}|\mathcal{F}_Q\rangle = -\frac{\lambda^2}{4}\sum_{\substack{k_N,k'_N\\ k_S\sigma}}\int_{-\infty}^{\infty}\mathrm{d}t_1\int_{-\infty}^{\infty}\mathrm{d}\epsilon_1\int_{-\infty}^{\infty}\mathrm{d}\epsilon_2\ \varphi(\epsilon_1)\varphi(\epsilon_2) \\ \times i\left[\frac{e^{-i\left[\epsilon_1-\epsilon_2-E_N(k_N)+E_N(k'_N)\right]t_1}u^2_{k_S}}{E_N(k'_N)-E_S(k_S)-\epsilon_2+i\alpha}c^\dagger_{k_N,\sigma}c_{k'_N,\sigma} - \frac{e^{i\left[\epsilon_1-\epsilon_2-E_N(k_N)+E_N(k'_N)\right]t_1}v^2_{k_S}}{E_N(k'_N)+E_S(k_S)-\epsilon_2-i\alpha}c_{k_N,\sigma}c^\dagger_{k'_N,\sigma}\right] \\ \times|F_\uparrow\rangle\otimes|F_\downarrow\rangle\otimes|\Psi_{\mathrm{BCS}}\rangle\ .\end{aligned} \quad \text{(E.27)}$$

As was done before, arguing that $E_N(k')$ is positive in the first term and negative in the second one, the $\varepsilon_2 \pm i\alpha$ can be removed from the denominator and the Fourier transform of the exponentiated phase can

be reverted. This term looks like this

$$\int_{\mathbb{R}} \mathrm{d}\varepsilon_1 \varphi(\varepsilon_1) e^{-i\epsilon_1 t_1} \int_{\mathbb{R}} \mathrm{d}\varepsilon_2 \varphi(\varepsilon_2) e^{i\epsilon_2 t_1} = e^{-i\phi(t_1)} e^{i\phi(t_1)} = 1\,, \tag{E.28}$$

which is surprising as it means that the voltage drive is not involved.

The integral over t_1 is simple and gives a delta function, common to both terms,

$$|\mathcal{F}_Q\rangle = -i\frac{\lambda^2}{4} \sum_{\substack{k,k' \\ k_S\sigma}} \delta\left[E_N(k_N) - E_N(k'_N)\right] \left[\frac{u_{k_S}^2}{E_N(k'_N) - E_S(k_S)} c^\dagger_{k_N,\sigma} c_{k'_N,\sigma} - \frac{v_{k_S}^2}{E_N(k'_N) + E_S(k_S)} c_{k_N,\sigma} c^\dagger_{k'_N,\sigma}\right] \times |F_\uparrow\rangle \otimes |F_\downarrow\rangle \otimes |\Psi_{\mathrm{BCS}}\rangle\ . \tag{E.29}$$

$k_N \leftrightarrow k'_N$ can be exchanged in the second term provided that the fermionic operators or inverted. One obtains

$$|\mathcal{F}_Q\rangle = -i\frac{\lambda^2}{4} \sum_{\substack{k_N,k'_N \\ k_S\sigma}} \delta\left[E_N(k_N) - E_N(k'_N)\right] \left[\frac{u_{k_S}^2}{E_N(k'_N) - E_S(k_S)} + \frac{v_{k_S}^2}{E_N(k_N) + E_S(k_S)}\right] \times c^\dagger_{k_N,\sigma} c_{k'_N,\sigma} |F_\uparrow\rangle \otimes |F_\downarrow\rangle \otimes |\Psi_{\mathrm{BCS}}\rangle\ . \tag{E.30}$$

Repeating what was done before, the k sums are shifted to kinetic energy integrals, so that the integral over E' can be performed. One is left with

$$|\mathcal{F}_Q\rangle = i\frac{L^3\lambda^2}{16\pi^3 v_F^3} \sum_\sigma \int_{-\omega_D}^{\omega_D} \mathrm{d}E \int_{-\omega_D}^{\omega_D} \mathrm{d}\xi \frac{u_\xi^2 - v_\xi^2}{E - \sqrt{\xi^2 + \Delta^2}} c^\dagger_{k(E),\sigma} c_{k(E),\sigma} |F_\uparrow\rangle \otimes |F_\downarrow\rangle \otimes |\Psi_{\mathrm{BCS}}\rangle\ . \tag{E.31}$$

The BCS coherence factors respect the following formula in terms of ξ

$$u_\xi^2 - v_\xi^2 = \frac{1}{2} \frac{\xi}{\sqrt{\xi^2 + \Delta^2}}\,. \tag{E.32}$$

The final state therefore reads as

$$|\mathcal{F}_Q\rangle = i\frac{L^3\lambda^2}{16\pi^3 v_F^3} \sum_\sigma \int_{-\omega_D}^{\omega_D} \mathrm{d}E \int_{-\omega_D}^{\omega_D} \mathrm{d}\xi \frac{\xi}{\sqrt{\xi^2 + \Delta^2}\left(E - \sqrt{\xi^2 + \Delta^2}\right)} c^\dagger_{k(E),\sigma} c_{k(E),\sigma} |F_\uparrow\rangle \otimes |F_\downarrow\rangle \otimes |\Psi_{\mathrm{BCS}}\rangle\ . \tag{E.33}$$

This is an odd function summed over a symmetric interval and therefore vanishes at zero temperature.

F. Computations for the QPC in the FQHE

In this Appendix, various computations used in the different chapters involving the fractional quantum Hall effect are presented.

F.1. Green's function

The Green's function of the quasiparticles is defined as

$$\left\langle \psi(x,\tau)\psi^{\dagger}(0,0)\right\rangle = \frac{1}{2\pi a}\left\langle e^{i\sqrt{\nu}\phi(x,\tau)}e^{-i\sqrt{\nu}\phi(0,0)}\right\rangle . \tag{F.1}$$

A very useful relation can be used, namely, for bosons operators[1],

$$\left\langle e^{i\sqrt{\nu}\phi(x,\tau)}e^{-i\sqrt{\nu}\phi(0,0)}\right\rangle = e^{\nu\left\langle \phi(x,\tau)\phi(0,0)-\phi(0,0)^2\right\rangle} . \tag{F.2}$$

One therefore introduces the bosonic Green's function, as

$$\mathcal{G}(x,t) = \left\langle \phi\left(t,x\right)\phi\left(0,0\right)-\phi\left(0,0\right)^2\right\rangle , \tag{F.3}$$

Hence

$$\left\langle e^{i\sqrt{\nu}\phi(x,\tau)}e^{-i\sqrt{\nu}\phi(0,0)}\right\rangle = e^{\nu\mathcal{G}(\tau)} , \tag{F.4}$$

and the bosonic Green's function can be computed from Eq. (9.27). The bosonic fields are written in k space in the continuous limit ($L\to\infty$)

$$\mathcal{G}(x,t) = \int_0^{\infty}\mathrm{d}k\int_0^{\infty}\mathrm{d}k'\frac{e^{-(k+k')a/2}}{\sqrt{kk'}}\left[\left(e^{ikx}-1\right)\left\langle b_k b_{k'}^{\dagger}\right\rangle + \left(e^{-ikx}-1\right)\left\langle b_k^{\dagger}b_{k'}\right\rangle\right] , \tag{F.5}$$

where the boson average value is evaluated on the equilibrium density matrix, enforcing the linear spectrum, it can be written directly in terms of k as

$$\left\langle b_k b_{k'}^{\dagger}\right\rangle = \delta_{k,k'}\left(1+\frac{1}{e^{v_F k/\theta}-1}\right) . \tag{F.6}$$

As a result the integral to compute is the following

$$\mathcal{G}(x,t) = \int_0^{\infty}\mathrm{d}k\left\{\frac{e^{-ka}-e^{-k[a-i(x-v_F t)]}}{k} - \frac{e^{-ka}}{k}\left[\frac{\left(e^{-ik[x-v_F t]}-1\right)\left(e^{ik[x-v_F t]}-1\right)}{e^{kv_F/\theta}-1}\right]\right\} . \tag{F.7}$$

[1] It can be derived with Gaussian integration techniques after performing a variation of the partition function with auxiliary fields in the path integral approach developed by Feynman [181].

The first term is tabulated [see Eq. (3.434.2) of Ref. [182]] and yields

$$\int_0^\infty \mathrm{d}k \frac{e^{-ka} - e^{-k[a-i(x-v_F t)]}}{k} = \log\left(1 - i\frac{x - v_F t}{a}\right) . \tag{F.8}$$

The second term can be written as

$$\begin{aligned}\int_0^\infty \mathrm{d}k \frac{e^{-ka}}{k} &\left[\frac{\left(e^{-ik[x-v_F t]} - 1\right)\left(e^{ik[x-v_F t]} - 1\right)}{e^{kv_F/\theta} - 1}\right] \\ &= \int_0^\infty \mathrm{d}u \frac{e^{-u(1+a\theta/v_F)}}{u}\left[\frac{\left(e^{-iu[x-v_F t]\theta/v_F} - 1\right)\left(e^{iu[x-v_F t]\theta/v_F} - 1\right)}{1 - e^{-u}}\right] ,\end{aligned} \tag{F.9}$$

which is also tabulated [see Eq. (3.413.1) of Ref. [182]] and yields

$$\begin{aligned}\int_0^\infty \mathrm{d}u \frac{e^{-u(1+a\theta/v_F)}}{u} &\left[\frac{\left(e^{-iu[x-v_F t]\theta/v_F} - 1\right)\left(e^{ik[x-v_F t]\theta/v_F} - 1\right)}{1 - e^{-u}}\right] \\ &= \log\left\{\frac{\Gamma^2(1 + \tau_0\theta)}{\Gamma\left(1 + \tau_0\theta + i\frac{[x-v_F t]\theta}{v_F}\right)\Gamma\left(1 + \tau_0\theta - i\frac{[x-v_F t]\theta}{v_F}\right)}\right\} ,\end{aligned} \tag{F.10}$$

where $\tau_0 = a/v_F$ is the short time cutoff. It is sometimes useful to actually consider that τ_0 is less than any other time scale, in this case [see Eq. (8.332.3) of Ref. [182]] and at the QPC ($x = 0$), one has

$$\begin{aligned}\int_0^\infty \mathrm{d}u \frac{e^{-u(1+a\theta/v_F)}}{u} &\left[\frac{\left(e^{-iu[x-v_F t]\theta/v_F} - 1\right)\left(e^{ik[x-v_F t]\theta/v_F} - 1\right)}{1 - e^{-u}}\right] \\ &= \log\left\{\frac{i\tau_0 \sinh\left[\pi\theta\left(i\tau_0 - t\right)\right]}{(i\tau_0 - t)\sinh(\pi\theta i\tau_0\theta)}\right\} ,\end{aligned} \tag{F.11}$$

Thus, adding the two terms of Eq. (F.7), the total bosonic Green's function can be written as

$$\mathcal{G}(\tau) = -\log\left[\frac{\sinh\left(\theta\pi(i\tau_0 - \tau)\right)}{\sinh\left(i\theta\pi\tau_0\right)}\right] . \tag{F.12}$$

Keldysh bosonic Green's functions. They are defined as

$$\mathcal{G}^{\eta\eta'}(t - t') = \left\langle \mathcal{T}_K \phi\left(t_\eta, x = 0\right)\phi\left(t'_{\eta'}, x = 0\right)\right\rangle , \tag{F.13}$$

where $\mathcal{T}_K$ as usual denotes ordering along the Keldysh contour. The four different Keldysh Green's functions can be written in terms of the bosonic one

$$\begin{aligned}\mathcal{G}^{++}(t) &= \mathcal{G}(|t|) \\ \mathcal{G}^{--}(t) &= \mathcal{G}(-|t|) \\ \mathcal{G}^{+-}(t) &= \mathcal{G}(-t) \\ \mathcal{G}^{-+}(t) &= \mathcal{G}(t) ,\end{aligned} \tag{F.14}$$

F.2. Current for Laughlin states

Evaluating the current to lowest order in λ yields

$$\begin{aligned}\langle I_B\rangle_t &= -\frac{i}{2}\sum_{\eta\eta_1}\eta_1\int_{-\infty}^{+\infty}\mathrm{d}t_1\,\langle T_K\left[I_B(t_\eta)H_B(t_{1,\eta_1})\right]\rangle \\ &= \frac{e^*}{2}\lambda^2\sum_{\eta\eta_1\epsilon\epsilon_1}\eta_1\epsilon\int_{-\infty}^{+\infty}\mathrm{d}t_1\,e^{i\epsilon\varphi(t)}e^{i\epsilon_1\varphi(t_1)}\left\langle T_K\left\{\left[\psi_R^\dagger(t_\eta)\psi_L(t_\eta)\right]^\epsilon\left[\psi_R^\dagger(t_{1,\eta_1})\psi_L(t_{1,\eta_1})\right]^{\epsilon_1}\right\}\right\rangle .\end{aligned} \tag{F.15}$$

One notices that terms $\epsilon=\epsilon'$ contain the combinations $\psi_s^\dagger(t_\eta)\psi_s^\dagger(t_{1,\eta_1})$, which will vanish. After removing these terms the current reads

$$\begin{aligned}\langle I_B\rangle_t = \frac{e^*}{2}\lambda^2\sum_{\eta\eta_1}\eta_1\int_{-\infty}^{+\infty}\mathrm{d}t_1\,\Big(&\exp\left\{i\left[\varphi(t)-\varphi(t_1)\right]\right\}\left\langle T_K\left\{\psi_R^\dagger(t_\eta)\psi_L(t_\eta)\psi_L^\dagger(t_{1,\eta_1})\psi_R(t_{1,\eta_1})\right\}\right\rangle \\ &-\exp\left\{-i\left[\varphi(t)-\varphi(t_1)\right]\right\}\left\langle T_K\left\{\psi_L(t_\eta)\psi_R^\dagger(t_\eta)\psi_R(t_{1,\eta_1})\psi_L^\dagger(t_{1,\eta_1})\right\}\right\rangle\Big) .\end{aligned} \tag{F.16}$$

Now one can use Wick's theorem and, using the usual definition of the quasiparticle operators in terms of bosonic fields, Eq. (9.32) one gets

$$\begin{aligned}\langle I_B\rangle_t = i\frac{e^*}{4\pi^2a^2}\lambda^2\sum_{\eta\eta_1}\eta_1\int_{-\infty}^{+\infty}\mathrm{d}t_1\,&\sin\left[\varphi(t)-\varphi(t_1)\right]\times \\ &\times\left\langle T_K\left[e^{i\sqrt{\nu}\phi_R(t_\eta)}e^{-i\sqrt{\nu}\phi_R(t_{1,\eta_1})}\right]\right\rangle\left\langle T_K\left[e^{-i\sqrt{\nu}\phi_L(t_\eta)}e^{i\sqrt{\nu}\phi_L(t_{1,\eta_1})}\right]\right\rangle .\end{aligned} \tag{F.17}$$

Using the formulas for the bosonic Green's functions, the current can be recast as

$$\langle I_B\rangle_t = i\frac{e^*}{4\pi^2a^2}\lambda^2\int_{-\infty}^{+\infty}\mathrm{d}t_1\,\sin\left[\varphi(t)-\varphi(t_1)\right]\sum_{\eta\eta_1}\eta_1e^{2\nu\mathcal{G}^{\eta\eta_1}(t-t_1)} . \tag{F.18}$$

From Eq. (F.14), one can show that

$$\sum_{\eta,\eta_1=\pm}\eta_1e^{2\nu\mathcal{G}^{\eta\eta_1}(t-t_1)} = 2\left[e^{2\nu\mathcal{G}(\tau)}-e^{2\nu\mathcal{G}(-\tau)}\right]\Theta(\tau) , \tag{F.19}$$

where $\tau=t-t_1$. Thus

$$\langle I_B\rangle_t = i\frac{e^*}{2\pi^2a^2}\lambda^2\int_0^{+\infty}\mathrm{d}\tau\,\sin\left[\varphi(t)-\varphi(t-\tau)\right]\left(e^{2\nu\mathcal{G}(\tau)}-e^{2\nu\mathcal{G}(-\tau)}\right) . \tag{F.20}$$

F.3. current for general Abelian edge states

In this appendix, the general model for Abelian fractional quantum Hall edge states introduced in Sec. 9.4.6 and it is shown that it leads to a tunneling current of the same form as the one obtained in Eq. (10.5). The QPC is set in the weak backscattering regime and is thus modeled by a Hamiltonian describing the

tunneling of quasiparticles between the two edges as

$$H_T = \sum_{\mathbf{g}} \Gamma_{\mathbf{g}} {\psi_{\mathbf{g}}^{(u)}}^\dagger(0)\psi_{\mathbf{g}}^{(d)}(0) + \text{H.c.} \tag{F.21}$$

where $(u)/(d)$ label the upper and lower edges (the standard R/L designation being ill-defined in the presence of non-chiral modes). In all generality, one would need to account for all possible tunneling events, i.e., the ones involving all possible quasiparticles. In practice, however, it makes sense to favor the one with the lowest scaling dimension, as it is the most relevant perturbations in the renormalization group sense. In what follows, this leading quasiparticle is labeled with the vector $\mathbf{g}^*$.

From the expression of the tunneling Hamiltonian, one readily obtains the tunneling current operator at the location of the QPC, as

$$I_T(t) = iQ_{\mathbf{g}^*}\left[\Gamma_{\mathbf{g}^*}(t)e^{iQ_{\mathbf{g}^*}V_{\text{DC}}t}{\psi_{\mathbf{g}^*}^{(u)}}^\dagger(0,t)\psi_{\mathbf{g}^*}^{(d)}(0,t) - \text{H.c.}\right], \tag{F.22}$$

where the QPC is driven by a DC voltage and has a time-dependent tunnel coupling.

Using the decomposition of the quasiparticle operators in terms of the bosonic fields ϕ_l, one can express the thermal average of the tunneling current in terms of the bosonic Green's function $\mathcal{G}_l^{\eta\eta'}(t-t')$ yielding

$$\begin{aligned}\langle I_T(t)\rangle = \frac{1}{2}Q_{\mathbf{g}^*}\sum_{\eta\eta'}\eta'\int \mathrm{d}t'\left[\Gamma_{\mathbf{g}^*}(t)\overline{\Gamma_{\mathbf{g}^*}(t')}e^{iQ_{\mathbf{g}^*}V_{\text{DC}}(t-t')} - \overline{\Gamma_{\mathbf{g}^*}(t)}\Gamma_{\mathbf{g}^*}(t')e^{iQ_{\mathbf{g}^*}V_{\text{DC}}(t-t')}\right] \\ \times\prod_l e^{2g_l^{*2}\mathcal{G}_l^{\eta\eta'}(t-t')}.\end{aligned} \tag{F.23}$$

At this stage, it is important to keep in mind that $\mathcal{G}_l^{\eta\eta'}(t-t')$ is a trivial generalization of the one presented in Sec. F.1. In particular, its Keldysh components follow the same relations as the ones introduced in Eq. (F.14), with the corresponding Green's function $\mathcal{G}_l(\tau)$ given by

$$\mathcal{G}_l(\tau) = -\log\left[\frac{\sinh\left(\frac{\pi}{\beta}(i\tau_l-\tau)\right)}{\sinh\left(i\frac{\pi}{\beta}\tau_l\right)}\right], \tag{F.24}$$

with $\tau_l = a/v_l$. It follows from this that the term involving the bosonic Green's function in Eq. (F.23) can be further rewritten as

$$\begin{aligned}\prod_l e^{2g_l^{*2}\mathcal{G}_l(\tau)} &= \prod_l e^{2g_l^{*2}\log\left[\frac{\sinh\left(i\frac{\pi}{\beta}\tau_l\right)}{\sinh\left(\frac{\pi}{\beta}(i\tau_l-\tau)\right)}\right]} = \prod_l e^{2g_l^{*2}\log\left[\frac{\sinh\left(i\frac{\pi}{\beta}\tau_0\right)}{\sinh\left(\frac{\pi}{\beta}(i\tau_0-\tau)\right)}\right]+2g_l^{*2}\log\left(\frac{\tau_l}{\tau_0}\right)} \\ &= e^{2\sum_l g_l^{*2}\mathcal{G}(\tau)}\prod_l\left(\frac{\tau_l}{\tau_0}\right)^{2g_l^{*2}}\end{aligned} \tag{F.25}$$

where the short time cutoff τ_l in the denominator only serves as a regularization and can be replaced by any infinitesimal. This allows to drop the l dependence in the bosonic Green's function and to perform the product over l, letting the scaling dimension appear naturally.

The tunneling current can now be rewritten as

$$\langle I_T(t)\rangle = \frac{1}{2} Q_{\mathbf{g}^*} \sum_{\epsilon} \epsilon \int \mathrm{d}t' e^{i\epsilon Q_{\mathbf{g}^*} V_{\mathrm{DC}}(t-t')} \left[\Gamma_{\mathbf{g}^*}(t)\right]^{\epsilon} \left[\Gamma_{\mathbf{g}^*}(t')\right]^{-\epsilon} \sum_{\eta\eta'} \eta' e^{2\delta_{\mathbf{g}^*}\mathcal{G}^{\eta\eta'}(t-t')}, \tag{F.26}$$

where, for convenience and without loss of generality, the prefactor in τ_l/τ_0 was absorbed into the definition of the tunneling amplitude. This expression perfectly mirrors the one obtained for the Laughlin case in Eq. (10.5), where the effective charge e^* and scaling dimension ν_D of the Laughlin quasiparticle are replaced with the corresponding effective charge $Q_{\mathbf{g}^*}$ and scaling dimension $\delta_{\mathbf{g}^*}$ of the leading tunneling quasiparticle.

F.4. Computation steps for the current

In this section a general formula for the current Eq. (10.5) is derived without any assumptions on the value of ν_D other than it being positive. In particular, Eq. (10.7) is obtained.

One starts by performing the sum over η in Eq. (10.5), using

$$\sum_{\eta,\eta'=\pm} \eta' e^{2\nu_D \mathcal{G}^{\eta\eta'}(t-t')} = 2\left[e^{2\nu_D\mathcal{G}(\tau)} - e^{2\nu_D\mathcal{G}(-\tau)}\right]\Theta(\tau)\,, \tag{F.27}$$

where $\tau = t - t'$. Then the sum over ϵ can be performed as

$$\sum_{\epsilon=\pm} \epsilon e^{i\epsilon\omega_0^*(t-t')} \left[\lambda^*(t)\right]^{\epsilon} \left[\lambda^*(t')\right]^{-\epsilon} = \lambda_0^2 \sum_{lm} \overline{p_l} p_m e^{i(l-m)\Omega t} \left(e^{i(m+q)\Omega\tau} - e^{-i(l+q)\Omega\tau}\right), \tag{F.28}$$

where $q = \frac{\omega_0^*}{\Omega}$. Inserting Eq. (F.27) and (F.28) in Eq. (10.5) gives

$$\begin{aligned}\langle I_{\mathrm{T}}(t)\rangle = e^* \left(\frac{1}{2\pi a}\right)^2 \lambda_0^2 \sum_{l,m} \overline{p_l} p_m e^{i(l-m)\Omega t} \int_0^{+\infty} \mathrm{d}\tau \left(e^{i(m+q)\Omega\tau} - e^{-i(l+q)\Omega\tau}\right) \\ \times \left[e^{2\nu_D\mathcal{G}(\tau)} - e^{2\nu_D\mathcal{G}(-\tau)}\right].\end{aligned} \tag{F.29}$$

The next step is to simplify the expression of the Green's function $\mathcal{G}(\tau)$, see Eq. (F.12), denoting $\eta = \pm$,

$$e^{2\nu_D\mathcal{G}(\eta\tau)} = (-i\eta)^{2\nu_D} \tanh\left(\frac{\pi}{\beta}\tau_0\right)^{2\nu_D} \frac{\cosh\left(\frac{\pi}{\beta}\tau\right)^{-2\nu_D}}{\left[\tanh\left(\frac{\pi}{\beta}\tau\right) - i\eta\tan\left(\frac{\pi}{\beta}\tau_0\right)\right]^{2\nu_D}}. \tag{F.30}$$

Thus, the current reads as

$$\begin{aligned}\langle I_{\mathrm{T}}(t)\rangle = e^* \left(2v\tau_0\right)^{-2} \pi^{-3} \beta \lambda_0^2 \sum_{l,m} \overline{p_l} p_m e^{i(l-m)\Omega t} \sum_{\eta=\pm} \eta(-i\eta)^{2\nu_D} \tanh\left(\frac{\pi}{\beta}\tau_0\right)^{2\nu_D} \\ \times \int_0^{+\infty} \mathrm{d}x \left[\exp\left(i\frac{m+q}{\pi\theta}x\right) - \exp\left(-i\frac{l+q}{\pi\theta}x\right)\right] \frac{\cosh\left(x\right)^{-2\nu_D}}{\left[\tanh\left(x\right) - i\eta\tan\left(\frac{\pi}{\beta}\tau_0\right)\right]^{2\nu_D}},\end{aligned} \tag{F.31}$$

where $\theta = (\beta\Omega)^{-1}$ is the reduced temperature. Changing variables to $y = \tanh(x)$, one is left with

$$\begin{aligned}\langle I_{\mathrm{T}}(t)\rangle = e^*\left(2v\tau_0\right)^{-2}\pi^{-3}\beta\lambda_0^2\sum_{l,m}\overline{p_l}p_m e^{i(l-m)\Omega t}\sum_{\eta=\pm}\eta \\ \times\int_0^1 \mathrm{d}y\left[(1-y)^{\nu_D-1-i\frac{m+q}{2\pi\theta}}(1+y)^{\nu_D-1+i\frac{m+q}{2\pi\theta}}\left(1+i\eta\tan\left(\frac{\pi}{\beta}\tau_0\right)^{-1}y\right)^{-2\nu_D}\right. \\ \left.-(m,q)\to(-l,-q)\right].\end{aligned} \tag{F.32}$$

Where the notation $f(a,b)-f(c,d) = f(a,b)-(a,b)\to(c,d)$ has been used. This integral can be expressed in terms of the first Appell hypergeometric series F_1, see Eq. (3.312) of Ref. [182], as long as ν_D is positive. The current therefore reads as

$$\begin{aligned}\langle I_{\mathrm{T}}(t)\rangle = e^*\left(2v\tau_0\right)^{-2}\pi^{-3}\beta\lambda_0^2\sum_{l,m}\overline{p_l}p_m e^{i(l-m)\Omega t}\sum_{\eta=\pm}\eta\left[\mathrm{B}\left(\nu_D-i\frac{m+q}{2\pi\theta},1\right)\right. \\ \times F_1\left(1,1-\nu_D-i\frac{m+q}{2\pi\theta},2\nu_D,1+\nu_D-i\frac{m+q}{2\pi\theta};-1;-i\eta\tan\left(\frac{\pi}{\beta}\tau_0\right)^{-1}\right) \\ \left.-(m,q)\to(-l,-q)\right],\end{aligned} \tag{F.33}$$

where $\mathrm{B}(x,y)$ is Euler's Beta function. Using the properties of Appell's hypergeometric series F_1, see Eq. (9.182.1) of Ref. [182], and the properties of Euler's Beta function, see Eq. (8.384.1) of [182], one finds that

$$\begin{aligned}\langle I_{\mathrm{T}}(t)\rangle = e^*\left(2v\tau_0\right)^{-2}\pi^{-3}\beta\lambda_0^2\sum_{l,m}\overline{p_l}p_m e^{i(l-m)\Omega t}\sum_{\eta=\pm}\eta\left[\frac{-i\eta\sin\left(\frac{\pi}{\beta}\tau_0\right)\exp\left(i\eta\frac{\pi}{\beta}\tau_0\right)}{\nu_D-i\frac{m+q}{2\pi\theta}}\right. \\ \times {}_2F_1\left(1,1-\nu_D-i\frac{m+q}{2\pi\theta};1+\nu_D-i\frac{m+q}{2\pi\theta};\exp\left(2i\eta\frac{\pi}{\beta}\tau_0\right)\right) \\ \left.-(m,q)\to(-l,-q)\right],\end{aligned} \tag{F.34}$$

where ${}_2F_1$ is Gauss' hypergeometric function. It is remarkable that this formula is valid to all orders in τ_0 and for any $\nu_D > 0$.

F.5. Weak backscattering regime

In this appendix, a formula for the current as a function of time s found in the regime where $0 < \nu_D < 1$, with $\nu_D \neq 1/2$. The weak backscattering regime for Laughlin fractions is a particular case of this regime of parameters. Therefore, performing an expansion in τ_0/β Eq. (10.11) is derived.

In this regime, as neither $-\nu_D$, nor $2\nu_D - 1$ are integer, and as $\left|1-\exp\left(2i\eta\frac{\pi}{\beta}\tau_0\right)\right| < \pi$, Eq. (2.10.1) of

Ref. [183] holds. Thus, to lowest order in τ_0/β

$$\langle I_{\mathrm{T}}(t)\rangle = \frac{\Gamma(2\nu_D)\mathcal{I}}{2}\sum_{l,m}\overline{p_l}p_m e^{i(l-m)\Omega t}\sum_{\eta=\pm}(i\eta)^{2\nu_D} \times\left[\frac{\Gamma(1-2\nu_D)\Gamma\left(1+\nu_D-i\frac{l+q}{2\pi\theta}\right)}{\left(\nu_D-i\frac{m+q}{2\pi\theta}\right)\Gamma\left(1-\nu_D-i\frac{m+q}{2\pi\theta}\right)}-(m,q)\to(-l,-q)\right], \tag{F.35}$$

where $\Gamma(z)$ is the Gamma function, $\Lambda=(\Omega\tau_0)^{-1}$ and

$$\mathcal{I}=\frac{e^*\Omega}{\pi}\left(\frac{\lambda_0}{v}\right)^2\left(\frac{2\pi\theta}{\Lambda}\right)^{2\nu_D-2}\frac{\theta}{\Gamma(2\nu_D)}\,. \tag{F.36}$$

Note that for $1/2<\nu_D<1$, the expansion of the hypergeometric function gives a leading contribution of order $O(\tau_0)$ which dominates over the one considered above, which is of order $O(\tau_0^{2\nu_D})$. However, this leading contribution simplifies when accounting for the second hypergeometric function obtained upon exchanging $(m,q)\to(-l,-q)$.

Using the fact that $i\eta=\exp\left(i\eta\frac{\pi}{2}\right)$, Euler's reflection formula for the Gamma function [see [182], Eq. (8.384.1)] and the fact that $\Gamma(z^*)=\Gamma(z)^*$ [which can be deduced from [182], Eq. (8.334.3)], the current is reduced to

$$\langle I_{\mathrm{T}}(t)\rangle = -i\frac{\mathcal{I}}{2\cos(\pi\nu_D)}\sum_{l,m}\overline{p_l}p_m e^{i(l-m)\Omega t} \times\left[\left|\Gamma\left(\nu_D-i\frac{m+q}{2\pi\theta}\right)\right|^2\sin\left(\pi\nu_D+i\frac{m+q}{2\theta}\right)-(m,q)\to(-l,-q)\right]. \tag{F.37}$$

Finally, after a change of indices, one is left with

$$\langle I_{\mathrm{T}}(t)\rangle = \mathcal{I}\sum_{l,m}\left|\Gamma\left(\nu_D+i\frac{m+q}{2\pi\theta}\right)\right|^2 \times\mathrm{Im}\left\{\overline{p_m}p_{m-l}e^{il\Omega t}\left[\tan(\pi\nu_D)\cosh\left(\frac{m+q}{2\theta}\right)+i\sinh\left(\frac{m+q}{2\theta}\right)\right]\right\}, \tag{F.38}$$

where $\mathrm{Im}(x)$ denotes the imaginary part of x. Assuming that $p_l\in\mathbb{R}$, this reduces to

$$\begin{aligned}\langle I_{\mathrm{T}}(t)\rangle = \mathcal{I}\sum_{l>0}\Bigg[&\cos(l\Omega t)\sum_m\left|\Gamma\left(\nu_D+i\frac{m+q}{2\theta\pi}\right)\right|^2(p_{m-l}p_m+p_m p_{l+m})\sinh\left(\frac{m+q}{2\theta}\right)\\ &+\sin(l\Omega t)\tan(\pi\nu_D)\sum_m\left|\Gamma\left(\nu_D+i\frac{m+q}{2\theta\pi}\right)\right|^2(p_m p_{l+m}-p_{m-l}p_m)\cosh\left(\frac{m+q}{2\theta}\right)\Bigg]\\ &+\mathcal{I}\sum_m\left|\Gamma\left(\nu_D+i\frac{m+q}{2\theta\pi}\right)\right|^2 p_m^2\sinh\left(\frac{m+q}{2\theta}\right).\end{aligned} \tag{F.39}$$

The current can finally be rewritten as

$$\langle I_{\mathrm{T}}(t)\rangle = I_0+\sum_{n>0}\mathcal{I}C_n\cos(n\Omega t+\varphi_n)\,, \tag{F.40}$$

where

$$\begin{aligned}
\varphi_n &= \arctan\left(\frac{B_n}{A_n}\right) \\
A_l &= \sum_m \left|\Gamma\left(\nu_D + i\frac{m+q}{2\theta\pi}\right)\right|^2 (p_{m-l}p_m + p_{l+m}p_m)\sinh\left(\frac{m+q}{2\theta}\right) \\
B_l &= \tan(\pi\nu_D)\sum_m \left|\Gamma\left(\nu_D + i\frac{m+q}{2\theta\pi}\right)\right|^2 (p_{m-l}p_m - p_{l+m}p_m)\cosh\left(\frac{m+q}{2\theta}\right) \\
C_n &= \frac{A_n}{\cos(\varphi_n)} \\
I_0 &= \mathcal{I}\sum_m \left|\Gamma\left(\nu_D + i\frac{m+q}{2\theta\pi}\right)\right|^2 p_m^2 \sinh\left(\frac{m+q}{2\theta}\right).
\end{aligned} \tag{F.41}$$

F.6. Strong backscattering regime

In this appendix, a formula for the current in the strong backscattering regime is derived. Applying the duality transformation to Eq. (F.34) taken for the Laughlin series, one has for the current in this regime

$$\begin{aligned}
\langle I_{\mathrm{T}}(t)\rangle = e\,(2v\tau_0)^{-2}\,\pi^{-3}\beta\lambda_0^2 \sum_{l,m}\overline{p_l}p_m e^{i(l-m)\Omega t}\sum_{\eta=\pm}\eta\Bigg[&\frac{-i\eta\sin\left(\frac{\pi}{\beta}\tau_0\right)\exp\left(i\eta\frac{\pi}{\beta}\tau_0\right)}{\nu^{-1} - i\frac{m+q}{2\pi\theta}} \\
&\times {}_2F_1\left(1, 1-\nu^{-1} - i\frac{m+q}{2\pi\theta}; 1+\nu^{-1} - i\frac{m+q}{2\pi\theta}; \exp\left(2i\eta\frac{\pi}{\beta}\tau_0\right)\right) \\
&- (m,q)\to(-l,-q)\Bigg],
\end{aligned} \tag{F.42}$$

where $q = \omega_0/\Omega$.

The next step is to perform an expansion in low τ_0/β for the Laughlin series (where ν^{-1} is an odd integer). The technique used in the case $0 < \nu_D < 1$ (see App. F.5) cannot be used here as $1 - 2\nu^{-1}$ is an integer, thus, Eq. (2.10.1) of Ref. [183] does not hold. However, another route is possible which allows to show that the leading contribution is of first order or less in τ_0.

Following Prudnikov *et. al.* [see Eq. (7.3.1.31) of Ref. [184]] a logarithmic expansion of the hypergeometric function is performed and all the terms of order higher than three are removed. The current can then be written as the sum of two terms:

$$\langle I_{\mathrm{T}}(t)\rangle = \langle I_{\mathrm{Fermi/DC}}(t)\rangle + \langle I_{\text{cor-AC}}(t)\rangle\,, \tag{F.43}$$

where the term containing the DC behavior as well as the Fermi limit is

$$\begin{aligned}\langle I_{\text{Fermi/DC}}(t)\rangle \approx ie\left(2v\tau_0\right)^{-2}\pi^{-3}\beta\lambda_0^2\sum_{l,m}\overline{p_l}p_m e^{i(l-m)\Omega t}\sum_{\eta=\pm}\sin\left(\frac{\pi}{\beta}\tau_0\right)\frac{\Gamma\left(\nu^{-1}-i\frac{m+q}{2\pi\theta}\right)}{\Gamma\left(1-\nu^{-1}-i\frac{m+q}{2\pi\theta}\right)}\\ \times\sum_{k,r=0}^{\infty}\sum_{s=0}^{2\nu^{-1}-1+k}\left\{\frac{(k+2\nu^{-1}-1)_k(2\nu^{-1})_k\left(\nu^{-1}-i\frac{m+q}{2\pi\theta}\right)_k\left(\frac{\pi}{\beta}\tau_0\right)^{2k-s+4\nu^{-1}-2}}{r!s!(k+2\nu^{-1}-1-s)!}\right.\\ \times(-1)^k 2^{k+2\nu^{-1}-1}(i\eta)^{2k-s-2}\left[\log\left(2\frac{\pi}{\beta}\tau_0\right)+i\eta\frac{\pi}{2}-\psi(k+1)+\psi\left(\nu^{-1}+k-i\frac{m+q}{2\pi\theta}\right)\right]\\ \left.-(m,q)\to(-l,-q)\right\},\end{aligned} \tag{F.44}$$

while the term corresponding to the AC current when correlations are present reads as

$$\begin{aligned}\langle I_{\text{cor-AC}}(t)\rangle \approx -ie\left(2v\tau_0\right)^{-2}\pi^{-3}\beta\lambda_0^2\sum_{l,m}\overline{p_l}p_m e^{i(l-m)\Omega t}\sum_{\eta=\pm}\sin\left(\frac{\pi}{\beta}\tau_0\right)\frac{1}{2\nu^{-1}-1}\\ \times\sum_{r=0}^{\infty}\sum_{k=0}^{2\nu^{-1}-2}\sum_{s=0}^{k}\left[(-1)^k(i\eta)^{r+2k-s}2^k\frac{(1)_k(1-\nu^{-1}-i\frac{m+q}{2\pi\theta})_k\left(\frac{\pi}{\beta}\tau_0\right)^{r+2k-s}}{r!s!(k-s)!(2-2\nu^{-1})_k}\right.\\ \left.-(m,q)\to(-l,-q)\right],\end{aligned} \tag{F.45}$$

with $(x)_n=\prod_{k=0}^{n-1}(x+k)$ is the Pochhammer symbol.

One sees indeed that for $\nu=1$ Eq. (F.45) vanishes and for $\nu^{-1}>1$ all terms in Eq. (F.44) are sub-leading. Therefore, the computation will be better understood if presented in two different sections.

F.6.1. Fermi liquid limit, $\nu=1$

The Fermi liquid limit is obtained by setting $\nu^{-1}=\nu=1$. The first sum over k in Eq. (F.45) vanishes and only the terms of Eq. (F.44) contribute. Performing the sum over η removes all terms containing odd powers of η, i.e., to lowest order in τ_0/β ($s=1$, $k=r=0$) the current reads as

$$\langle I_{\text{T}}(t)\rangle=\frac{e\lambda_0^2\Omega}{4\pi v_{\text{F}}^2}\sum_{l,m}\overline{p_l}p_m e^{i(l-m)\Omega t}(2q+l+m)\,. \tag{F.46}$$

F.6.2. Filling factors, $\nu^{-1}>1$

The general case of integer ν^{-1} greater than one is obtained by remarking that the leading term in Eq. (F.44) is a polynomial of order five or more in τ_0/β. Therefore, the main contribution to the current can be extracted from Eq. (F.45) only. It can be shown that the term of order minus one in τ_0/β does not depend on q nor l or m, thus it does not contribute in the current. The sum over η removes the zeroth order term in τ_0/β so one is left with the first order contributions. They arise when the indices respect $r+2k-s=2$, i.e., there are four possibilities:

- $r=0$, $k=s=2$;

- $r = 0$, $k = 1$, $s = 0$;
- $r = k = s = 1$;
- $r = 2$, $k = s = 0$.

The last possibility gives rise to a term independent of q, l, m which thus vanishes. Selecting the three first possibilities only and removing the Fermi/DC term in Eq. (F.43), the current ultimately reads as

$$\langle I_{\mathrm{T}}(t)\rangle \approx \frac{-e}{\pi^2(1-2\nu^{-1})_3}\left(\frac{\lambda_0}{v}\right)^2\frac{\Omega}{\Lambda}\,\mathrm{Im}\left[\sum_{l,m}\overline{p_l}p_m e^{i(l-m)\Omega t}\,(m+q)^2\right]. \tag{F.47}$$

F.7. Fermi liquid approach

This section describes a computation of the Fermi liquid behavior using standard Fermi liquid theory In this picture, the Hamiltonian is written in analogy with Eq. (10.1), in terms of electron creation and annihilation operators $\Psi_{\mathrm{L,R}}$ at position $x = 0$ in the left or right leads. It reads

$$\mathcal{H}_{\mathrm{T}} = \lambda(t)\Psi_{\mathrm{L}}^\dagger\Psi_{\mathrm{R}} + \mathrm{H.c.} \tag{F.48}$$

Thus the current operator is

$$I_{\mathrm{T}} = ie\lambda(t)\Psi_{\mathrm{L}}^\dagger\Psi_{\mathrm{R}} + \mathrm{H.c.} \tag{F.49}$$

Keldysh Green's functions for electron operators are defined as

$$G_{\mathrm{ss'}}^{\eta\eta'} = -i\left\langle \mathcal{T}_K \Psi_{\mathrm{s}}(t_\eta)\Psi_{\mathrm{s'}}^\dagger(t'_{\eta'})\right\rangle, \tag{F.50}$$

where $\mathcal{T}_{\mathrm{K}}$ is the time ordering operator along the Keldysh contour, s and s' can be either L or R and the Keldysh contour indices η and η' can be $+$ or $-$. The current can be written with Keldysh Green's function for electron operators:

$$\langle I_{\mathrm{T}}(t)\rangle = -e\left[\lambda(t)G_{\mathrm{RL}}^{+-}(t,t) - \lambda^*(t)G_{\mathrm{LR}}^{+-}(t,t)\right]. \tag{F.51}$$

Working in the wide band limit allows to simplify the Green's functions, the current can therefore be simplified into

$$\langle I_{\mathrm{T}}(t)\rangle = \frac{\lambda_0^2 e}{4\pi v_{\mathrm{F}}^2}\sum_{l,m}\overline{p_l}p_m e^{i(l-m)\Omega t}\int \mathrm{d}\omega\left[f(\omega-\mu_{\mathrm{R}}) - f(\omega+l\Omega-\mu_{\mathrm{L}}) - f(\omega-\mu_{\mathrm{L}}) + f(\omega+m\Omega-\mu_{\mathrm{R}})\right]. \tag{F.52}$$

where $f(x)$ is the usual Fermi distribution and $\mu_{R/L}$ is the chemical potential of edge R/L. Performing the integration yields

$$\langle I_{\mathrm{T}}(t)\rangle = \frac{e\Omega\lambda_0^2}{4\pi v_F^2}\sum_{l,m}\overline{p_l}p_m e^{i(l-m)\Omega t}(2q+l+m). \tag{F.53}$$

Using Eq. (10.4) to write the derivative $\partial_t\lambda(t) = i\Omega\sum_l l\overline{p_l}e^{il\Omega t}$, the current can be rewritten as

$$\langle I_{\mathrm{T}}(t)\rangle = \frac{e\Omega}{4\pi v_{\mathrm{F}}^2}\left[2q\,|\lambda(t)|^2 + \frac{1}{i\Omega}\partial_t\,|\lambda(t)|^2\right]. \tag{F.54}$$

Finally, substituting the expression for the time-dependent tunnel coupling $\lambda(t)$ for the two types of drive,

one has

$$\langle I_{\mathrm{T}}(t)\rangle = \frac{e^2}{2\pi v_{\mathrm{F}}^2}\begin{cases}\lambda(t)^2 V_{\mathrm{DC}} & \text{for a gate drive}\\ \lambda_0^2 V(t) & \text{for a voltage drive.}\end{cases} \tag{F.55}$$

G. Computations for interacting pulses

In this Appendix, various results related to Chapter 11 are presented and derived.

G.1. Leviton and anti-Leviton case

As a first computation, the charge backscattered at the QPC is obtained when terminal 1 is driven by the voltage

$$V(t) = \sum_{s=\pm} s \sum_{k=-\infty}^{+\infty} \frac{V_0}{\pi} \frac{\gamma^2}{\gamma^2 + (t - k\mathcal{T} + s\Delta t/2)^2}, \tag{G.1}$$

which corresponds to the injection of a Leviton and an anti-Leviton in the same period separated by a time delay Δt. In this case, $V(t) = V(-t)$ and the phase $\varphi(t)$ becomes

$$\begin{aligned} \varphi(t) &= e^* \int_{-\infty}^{t} \mathrm{d}t' \sum_{s=\pm} s \sum_{k=-\infty}^{+\infty} \frac{V_0}{\pi} \frac{\gamma^2}{\gamma^2 + (t' - k\mathcal{T} + s\Delta t/2)^2} \\ &= e^* \int_{t-\Delta/2}^{t+\Delta/2} \mathrm{d}t' \sum_{k=-\infty}^{+\infty} \frac{V_0}{\pi} \frac{\gamma^2}{\gamma^2 + (t' - k\mathcal{T})^2}, \end{aligned} \tag{G.2}$$

and, as a result, $\varphi(t) = \varphi(-t)$. By using the latter property, it can be shown that the integral over t in Eq. (11.10) vanishes. Indeed,

$$\int_{-\infty}^{\infty} \mathrm{d}t \, \sin\left[\varphi(t) - \varphi(t-\tau)\right] = \int_{-\infty}^{\infty} \mathrm{d}t \, \sin\left[\varphi(-t+\tau/2) - \varphi(-t-\tau/2)\right]. \tag{G.3}$$

By using $\varphi(t) = -\varphi(-t)$, one sees the integral vanishes.

G.2. Floquet weights for double pulses

A computation of Floquet coefficients for two pulses of charge $q = \pm 1$ and separated by a time shift δt is proposed. The first section focuses on a signal made of two Levitons while the second one relates to a Leviton added to an anti-Leviton. In both cases, the coefficients are defined by the following relation

$$e^{-i\phi(t)} = \sum_l p_l e^{-il\Omega t}, \tag{G.4}$$

where $\phi(t) = \phi_1(t) + \phi_2(t + \delta t)$. From Ref. [174] the coefficients for a single pulse read as

$$p_l = \begin{cases} e^{-2\pi l\eta}\left(1 - e^{-4\pi\eta}\right) & l \geq 0 \\ -e^{-2\pi\eta} & l = -1 \\ 0 & l < -1\,. \end{cases} \tag{G.5}$$

G.2.1. Two-Levitons drive

In this case, $\phi_2(t) = \phi_1(t)$, thus

$$e^{-i\phi(t)} = \sum_l p_l e^{-il\Omega t} \sum_m p_m e^{-im\Omega(t+\delta t)} \,. \tag{G.6}$$

writing $l + m = \tilde{l}$, one obtains

$$e^{-i\phi(t)} = \sum_{lm} p_{l-m} p_m e^{-il\Omega t} e^{-im\Omega\delta t} \,. \tag{G.7}$$

Which is equivalent to defining the corresponding coefficients $\tilde{p}_l = \sum_m p_{l-m} p_m e^{-im\Omega\delta t}$. A formula can be obtained for the $\tilde{p}_l$. Defining $\alpha = \Omega\delta t$, the $l = -2$ coefficient can be written as

$$\tilde{p}_{-2} = \sum_m p_{-2-m} p_m e^{-im\alpha} \,. \tag{G.8}$$

as $p_k = 0$ for any $k < -1$, the only non-vanishing term is that corresponding to $m = -1$, it reads as

$$\begin{aligned} \tilde{p}_{-2} &= p_{-1}^2 e^{i\alpha} \\ &= e^{-4\pi\eta} e^{i\alpha} \,. \end{aligned} \tag{G.9}$$

The second particular term to compute is the $l = -1$ term, for the same reasons as before, the only non-vanishing terms are the $m = 0$ and $m = -1$, thus

$$\begin{aligned} \tilde{p}_{-1} &= p_{-1} p_0 \left(e^{-im\alpha} + 1\right) \\ &= -e^{-2\pi\eta} \left(1 - e^{-4\pi\eta}\right) \left(e^{i\alpha} + 1\right) \,. \end{aligned} \tag{G.10}$$

For other values of l, one can show than the sum is limited to $-1 \leq m \leq l + 1$. Thus,

$$\tilde{p}_l = \sum_{m=-1}^{l+1} p_{l-m} p_m e^{-im\alpha} \,. \tag{G.11}$$

It is useful to isolate the $m = -1$ and $m = l + 1$ terms and write

$$\tilde{p}_l = \sum_{m=0}^{l} p_{l-m} p_m e^{-im\alpha} + p_{-1} p_{l+1} \left(e^{i\alpha} + e^{-i(l+1)\alpha}\right) \,. \tag{G.12}$$

One can show that $p_k = e^{-2\pi k\eta} p_0$, thus

$$\begin{aligned} \tilde{p}_l &= e^{-2l\pi\eta} p_0 \left[p_0 \sum_{m=0}^{l} e^{-im\alpha} + p_{-1} e^{-2\pi\eta} \left(e^{i\alpha} + e^{-i(l+1)\alpha}\right] \right) \\ &= e^{-2l\pi\eta} \left(1 - e^{-4\pi\eta}\right) \left[\left(1 - e^{-4\pi\eta}\right) \sum_{m=0}^{l} e^{-im\alpha} - e^{-4\pi\eta} \left(e^{i\alpha} + e^{-i(l+1)\alpha}\right) \right] \,. \end{aligned} \tag{G.13}$$

The sum can be performed as it is just a geometric series, one is left with

$$\begin{aligned}\tilde{p}_l &= e^{-2l\pi\eta}\left(1-e^{-4\pi\eta}\right)\left[\left(1-e^{-4\pi\eta}\right)\frac{1-e^{-i(l+1)\alpha}}{1-e^{-i\alpha}} - e^{-4\pi\eta}\left(e^{i\alpha}+e^{-i(l+1)\alpha}\right)\right] \\ &= \frac{e^{-2l\pi\eta}\left(1-e^{-4\pi\eta}\right)}{1-e^{-i\alpha}}\left[1-e^{-i(l+1)\alpha}-e^{-4\pi\eta}\left(e^{i\alpha}-e^{-i(l+2)\alpha}\right)\right].\end{aligned} \tag{G.14}$$

G.3. Leviton and anti-Leviton drive

In this case $\phi_2(t) = -\phi_1(t)$

$$e^{-i\phi(t)} = \sum_l p_l e^{-il\Omega t}\sum_m p_m^* e^{im\Omega(t+\delta t)}. \tag{G.15}$$

writing $l+m=\tilde{l}$, one obtains

$$e^{-i\phi(t)} = \sum_{lm} p_{l+m}p_m e^{-il\Omega t}e^{+im\Omega\delta t}. \tag{G.16}$$

Which is equivalent to defining corresponding coefficients $\tilde{p}_l = \sum_m p_{l+m}p_m e^{+im\Omega\delta t}$. It is handy to separate between the $l=0$, $l>0$ and $l<0$ cases,

Case $l=0$ In this case,

$$\begin{aligned}\tilde{p}_0 &= \sum_{m=-1}^{\infty} p_m^2 e^{im\alpha} \\ &= p_{-1}^2 e^{-i\alpha} + \sum_{m=0}^{\infty} e^{(-4\pi\eta+i\alpha)m} \\ &= \frac{e^{-4\pi\eta}e^{-i\alpha} - e^{-8\pi\eta}+1}{1-e^{-4\pi\eta+i\alpha}}.\end{aligned} \tag{G.17}$$

Case $l>0$ One starts by remarking that the sum runs over $m>-1$ and separating the first term from the rest of the sum, the following steps are straightforward computation steps.

$$\begin{aligned}\tilde{p}_{l>0} &= p_{l-1}p_{-1}e^{-i\alpha} + p_0^2 e^{-2\pi l\eta}\sum_{m=0}^{\infty} e^{m(-4\pi\eta+i\alpha)} \\ &= -e^{-2l\pi\eta}\left(1-e^{-4\pi\eta}\right)e^{-i\alpha} + e^{-2\pi l\eta}\left(1-e^{-4\pi\eta}\right)^2\frac{1}{1-e^{-4\pi\eta+i\alpha}} \\ &= \frac{2i\sin\left(\frac{\alpha}{2}\right)\left(1-e^{-4\pi\eta}\right)}{1-e^{-4\pi\eta+i\alpha}}e^{-2l\pi\eta-i\frac{\alpha}{2}}.\end{aligned} \tag{G.18}$$

Case $l<0$ In this case, the sum runs from $m=-l-1$ up to infinity, thus a change of variables into $\tilde{m}=m+l$ allows to write

$$\tilde{p}_{l<0} = \sum_{m=-1}^{\infty} p_{m-l}p_m e^{i\alpha(m-l)}. \tag{G.19}$$

writing $-l = |l|$, one recognize the formula for the $l > 0$ case:

$$\begin{aligned} \tilde{p}_{l<0} &= e^{-i\alpha l}\tilde{p}_{|l|} \\ &= \frac{2i\sin\left(\frac{\alpha}{2}\right)\left(1-e^{-4\pi\eta}\right)}{1-e^{-4\pi\eta+i\alpha}} e^{-2|l|\pi\eta - i\frac{\alpha+2l}{2}} . \end{aligned} \tag{G.20}$$

Both cases can be summarized by

$$\tilde{p}_{l\neq 0} = \frac{2i\sin\left(\frac{\alpha}{2}\right)\left(1-e^{-4\pi\eta}\right)}{1-e^{-4\pi\eta+i\alpha}} e^{-2|l|\pi\eta - i\alpha\frac{1+l-|l|}{2}} . \tag{G.21}$$

Bibliography

[1]D. C. Glattli and P. S. Roulleau, "Levitons for electron quantum optics", Physica Status Solidi (b) **254**, 1600650 (2017).

[2]C. Bäuerle, D. C. Glattli, T. Meunier, F. Portier, P. Roche, P. Roulleau, S. Takada, and X. Waintal, "Coherent control of single electrons: a review of current progress", Reports on Progress in Physics **81**, 056503 (2018).

[3]Y. Imry, *Introduction to mesoscopic physics*, 2 (Oxford University Press on Demand, 2002).

[4]Y. V. Nazarov and Y. M. Blanter, *Quantum transport: introduction to nanoscience* (Cambridge university press, 2009).

[5]R. Landauer, "Spatial variation of currents and fields due to localized scatterers in metallic conduction", IBM Journal of research and development **1**, 223–231 (1957).

[6]G. Lesovik, "Excess quantum noise in 2d ballistic point contacts", ZhETF Pisma Redaktsiiu **49**, 513 (1989).

[7]R. Landauer, "Johnson-nyquist noise derived from quantum mechanical transmission", Physica D: Nonlinear Phenomena **38**, 226–229 (1989).

[8]R. Landauer and T. Martin, "Equilibrium and shot noise in mesoscopic systems", Physica B: Condensed Matter **175**, 167–177 (1991).

[9]M. Büttiker, "Scattering theory of current and intensity noise correlations in conductors and wave guides", Phys. Rev. B **46**, 12485–12507 (1992).

[10]T. Martin and R. Landauer, "Wave-packet approach to noise in multichannel mesoscopic systems", Physical Review B **45**, 1742 (1992).

[11]L. Levitov and G. Lesovik, "Charge-transport statistics in quantum conductors", Eksp. Teor. Fiz **55**, 534 (1992).

[12]R. Landauer, "Solid-state shot noise", Physical Review B **47**, 16427 (1993).

[13]L. S. Levitov and G. B. Lesovik, "Charge distribution in quantum shot noise", Jetp Letters **58**, 230–235 (1993).

[14]J. Torres and T. Martin, "Positive and negative hanbury-brown and twiss correlations in normal metal-superconducting devices", Eur. Phys. J. B **12**, 319–322 (1999).

[15]M. Reznikov, M. Heiblum, H. Shtrikman, and D. Mahalu, "Temporal correlation of electrons: suppression of shot noise in a ballistic quantum point contact", Phys. Rev. Lett. **75**, 3340–3343 (1995).

[16]A Kumar, L Saminadayar, D. Glattli, Y Jin, and B Etienne, "Experimental test of the quantum shot noise reduction theory", Physical Review Letters **76**, 2778 (1996).

[17]L. S. Levitov, "The statistical theory of mesoscopic noise", 10.48550/ARXIV.COND-MAT/0210284 (2002).

[18]A. Dayem and R. Martin, "Quantum interaction of microwave radiation with tunneling between superconductors", Physical Review Letters **8**, 246 (1962).

[19]P. K. Tien and J. P. Gordon, "Multiphoton process observed in the interaction of microwave fields with the tunneling between superconductor films", Phys. Rev. **129**, 647–651 (1963).

[20]H. Lee and L. Levitov, "Orthogonality catastrophe in a mesoscopic conductor due to a time-dependent flux", arXiv preprint cond-mat/9312013 (1993).

[21]G. Lesovik and L. Levitov, "Noise in an ac biased junction: nonstationary aharonov-bohm effect", Physical review letters **72**, 538 (1994).

[22]L. S. Levitov, H. Lee, and G. B. Lesovik, "Electron counting statistics and coherent states of electric current", Journal of Mathematical Physics **37**, 4845–4866 (1996).

[23]J Dubois, T Jullien, F Portier, P Roche, A Cavanna, Y Jin, W Wegscheider, P Roulleau, and D. Glattli, "Minimal-excitation states for electron quantum optics using levitons", Nature **502**, 659–663 (2013).

[24]B. J. van Wees, H. van Houten, C. W. J. Beenakker, J. G. Williamson, L. P. Kouwenhoven, D. van der Marel, and C. T. Foxon, "Quantized conductance of point contacts in a two-dimensional electron gas", Phys. Rev. Lett. **60**, 848–850 (1988).

[25]J. M. Raimond, M. Brune, and S. Haroche, "Manipulating quantum entanglement with atoms and photons in a cavity", Rev. Mod. Phys. **73**, 565–582 (2001).

[26]E. Knill, R. Laflamme, and G. J. Milburn, "A scheme for efficient quantum computation with linear optics", Nature **409**, 46–52 (2001).

[27]P. Kok, W. J. Munro, K. Nemoto, T. C. Ralph, J. P. Dowling, and G. J. Milburn, "Linear optical quantum computing with photonic qubits", Rev. Mod. Phys. **79**, 135–174 (2007).

[28]S. Haroche, "Nobel lecture: controlling photons in a box and exploring the quantum to classical boundary", Rev. Mod. Phys. **85**, 1083–1102 (2013).

[29]A. Blais, A. L. Grimsmo, S. M. Girvin, and A. Wallraff, "Circuit quantum electrodynamics", Rev. Mod. Phys. **93**, 025005 (2021).

[30]A. Peruzzo, J. McClean, P. Shadbolt, M.-H. Yung, X.-Q. Zhou, P. J. Love, A. Aspuru-Guzik, and J. L. O'Brien, "A variational eigenvalue solver on a photonic quantum processor", Nature Communications **5**, 4213 (2014).

[31]P. Lodahl, "Quantum-dot based photonic quantum networks", Quantum Science and Technology **3**, 013001 (2017).

[32]S. Wehner, D. Elkouss, and R. Hanson, "Quantum internet: a vision for the road ahead", Science **362**, eaam9288 (2018).

[33]D. Dasenbrook and C. Flindt, "Dynamical generation and detection of entanglement in neutral leviton pairs", Phys. Rev. B **92**, 161412 (2015).

[34]D. Dasenbrook and C. Flindt, "Dynamical scheme for interferometric measurements of full-counting statistics", Phys. Rev. Lett. **117**, 146801 (2016).

[35]D. Dasenbrook, J. Bowles, J. B. Brask, P. P. Hofer, C. Flindt, and N. Brunner, "Single-electron entanglement and nonlocality", New Journal of Physics **18**, 043036 (2016).

[36]H. Edlbauer, Wang, Junliang, Crozes, Thierry, Perrier, Pierre, Ouacel, Seddik, Geffroy, Clément, Georgiou, Giorgos, Chatzikyriakou, Eleni, Lacerda-Santos, Antonio, Waintal, Xavier, Glattli, D. Christian, Roulleau, Preden, Nath, Jayshankar, Kataoka, Masaya, Splettstoesser, Janine, Acciai, Matteo, da Silva Figueira, Maria Cecilia, Oztas, Kemal, Trellakis, Alex, Grange, Thomas, Yevtushenko, Oleg M., Birner, Stefan, and Bauerle, Christopher, "Semiconductor-based electron flying qubits: review on recent progress accelerated by numerical modelling", EPJ Quantum Technol. **9**, "21" (2022).

[37]A. K. Ekert, "Quantum cryptography based on bell's theorem", Physical review letters **67**, 661 (1991).

[38]C. H. Bennett, G. Brassard, and N. D. Mermin, "Quantum cryptography without bell's theorem", Physical review letters **68**, 557 (1992).

[39]C. H. Bennett, G. Brassard, C. Crépeau, R. Jozsa, A. Peres, and W. K. Wootters, "Teleporting an unknown quantum state via dual classical and einstein-podolsky-rosen channels", Phys. Rev. Lett. **70**, 1895–1899 (1993).

[40]G.-L. Long and X.-S. Liu, "Theoretically efficient high-capacity quantum-key-distribution scheme", Physical Review A **65**, 032302 (2002).

[41]I. Neder, N. Ofek, Y. Chung, M. Heiblum, D. Mahalu, and V Umansky, "Interference between two indistinguishable electrons from independent sources", Nature **448**, 333–337 (2007).

[42]E. Bocquillon, F. Parmentier, C. Grenier, J.-M. Berroir, P. Degiovanni, D. Glattli, B. Plaçais, A Cavanna, Y. Jin, and G. Fève, "Electron quantum optics: partitioning electrons one by one", Physical Review Letters **108**, 196803 (2012).

[43]T Jullien, P Roulleau, B Roche, A Cavanna, Y Jin, and D. Glattli, "Quantum tomography of an electron", Nature **514**, 603–607 (2014).

[44]R. H. Brown and R. Q. Twiss, "Correlation between photons in two coherent beams of light", Nature **177**, 27–29 (1956).

[45]W. D. Oliver, J. Kim, R. C. Liu, and Y. Yamamoto, "Hanbury brown and twiss-type experiment with electrons", Science **284**, 299–301 (1999).

[46]M Henny, S. Oberholzer, C. Strunk, T Heinzel, K Ensslin, M Holland, and C Schonenberger, "The fermionic hanbury brown and twiss experiment", Science **284**, 296–298 (1999).

[47]D. Glattli and P. Roulleau, "Hanbury-brown twiss noise correlation with time controlled quasi-particles in ballistic quantum conductors", Physica E: Low-dimensional Systems and Nanostructures **76**, 216–222 (2016).

[48]C.-K. Hong, Z.-Y. Ou, and L. Mandel, "Measurement of subpicosecond time intervals between two photons by interference", Physical review letters **59**, 2044 (1987).

[49]M. Vanević, J. Gabelli, W. Belzig, and B. Reulet, "Electron and electron-hole quasiparticle states in a driven quantum contact", Phys. Rev. B **93**, 041416 (2016).

[50]J. G. Rarity and P. R. Tapster, "Experimental violation of bell's inequality based on phase and momentum", Phys. Rev. Lett. **64**, 2495–2498 (1990).

[51]T. Jonckheere, J. Rech, C Wahl, and T Martin, "Electron and hole hong-ou-mandel interferometry", Physical Review B **86**, 125425 (2012).

[52]J. Rech, D. Ferraro, T. Jonckheere, L. Vannucci, M. Sassetti, and T. Martin, "Minimal Excitations in the Fractional Quantum Hall Regime", Physical Review Letters **118**, 10.1103/PhysRevLett.118.076801 (2017).

[53]C. Wahl, J. Rech, T. Jonckheere, and T. Martin, "Interactions and charge fractionalization in an electronic hong-ou-mandel interferometer", Physical review letters **112**, 046802 (2014).

[54]F. Ronetti, L. Vannucci, D. Ferraro, T. Jonckheere, J. Rech, T. Martin, and M. Sassetti, "Crystallization of levitons in the fractional quantum hall regime", Physical Review B **98**, 075401 (2018).

[55]C. Wahl, "Decoherence and interactions in electron quantum optics setups", Theses (Aix-Marseille Université, 2014).

[56]M. Acciai, M. Carrega, J. Rech, T. Jonckheere, T. Martin, and M. Sassetti, "Probing interactions via nonequilibrium momentum distribution and noise in integer quantum hall systems at $\nu = 2$", Phys. Rev. B **98**, 035426 (2018).

[57]D. Ferraro, F. Ronetti, L. Vannucci, M. Acciai, J. Rech, T. Jockheere, T. Martin, and M. Sassetti, "Hong-ou-mandel characterization of multiply charged levitons", The European Physical Journal Special Topics **227**, 1345–1359 (2018).

[58]L. Vannucci, F. Ronetti, D. Ferraro, J. Rech, T. Jonckheere, T. Martin, and M. Sassetti, "Photoassisted shot noise spectroscopy at fractional filling factor", Journal of Physics: Conference Series **969**, 012143 (2018).

[59]F. Ronetti, L. Vannucci, D. Ferraro, T. Jonckheere, J. Rech, T. Martin, and M. Sassetti, "Hong-ou-mandel heat noise in the quantum hall regime", Phys. Rev. B **99**, 205406 (2019).

[60]M. Acciai, A. Calzona, M. Carrega, T. Martin, and M. Sassetti, "Spectral properties of interacting helical channels driven by lorentzian pulses", New Journal of Physics **21**, 103031 (2019).

[61]G. Rebora, M. Acciai, D. Ferraro, and M. Sassetti, "Collisional interferometry of levitons in quantum hall edge channels at $\nu = 2$", Phys. Rev. B **101**, 245310 (2020).

[62]G. Rebora, D. Ferraro, R. H. Rodriguez, F. D. Parmentier, P. Roche, and M. Sassetti, "Electronic wave-packets in integer quantum hall edge channels: relaxation and dissipative effects", Entropy **23**, 10.3390/e23020138 (2021).

[63]I. Giaever, "Electron tunneling between two superconductors", Physical Review Letters **5**, 464 (1960).

[64]M. Acciai, F. Ronetti, D. Ferraro, J. Rech, T. Jonckheere, M. Sassetti, and T. Martin, "Levitons in superconducting point contacts", Phys. Rev. B **100**, 085418 (2019).

[65]W. Belzig and M. Vanevic, "Elementary Andreev processes in a driven superconductor-normal metal contact", Physica E: Low-Dimensional Systems and Nanostructures **75**, 22–27 (2016).

[66]P.-G. De Gennes, *Superconductivity of metals and alloys* (CRC press, 1999).

[67]G. E. Blonder, M. Tinkham, and T. M. Klapwijk, "Transition from metallic to tunneling regimes in superconducting microconstrictions: Excess current, charge imbalance, and supercurrent conversion", Physical Review B **25**, 4515–4532 (1982).

[68]D. C. Tsui, H. L. Stormer, and A. C. Gossard, "Two-dimensional magnetotransport in the extreme quantum limit", Physical Review Letters **48**, 1559 (1982).

[69]R. B. Laughlin, "Anomalous quantum hall effect: an incompressible quantum fluid with fractionally charged excitations", Physical Review Letters **50**, 1395 (1983).

[70]S. An, P Jiang, H Choi, W Kang, S. Simon, L. Pfeiffer, K. West, and K. Baldwin, "Braiding of abelian and non-abelian anyons in the fractional quantum hall effect", arXiv preprint arXiv:1112.3400 (2011).

[71]N. P. Sandler, C. d. C. Chamon, and E. Fradkin, "Andreev reflection in the fractional quantum hall effect", Physical Review B **57**, 12324 (1998).

[72]C. Nayak, S. H. Simon, A. Stern, M. Freedman, and S. Das Sarma, "Non-abelian anyons and topological quantum computation", Rev. Mod. Phys. **80**, 1083–1159 (2008).

[73]M. Hashisaka, T. Jonckheere, T. Akiho, S. Sasaki, J. Rech, T. Martin, and K. Muraki, "Andreev reflection of fractional quantum hall quasiparticles", Nature Communications **12**, 2794 (2021).

[74]T. Jonckheere, J. Rech, B. Grémaud, and T. Martin, "Anyonic statistics revealed by the hong-ou-mandel dip for fractional excitations", Phys. Rev. Lett. **130**, 186203 (2023).

[75]P. Glidic, O. Maillet, C. Piquard, A. Aassime, A. Cavanna, Y. Jin, U. Gennser, A. Anthore, and F. Pierre, "Quasiparticle andreev scattering in the $\nu = 1/3$ fractional quantum hall regime", Nature Communications **14**, 514 (2023).

[76]T. Martin, "Wave packet approach to noise in n-s junctions", Physics Letters A **220**, 137–142 (1996).

[77]G. Lesovik, T. Martin, and G. Blatter, "Electronic entanglement in the vicinity of a superconductor", Eur. Phys. J. B **24**, 287–290 (2001).

[78]D. Chevallier, J. Rech, T. Jonckheere, and T. Martin, "Current and noise correlations in a double-dot cooper-pair beam splitter", Phys. Rev. B **83**, 125421 (2011).

[79]J. Rech, D. Chevallier, T. Jonckheere, and T. Martin, "Current correlations in an interacting cooper-pair beam splitter", Phys. Rev. B **85**, 035419 (2012).

[80]M. P. Anantram and S. Datta, "Current fluctuations in mesoscopic systems with andreev scattering", Phys. Rev. B **53**, 16390–16402 (1996).

[81]P. Recher, E. V. Sukhorukov, and D. Loss, "Andreev tunneling, coulomb blockade, and resonant transport of nonlocal spin-entangled electrons", Phys. Rev. B **63**, 165314 (2001).

[82]O. Sauret and D. Feinberg, "Spin-current shot noise as a probe of interactions in mesoscopic systems", Phys. Rev. Lett. **92**, 106601 (2004).

[83]O. Sauret, T. Martin, and D. Feinberg, "Spin-current noise and bell inequalities in a realistic superconductor-quantum dot entangler", Phys. Rev. B **72**, 024544 (2005).

[84]D. Pan, K. Li, D. Ruan, S. X. Ng, and L. Hanzo, "Single-photon-memory two-step quantum secure direct communication relying on einstein-podolsky-rosen pairs", IEEE Access **8**, 121146–121161 (2020).

[85]C. H. Bennett and S. J. Wiesner, "Communication via one- and two-particle operators on einstein-podolsky-rosen states", Phys. Rev. Lett. **69**, 2881–2884 (1992).

[86]Y. V. Nazarov, "Novel circuit theory of andreev reflection", Superlattices and microstructures **25**, 1221–1231 (1999).

[87]A. Crépieux, P. Devillard, and T. Martin, "Photoassisted current and shot noise in the fractional quantum hall effect", Phys. Rev. B **69**, 205302 (2004).

[88]B. Bertin-Johannet, J. Rech, T. Jonckheere, B. Grémaud, L. Raymond, and T. Martin, "Microscopic theory of photoassisted electronic transport in normal-metal/bcs-superconductor junctions", Phys. Rev. B **105**, 115112 (2022).

[89]B. Bertin-Johannet, L. Raymond, F. Ronetti, J. Rech, T. Jonckheere, B. Grémaud, and T. Martin, "An on-demand source of energy-entangled electrons using levitons", Appl. Phys. Lett. **122**, 10.1063/5.0148041 (2023).

[90]F. Ronetti, B. Bertin-Johannet, L. Raymond, and T. Martin, "Correlated two-leviton states in the fractional quantum hall regime", in preparation (2023).

[91]B. Bertin-Johannet, B. Grémaud, L. Raymond, J. Rech, T. Jonckheere, and T. Martin, "Current and shot noise in a spin dependent driven normal metal - bcs superconductor junction.", in preparation (2023).

[92]B. Bertin-Johannet, L. Raymond, J. Rech, T. Jonckheere, B. Grémaud, D. C. Glattli, and T. Martin, "Photo-assisted current in the fractional quantum hall effect as a probe of the quasiparticle operator scaling dimension", arXiv preprint cond-mat/2301.10021 (2023).

[93]B. Bertin-Johannet, A. Popoff, F. Ronetti, J. Rech, T. Jonckheere, L. Raymond, B. Grémaud, and T. Martin, "Correlated two-leviton states in the fractional quantum hall regime", in preparation (2023).

[94]P. Dutta and P. Horn, "Low-frequency fluctuations in solids: 1 f noise", Reviews of Modern physics **53**, 497 (1981).

[95]T. Martin, "Course 5 Noise in mesoscopic physics", Les Houches Summer School Proceedings **81**, 283–359 (2005).

[96]H. Nyquist, "Thermal agitation of electric charge in conductors", Physical review **32**, 110 (1928).

[97]W. Schottky, "Uber spontane stromschwankungen in verschiedenen elektrizitatsleitern", Annalen der physik **362**, 541–567 (1918).

[98]J. C. Cuevas, "Electronic transport in normal and superconducting nanocontacts", PhD thesis (Universidad Autonoma, 1999).

[99]J. Bardeen, "Tunnelling from a many-particle point of view", Phys. Rev. Lett. **6**, 57–59 (1961).

[100]W. A. Harrison, "Tunneling from an independent-particle point of view", Phys. Rev. **123**, 85–89 (1961).

[101]M. H. Cohen, L. M. Falicov, and J. C. Phillips, "Superconductive tunneling", Phys. Rev. Lett. **8**, 316–318 (1962).

[102]R. E. Prange, "Tunneling from a many-particle point of view", Physical Review **131**, 1083 (1963).

[103]G Rickayzen, *Theory of superconductivity* (Interscience Publishers), p. 330.

[104]J. H. Shirley, "Solution of the schrodinger equation with a hamiltonian periodic in time", Physical Review **138**, 10.1103/PhysRev.138.B979 (1965).

[105]P. Danielewicz, "Quantum theory of nonequilibrium processes, i", Annals of Physics **152**, 239–304 (1984).

[106]J Keeling, I Klich, and L. S. Levitov, "Minimal excitation states of electrons in one-dimensional wires", Physical Review Letters **97**, 1–5 (2006).

[107]M. Vanević, Y. V. Nazarov, and W. Belzig, "Elementary charge-transfer processes in mesoscopic conductors", Physical Review B **78**, 245308 (2008).

[108]A. Abrikosov, L. Gorkov, I. Dzyaloshinski, and R. Silverman, *Methods of quantum field theory in statistical physics, prentice hall* (Inc. NJ, 1963).

[109]L. N. Cooper, "Bound electron pairs in a degenerate fermi gas", Physical Review **104**, 1189 (1956).

[110]J. R. Schrieffer, *Theory of superconductivity* (CRC press, 1983).

[111]N. N. Bogolyubov, "The compensation principle and the self-consistent field method", Soviet Physics Uspekhi **2**, 236 (1959).

[112]V. Khlus, "Current and voltage fluctuations in microjunctions between normal metals and superconductors", Zh. Eksp. Teor. Fiz **93**, 2179 (1987).

[113]X Jehl, M Sanquer, R Calemczuk, and D Mailly, "Detection of doubled shot noise in short normal-metal/superconductor junctions", Nature **405**, 50–53 (2000).

[114]N. M. Chtchelkatchev, G. Blatter, G. B. Lesovik, and T. Martin, "Bell inequalities and entanglement in solid-state devices", Phys. Rev. B **66**, 161320 (2002).

[115]P. Samuelsson, E. V. Sukhorukov, and M. Büttiker, "Orbital entanglement and violation of bell inequalities in mesoscopic conductors", Phys. Rev. Lett. **91**, 157002 (2003).

[116]J. Torres, T. Martin, and G. B. Lesovik, "Effective charges and statistical signatures in the noise of normal metal–superconductor junctions at arbitrary bias", Physical Review B **63**, 134517 (2001).

[117]A. Das, Y. Ronen, M. Heiblum, D. Mahalu, A. V. Kretinin, and H. Shtrikman, "High-efficiency cooper pair splitting demonstrated by two-particle conductance resonance and positive noise cross-correlation", Nature communications **3**, 1–6 (2012).

[118]G. Deutscher and D. Feinberg, "Coupling superconducting-ferromagnetic point contacts by andreev reflections", Applied Physics Letters **76**, 487–489 (2000).

[119]M. Tinkham, *Introduction to superconductivity* (Courier Corporation, 2004).

[120]C. Grenier, J. Dubois, T. Jullien, P. Roulleau, D. C. Glattli, and P. Degiovanni, "Fractionalization of minimal excitations in integer quantum hall edge channels", Phys. Rev. B **88**, 085302 (2013).

[121]A. A. Kozhevnikov, R. J. Schoelkopf, and D. E. Prober, "Observation of photon-assisted noise in a diffusive normal metal–superconductor junction", Phys. Rev. Lett. **84**, 3398–3401 (2000).

[122]E. H. Hall et al., "On a new action of the magnet on electric currents", American Journal of Mathematics **2**, 287–292 (1879).

[123]K. v. Klitzing, G. Dorda, and M. Pepper, "New method for high-accuracy determination of the fine-structure constant based on quantized hall resistance", Phys. Rev. Lett. **45**, 494–497 (1980).

[124]B. I. Halperin, "Quantized hall conductance, current-carrying edge states, and the existence of extended states in a two-dimensional disordered potential", Physical Review B **25**, 2185 (1982).

[125]R. B. Laughlin, "Quantized hall conductivity in two dimensions", Physical Review B **23**, 5632 (1981).

[126]P. Streda, J. Kucera, and A. H. MacDonald, "Edge states, transmission matrices, and the hall resistance", Phys. Rev. Lett. **59**, 1973–1975 (1987).

[127]J. K. Jain and S. A. Kivelson, "Quantum hall effect in quasi one-dimensional systems: resistance fluctuations and breakdown", Phys. Rev. Lett. **60**, 1542–1545 (1988).

[128]M. Büttiker, "Absence of backscattering in the quantum hall effect in multiprobe conductors", Phys. Rev. B **38**, 9375–9389 (1988).

[129]D. J. Thouless, M. Kohmoto, M. P. Nightingale, and M. den Nijs, "Quantized hall conductance in a two-dimensional periodic potential", Physical review letters **49**, 405 (1982).

[130]B. Simon, "Holonomy, the quantum adiabatic theorem, and berry's phase", Physical Review Letters **51**, 2167 (1983).

[131]R. Bott and S. S. Chern, "Hermitian vector bundles and the equidistribution of the zeroes of their holomorphic sections", Acta Mathematica **114**, 71 –112 (1965).

[132]Y. Hatsugai, "Chern number and edge states in the integer quantum hall effect", Physical review letters **71**, 3697 (1993).

[133]Y. Hatsugai, "Edge states in the integer quantum hall effect and the riemann surface of the bloch function", Physical Review B **48**, 11851 (1993).

[134]X.-G. Wen, "Topological orders and edge excitations in fractional quantum hall states", Advances in Physics **44**, 405–473 (1995).

[135]A. Lopez and E. Fradkin, "Fractional quantum hall effect and chern-simons gauge theories", Physical Review B **44**, 5246 (1991).

[136]D. Tong, "Lectures on the quantum hall effect", arXiv preprint arXiv:1606.06687 (2016).

[137]E. Witten, "Three lectures on topological phases of matter", La Rivista del Nuovo Cimento **39**, 313–370 (2016).

[138]F. Wilczek, "Magnetic flux, angular momentum, and statistics", Physical Review Letters **48**, 1144 (1982).

[139]F. Wilczek, "Quantum mechanics of fractional-spin particles", Physical review letters **49**, 957 (1982).

[140]X.-G. Wen, "Gapless boundary excitations in the quantum hall states and in the chiral spin states", Physical Review B **43**, 11025 (1991).

[141]J.-S. Caux and C. M. Smith, "Celebrating haldane's 'luttinger liquid theory'", Journal of Physics: Condensed Matter **29**, 151001 (2017).

[142]J. von Delft and H. Schoeller, "Bosonization for beginners - refermionization for experts", Annalen der Physik **510**, 225–305 (1998).

[143]X.-G. Wen, "Theory of the edge states in fractional quantum hall effects", International journal of modern physics B **6**, 1711–1762 (1992).

[144]M. Kohmoto, "Topological invariant and the quantization of the hall conductance", Annals of Physics **160**, 343–354 (1985).

[145]C. L. Kane and M. P. Fisher, "A shot in the arm for fractional charge", Nature **389**, 119–120 (1997).

[146]X.-G. Wen, "Edge transport properties of the fractional quantum hall states and weak-impurity scattering of a one-dimensional charge-density wave", Physical Review B **44**, 5708 (1991).

[147]C. Kane and M. P. Fisher, "Nonequilibrium noise and fractional charge in the quantum hall effect", Physical review letters **72**, 724 (1994).

[148]C. d. C. Chamon, D. E. Freed, and X. G. Wen, "Tunneling and quantum noise in one-dimensional luttinger liquids", Phys. Rev. B **51**, 2363–2379 (1995).

[149]L Saminadayar, D. Glattli, Y Jin, and B. c.-m. Etienne, "Observation of the e/3 fractionally charged laughlin quasiparticle", Physical Review Letters **79**, 2526 (1997).

[150]R. de Picciotto, M. Reznikov, M. Heiblum, V. Umansky, G. Bunin, and D. Mahalu, "Direct observation of a fractional charge", Nature **389**, 162 (1997).

[151]M. Kapfer, P. Roulleau, M Santin, I. Farrer, D. Ritchie, and D. Glattli, "A josephson relation for fractionally charged anyons", Science **363**, 846–849 (2019).

[152]R. Bisognin, H. Bartolomei, M. Kumar, I. Safi, J.-M. Berroir, E. Bocquillon, B. Placais, A. Cavanna, U. Gennser, Y. Jin, et al., "Microwave photons emitted by fractionally charged quasiparticles", Nature communications **10**, 1–7 (2019).

[153]I. Safi, P. Devillard, and T. Martin, "Partition noise and statistics in the fractional quantum hall effect", Phys. Rev. Lett. **86**, 4628–4631 (2001).

[154]S. Vishveshwara, "Revisiting the hanbury brown–twiss setup for fractional statistics", Phys. Rev. Lett. **91**, 196803 (2003).

[155]E.-A. Kim, M. Lawler, S. Vishveshwara, and E. Fradkin, "Signatures of fractional statistics in noise experiments in quantum hall fluids", Physical review letters **95**, 176402 (2005).

[156]E.-A. Kim, M. J. Lawler, S. Vishveshwara, and E. Fradkin, "Measuring fractional charge and statistics in fractional quantum hall fluids through noise experiments", Physical Review B **74**, 155324 (2006).

[157]B. I. Halperin, A. Stern, I. Neder, and B. Rosenow, "Theory of the fabry-pérot quantum hall interferometer", Phys. Rev. B **83**, 155440 (2011).

[158]B. Rosenow, I. P. Levkivskyi, and B. I. Halperin, "Current correlations from a mesoscopic anyon collider", Physical Review Letters **116**, 156802 (2016).

[159]D. E. Feldman and B. I. Halperin, "Fractional charge and fractional statistics in the quantum hall effects", Reports on Progress in Physics (2021).

[160]J. Nakamura, S. Liang, G. C. Gardner, and M. J. Manfra, "Direct observation of anyonic braiding statistics", Nature Physics **16**, 931–936 (2020).

[161]H. Bartolomei, M. Kumar, R. Bisognin, A. Marguerite, J.-M. Berroir, E. Bocquillon, B. Placais, A. Cavanna, Q Dong, U. Gennser, et al., "Fractional statistics in anyon collisions", Science **368**, 173–177 (2020).

[162]B. Lee, C. Han, and H.-S. Sim, "Negative excess shot noise by anyon braiding", Phys. Rev. Lett. **123**, 016803 (2019).

[163]J.-Y. M. Lee, C. Han, and H.-S. Sim, "Fractional mutual statistics on integer quantum hall edges", Phys. Rev. Lett. **125**, 196802 (2020).

[164]T. Morel, J.-Y. M. Lee, H.-S. Sim, and C. Mora, "Fractionalization and anyonic statistics in the integer quantum hall collider", Phys. Rev. B **105**, 075433 (2022).

[165]N. Schiller, Y. Oreg, and K. Snizhko, "Extracting the scaling dimension of quantum hall quasiparticles from current correlations", Phys. Rev. B **105**, 165150 (2022).

[166]P. Roche, V. Rodriguez, and D. Glattli, "Quantum hall effect, chiral luttinger liquids and fractional charges", Comptes Rendus Physique **3**, 717–732 (2002).

[167]L. V. Keldysh, Zh. Eksp. Teor. Fiz. **47**, [Sov. Phys.-JETP 20, 1018 (1965)], 1515 (1965).

[168]D. E. Feldman and Y. Gefen, "Backscattering off a point impurity: current enhancement and conductance greater than e^2/h per channel", Phys. Rev. B **67**, 115337 (2003).

[169]M. Moskalets, "High-temperature fusion of a multielectron leviton", Phys. Rev. B **97**, 155411 (2018).

[170]E. Bocquillon, V. Freulon, J.-M Berroir, P. Degiovanni, B. Plaçais, A. Cavanna, Y. Jin, and G. Fève, "Coherence and indistinguishability of single electrons emitted by independent sources", Science **339**, 1054–1057 (2013).

[171]A. Marguerite, C. Cabart, C. Wahl, B. Roussel, V. Freulon, D. Ferraro, C. Grenier, J.-M. Berroir, B. Plaçais, T. Jonckheere, J. Rech, T. Martin, P. Degiovanni, A. Cavanna, Y. Jin, and G. Fève, "Decoherence and relaxation of a single electron in a one-dimensional conductor", Phys. Rev. B **94**, 115311 (2016).

[172]T. Jonckheere, M. Creux, and T. Martin, "Time-controlled charge injection in a quantum hall fluid", Phys. Rev. B **72**, 205321 (2005).

[173]L. Vannucci, F. Ronetti, J. Rech, D. Ferraro, T. Jonckheere, T. Martin, and M. Sassetti, "Minimal excitation states for heat transport in driven quantum hall systems", Phys. Rev. B **95**, 245415 (2017).

[174]F. Ronetti, "Charge and heat transport in topological systems", Thèse de doctorat dirigée par Sassetti, Maura et Martin, Thierry Sciences des Matériaux, Physique, Chimie et Nanosciences Aix-Marseille 2018, PhD thesis (2018).

[175]A. Crépieux, P. Devillard, and T. Martin, "Photoassisted current and shot noise in the fractional quantum hall effect", Phys. Rev. B **69**, 205302 (2004).

[176]B. Heshmat, H. Pahlevaninezhad, Y. Pang, M Masnadi-Shirazi, R. B. Lewis, T. Tiedje, R. Gordon, and T. E. Darcie, "Nanoplasmonic terahertz photoconductive switch on gaas", Nano letters **12 12**, 6255–9 (2012).

[177]D. Chevallier, J. Rech, T. Jonckheere, C. Wahl, and T. Martin, "Poissonian tunneling through an extended impurity in the quantum hall effect", Phys. Rev. B **82**, 155318 (2010).

[178]L. Vannucci, F. Ronetti, G. Dolcetto, M. Carrega, and M. Sassetti, "Interference-induced thermoelectric switching and heat rectification in quantum hall junctions", Phys. Rev. B **92**, 075446 (2015).

[179]F. Ronetti, L. Vannucci, G. Dolcetto, M. Carrega, and M. Sassetti, "Spin-thermoelectric transport induced by interactions and spin-flip processes in two-dimensional topological insulators", Phys. Rev. B **93**, 165414 (2016).

[180]J. Rammer and H. Smith, "Quantum field-theoretical methods in transport theory of metals", Rev. Mod. Phys. **58**, 323–359 (1986).

[181]J. W. Negele and H. Orland, *Quantum many-particle systems* (Perseus Books, 1998).

[182]D. Zwillinger and A. Jeffrey, *Table of integrals, series, and products* (Elsevier Science, 2007).

[183]H. Bateman, *Higher transcendental functions [volumes i-iii]*, Vol. 1 (McGraw-Hill Book Company, 1953).

[184]A. Prudnikov, Y. A. Brychkov, and O. Marichev, *More special functions (integrals and series vol 3)* (New York: Gordon and Breach, 1990).